CONTRIBUTION OF BIOMECHANICAL MEASUREMENTS TO DETECTION OF TOXICITY IN VITRO: AN ATOMIC FORCE MICROSCOPE STUDY

by

OLIVIA LEE MACNEILL

2017

her innocence made difficulties seem insignificant. These few sentences do not justify my gratitude towards everyone who was there throughout my journey.

ABSTRACT

The liver has a wide range of capabilities and is the key organ for drug metabolism, detoxification and elimination. Molecules are absorbed from the GI tract into the bloodstream and transported to the liver through the portal vein circulation system. Most of the metabolic functions within the liver are processed by hepatocytes. The project aim was to test two drugs (5-Fluorouracil (5-FU) and diclofenac) with different metabolic pathways, interpret their toxic effects in hepatocytes and relate these to mechanical and morphological alterations in the cells. The findings of this project thereby allow development of a cell mechanics model for toxicity profiling and drug efficacy at a subcellular level.

Hepatocellular carcinoma (HCC) is the second most common cancer in the world and the most frequent type of liver cancer. Therefore, a great amount of effort has been aimed at the discovery of anticancer compounds to treat it. The majority of conventional chemotherapeutic drugs work on the principle of halting DNA synthesis, and 5-FU follows this principle. This drug is also commonly used for treatment for most gastrointestinal tract cancers. When 5-FU is administered, the toxic adverse effects need to be considered as there is a possibility of severe side effects. To characterise toxic changes in hepatocytes, an Atomic Force Microscope (AFM) was used, which can produce high-resolution images by probing the surface of the cell, to provide information on the cell's mechanical properties (such as Young's modulus). However, with the complexity of this technique it has proved to be challenging to measure relative Young's modulus values that minimise artefacts which affected the image quality of the cells.

Using 5-FU as a model drug, apoptosis was detected by relating surface morphology and mechanical measurements. The surface morphology of HepG2 cells was examined with AFM, and the images produced showed cells exhibiting networking lines of a fibrous nature

on the cell surface and protrusions from the cell membrane after the application of 5-FU. This is thought to be related to apoptotic behaviour occurring within the cell but this is not conclusive and further investigations need to be conducted.

Mitochondria are the main source of adenosine triphosphate (ATP), which is vital for energy, and therefore control all active processes within the cell. Mitochondrial injury often occurs due to drug toxicity, causing altered metabolic function within the cells. Diclofenac is a widely prescribed NSAID, which may cause serious hepatotoxicity, and is thought to be a mitochondrial toxicant.

When altering the physiological conditions from glucose containing medium to galactose containing medium, it was shown that the growth and metabolic function of HepG2 cells decreased. Diclofenac caused a depletion of ATP within the cells. When imaging the cell with AFM, after treatment with diclofenac, there were alterations at surface of HepG2 cells. When the cantilever was separated from the cell surface, the retraction curves showed intermolecular interactions occurring, after treatment with diclofenac which were not observed if the cells were untreated. Microscopic evidence suggested apoptosis may have occurred and it is proposed that the changes in the cell surface reflect this.

Liposomes consisting of lipid bilayers can encapsulate a wide range of drugs, and their behaviour can be controlled by modifying their surface properties. This research also studied the production of liposomes in order to understand their interaction with cells. Liposomal delivery systems are used to improve the bioavailability of drugs and can reduce toxic effects. The liposomes were shown to engage with the cell surface by use of AFM but did not influence the cells viability, suggesting that they had potential as a non-toxic delivery system.

This thesis has produced initial data to suggest that changes in cell mechanical properties can be used to detect changes in cell behaviour, such as apoptosis, but the method is still fraught with complexity.

LIST OF ABBREVIATIONS

7-AAD - 7-Aminoactinomycin D

ANOVA - Analysis of variance

AFM - Atomic Force Microscope

AO - Acridine orange

ATP - Adenosine triphosphate

BrdU - Bromodeoxyuridine

CV - Crystal Violet

DAPI - 4', 6-Diamidino-2-Phenylindole, Dihydrochloride

Dic - Diclofenac

DMEM - Dulbecco's Modified Eagle's Media

DMPC - 1, 2-dimyristoyl-*sn*-glycero-3-phosphocholine

DMSO - Dimethyl Sulfoxide

DNA - Deoxyribonucleic acid

DPBS- Dulbecco's phosphate buffered saline

ECACC- European Collection of Authenticated Cell Cultures

ELISA - Enzyme-linked immunosorbent assay

FACS - Fluorescence-activated cell sorting

FCS - Foetal calf serum

FITC - Fluorescein isothiocyanate

FM - Fluorescence microscope

5-FU - 5-Fluorouracil

HCC - Hepatocellular carcinoma

HEPES - Hydroxyethyl piperazine ethanesulfonic acid

HPLC - High Performance Liquid Chromatography

HUVEC - Human Umbilical Vein Endothelial Cells

MLV - Multilamellar vesicles

MTT- 3-(4,5-Dimethylthiazol-2-yl)-2,5-diphenyltetrazolium bromide

NR- Neutral Red

NTA - Nanoparticle Tracking Analysis

NSAID - Nonsteroidal anti-inflammatory drug

OXYPHOS - Oxidative phosphorylation

PBS - Phosphate buffered saline

PI - Propidium Iodide

POD - peroxidase

Q - Quality factor

QNM - Quantitative Nanoscale Mechanical

SEM - Scanning Electron Microscope

SEM - Standard error of mean

YM - Young's modulus

Table of Contents

Chapter 1 - INTRODUCTION

This thesis focuses on the relationship between toxicity and biomechanical properties of the liver by using two different drugs. In this section, an overview is given of the liver and hepatoma carcinoma (HCC). The diagnosis and treatment plan of HCC is described, as well as the future of drug delivery systems. Atomic force microscopy is explained in detail and its uses to obtain imaging and mechanical information from the cell surface.

1.1. THE LIVER

A healthy liver constitutes approximately 2.5% of the total body weight in human adults. The principal cell type is the hepatic parenchymal cell (hepatocytes), which takes up 60% of the population of cells and 80% of the organ volume (Esrefoglu, 2013). The liver is essentially an exocrine gland that secretes bile into the intestine. However, it is more commonly regarded as an organ with a diverse range of functions. The remarkable micro-anatomical arrangement within the tissue gives the opportunity for the liver to have several roles, for example; detoxication, regulation of glycogen storage and hormone production. The main role of the liver is primarily a metabolic organ.

1.1.1. STRUCTURE AND FUNCTION

The liver lies in the abdominal cavity and is attached to the diaphragm, protected by the ribs. It is divided into four lobes and receives a dual vascular blood supply, originating from the portal vein (~75%) and hepatic artery (~25%) (Burroughs, 2011). The total blood supply to the liver is approximately 25% of the resting cardiac output and the liver also receives at least 20% of oxygen available for consumption (Young, 2010). The liver is organised into polygonal prism shaped lobules. The hepatic vein is the centre point of the lobules. Each lobule has hepatocytes which are organised within the hepatic cord and the cords are separated by adjacent sinusoids (Figure 1.1).
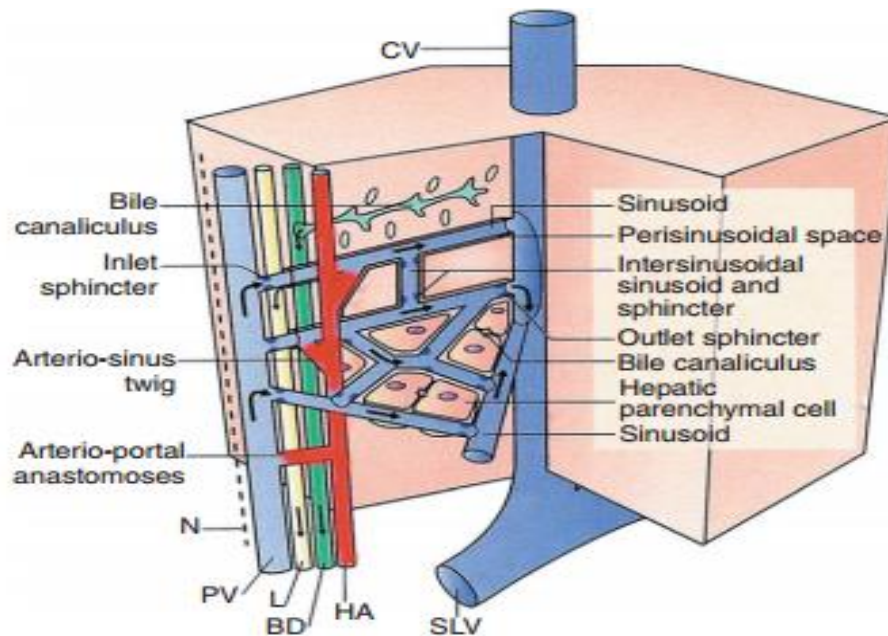
Figure 1.1 - Structural layout of the liver. This organ has a complex microvasculature system and in schematic, it is shown above. Bile ductile (BD), central venule (CV), hepatic arteriole (HA), Lymphatic (L), nerve (N), portal venule (PV), sub lobular HV. Image obtained from the McCuskey RS Functional morphology of the liver with emphasis on its microvasculature, Tavoloni N Berk.

The body relies on various functions occurring in the liver and diseases can often change the efficiency of these functions. It has a range of functions: from formation, storage, synthesis, metabolism and processing of both endogenous and exogenous compounds. Most of the organisation of the liver is designed for one of its main role of removing unwanted materials from the blood.

The liver has been recognised for a long time to be a key organ for drug metabolism and elimination. The liver has a the central role in drug processing, whereby a drug can alter the metabolism and pharmacokinetics of a second drug through various mechanisms of induction or inhibition of enzymes, and altered transporter activates (Sousa et al., 2008). The liver also plays an important role in drug absorption due to the distinctive placement between the systemic and portal circulation. Hepatic first-pass metabolism can alter the structure of a drug or substance ingested by mouth, removing some of the active components of chemicals from

the blood before they enter the general circulation. If a drug is known to have high hepatic first-pass metabolism this results in a low oral bioavailability (Lin and Lu, 1997).

1.1.2. TISSUE STRUCTURE AND FUNCTION

There are different types of cells in the liver each having their different roles. Nevertheless, the cells within the liver are in contact with other components; hepatocytes and other cell types, bile canaliculi, the space of Disse and the liver extracellular matrix along with other interactions. In the space of Disse (the area between the hepatocytes and the endothelial sinusoidal cells), the extracellular matrix components can vary along the different axes. The liver extracellular matrix is composed mainly of collagen, laminin and other proteins (Zeisberg et al., 2006).

Hepatocytes are polyhedral cells approximately 15 to 30 μm in diameter and have a volume of approximately 5000 μm^3. Neighbouring cells are structured into plates which are organised to form a continuous lattice. There are spaces between the plates of the hepatocytes which are occupied by hepatic sinusoids. These sinusoids provide a gateway to nourish each parenchymal cell. Hepatocytes execute most of the metabolic functions within the liver. Endogenous functions range from extracting and processing nutrients from the blood, to producing exocrine and endocrine secretions (Kamimura and Liu, 2008).

Kupffer cells are the liver sinusoidal macrophages which make up a large part of the tissue based macrophage cells in the body. They are vital components of the innate immune system performing specialised scavenger and phagocytic functions which remove complexes formed with microorganisms and cell debris from the blood. They are the first barrier in the portal vein guarding entry into the liver. When pathogens enter the portal vein from the GI tract, it is important to avoid systemic immune activation (Vollmar and Menger, 2009). Kupffer cells are known to contribute to regulation of hepatocellular carcinoma and cirrhosis development, and during chronic viral hepatitis, by the ongoing release of cytokines and chemokines causing an increased chance of spontaneous mutations and DNA damage (Boltjes et al., 2014).

Hepatic stellate cells regulate the regeneration of the liver and inflammation. They are also known to have the ability to store vitamin A and distribute this to other areas of the body (Zhao and Burt, 2007). Vitamin A in the body can be regulated by the use of retinoids. The

stellate cell system is made up of hepatic and extrahepatic stellate cells which can regulate homeostasis of retinoid in the whole body (Senoo, 2004). This cell type also exists in other extrahepatic organs such as the intestine, kidney and pancreas enabling them to regulate the fat and vitamin A required in these organs.

For all above cell types to maintain their function, energy is required and the majority is providing by the mitochondria by means of ATP. In liver tissue, the number of mitochondria is high in terms of density and number. This makes it one of the richest organs in relation to distribution of mitochondria (Degli Esposti et al., 2012).

1.1.3. BIOENERGETICS

Bioenergetics is an important area of biochemistry which assists in the understanding of how the cell processes and produces energy. This term, bioenergetics, provides an understanding of different forms of oxidation reactions and how they aid the cell. The relationship between ATP synthesis by the glycolytic pathway and oxidative phosphorylation is achieved by the chemiosmotic mechanism. Over recent years, this process has been helpful to provide an understanding on diseases and drugs which have a metabolic dependency (Kakimoto and Kowaltowski, 2016).

1.1.4. CELLULAR STRUCTURE

For cells to interact and organise themselves in their surrounding environment, their internal structure and shape needs to be adaptable. All cells contain organelles and cellular structures which have defined functions. Hepatocytes are rich with organelles due to their important metabolic and secretory functions. They may have one nucleus but typically have two nuclei or more, with their cytoplasm containing numerous mitochondria. Also, a defined Golgi apparatus is positioned at the point where the bile canaliculi, rough and smooth endoplasmic reticulum and nucleus meet (Boyer et al., 2011). The cell is surrounded by a thin membrane which is approximately 5-10 nm in thickness (Karp, 2002), which controls both the intra- and extra-cellular environment.

1.1.5. MITOCHONDRIA

The mitochondria are typical lozenge shaped organelles and have relatively open connections within the intermembrane and cristae space. They have unusual properties compared to other organelles; for example, they divide independently meaning that cell division is not coupled with mitochondrial replication. The replication of mitochondria is increased if there is an increased energy demand. Mitochondria have two membranes and their own genome. These two membranes have contrasting purposes. The outer mitochondrial membrane is freely permeable to most metabolites and ions. The inner membrane contains proteins which are involved in ATP synthesis and electron transport. Oxidative phosphorylation occurs in the area surrounded by the inner membrane. Firstly, the citric acid cycle generates the electrons which move between several membrane-bound protein complexes, where at the end of this chain, the final electron acceptor is oxygen and at the same instant ATP is produced.

The primary role of mitochondria in the cell is to supply ATP. However, these organelles have many other processes to undertake such as metabolic interconversion, ion transport and, the generation and removal of oxygen species. More importantly however, the liver requires mitochondria to adjust for the required energetic demand by regulating the flux of various metabolites. Moreover, ammonia is metabolised into urea (less toxic) in the liver which occurs at unique site of the mitochondria.

1.1.6. CYTOSKELETON

The cytoskeleton is a fundamental structural organelle for many processes such as maintaining cell architecture movement, polarity and morphology (Canton and Litchfield, 2006). It is an intricate network of three types of protein filaments: intermediate filaments, actin microfilaments and microtubules. These filamentous proteins can determine the viscoelastic behaviour of cells due to their complex physical properties. All three filament types are critical for different functions in the cell. Specifically in hepatocytes the cytoskeleton is known to contribute to regulation of the activity of drug biotransformation (Chang et al., 2009). Disturbances in the cytoskeleton can result in dysfunction throughout the cell or even cell death.
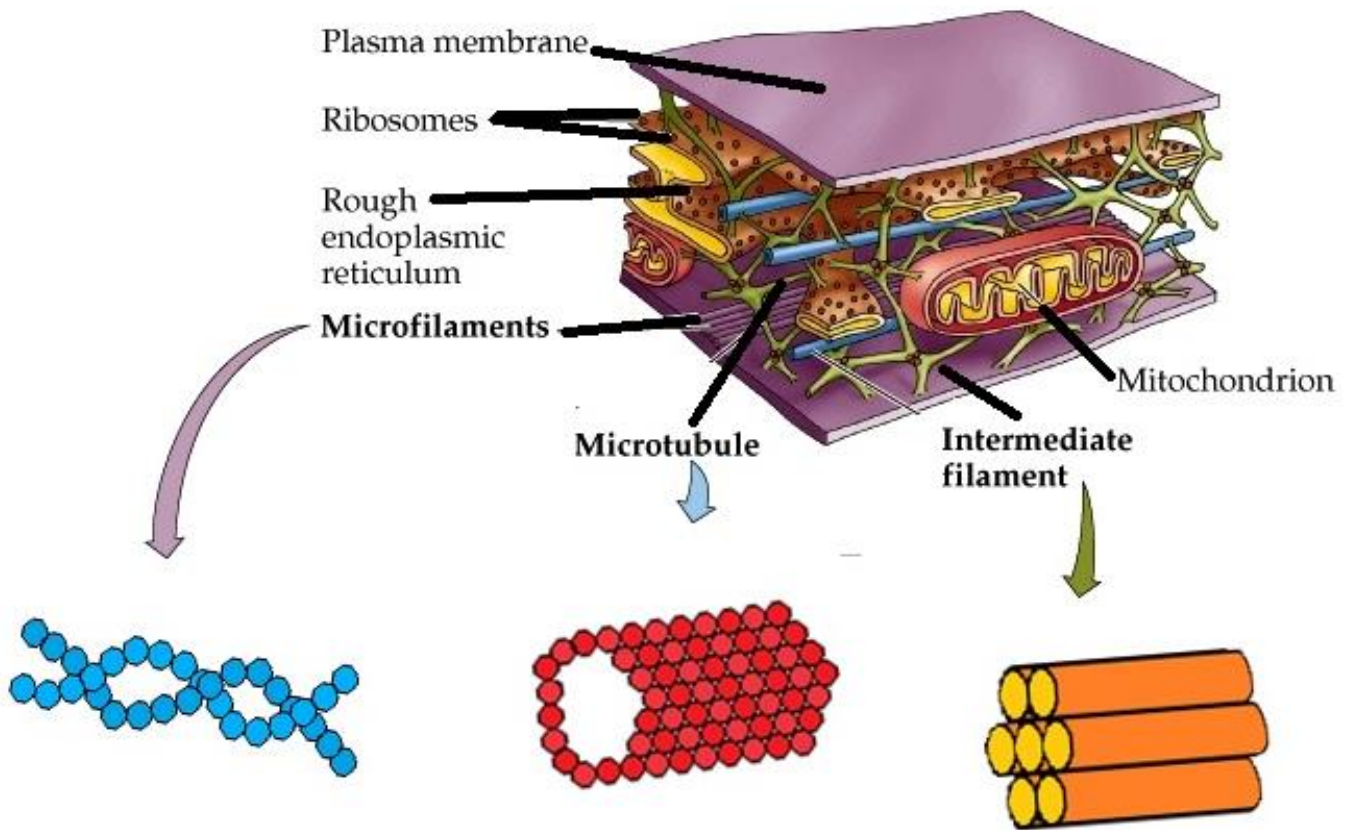
Figure 1.2 – The living cell and its cytoskeleton components. The schematic was adapted from Alberts et al, 2009. The cytoskeleton is required to give the cell structure. A segment of the cell is shown in the schematic where different components of the cell are displayed. Three protein filaments which make up the cytoskeleton and their typical formation: intermediate filament (orange), actin filaments (blue), and microtubules (red). Intermediate filaments are parallel to each other and can be seen to gather in small clusters. Actin filaments are a double stranded molecule. Microtubules are formed in a helical layer which forms a hollow tube.

Intermediate filaments occur in only specialised cells and usually exist in rods which are clustered together (Figure 1.2). These types of filaments are important for maintaining the cell shape. In living cells, the intermediate filaments appear wavy, suggesting a contribution to the viscoelastic properties of the cell, even if this appears to be only very minor (Fudge et al., 2003). Large deformations in the cell will cause the intermediate filaments to stretch and become fully extended. The intermediate filament proteins (cytokeratin) have been found to be helpful in the diagnostic pathology of cancer (Barak et al., 2004).

Actin filaments in the cytoskeleton are the primary structures involved the maintenance of forces required for movement. Other functional roles of actin include secretion, vesicle

6

transfer and endo/exocytosis, with actin filaments being the most abundant fibres in hepatocytes (Stamenović, 2008). The actin filaments are composed of double stranded molecules of monomeric globular (G) actin which exists in equilibrium with the polymerised fibrous (F) actin in the cell. G-actin is a single globular actin monomer and this polymerises to form F-actin. These fibres can extend into microvilli but are predominantly located on the plasma membrane. The elasticity modulus of F-actin is between 1- 2 GPa, which is larger in magnitude than that of the living cell which would be typically be 0.1-1kPa (Stamenović et al., 2007). These filaments can go through a rapid process of polymerisation-depolymerisation in response to chemical (drug) or physical signals.

Microtubules are composed of α-tubulin and β-tubulin monomers alternating in helical layers to form a hollow tube (Figure 1.2). Microtubules are involved in cell division as they form in the mitotic apparatus. They exist generally in small numbers compared to the other filament types and indirectly play a mechanical role such as in the regulation of myosin-II mediated contraction of the actin network (Pullarkat et al., 2007). They also have involvement with blood bound secretion and the intracellular translocation of vesicles. In recent years, microtubules have become an interesting research area with relation to several proteins which known to cause cell death (Braguer et al., 2007).

1.2.   CELL DEATH

The first paper to mention apoptosis that described the death of cells in a distinctive way was published in 1972, although the conceptual idea had been described years previously (Kerr et al., 1972). Apoptosis can occur to maintain cell populations during development or cell aging. It is also a defence mechanism when cells are damaged by different sources (toxic agents or disease) to prevent that damage being passed on when cells proliferate. It is known that both pathological and physiological stimuli have an effect on the apoptosis response (Thompson, 1995). For example, changes in hormonal environment and lack of growth factors (Figure 1.3).

Necrosis, on the other hand, has properties which are seen to differ to apoptosis such as the cell death begins with swelling of mitochondria and cytoplasm, no vesicles are formed and no energy is required for this process which can be seen in the Appendix (Figure A.1). During this process, there is a break down in the plasma membrane where cytoplasmic contents are

unconfined leading to leakage into the extracellular fluid. There is a significant inflammatory response due to necrosis causing extensive tissue damage.

Issues have arisen when scientists attempted to distinguish apoptosis from necrosis when both processes are occurring either simultaneously, sequentially or independently (Table 1.1). Necrosis is cell death which is energy-independent and causes an unregulated signalling (Ankarcrona et al., 1995). In the case of cytotoxic anticancer drugs, a selected low dose could cause apoptosis but higher concentrations of the drug can stimulate necrosis. Cell shrinkage occurs during apoptosis as the organelles become closely packed, this is not found in necrosis (see appendix Figure A.1 for schematic). The apoptotic cell forms small apoptotic bodies and no obvious inflammation can be seen. In comparison, a necrotic cell swells and burst, releasing cytotoxic mediators which cause an inflammatory response. (Ziegler and Groscurth, 2004).

To date, apoptosis can be initiated via two pathways and these pathways merge during activation of execution caspases (Figure 1.3). The two pathways which lead to the execution pathway are known as intrinsic and extrinsic. The intrinsic pathway is mediated by stress signals which causes mitochondrial changes followed by activation of caspase-9. The extrinsic pathway occurs by the binding of Fas/CD95/TNF ligands to the membrane (Desouza et al., 2012). There is evidence stating that the pathways are linked and can influence each other (Fulda and Debatin, 2006).
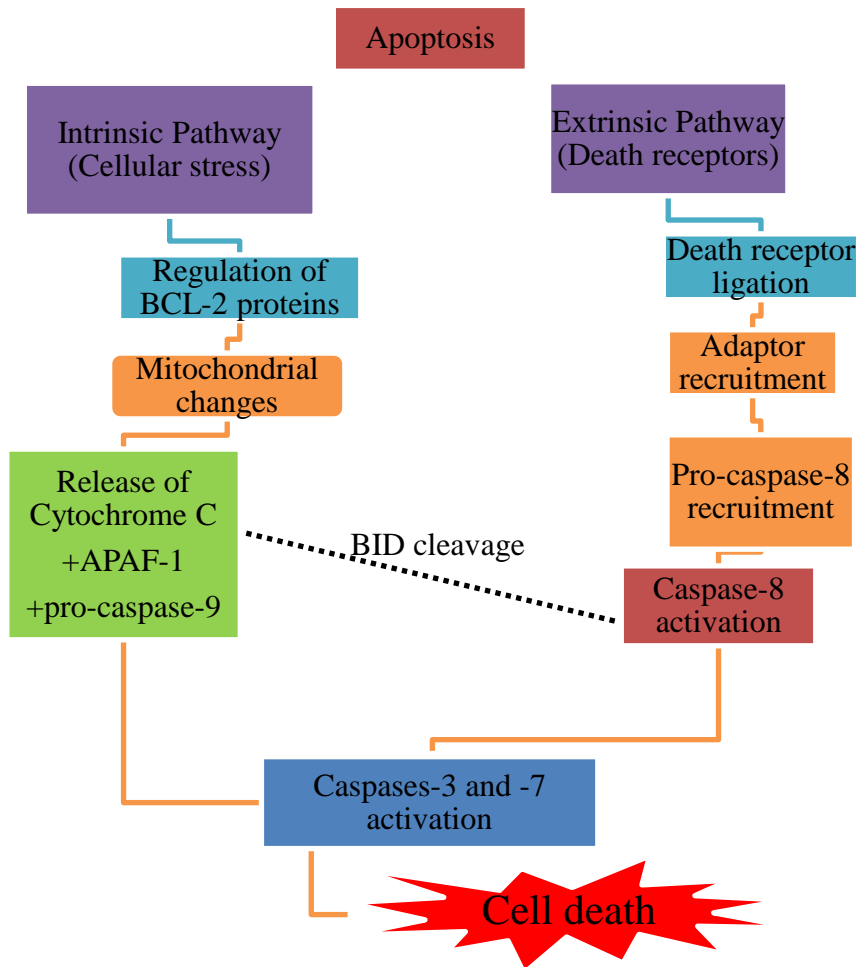
Figure 1.3 - Overview of pathways which can lead to cell death. The normal cell is induced with death stimuli by initiating many of the possible pathways which result in cell death. During apoptosis, the initiator caspase is activated causing an effector caspase to cleave onto cellular components. Apoptosis displays nuclear and cytoplasmic condensation, maintaining an intact membrane, DNA damage and formation of apoptotic bodies. Apoptotic bodies can proceed to lysis or secondary cell death if there are no phagocytes.

Apoptosis	Necrosis
- Affects individual cells - No inflammatory response - Induced due to physiological stimuli - Energy dependent - Release of various factors in cytoplasm - Activation of caspase cascade - Membrane blebbing - Apoptotic bodies - Shrinkage of cytoplasm	- Affects groups of cells - Significant inflammatory response - Evoked by non-physiological disturbances - No energy required - Loss of membrane integrity - No vesicle formation - Swelling of organelles

Table 1-1 –Comparison between apoptosis and necrosis with regards to morphological, biochemical and physiological features

A cascade of complex biochemical changes accompanies the apoptosis process. These range from DNA fragmentation, membrane blebbing, cell shrinking/organelle compaction, formation of intact apoptotic bodies and chromatin condensation. Chromatin condensation is related to pyknosis (irreversible condensation of chromatin in the nucleus) and is one of the most prominent features of apoptosis and can be readily observed by microscopy.

Caspases are contained in most cells as an inactive proenzyme form but once activated can catalyse complex protease events which can lead to apoptotic signalling events. The range of caspases can be broken down into different categories, inflammatory caspases, initiators and executioners. The inflammatory response proceeds through the pathway of necrosis, in which the following caspases partake (caspase -1, -4, -5). However, during apoptosis the following caspases initiate (caspase -2,-9,-10) the process of cell death, and then activate the executioners (caspase-3,-6,-7) (Rai et al., 2005). There are another four caspases which have been identified and have other related mechanisms which are not as easily related to the mechanisms of cell death. The relationship between the caspases and disease is essential for

understanding the specific process of cell death. It is thought the overexpression of a certain caspase can aid in the diagnosis of cancers (Persad et al., 2004).

1.3. HEPATOCELLULAR CARCINOMA

Hepatocellular carcinoma (HCC) is a leading cause of cancer-related death in cirrhotic patients (Sun et al., 2014). With 70- 85% of primary liver cancer was HCC (Jemal et al., 2011). Specifically in the UK, HCC was diagnosed in 1,836 new cases, on average per year over the last five years (Costella et al., 2016). There have been concerns in recent years due to the rise of people with the hepatitis C virus which can lead to HCC (de Oliveria Andrade et al., 2009). This has led to more screening for hepatitis in the UK (Ryder, 2003). There are many influencing factors which can increase the chances of HCC occurring, such as gender (males being more susceptible), age, and presence of hepatic cirrhosis. Diabetes mellitus is a known risk factor for possible development of HCC, a study reported a baseline history of diabetes can increase the chances of HCC by approximately two-fold (King et al., 2014, Yang et al., 2011). The patients with a high risk of development should be offered liver function surveillance and if a definite diagnosis is obtained, the most appropriate treatment initiated.

1.3.1. DIAGNOSIS AND TREATMENT

Diagnosis of HCC is normally based on an imaging technique such as magnetic resonance imaging (MRI), Computerised Topography (CT) or angiography with lipiodol injection (mostly used in the USA). The concentration of the plasma protein, α-fetoprotein (AFP), has been used to test for HCC but it is not satisfactory due to lack of specificity and sensitivity (Zhao Y., 2013).

The prognosis of HCC can be variable as a result of factors such as tumour size, location and stage of liver disease. An understanding of prognostic factors in patients is vital for designing a treatment plan. In the early stages, most patients are treated with potentially curative therapies. Patients who are at a critical stage of treatment are normally treated with Transcatheter Arterial Chemoembolization (TACE) or interventional radiology, which achieves a partial response or a complete necrosis because the blood supply to the tumour is

restricted (Deng et al., 2012). Only 30-40% of patients are eligible for curative intervention such as liver transplantation (Cao et al., 2012). Unfortunately, only a minority of patients with HCC are diagnosed early enough to benefit from most types of treatment. There is a significantly high treatment failure rate when the tumour size is found to be greater than 3 cm (Mulier et al., 2005). Conventional chemotherapy for inoperable HCC patients is ineffective and produces a low response rate. In the advanced stages, the drug sorafenib (multi-kinase inhibitor) is the most favourable in the literature, but there is uncertainty on how effective this drug is alone (Bruix and Sherman, 2011, Cao et al., 2012, Deng et al., 2012, Sherman, 2014, Ryder, 2003). There are other non-surgical options ranging from percutaneous ethanol injection, chemoembolization, radiofrequency ablation, systemic chemotherapy or hormonal therapy (Yu, 2016). Prior to sorafenib, doxorubicin was used but it gives a low response rate of 15- 20% (Cao et al., 2012), due to the short half-life of the drug in plasma (approximately 3 min).

Preclinical research originates from *in vitro* cellular studies on hepatocytes. The most common *in vitro* research model for analysis of HCC are cultures of HepG2 cells derived from a human patient with liver cancer in 1972 (Aden et al., 1979). These cells are used as an alternative to cultures of primary human hepatocytes which are difficult to obtain. HepG2 cells have lost growth control regulation so have unlimited proliferation. Suspensions of HepG2 cells can easily be preserved in liquid nitrogen and they reattach readily to the surfaces of cultures dishes after thawing. HepG2 cells share many of the properties of hepatocytes, such as plasma membrane polarity, secretion of various lipoproteins and biosynthesis of multiple plasma proteins (Altmann et al., 2008). Even though there are many advantages in using HepG2 cells, the cells are highly de-differentiated with little liver-like function (Zhang et al., 2014). This cell line is commonly used for toxicity testing, but it possesses low activities of the enzymes which are used for detoxification of xenobiotics (Bandele et al., 2012, Nikoloff et al., 2014).

Several studies have used HepG2 cells to investigate the metabolism and the toxicity of compounds which have an adverse impact on biological processes (Bandele et al., 2012, Sharma et al., 2009). The main objective of these types of *in vitro* experiments was to produce data that were reliable, sensitive and accurate enough to identify alterations for example, in mitochondrial activity, cell viability and oxidative stress, which would aid in prediction of *in vivo* biological effects. *In vitro* human cell culture systems represent a

valuable approach to assess the toxicity of compounds which can then be reproduced in *in vivo* models.

Ultimately, to assess biological effects and safety of new candidate drugs there is more direct clinical research in the form of clinical trials. For HCC, most clinical trials are conducted in the area of inoperable HCC. These were mostly found to have minimal chemotherapeutic activity in patients but proved that the drugs have an acceptable safety profile (Llovet et al., 2001, Wagner and Vorauer-Uhl, 2011, Yopp and Jarnagin, 2010, Londoño et al., 2015).

Various drug models have been established to define the most successful treatment plan for HCC. The uses of specific chemotherapeutics are known to cause a toxic effect not only to the cancer cells but to healthy cells. Understanding individual drugs models would give hope to a possible combination therapy to enhance the bioavailability of conventional drugs.

1.3.2. 5-FU AS A MODEL ANTI-CANCER AGENT

5-Fluorouracil is an anti-cancer agent and can be used for treating many tumours in different parts of the body. It is a heterocyclic aromatic organic compound with a structure similar to the pyrimidine molecules of DNA and RNA. From a study of the literature, researchers are most interested in the site-specific drug delivery of 5-FU to the colon (Shahbazi and A Santos, 2013).

The metabolic pathway of 5-FU is complex (Figure 1.4) and ultimately can give rise to active metabolites known as fluorodeoxyuridine monophosphate (5-F-dUMP), fluorodeoxyuridine triphosphate (5-F-dUTP) and fluorouridine triphosphate (5-FUTP). The main pathway for the action of 5-FU is to form a stable complex with thymidylate synthase (TS) after being converted to fluorodeoxyuridine monophosphate (5-F-dUMP), and overall it causes an inhibition of deoxythymidine monophosphate (dTMP) production (a detailed schematic can be found in the appendix, Figure A.2. This leads to an imbalance of nucleotides, as well as to altered incorporation of uridine into DNA. The stability and function of DNA and RNA is altered due to 5-FU converting the nucleotides to fluoronucleotides (Pettersen et al., 2011). Cytotoxicity is known to occur because of depletion of dTMP which is vital for DNA repair and replication. Up to 80% of administered 5-FU is broken down by dihydropyrimidine dehydrogenase (DPD) in the liver (He et al., 2008). The enzyme is important for the rate-

limiting step of 5-FU catabolism in all types of cells. Indeed, *in vitro* studies showed DPD overexpression occurs if a cancer cell line becomes resistant to 5-FU (Takebe et al., 2001).
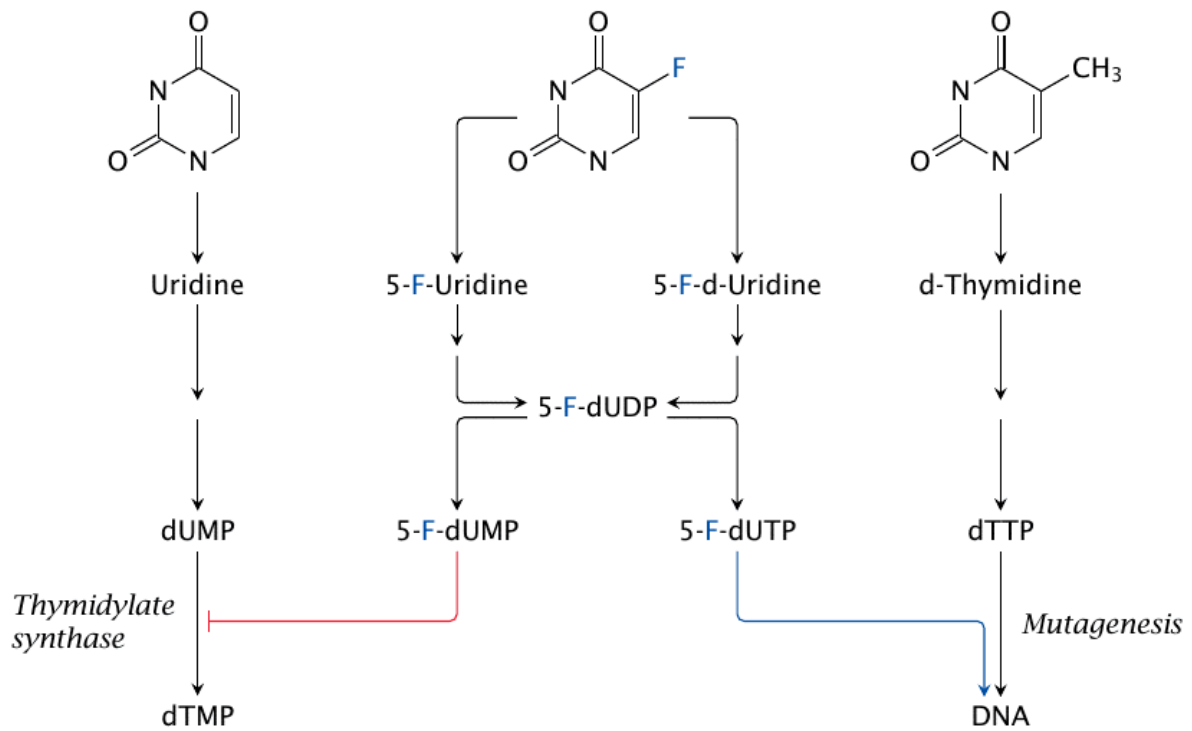
Figure 1.4 – Schematic of 5-FU metabolism. Adapted from Palmer et al. The active metabolites, (fluorodeoxyuridine monophosphate (5-F-dUMP) and fluorodeoxyuridine triphosphate (5-F-dUTP)) allow 5-FU to mimic both uracil and thymine. The main mechanism is the conversion to FUMP from activation of 5-FU by several possible cofactors. The metabolite 5-F-d-Uridine causes further phosphorylation to fluorodeoxyuridine diphosphate (FdUDP) by ribonucleotide reductase. 5-F-dUDP can then generate active metabolites 5-F-dUMP and 5-F-dUTP, respectively.

5-FU is known for the toxic effect it has on the body from severe haematological, to mucosal and gastrointestinal toxicities, which often occur during dose intensification strategies (Zhang N., 2008, Garg et al., 2002). It also interferes with nucleoside metabolism and can be incorporated into RNA and DNA (Noordhuis et al., 2004), making it an enzyme inhibitor. Enzyme inhibitors are beneficial substances in certain diseases. The bioavailability of the drug is known to be erratic; it has as a short half-life in plasma (8-14 minutes) and hence is

not ideal for oral use (Fleming et al., 2003). The treatment plan for this drug is normally continuous low-dose infusion as there has been shown to be a higher response rate by this route (Borner et al., 1993).

5-FU is used for the treatment of HCC, but the tumour is known to show resistance which is a major obstacle for successful treatment (Uchibori, 2012). Also, the half-life of the drug would need to be improved, and the toxic effect it has on healthy cells moderated. Hence, there is literature on different drug delivery systems such as; liposomes (Fresta et al., 1993, Pentak et al., 2012, Zhang N., 2008), silver nanostructures (Sardo et al., 2009) and micelles. Ideally, 5-FU would be able to incorporate into the cancerous cells but to achieve this, the lipophilicity of the drug would need to be increased and improved its delivery formulation.

1.3.3. Mitochondria in Cancer

The density of mitochondria in cells is dependent upon numerous factors, mostly relating to oxidative phosphorylation. There is a known difference between cancer and normal cells when it comes to energy metabolism, thus giving the opportunity to provide more effective treatment for cancer. The Warburg effect states that there is a higher level of glycolysis in a cancer cell, which is vital for their survival (Warburg, 1956). As the tumour progresses, there is a reduction in mitochondrial function as the microenvironment differs from normal tissues especially with regards to regions of hypoxia and interior vasculature areas (Vaupel, 2008). These regions will suffer changes in transcription factors within the cell, leading to the possible outcome of gene expression alterations.

In physiological and pathological scenarios, the mitochondria are known to exert both lethal and vital functions. Within the cell, the mitochondria aids in the production of energy. However, the mitochondria can regulate a trigger leading to the intrinsic pathway of apoptosis due to intracellular stimuli such as overproduction of reactive oxygen species (Kroemer et al., 2007). Additionally, malignant cells are shown to have altered metabolic capacity to engage in processes such as apoptosis (Galluzzi et al., 2008). These modifications may be related to the bioenergetic functions of mitochondria which could allow these organelles to be attractive drug targets (Fulda et al., 2010).

Mitochondria can exhibit differences in shape, size and number depending on cell type. In a study analysing the copy number of mitochondria DNA in HCC, the number in male and

females was found to be significantly different (Yin et al., 2004). Additionally, HCC is more commonly diagnosed in males than females but the link between gender and mitochondria content in the liver has not been researched in detail. Also, in this study it was stated that the content of mitochondrial respiratory proteins significantly decreases in HCC. Also, studies have tried to ascertain the number of mitochondria in a single hepatocyte which was calculated to be 500 to 4000 (Degli Esposti et al., 2012). There are many drugs which can cause mitochondrial toxicity and could perhaps therefore aid in the treatment with HCC. In recent years, studies have reported that cancers can been successfully treated by NSAIDs, where inducing cell cycle arrest and apoptosis has occurred (Hosomi et al., 2000, Rao and Reddy, 2004, Jana, 2008).

1.3.4. AN INTRODUCTION TO DICLOFENAC

Diclofenac (Dic) is a non-steroid anti-inflammatory drug which was synthesized in the 1960s by Ciba-Giegy and was officially launched in 1973 as an oral formulation. Diclofenac provides inhibition of cyclooxygenase enzyme 1 (COX 1) and cyclooxygenase II (COX II) causing an anti-inflammatory response (Warner et al., 1999, Goh and Lane, 2014). Additional mechanisms of action have been proposed including the possibility of inhibition the of thromboxane-prostanoid receptor and the inhibition of lipoxygenase enzymes (Gan, 2010). Diclofenac has a half-life in plasma of approximately 1.5h and is metabolised in the liver to 4-hydroxydiclofenac and other hydroxylated forms (Figure 1.5).
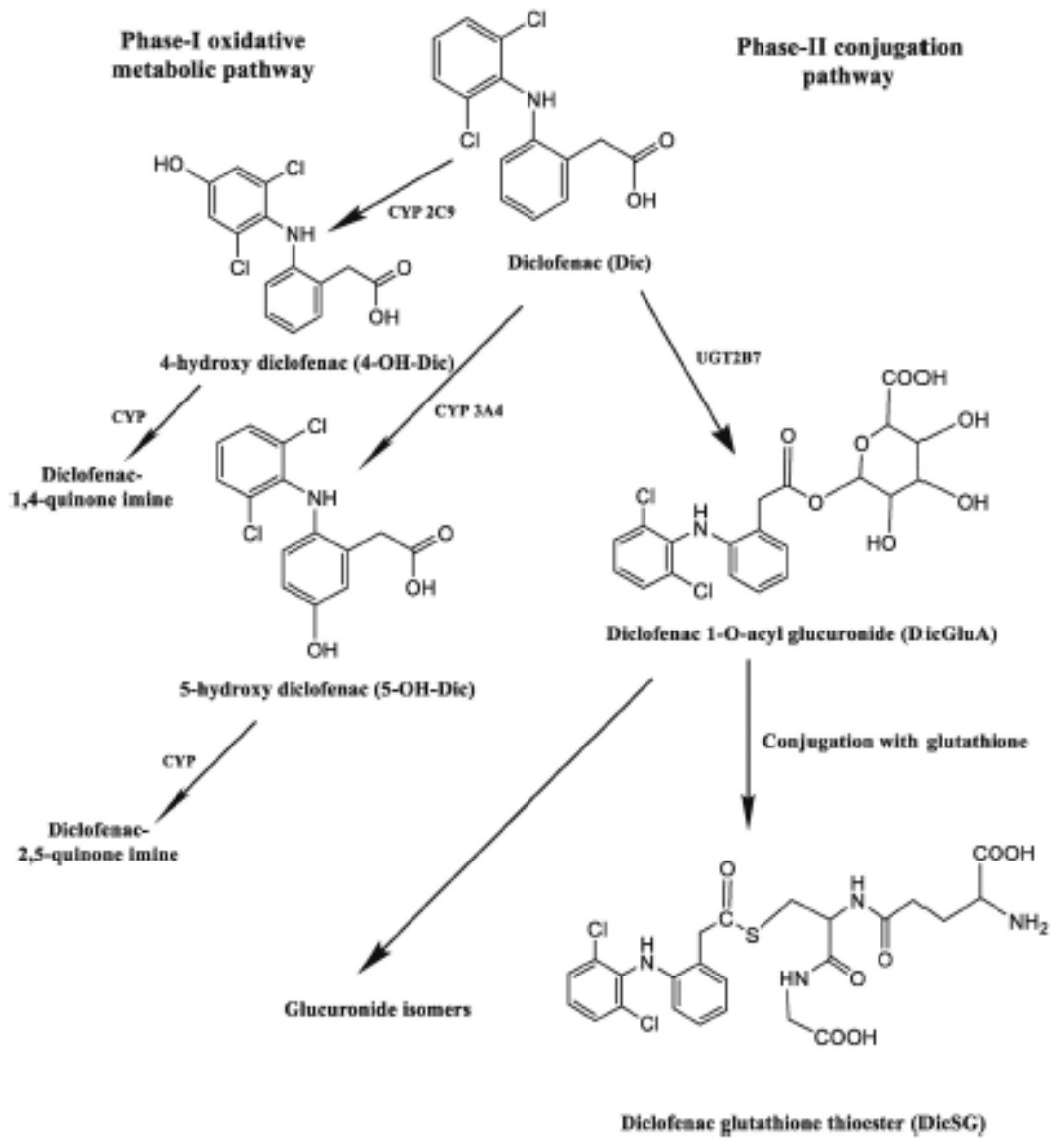
Figure 1.5 - Diclofenac and its major of metabolites found in human. The schematic was adapted from Syed et al, 2012. As seen, diclofenac can be metabolised by phase-I and phase II reactions. There is a possibility of oxidation to p-benzoquinone imines by 4'-OH-Dic and 5-OH-Dic metabolites

The pharmacokinetics and metabolism of diclofenac have been defined in past studies. The bioavailability of diclofenac is approximately 90% when administrated orally. After two hours, a dose of 50mg will equate to 1.0μg/ml in terms of plasma levels (Riess et al., 1978).

1.4. DRUG DELIVERY SYSTEMS

Targeting the delivery of drugs to improve efficacy in chemotherapy has been achieved using drug delivery systems. Most of the work carried out in the drug delivery area has in fact been focused toward cancer chemotherapy, in order to reduce its toxic effects and increase the accuracy and specificity of its targeting towards tumour tissue only. The success is debatable, but the objective is to improve the therapeutic efficacy. The delivery of many drugs can be improved by altering their pharmacological properties to enhance circulation half-life and efficacy (Allen and Cullis, 2004). Description of the surface area, shape and size of the cancers to be treated would assist the drug delivery systems to efficiently reach the target. An ideal drug delivery system would be non-toxic over a long period, excluded from other sites, target the site of a cancer associated receptor, and could be rapidly removed when the set goal was achieved. The drug should also remain active for the optimum time and concentration.

Tablets are the most common and stable oral dosage form of delivery system. The advantage of using tablets is their affordability for both patients and manufacturers. The main objective in designing a drug delivery system is to increase the effectiveness of the drug and reduce the need for frequent dosing. Oral ingestion is a convenient route for drug administration and is more feasible compared with any other route.

Evaluation of a controlled release drug delivery system requires biopharmaceutical information regarding absorption, the molecular weight, effects at different pH, pKa value, apparent partition coefficient and overall knowledge of the GI tract absorption mechanism of the drug. This information can aid prediction of the optimum drug release rate.

Conventional drug delivery systems can be modified to improve parameters such as release and targeting. There are two types of release systems; delayed (uses intermittent, repetitive dosing) and sustained (achieves slow release over extended periods). Targeting can be site-specific or use receptor facilitated release depending on the location within an organ or at adjacent biological locations to the target. Sustained release is advantageous as the drug can then have improved efficacy. The optimum way forward is to use well established drugs encapsulated them and then delivered them to the target site.

1.5.   NANOPARTICLES

Nanoparticles are used in the research of drug delivery systems as carriers of drug molecules and these can range in size from 10-1000nm. Nanoparticles as a drug delivery system demonstrate potential sophistication for cancer treatment. It is hoped these nanoparticles will help solve difficult challenges faced, such a metastatic disease, toxicity and drug resistance. Nanoparticles can have many different structures (Figure 1.6). Over the decades, a variety of types of nanoparticles have been developed and characterised including liposomes, micelles and dendrimers, to name a few. In the schematic below (adapted by (Cho et al., 2008)) the nanoparticles shown have different physiochemical properties which is beneficial to trigger different responses. The physicochemical properties that can be altered can range from shape, size, surface charge, solubility and hydrophobicity. There can be different advantages depending on the type of nanoparticle used – often linked to its physicochemical properties (Brannon-Peppas and Blanchette, 2012, Singh, 2016).
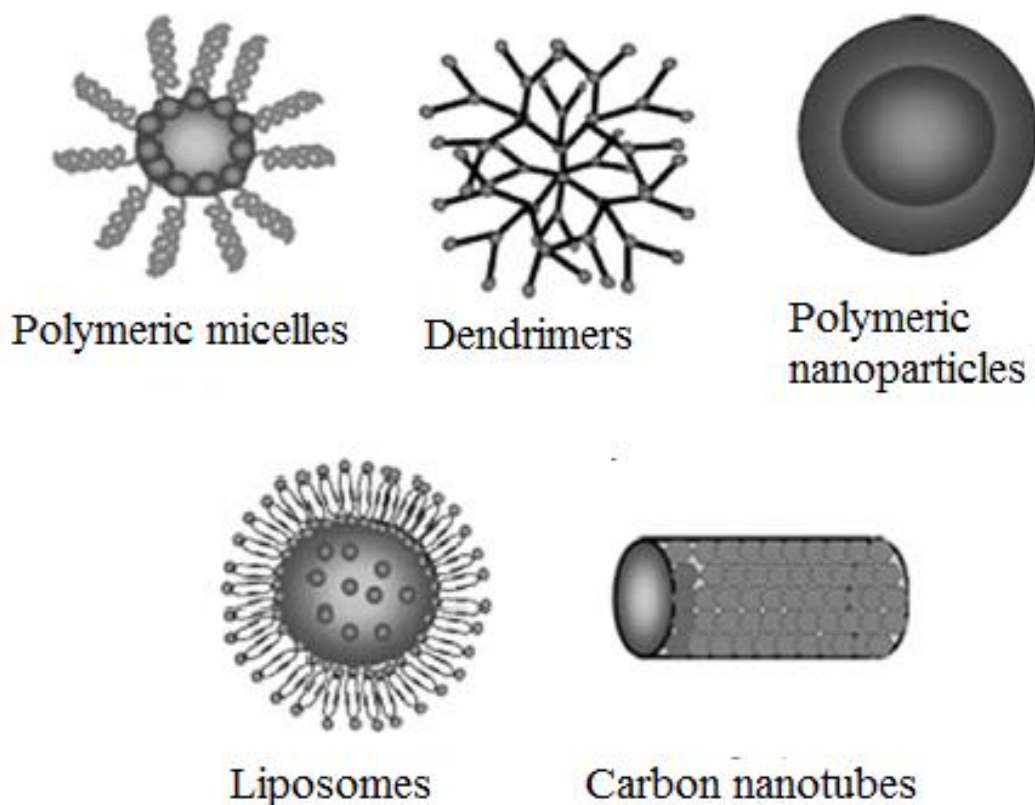
Figure 1.6 – Drug delivery nanoparticles. There is a range of possible nanoparticles which can be used as drug delivery systems. The manipulation of these nanoparticle properties can aid bio-compatibly and purpose of function. In this schematic (adapted from by Cho et al.), different nanoparticles can be used in nanomedicine: Polymeric micelles, dendrimers, polymeric nanoparticles, liposomes and carbon nanotubes.

The use of nanoparticles in therapeutic processes has increased significantly in recent years. Nanoparticles harness opportunities to make drug delivery system more precise, and also improve other characteristics such as therapeutic index. The shape, size and surface characteristics of a nanoparticle have an important role to play in the *in vivo* biodistribution.

Spherically shaped nanoparticles have been extensively studied (Kumar and Kumar, 2014). Smaller nanoparticles (<5 nm) are known to be cleared rapidly from the body due to renal clearance or extravasation (drug leaked into surrounding tissue) (Vinogradov et al., 2004, Torchilin, 2008), with the accumulation of nanoparticles occurring as size increases to within the micrometre range. Accumulation in areas such as the liver occurs with these larger particles (Petros and DeSimone, 2010). Cellular uptake and biodistribution of nanoparticles

therefore depends on size, but also on the cell type. Nanoparticles within the range of 40-80 nm have been found to be the most effective in altering cell function (Jiang et al., 2008).

Shape of nanoparticles is a critical parameter and is a useful one to manipulate for effective drug delivery system design (Champion et al., 2007). Differently shaped nanoparticles can utilise different ways of transportation, degradation and targeting. Spherical nanoparticles were found to be noticeably less toxic than rod shaped nanoparticles (Hsiao and Huang, 2011), with a possible reason being related to the van der Waals forces of the rod shaped particle nanoparticles are larger than those of spherical. Surface properties are thought to have significant impact on the cytotoxicity and cellular uptake of nanoparticles (Ahn et al., 2013). The cell uptake of particles, and subsequent effects on proliferation and viability were shown to be altered when a nanoparticle had a charged surface (Chen et al., 2006). It was shown for example, that nanoparticles with a positive surface charge are internalised to a greater extent within HepG2 cells compared with negatively charged particles (Liu et al., 2013).

Delivery systems in the form of nanoparticles can be segregated into categories of passively or actively targeted. In passive targeting, the enhanced permeation and retention (EPR) effect is used to enable a drug to permeate more readily through a tumour. This phenomenon of EPR-effect was discovered by Maeda and Matsumura and was then used by them when designing cancer-targeting drug delivery systems (Maeda and Matsumura, 1988). In general, passive targeting relates to both the blood circulation and the extravaculative and is achieved through locally activated delivery within the body. In active targeting, the drug is conjugated with a carrier system that targets cell ligands and when in close proximity (<0.5nm), the two components can interact (Bae and Park, 2011). It has been shown that such ligand-receptors do not always improve accumulation of nanoparticles in tumours (Pirollo and Chang, 2008).

1.6.   LIPOSOMES

The first drug delivery system in the form of nanoparticles was lipid vesicles, and they were first described in the 1960s (Bangham et al., 1965). The lipids form a bilayer due to the hydrophobic interactions; therefore, the hydrophilic heads of the lipids are facing the aqueous surroundings. The physiochemical parameters can be changed to suit functionality, size and surface charge.

Liposomes are ideal mainly for carrying very potent drugs as the encapsulation efficacy tends to be low. There are many challenges when using liposomes such as rapid release. Liposomes are, however, reputable as delivery systems and have a wide application. The conventional methods of production are known to produce a broad distribution of size, poor stability and low reproducibility of size, hence they can be restricting (Huang et al., 2014). The size of liposomes is important for drug delivery, and conventional methods are not capable of giving a homogenous distribution (Wagner and Vorauer-Uhl, 2011). The stability of the liposomes can be increased with the use of cholesterol in the formulations and can determine the size of particles achieved. Drug incorporation and release rate depends on the drug but also on the lipid choice, composition and concentration.

1.6.1.   PRODUCTION OF LIPOSOMES

There are many methods for the production of liposomes, for example; thin-film hydration, reversed phase evaporation, solvent-injection technique and detergent dialysis (Krämer, 2007, van Balen et al., 2004). Each one of these production methods has its advantages and disadvantages. The most common way for the preparation of liposomes is the thin-film hydration method. This is achieved by using an organic solvent to dissolve the lipids before emulsifying them in an aqueous phase and then slowly evaporating the solvent. The liposomes are extruded through filters with specific pore sizes at a temperature above the phase transition (Toh and Chiu, 2013). Despite advantages, the shape and size of multi-lamellar vesicles (MLV) liposomes are heterogeneous but can be down-sized using techniques such as sonication or extrusion (Akbarzadeh et al., 2013).

A recent advance in the area of microfluidic-based methodologies for drug development (lab-on-a-chip, Figure 1.7), which investigates rapid controlled mixing, is gaining popularity in research laboratories and hopefully the end point will be industrial applied (Kastner et al.,

2015, Belliveau et al., 2012). The production of liposomes using this technology depends on an alteration in polarities of the lipids followed by a nanoprecipitation reaction. The flow profiles of the inlets into the chambers have a low Reynolds number and are defined by laminar flow. The use of microfluidics arrangement gives the opportunity to control the ratio between solvent and aqueous streams and the mixing rate (Figure 1.7). The ecological factors are facilitated reducing time, liquid volumes and costs. Compared to the conventional methods, there is a higher throughput and it is considered to be less harsh.
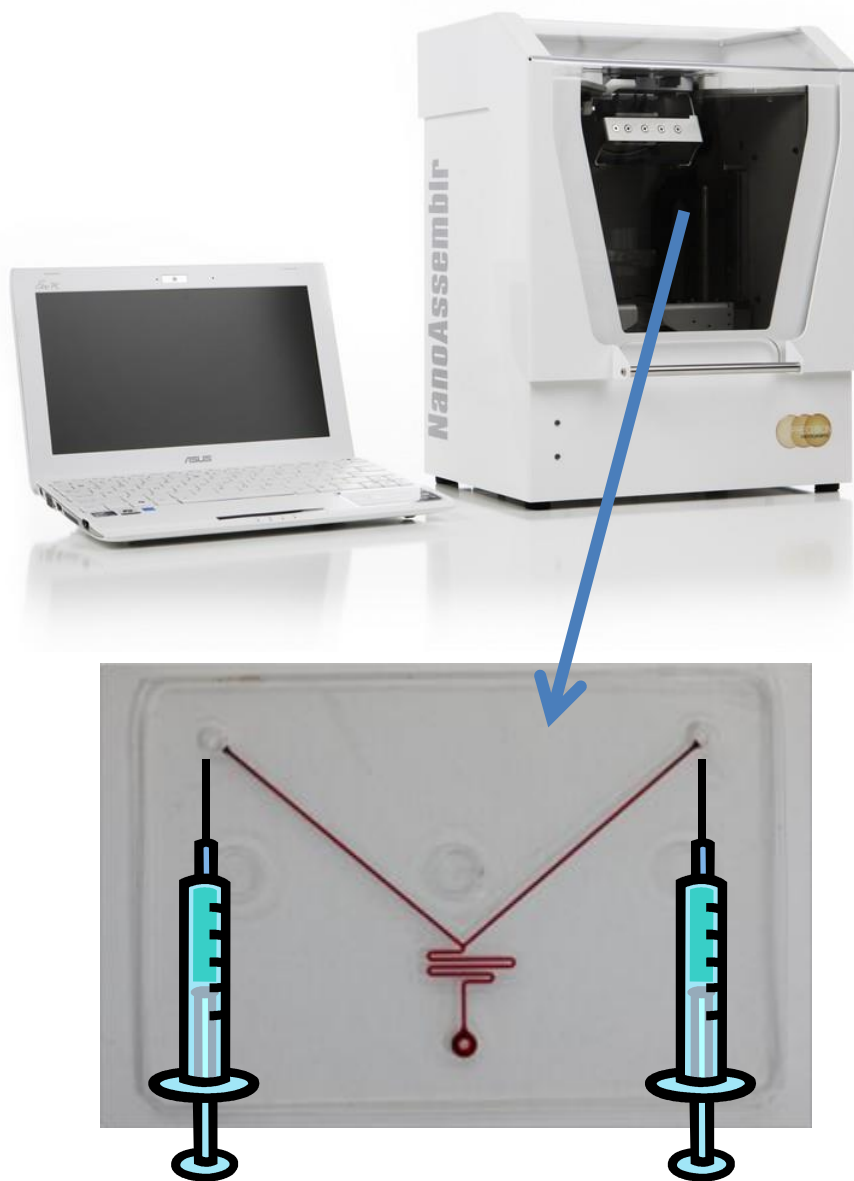
Figure 1.7 - Nanoassemblr desktop system (adapted from precision systems catalogue (NanoSystems, 2015). The development of this microfluidic based equipment can exploit the use of micro-sized channels for controlled mixing to generate liposomes

Liposomes have been used for drug targeting especially in cancer therapy. The toxic side effects of drugs can severely restrict chemotherapy. It is hoped that liposome encapsulation could alter the distribution of the chemotherapeutic drug in the body both temporally and spatially which would increase the efficacy of the treatment and reduce toxic side effects (Dorasamy et al., 2012, Dash and Konkimalla, 2013). Liposomal products have currently either entered clinical trials (53 products), or have been successfully launched commercially (8 products) (Nagarsenker et al., 2015). For example, ThermoDox is a lyso-thermosensitive liposomal preparation containing doxorubicin, and in the phase III HEAT trial this is to be used to treat inoperable hepatocellular carcinoma with or without radiofrequency ablation (Shah et al., 2014, Spence et al., 2015).

ThermoDox is an enhanced Lyso-Thermosensitive Liposomal Doxorubicin delivery system which is delivered intravenously and uses mechanisms to deliver the drug in higher concentration to the site of the tumour than conventional therapy. The phospholipid chosen has a gel-to-liquid temperature transition which can be attainable by local hyperthermia (~41ºC). Hence, at this temperature the lipid membrane becomes unstable which triggers drug release into the tissue. There have been case studies (OPTIMA) which evaluated ThermoDox in combination with radiofrequency ablation and they suggest an improvement in chemotherapy compared to free drug (Hong et al., 2013).

1.7. BIOMECHANICAL PROPERTIES OF CELLS

The multidisciplinary field of cell biomechanics (which links cell biology with nanomechanics) helps give an understanding of the complexity of cells within their own environment. Cells in their own environment are constantly exposed to mechanical stimuli which cue a response. Mechanical stimuli can alter the cell growth, differentiation, and migration when external forces are applied. The response of these applied forces can give a biochemical signal (leading to an induced change in phenotype) or a mechanical response (deformations of the cell structure). These responses can change the viscoelastic behaviour of a cell (Moeendarbary and Harris, 2014). Viscoelasticity is a stress-strain relationship which is non-linear and in addition the deformation energy does not return to the original state. Mechanical analysis of cells is becoming sought after information in several areas of biology. The difference between normal and malignant cell stiffness has been related to processes occurring within the cell (Lekka, 2016). Young's Modulus is a value to represent the stress-strain relationship of a material. In most circumstances, the Young's modulus remains a constant value (example -metals). However, each different cell type has a different Young's modulus, and within every cell type, this value can change due to many factors. There is a great difference in the magnitude of the Young's modulus in different types of tissue. For example, the Young's modulus values for cartilage have been quoted at ~950 kPa, kidney ~2 kPa, liver ~640 Pa, mammary gland ~150 Pa and fat ~17 Pa (Kumar and Weaver, 2009) (Table 1.2). Mechanical parameters associated with each type of cell group can be related to their ability to store mechanical energy internally and the cell structure.

Table 1 A summary of elastic moduli of several different tissues. Experimental elastic moduli of a variety of tissues, including the animal of origin of the tissue, and the testing modality used to determine the modulus. When multiple stiffness values were available, the value at the lowest strain rate and lowest pre-strain was used to approximate the "resting stiffness" of the tissue

Tissue type	Animal	Testing method	Elastic modulus	Ref
Achilles' tendon	Rat	Tension	310 Mpa	15
Articular cartilage	Bovine	Compression	950 kPa	86
Skeletal muscle	Rat	Tension	100 kPa	87
Carotid artery	Mouse	Perfusion	90 kPa	88
Spinal cord	Human	Tension	89 kPa	89
Thyroid cancer[a]	Human	Compression	45 kPa	16
Spinal cord	Rat	Tension	27 kPa	90
Cardiac muscle	Mouse	Tension	20–150 kPa	91
Skeletal muscle	Mouse	AFM	12 kPa	13
Thyroid	Human	Compression	9 kPa	16
Lung	Guinea pig	Tension	5–6 kPa	5
Breast tumor	Human	Compression	4 kPa	7
Kidney	Swine	Rheology	2.5 kPa	92
Premalignant breast[b]	Human	Indentation	2.2 kPa	14
Fibrotic liver	Human	Compression	1.6 kPa	93
Liver	Human	Compression	640 Pa	93
Lymph containing metastases	Human	Vibrational resonance	330 Pa	17
Brain	Swine	Indentation	260–490 Pa	94
Lymph node	Human	Vibrational resonance	120 Pa	17
Mammary gland	Human	Compression	160 Pa	7
Fat	Human	Indentation	17 Pa	14

[a] Thyroid papillary adenocarcinoma. [b] Mammary ductal carcinoma *in situ*.

Table 1-2 – List of various tissue types and their elastic modulus from Levental et al. 2006. This table illustrates the array of testing methods and tissue types, which produced elastic modulus values in the range of Pascals (Pa) to mega Pascals (MPa).

Rheology describes the viscoelastic properties of a material and can also measure its deformation when an external force is applied. Deformation can be represented along only one axis and analogies can be used to express viscosity or elastic behaviour. The deformation is expressed in moduli depending on the applied force direction to the material. The stress (σ) can be defined as the force (F) applied to an area (A) (Equation 1.1).

$$\sigma = \frac{F}{A}$$

Equation 1.1 - Force acting on an area (such as tensile or compressive stress); where σ is the normal force ((Pa), N/m^2, psi), normal component force (N) and the area (m^2)

There are different ways of abbreviating the forces applied. These force moduli can be described as a response to tension (Young's modulus), hydrostatic compression (Bulk moduli), shear and bending. Force application techniques can be categorised into different areas such as optical, magnetic, flow, electrical and cantilever type of techniques (Figure 1.8).
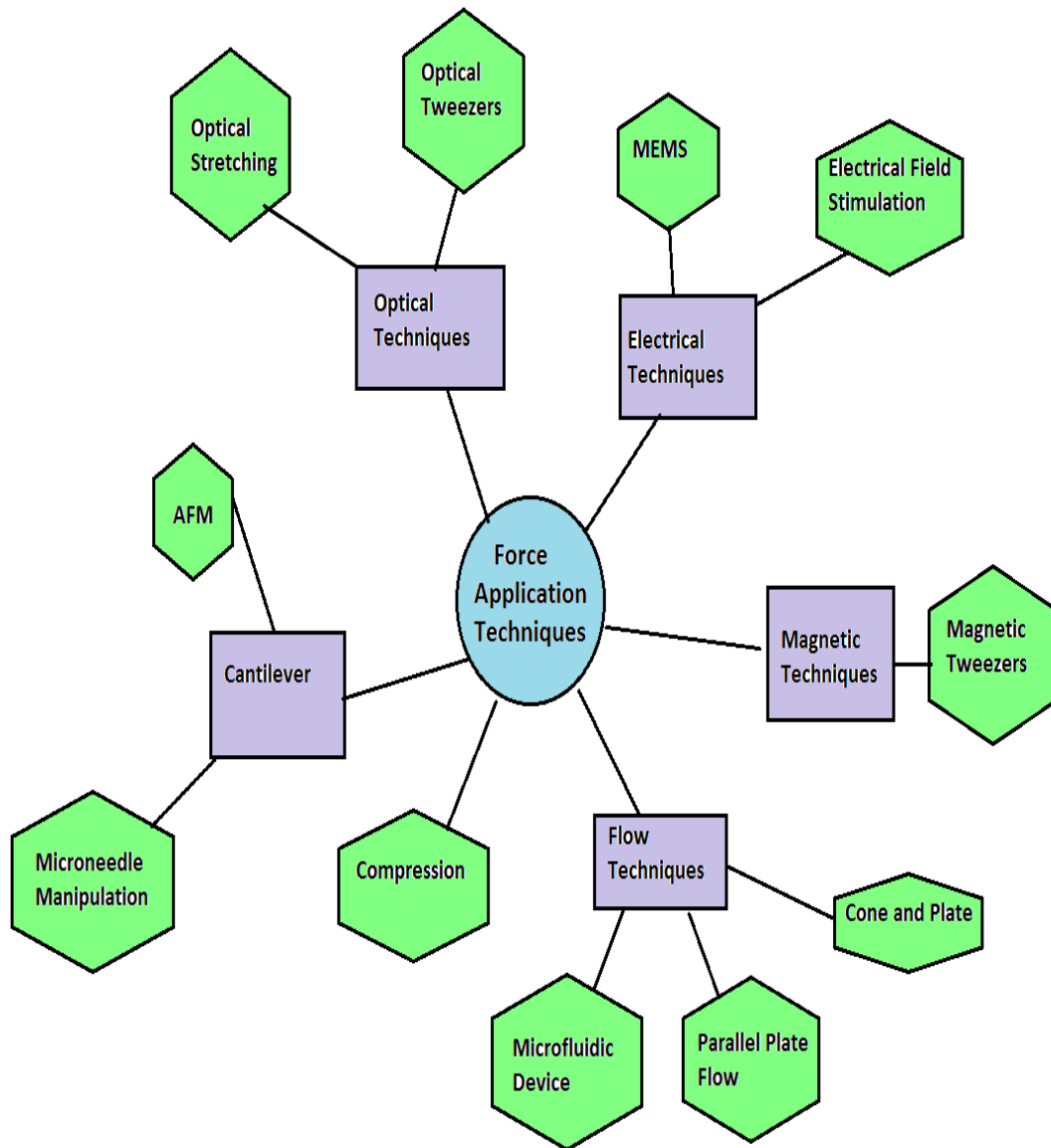
Figure 1.8 - Different Force Applications Techniques . All the above have their advantages and disadvantages which are briefly stated below, adapted from Rodriguez et al., 2013.

Optical techniques are advantageous due to the lack of physical contact between the force producing mechanisms (laser) and the cell, which allows the cell to alter mechanical properties without restrictions. Limitations of this type of experiment can be related to the heat produced from the laser. Advantages associated with magnetic tweezers are related to the bead attachment variability as numerous molecules could bind to the bead. Additionally, the magnetic tweezers induce minimal heat to the cellular sample but the resolution achieved from this technique is limited. Experiments which induce shear stress apply a homogeneous force and are relatively simplistic. However, the lack of sophistication does not allow complete control of the cell mechanical environment. Microfluidic set ups can manipulate the cell mechanics with ease and can be designed to analysis adherent and suspension cell types.

The choice of experiment is based on the sample type or size which is being investigated. Some of these techniques are preferable for microscale and others for nanoscale (Rodriguez et al., 2013). The development of techniques allows advances in technology and the possibility to specialise these approaches further.

Current techniques developed for force measurements of single cells encompass such methods as micropipette aspiration, magnetic bead twisting, optical tweezers and atomic force microscopy (AFM) (Dörig et al., 2013, Friedrichs et al., 2013, Zhou et al., 2012). The advantages of these methods lie in the capability to measure living cells at a single cell level and in liquid conditions imitating their natural environment. These methods cover a wide range of forces (approximately 0.1pN to 100nN) and length scale (approximately 0.1nm to 100µm) (Müller and Dufrêne, 2011a). Overall, there are two ways to apply forces either via a mechanical force transducer or via external fields acting on the sample from a distance. When a force application technique is chosen, the ideal setup for the experiment needs to be assessed.

1.8. ATOMIC FORCE MICROSCOPY

Scanning probe microscopy was first introduced in the early 1980s with the use of tunnelling currents to image conductive surfaces (scanning tunnelling microscope). The invention of the AFM was a few years later by Binning, where a sharp tip was used to interact with the surface to monitor force and thereby generate a topographical surface image. The AFM

consists of a cantilever, sample stage, and optical deflection system. The cantilever moves down towards the surface and deflects which puts a force onto the sample. The deflection of the cantilever is tracked by a laser which is measured by photodiode. Most AFM today (Figure 1.9) uses an optical method with high resolution to measure the cantilever deflection. AFM has been used to investigate many sample types including biomaterials, crystals, DNA and proteins (Variola, 2015, Cubillas et al., 2013, Lyubchenko, 2013).
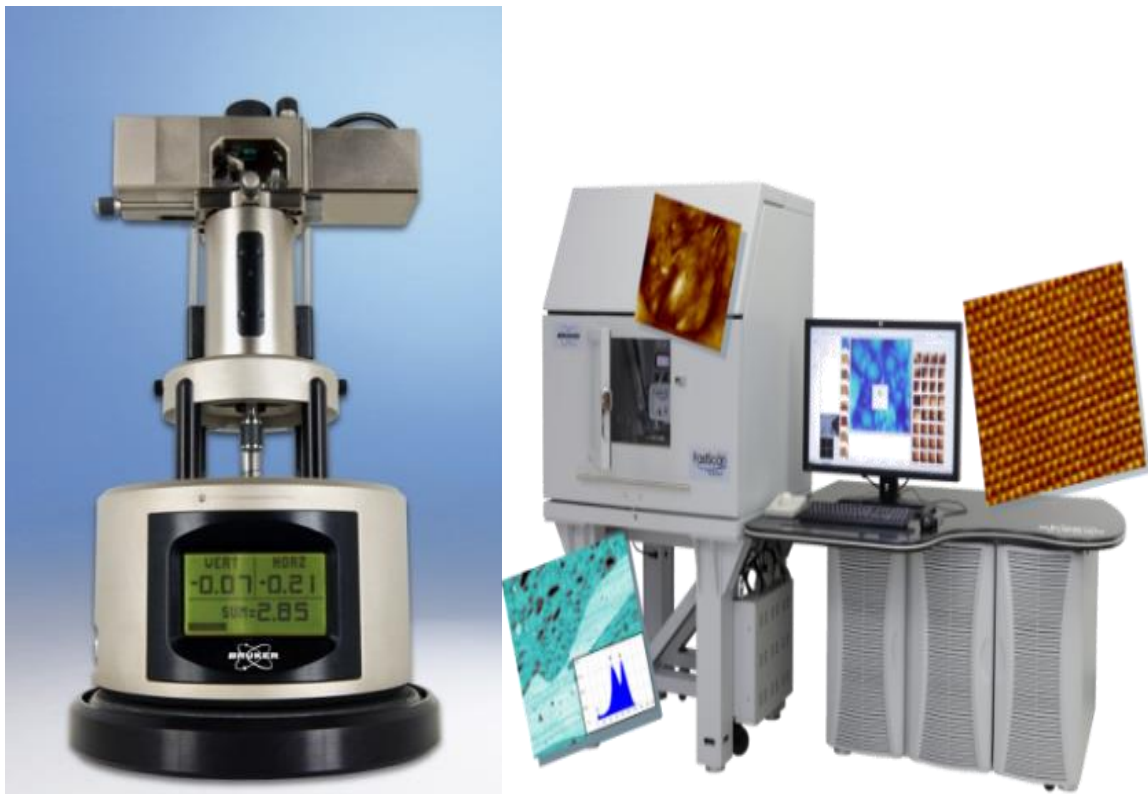
Figure 1.9 - Two modern AFM systems; Bruker Multimode 8 (Left) and Bruker FastScan Dimension (Right). Both instruments are complex and have many variations of contact and tapping mode to choose from.

There are many possibilities with AFM, including imaging, conductive measurement and force spectroscopy. There are two modes in AFM which are mainly described in the literature; contact and tapping mode (also known as AC).

The first imaging mode developed was known as contact mode. Contact mode can be set as a constant force, with the sample height being adjusted and a feedback loop used to keep a constant deflection of the cantilever (Figure 1.10). The piezo-vertical position is monitored to create an image at a constant force; this mode is good for electrical measurements (piezo

response) (Alsteens et al., 2012). The higher the force, the more deformed the sample can become, with the area of scanning being as flat as possible in order to lessen the deformation. Also, the lateral movement can cause drag forces which is not ideal for cells as they tend to be easily damaged or loosely bound to the surface. Image artefacts are known to appear when scanning over larger areas, therefore the feedback response time has to be as fast as possible, see Section 2.5.4 (Colaço and Carvalho, 2013). There is also a disadvantage with contact mode due to the laser signal drift which is likely to occur over a period of time.

Tapping mode makes the cantilever oscillate near its resonance frequency, allowing the amplitude of the oscillation to be measured (Figure 1.10). The feedback is kept constant which helps to produce the image. The cantilever tip goes through stages of attraction and repulsion areas with regards to the surface during the period of oscillation. There are many parameters which can be altered to reduce damage to the soft sample and cantilever. The cantilever should have a spring constant in the correct region to minimise damage (see section 2.7), and software parameters which can be altered to improve experimental conditions. The setpoint parameter (force applied) allows the oscillation signal to be damped if required which can reduce dominant attractive forces and hence reduce damage to the sample. The feedback gain is again related to the signal and if this value was to be increased, overall the noise will increase but it can improve image quality. A reduction in scan rate (time taken to capture an image) can decrease the chances of damage as the cantilever will be moving more slowly along the surface.
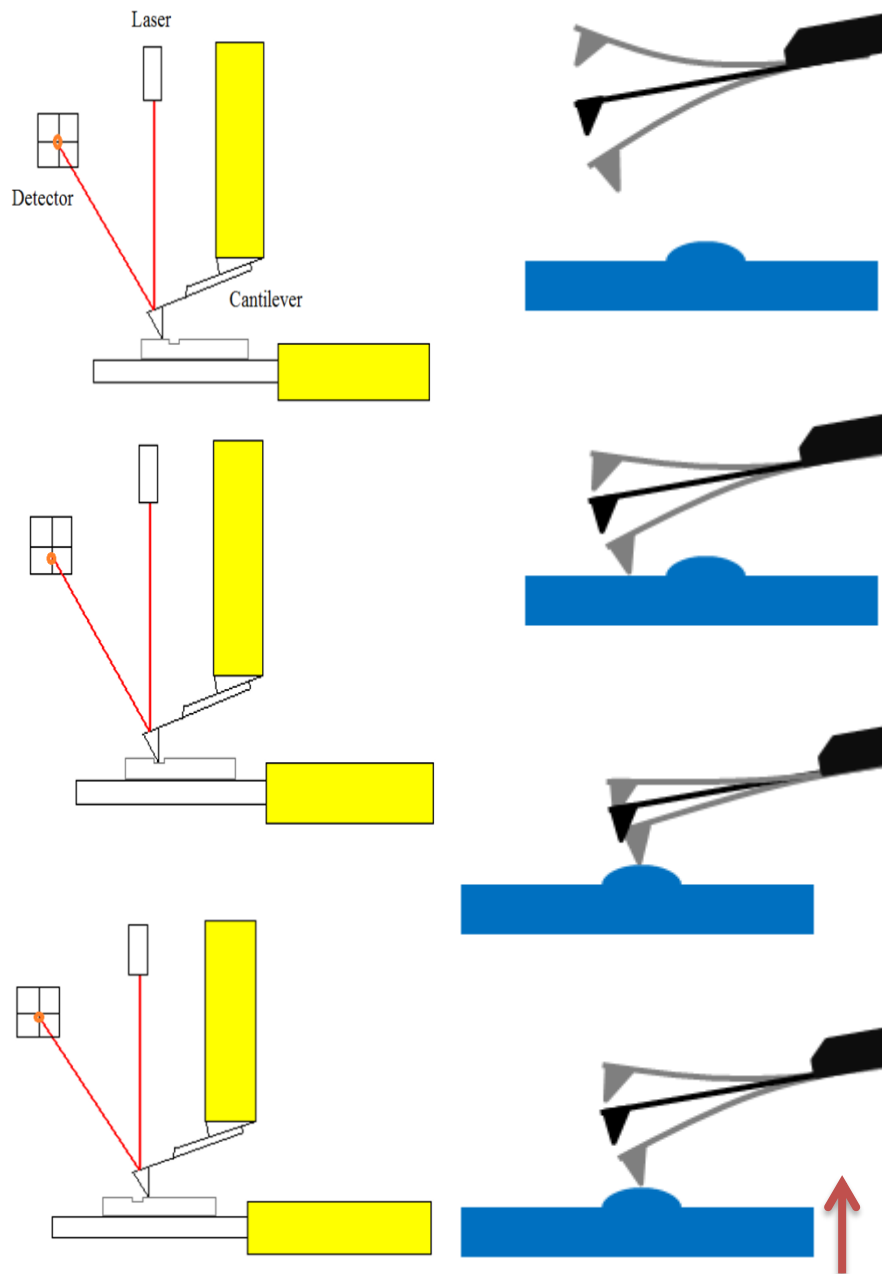
Figure 1.10 – Two of the most common modes used with AFM - Contact mode (Left) and Tapping mode (Right). Contact mode (depicted by diagram) – The cantilever is engaged on the sample; the tip encounters a particle and then the cantilever is pushed up (vertically) which increases the generated error signal. The AFM scanner (Z piezo) lifts the cantilever upwards and the vertical deflection is back to the setpoint. In tapping mode (depicted by diagram) – the cantilever is oscillating in free air/liquid and the amplitude will be larger than the setpoint. When the cantilever is tapping along the sample, there is an oscillation occurring at the setpoint amplitude. When the cantilever moves towards the particle, the oscillation amplitude lowers which leads to feedback to the z piezo which reduces damage to the cantilever and surface.

Force spectroscopy analyses the forces between the sample and tip, which can be as small as a piconewton. Questions can be addressed with the use of this mode about certain molecular interactions on the cell surface (Müller et al., 2009). These interactions can be from weak van der Waals forces to covalent bonds and can be related to typical interactions at the surface. This mode requires a soft cantilever and an accurate piezoelectric system to give precise force results. In force spectroscopy techniques, such as chemical force microscopy and single- cell force spectroscopy, the AFM tip is functionalised with chemical groups. Force volume measurements can give out images and map mechanical properties which add to the application of force spectroscopy. The array of force curves are taken from all planes. This method has drawbacks relating to the resolution, both lateral and temporal.

Biologists can use the information provided by AFM to provide a detailed description of the mechanisms behind metastasis and differentiation by examining cell surface details. Cellular behaviour can manifest as structural changes of the cytoskeleton and hence with the use of AFM these changes can be used as an early indication of important abnormalities. Live cell imaging by AFM allows analysis at the nanoscale which can create an accurate representation at cellular level. The cell has many processes and imaging the living cell is essential for understanding communications within and between cells. The development of AFM has enabled the detection of structures beyond the cellular level.

Various cells have been imaged by AFM, however, the majority of the cells imaged are in a fixed or dried environment. Table 1.2 depicts a few cellular studies conducted by AFM. Over recent years, the instrument is becoming more versatile, resolution is improving and time to produce an image is reducing.

Since the early studies conducted by Henderson and co-workers, there are several papers which used AFM to characterise cells by imaging (Henderson et al,. 1992). Some studies have published with cells imaged in a dried and fixated environment (Francis et al,. 2010), which is known to alter the cells dynamics. This is explained in more detail in the next section.

AFM can depict the cell in three dimensions, in contrast to fluorescence microscopy, which is a two-dimensional technique. This additional dimension provides data regarding the cell volume. In the table below, Calzado and colleagues, demonstrated that the roughness and

33

elasticity of cells could allow the characterisation of different *in vitro* cell lines (Calzado et al,. 2015).

Table 1.3 portrays an overview of studies which have been conducted by AFM. Each study, has a main aim and the outcome is mainly to produce images to define individual cell types.

Paper authors	Cell Type	Environment	Aim
Henderson et al,. 1992	Glial cell	Liquid, fixed	Demonstration of actin filaments in living cells
Francis et al,. 2010	Epithelial adenocarcinoma	Fixed, dried cells	High resolution images producing detailed images
Mêndez-Vilas et al,. 2012	Hela cells	Liquid, 37°C	Partial images and Young's modulus of cells
Calzado et al,. 2016	Epithelial breast cancer cell lines	Liquid, 37°C	Distinguishing between three different cell lines
Pi et al,. 2015	HepG2 cells	Liquid, fixed	Application of quercetin to analysis cellular alterations

Table 1-3 – Published papers investigating different cell types and properties by use of AFM. The table shows the small number of papers which have been published in this area. All the above experiments have been conducted differently and hence it is complex to define standard experimental values for comparison.

Throughout this thesis, the human hepatoma cell line, HepG2 was experimented on. There is a limited amount of literature on this specific cell line using AFM. Most experiments, used a fixed or/and dried environment to reduce the complexity of the study. In a recent study, Pi and co-workers investigated apoptosis in HepG2 cells after application of quercetin and used AFM to examine cell properties, but the experimental setup was in a fixation environment (Pi et al,. 2015). Fixed cells are well documented as not representing the mechanical properties of living HepG2 cells, as the elasticity of the cell increases dramatically after fixing.

Most studies which use AFM, are found to use elongated cells and HepG2 cells do not have this morphology, and their shape adds complexity to the imaging process. The morphology changes monitored by the imaging process could be related to a volume change, but additional observations can be made when analysing cell mechanical measurements, as described in the next section.

Cantilevers follow the principles of Hooke's law: the force F which is applied is proportional to the deflection Δx of the cantilever;

$$F = k\Delta x$$

Equation 1.2 - Hooke's Law, where k is the spring constant and x is the deflection of the cantilever.

The sample stiffness can be used to indicate the spring constant required, as the wrong value could damage the surface. Typical cantilevers were ideally found to have a spring constant ranging from 0.01 to 0.4N/m for mammalian cells. Actual spring constants of cantilevers can substantially differ from quoted manufacturer values. In the ideal case, the cantilever stiffness should be small (< 1 N/m) to avoid stresses from the cantilever movement which are not compensated for by feedback systems (Freidrich et al, 2013). In the case of live cells, the actual spring constant of the cantilever can be determined in situ, using the thermal noise method (Canale et al, 2013). The thermal noise method is related to the equipartition theorem where ideally the cantilever is classified as a perfect spring, this is not the case. The cantilever is fixed a one end, however it is constantly oscillating due to the thermal vibrations from the environment. Therefore, the thermal environment and the deflection of the cantilever can be measured accurately. Hence, both these values can assist in the calculation of the spring constant.
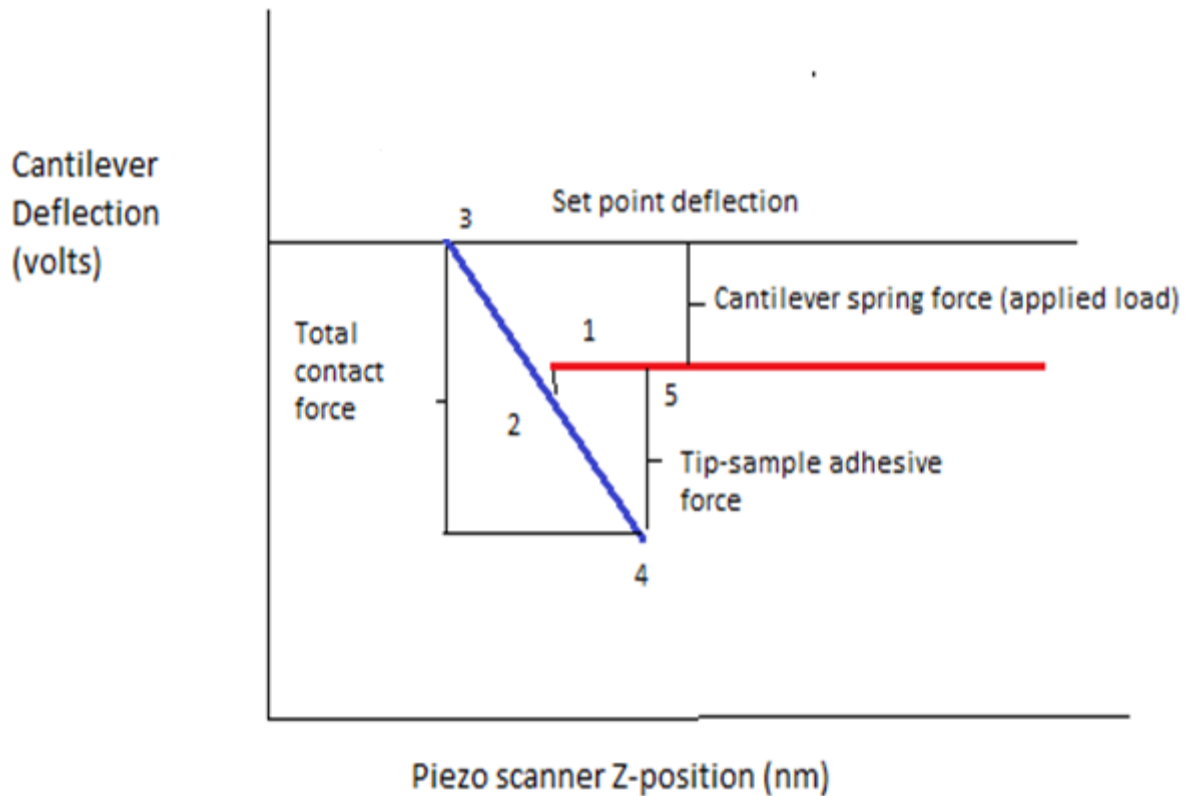
Figure 1.11 - Typical force curve   adapted from Stefan B. Kaemmer (2013). The force curve shown has a line of approach and withdrawal. It should be noted as well as the applied force, adhesion should be accounted for when analysing the total contact force. In the schematic, the cantilever will approach the surface (1), the cantilever will try to balance the restoring force (2), there is a possibility of a setpoint (3- mainly used in contact mode), the cantilever is being removed from the surface (4) and adhesive forces can occur which attract the cantilever back to the surface (5) (Stefan B. Kaemmer, 2013).

When a force distance curve (Figure 1.11) is obtained, mechanical measurements can be extracted, such as Young's modulus. To obtain values, a mathematical model can be applied to the force distance curve. The most common mathematical model used to obtain Young's modulus, is adapted from Hooke's law, and is known as the Hertz model (Equation 1.3). The Hertzian contact model can be used to understand the contact between spherical particles and the indenter, where there is deformation of the contacting bodies occurring.

$$F = \frac{4}{3} \frac{E}{(1 - v^2)} \sqrt{R} \partial^{\frac{3}{2}}$$

Equation 1.3 - Adaptation from Hooke's Law for cantilever selection, so that the spring constant suits the surface of the sample. Where F is the force, E is the Young's Modulus, v is Poisson ratio, R is radius of the tip and ∂ is the indentation depth

The Hertz model can be altered to suit various experimental conditions. The tip geometry can be changed and then the dimensions of the indenter can be applied to the Hertz model. The possible tip geometry can range from pyramidal, cone, cylindrical or spherical (which is the most preferable).

The use of spherical colloidal probe is one way to facilitate the understanding of the whole cell mechanics. These spheres are less likely to deeply penetrate the cells surface, therefore less damage and more realistic measurements are obtained if the same amount of force is applied. Many studies (Sokolov et al, 2013, Dufrene et al, 2013) explain the benefits of this type of probe compared to conventional probes. These benefits range from the probe being dependent on the local stress-strain response to being preferable for analysis of cell mechanics. Also, the spherical probe can substantially reduce the heterogeneity of the results as it is measuring the whole cell rather than a single point. This could lead to one measurement of the spherical probe being equivalent to an average of many measurements with use of a sharp tip.

Colloidal probe AFM is used to investigate the force between a substrate and single colloids. To obtain a spherical probe a microsphere is glued precisely to a tipless AFM cantilever, or the apex of an AFM pyramid is rounded to give a half-sphere (Hilal et al, 2010). There are different types of polystyrene latex microspheres (NH_2, COOH, OH). In studies, it is stated that it is important that the contact radius is much larger than the separation distance (between the cantilever and the sample surface), in the case of the spherical colloid (Mi et al., 2012).
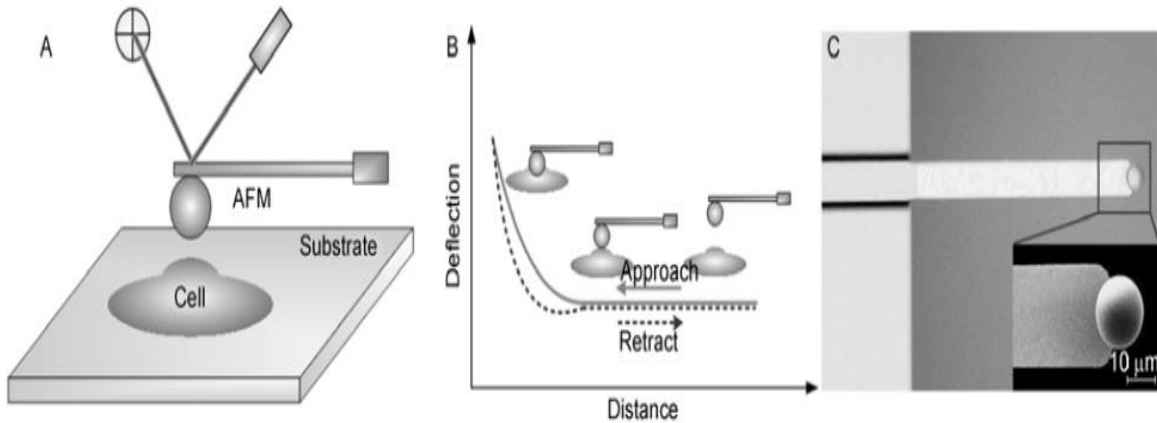
Figure 1.12 - Principle of measuring with a colloid probe . The schematic was obtained from Mi et al, 2013. A – Typical set up for an AFM experiment with spherical probe. B – The trace graph of the cantilever with regards to distance from the surface and deflection. C- Microscope image of the spherical probe

In the study conducted by (Mi et al., 2013), the microspheres were glued on with epoxy resin. In the schematic (Figure 1.12), it shows how the force profile is formed and hence Young's modulus is produced. Another common way of probe preparation (Mi et al., 2012) is by taking the tipless cantilever and mounting it onto the AFM where the laser signal was modulated. A drop of the polystyrene sphere solution was placed onto a fresh glass slide and a drop of the epoxy resin was placed on another section on the same slide. The cantilever was moved to contact the resin and retracted, the same process was completed with the sphere. To ensure the probe was in the correct position, a scanning electron microscopy (SEM) was used.

1.8.1. RELATING AFM INDENTATION TO CELL BIOMECHANICS

Every cell type has a different location and function throughout the body which allows the body to maintain homeostasis. When analysing at a cellular level, there are various physical stresses that can be applied to the cell, as explained previously. These physical stresses could monitor or trigger modification occurring structurally or biochemically. Therefore, an understanding at this level is essential to understand mechanical responses and functionalities of cells in both pathological and native environments. The validation of models used to derive values for mechanical measurements is important. The interpretation of mechanical

measurements in a quantitative way is important and is typically conducted with regards to the elastic moduli which is assigned to the material (Guz et al,. 2014).

AFM is a useful tool for cell biology as it can assist with the visualisation of the cell surface. Additionally, AFM can be implemented by nanoindentation of live cells, which allows mechanical properties to be calculated and correlated with structural components within the cell. Various experiments have investigated the cell phenotype, however, the quantitative evaluation and analysis of the mechanical properties of subcellular organelles has not (Szymonski et al,. 2015). The reason for this is mainly because of the resolution of AFM required. The use of the AFM could allow for investigation and application the tip of the AFM as a nanoindentation and an imaging tool.

In Figure 1.13, displays a schematic of a cell probed by AFM which illustrates the cellular components that could have an external force applied to them. Hence, if the cell was to be indented a small amount (~50nm), the force curve produced will only portray mechanical information about glycocalyx. At the other end of the spectrum, if the cantilever indents to a value greater than the cell height, data produced will represent the surface to which the cell is adhered. Ideally, the cell should be indented where the "whole" cell can be represented by various organelles (Figure 1.13). Further discussion on indentation depth is documented in 2.5.9.2.
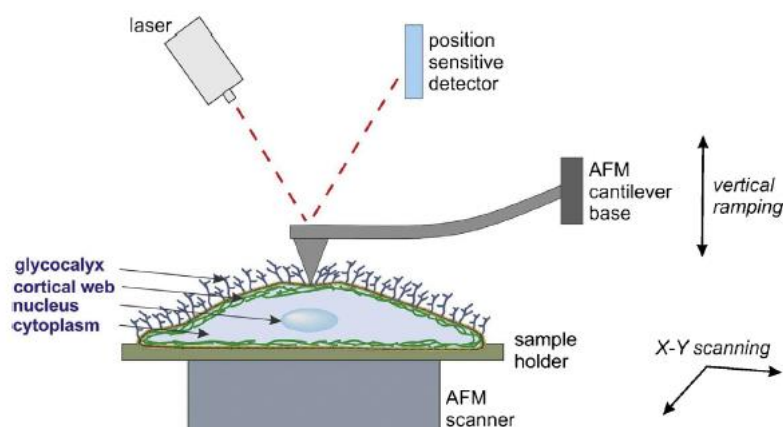
Figure 1.13 - A schematic of a cell in an AFM experiment. Obtained from Szymonski et al (2015). This image illustrates different structures within the cell which can be indented with a tip of a cantilever.

The application of Young's modulus through AFM can be applied from Hooke's law (Equation 1.1), as explained previously. The force curves obtained from the nanoindentation procedure allows for the application of Hertz model to produce a value for Young's modulus. Most models of elasticity have principles which originate from the Hertz model and this is still commonly implemented (Figure 1.14). The Hertz model is discussed in more detail in section 2.5.10.

Young's modulus of mammalian cells

Cell type	E (kPa)	Commentary	References
Endothelial cells			
HUVEC	10–11		Sato et al. (2004)
–	1.3–7.2	Spatial heterogeneity	Mathur et al. (2000)
–	0.9–1.7; 12.0–18	Shear stress, different models	Ohashi et al. (2002)
BPAEC	0.2–2.0	Spatial heterogeneity	Pesen and Hoh (2005)
Leukocytes			
Leukemia myeloid cells (HL60)	0.2–1.4		Rosenbluth et al. (2006)
Leukemia lymphoid (Jurkat) cells	0.02–0.08		
Neutrophils	0.2–0.07		
Corti organ's cells			
Outer hair cells	300–400	Cortical lattice	Tolomeo et al. (1996)
Guinea pig's outer hair cells	2–4	Different levels of cochlea	Sugawara et al. (2002)
Mouse outer hair cells	2–4		Murakoshi et al. (2006)
Guinea pig's inner hair cells	0.1–0.5		Sugawara et al. (2002)
Hensen's cells	0.3–1.1		–
Osteoblasts	0.3–20.0	Changes at adhesion	Simon et al. (2003)
Astrocytes	2–20	Spatial heterogeneity	Yamane et al. (2000)
Fibroblasts	4–5		Bushell et al. (1999)
Migrating 3T3 cells	3–12	Spatial heterogeneity	Rotsch et al. (1999)
–	0.6–1.6	Changes at adhesion	Mahaffy et al. (2004)
L 929	4–5		Wu et al. (1998)
Epidermal keratocytes	10–55	Spatial heterogeneity	Laurent et al. (2005)
Platelets	1–50	Spatial heterogeneity at activation	Radmacher et al. (1996)

Figure 1.14 – Young's modulus values of mammalian cell conducted by AFM. The table was obtained from Kuzenetsova et al,. (2007), where a range of cells have values for Young's modulus calculated with AFM. Example of heterogeneity of results circled (blue circle).

In Figure 1.14, an array of cell types are presented with their calculated Young's moduli. Many studies revealed that the results have spatial heterogeneity. Again, the Young's modulus value of the same cell type in Figure 1.14 demonstrated inconsistencies. This table confirms there are no standard values for Young's modulus for individual cell types and there are multiple explanations for this outcome which are explained in section 2.5.8.

The liver is the most resilient organ of our body with reported values of elasticity between 1.5 and 5.0 kPa *in vivo* (Umut Ozcan et al., 2011, Leal-Egaña et al., 2012). In liver disease, the elasticity of this organ depends on the degree of fibrosis, with the more advanced stages

causing an elasticity of greater than 10kPa (Masuzaki et al., 2007, Pang et al., 2014). A study conducted on liver cells *in vitro* found the elasticity values to be 2kPa in a DMEM medium environment, but if glutaraldehyde was applied, the elasticity of the cells increased to 100kPa (Braet and Radmacher, 2012). An *in vitro* study used HepG2 cells in a fixed environment (Pi et al., 2015), and the Young's modulus was found to be 50kPa in untreated cells and 109kPa after treatment with quercetin at a concentration which was known to effect the cell viability. Another study, used SK-Hep-1 cells and HepG2 cells, and Young's modulus showed a broad distribution of a range of 1-500kPa. The probe used had a sharp tip with spring constant of 0.05N/m and also fixation was used. The comparison between studies is complex, as not one study can be found to use the same parameters as the next. Also, other conditions such as the surface underneath cells, liquids used, and temperature under which experiments were carried out, and how long cells have been attached to the surface influence stiffness outcome.

Overall, the investigation of mechanical measurements on cells could be related to cell function by application of AFM, as the technique is versatile allowing the probe to both image and indent the cell surface. The overall aim would be to focus on the findings obtained by AFM and validate the nanoindentation method which could then be applied to *in vitro* toxicity evaluation and drug testing at the cellular level.

1.9. SUMMARY OF INTRODUCTION

The liver is a complex structure and at a cellular level mechanical characteristics can alter the organ as a whole. It is composed of four lobes which are vital for purification of blood. Hepatocytes take up most of the volume of the liver and provide structure and regulation factors.

Atomic Force Microscopy gives the ability to produce high quality images as well as mechanical measurements of cells. Force distance curves obtained from AFM can produce mechanical information about the cell, with the hope that it can be related to the early changes occurring within the cell which precede toxicity.

In HCC, 5-FU can be used for treatment but as with most traditional chemotherapeutic drugs it is aimed at inhibiting DNA replication. In most cases, only limited success is achieved and therefore investigating early indications of toxic effects could assist in more specific targeted future treatment.

Drugs, such as NSAIDs, are known to have potentially toxic effect on the liver, and more specifically on the mitochondria. The use of these drugs could aid in cellular targeting as there is a significant difference in mitochondrial metabolism between normal and cancer cells.

Drug delivery systems are seen to be the future direction when improving the bioavailability of developed drugs. Additionally, it is also hoped, they will reduce the toxic effect of drugs on healthy cells. There are a range of possible nanoparticles which could be beneficial for drug delivery purposes. Liposomes are becoming an increasingly researched area due to the ease of production.

The essential aims of this study were to relate the toxicity of drugs to biomechanical information about the cell. To do this 5-FU and diclofenac were used as toxins. Their effects were analysed in terms of biochemical and biomechanical effects on the cells. Delivery of 5-FU by liposomes was investigated as a means to improve targeting and reduce toxicity.

The specific objectives were to:

- Use HepG2 cells to analyse cell viability and toxicity mechanisms with free drug at different concentrations. This used specifically a chemotherapeutic drug (5-FU) and mitochondrial toxicant (diclofenac).
- Analyse the cell surface by AFM when HepG2 cells were treated with the free drugs.
- Capture force curves and obtain Young's modulus values when HepG2 are treated with both drugs to observe any alterations occurring.
- Investigate the Young's modulus of HepG2 cells by applying two different tip geometries (pyramidal and spherical indenters).
- Prepare liposomes by means of rotary evaporator and microfluidics.
- Use NanoAssemblr to produce liposomes with different compositions, flow rates and drug to lipid ratio.
- Use different equipment to characterise liposomes (by size, encapsulation efficiency, charge and shape).
- Investigate the interactions with the liposome nanocarriers, free drugs and the liposome encapsulated drug and the HepG2 cells in terms of the cellular nanomechanical properties.

Chapter 2 - GENERAL METHODS INCLUDING DEVELOPMENT OF THE AFM

This chapter provides a general description of methods which were reapplied throughout the thesis and more where appropriate specific methods are explained in the relevant chapters.

2.1. MAINTAINING STOCKS OF CELLS BY CELL CULTURE

HepG2 cells (obtained from Public Health England on behalf of ECACC (European Collection of Authenticated Cell Cultures), Porton Down) were used throughout the conducted research. They were chosen to monitor the nanomechanical properties and relate this to the toxic effects occurring.

HepG2 cells were cultured in DMEM (Dulbecco's modified Eagle's medium) in $25cm^2$ or $75cm^2$ culture flasks (Nunc™ EasYFlask, Thermo Fisher, Paisley) at $37°C$, under an atmosphere of 5% CO_2 in air. The medium was supplemented with 10% (v/v) foetal bovine serum (FBS) (Biosera), streptomycin (5mg/ml) and penicillin (5000 units/ml) (Sigma) and NEAA (Lonza). Routinely, these cells were passaged every three days at a ratio of 1:4. This was completed by use of trypsin (0.05%) in versene, which detached the cells from the flask. Versene was prepared by dissolving 0.3g of KCl, 0.3g of KH_2PO_4, 12g of NaCl, 1.73g of anhydrous Na_2HPO, 0.3g of EDTA and 4.5ml of 0.5% solution of Phenol Red in 1.5 l of distilled water and was stored at room temperature after sterilisation.

2.2. STOCK SOLUTIONS

2.2.1. PREPARATION OF 5-FU

5-Fluorouracil (5-FU) (Sigma-Aldrich, Dorset, UK), was stored at $2°C$ dissolved in dimethylsulpoxide (DMSO) at a concentration of 50mg/ml which was diluted with Dulbecco's phosphate-buffered saline (DPBS) when required.

2.2.2. PREPARATION OF DICLOFENAC

Diclofenac (Sigma-Aldrich, Dorset, UK), was stored at $-20°C$ dissolved in DMSO at a concentration of 40 mg/ml which was diluted with DPBS when required.

2.3. MEASURING CELL VIABILITY

Methods of studying cytotoxicity can provide information other than cell viability, including cell metabolism, organelle function and cell cycle phase. Many methods of investigating cytotoxicity analyse alterations of the membrane, most often by the uptake or exclusion of dyes. All assay and chemicals used, unless otherwise stated, were bought from Sigma-Aldrich; Dorset, UK. All 96 well plate experiments were carried out with HepG2 cells (10^4 cell/well) unless otherwise stated.

2.3.1. MEASURING CELL VIABILITY BY TRYPAN BLUE

A solution of Trypan Blue (0.1% w/v) was diluted with sterile phosphate buffered saline, pH7.4 (PBS). Cell suspension (100 µl) was added to an equal volume of the Trypan Blue solution. A haemocytometer was used to count the live/dead cells and a percentage of viability was calculated.

2.3.2. THE MTT ASSAY

The colourmetric assay for reduction of MTT (3-(4,5-Dimethylthiozol-2-yl)-2,5-diphenyltetrazolium bromide) can be used to measure the metabolic activity of cells by the reduction of the yellow tetrazolium salt into a blue formazan product by cellular dehydrogenases. There is an accumulation of formazan in the viable cells and this can be extracted using organic solvents (Zhang et al., 2011b).

The solution for MTT in PBS pH 6.75 (10 mM, 0.4143 g /100 ml) was filtered through a 0.2 µm filter and it can be stored for up to 2 weeks at 4ºC. The cells were set up in a 96 well plate, incubated for the required time, and at the end of the incubation time 50µl MTT solution/well was added. Thereafter, the cells were incubated at 37ºC in the incubator for 4 h. The solution was removed and 200µl DMSO added to each well to dissolve the formazan product. The colour was mixed evenly on a shaker for 30min and absorbance was measured at 540 nm in Multiskan Ascent 96 well plate reader.

2.3.3. THE NEUTRAL RED ASSAY

The Neutral Red assay (NR) involves use of a vital dye (Toluylene Red). The dye is taken up and processed by the viable cells by active transport (Barbosa and Peters, 1971). It is known

to interact with lysosomes and if the cell is non-viable, they will not up take the dye. The dye is a weakly cationic dye which binds to the lysosomes due to the electrostatic hydrophobic bonds. Viable cells are stained red, and percentage of cell viability compared with the control cell sample.

A stock solution of NR (4 mg/ml) in PBS was filtered and stored for at room temperature. When required, the NR stock was diluted 1:100 in medium and then incubated overnight at 37°C. After this time period, the NR solution was centrifuged and 200µl of the NR was added to each well to assess viability. The cells were then incubated at 37ºC for 3 h. NR solution was then removed and cells washed once with PBS (200µl/well), then 100µl destain (50:1:49 of ethanol, glacial acetic acid and distilled water) was added to each well and the plate was shaken for ~30 min until a homogeneous colour was obtained in each well. The absorbance was then measured with 540nm filter in a plate reader.

2.3.4. THE CRYSTAL VIOLET ASSAY

Crystal violet (CV) binds to proteins and DNA. The stain (CV) was weighed (100mg) and dissolved into 100ml of distilled water and then filtered prior to use. Post-treatment the cells were fixed with 1% formalin solution for 10min. Cells were then washed with PBS, pH 7.4, before adding the CV solution for 20 minutes at room temperature. The stained cells were then again washed with PBS for a further 3 times. After this, 200µl 0.1% Triton-x100 (0.1% (v/v) in PBS) was added and left on the plate for an hour to release the colour from the cells, and then absorbance was measured at 540nm in the plate reader. This method measures cells which are firmly attached to the plate, and are therefore viable.

2.3.5. THE BRDU ASSAY

Cell proliferation was analysed by BrdU Cell Proliferation ELISA using antibodies to BrdU (Roche; West Sussex, UK). The cell proliferation ELISA is a simple colourmetric assay used to measure the extent of BrdU incorporation during new DNA synthesis. This assay is an alternative to the thymidine incorporation assay which uses radioactive isotopes instead. Hence, the use of BrdU avoids the use of radioactivity.

The cells were cultured on a 96 well plate for 24h and then cells were treated with the toxins as desired. The BrdU labelling reagent was diluted 1:100 with sterile medium. This labelling

solution was then added to the wells (10μl) and left for 2h in the incubator which labelled the DNA. After this time, the medium was removed and 200μl of FixDenat was added (to fix the cells to the bottom of the wells). The FixDenat solution was removed after 30min and 100 μl of anti-BrdU-POD working solution was left to incubate with the cells for 90min. Cells were washed three times with washing buffer before a chromogenic substrate solution was added, and incubated for 10min until colour had developed. Thereafter, a stopping solution was added. The absorbance of the sample was measured at 450nm (reference wavelength: 690nm). The blank control absorbance value should not exceed 0.1 and this value must be subtracted from all sample values.

2.4. CELL MORPHOLOGY MEASURED USING FLUORESCENCE MICROSCOPY

Cell morphology and viability can be analysed by use of a fluorescence microscope (Carl Zeiss Axio Imager). There are many stains which can be used to investigate different components of the cell, such as Acridine Orange (AO; Sigma-Aldrich; Dorset, UK), Propidium Iodide (Life Technologies; Paisley, UK), Phalloidin-FITC and 4', 6-Diamidino-2-Phenylindole, Dihydrochloride (DAPI; Sigma-Aldrich; Dorset, UK). AO (Excitation wavelength – 502nm, Emission wavelength -525nm) is a cationic dye that is bound to the nucleic acids producing a green fluorescent complex. PI (Excitation wavelength – 540nm, Emission wavelength – 610nm) penetrates the plasma membrane and can be detect dead cells where it forms a red nuclear fluorescent stain. Phalloidin-FITC is used for labelling actin filaments and provides a green fluorescence. DAPI nuclear stain shows a blue fluorescence by strongly binding to DNA in the nucleus (specifically binds at A-T regions).

When using the fluorescence microscope, the cells are plated onto 35mm^2 petri dishes (BD Falcon; Oxford, UK) and then treated as required. Where required cells were fixed using 4% paraformaldehyde (Sigma-Aldrich; Dorset, UK) and left for 15 min at room temperature. Cells were then washed using PBS before applying the appropriate fluorescence dye. After the dye was applied, the images were viewed using a Carl Zeiss Axio Imager microscope under a 40X (Numerical aperture, (NA) =0.8) or 20X (NA=0.5) water immersion lens. The mercury lamp excited the florescence and the emission was recorded using a fluorescein isothiocyanate (FITC)/Rhodamine filter block (485/515-530nm; 546/580-563nm) for AO and PI. After the cells were clearly focused the images were captured by using AxioVision v.4.6

(Zeiss, Germany). The images were analysed with Zen (blue edition, Zeiss). Details of individual fluorescent stains will follow.

Phalloidin binds to cellular actin and is known to be extremely toxic so caution is required. After a washing stage, 100 μl of FITC- Phalloidin (0.2% (w/v) in PBS pH7.4) was added to the well plates and then was incubated for an hour in a moist chamber at room temperature in the dark. The stained cells were then washed with PBS pH 7.4 and samples could be stored in foil in the cool room at 4-6°C in the dark until viewed.

PI and AO stains are used when the interest is around live/dead percentage of cells. The cells were washed with pH 7.4 PBS, and 1 ml of PI (20μg/ml (w/v) in PBS pH7.4) was added and then the cells were left to incubate for 1 min at room temperature. The solution was then discarded and the cells were washed gently with 1ml PBS three times. The cells were then incubated for 5 min with AO (100μg/ml (w/v) in PBS pH7.4) at room temperature. After incubation, the solution was removed, 1ml PBS was added and the samples were viewed.

DAPI develops a blue fluorescence and is used for nuclear staining of cells. After washing with 1ml of PBS, the DAPI stain (10μg/ml (w/v) in PBS p7.4) was added to cells and left for a short time (30 sec) followed by a washing stage occurred after, with viewing immediately after.

2.5.   ATOMIC FORCE MICROSCOPE

As explained in Chapter 1, AFM is a complex technique which has various parameters which can be optimised. In this section, the general setup will be explained, and then in detail the complexity of imaging in cells (HepG2 cells).

The surface morphology and nanomechanical values of the samples were analysed by Atomic force microscopy Dimension Icon/FastScan (AFM, Digital Instruments, Santa Barbara, CA, USA; Bruker Nanoscope analysis software Version 1.50)

2.5.1.   CANTILEVER SELECTION

Each experiment with AFM has various options for cantilever type but the majority can be used in every mode. The cantilevers all have different structures such as tip geometry, spring constant and coatings. Each individual application requires the cantilever to be in optimal

condition but this was not always possible. Most cantilevers are made by micro fabrication techniques from silicon nitride and silicon and it can be assumed that every cantilever is similar (Section 2.5.2). Some cantilevers are covered on the backside with a thin gold layer which enhances reflectivity, and the advantages and disadvantages of this will be discussed.

The initial AFM measurements were obtained using ScanAsyst-air probes, and spring constant (~ 0.4 N/m). For live cell imaging, the cantilever of choice was MCLT-A (~ 0.07 N/m) or preferably PEAKFORCE-HIRS-F-B (~ 0.12 N/m) due to the long sharp tip which is known to detect fine details on the cell surface. For force measurement, cells were indented with a colloidal probe fabricated from Arrow TL1 tipless cantilevers (see Section 2.5.3 for preparation) and a pyramidal cantilever (SNL-10d) for comparison as they have similar spring constants (~0.03 N/m).

2.5.2. TIP GEOMETRY

The most common tip shape is pyramidal, this tip is most useful for imaging. The resolution obtained is highly dependent on the tip geometry. When imaging, the tip should be able to follow the surface with ease and if there is a dramatic change in height, the cantilever tends to overshoot, resulting in the sample or cantilever getting damaged leading to discrepancies in the image. Hence, to minimise the overshoot, the cantilever should have minimal contact with the surface; meaning ideally, the sharper the tip, the higher the resolution that can be achieved.

The pyramidal tip can be used for force mapping but can only resolve local elasticities. The main concern is regarding the exact dimensions of the tip. This is required when a mathematical model is to be applied, and a lack of precise tip dimension makes it hard to quantify mechanical data of the sample.

The figure below (Figure 2.1) emphasises the importance of the dimensions. The two cantilevers below were from the same box, they are very similar, but the slightest change in the tip geometry will have onward effect on the mechanical measurements using these.
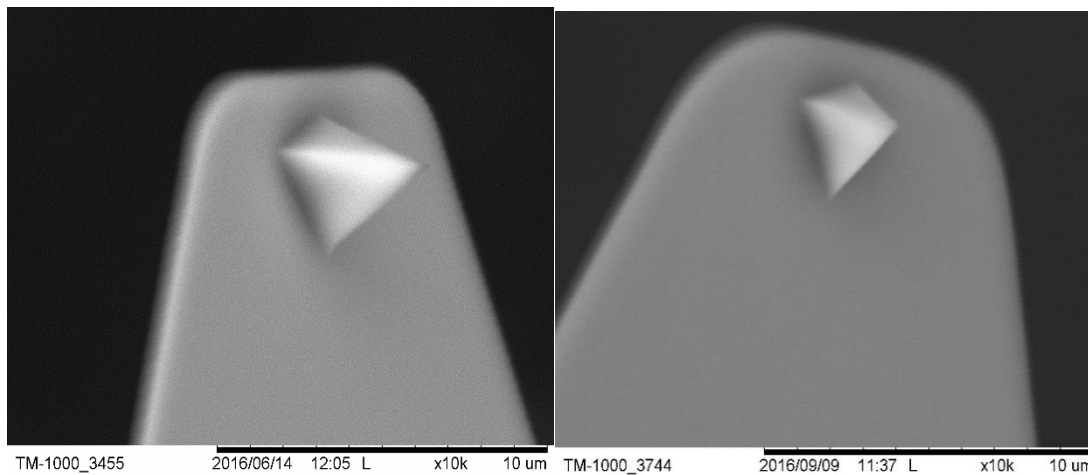
Figure 2.1 - SEM images of cantilevers. These cantilevers were from the same box, and found to have slightly different tip shape geometry. This shows that it should not be assumed, that every type of tip geometry is the same, with regards to dimensions, which is valuable when calculating mechanical measurements. If more than one cantilever was to be used in a study, it becomes more complex when quantifying force measurements. Images were obtained with FE-SEM Hitachi SU-6600 X10K

If a cantilever is to be used to measure mechanical properties it is always advised to firstly take an image of the tip with an SEM or other equipment, to analysis the tip geometry, ensuring there is no damage. Also, ideally, the cantilever should be sterilised by UV as a precaution to minimise the chance of debris. After an experiment, the tip should be washed to remove any contamination, especially if the imaging was carried out in fluid.

2.5.3. AFM COLLOIDAL PROBE PREPARATION

Colloidal probes (~2-15µm) were prepared to give the overall elasticity of the cell rather than the elasticity at a defined point (~2-20nm) which was obtained with the use of the sharp pyramidal tips. The geometry of spheres is well-defined and the data can be fitted with specific models to estimate the elastic modulus (Hertz model). Other tip geometry can be used, but alterations of the model are required (Section 2.5.11)

The colloidal probes were prepared in-house for the indentation measurements. A silica microsphere (Sigma-Aldrich, Dorset, UK) was attached to a tipless silicon nitride cantilever (Arrow-TL1, Nanoworld). To do this, a small number of microspheres were spread across a glass slide and one microsphere was isolated by sterile tweezers, then the other spheres were gently removed. On the same glass slide a droplet of resin (Sigma-Aldrich, Dorset, UK) was added and it spread out evenly. The cantilever was lowered onto the resin momentarily and

then raised up whilst ensuring there was no excess glue. After the relocation of the cantilever towards the microsphere, the cantilever was slowly lowered by use of the manual step motor controls ensuring the tip was aligned with the microsphere where required. The cantilever was left there momentarily and then removed from the surface, leaving no microsphere on the glass slide. To ensure the microsphere was positioned correctly, an SEM image was taken after the glue had set (optimal time was 1h). Before indentation, the cantilever was mounted and calibrated (see Section 2.5.4). The spring constant obtained was generally found to be ~0.02N/m.

Throughout the experiments conducted with AFM, the cantilevers were analysed by the AFM to ensure there was no damage or contamination to the cantilevers that could affect future results. However, not all angles can be seen with AFM so hence SEM was used. In Figure 2.2, SEM images were produced on two types of indenters that were used in experiments to clarify that placement of the microsphere was correct, and to ensure that the cantilevers were fit for purpose as this was not always the case.
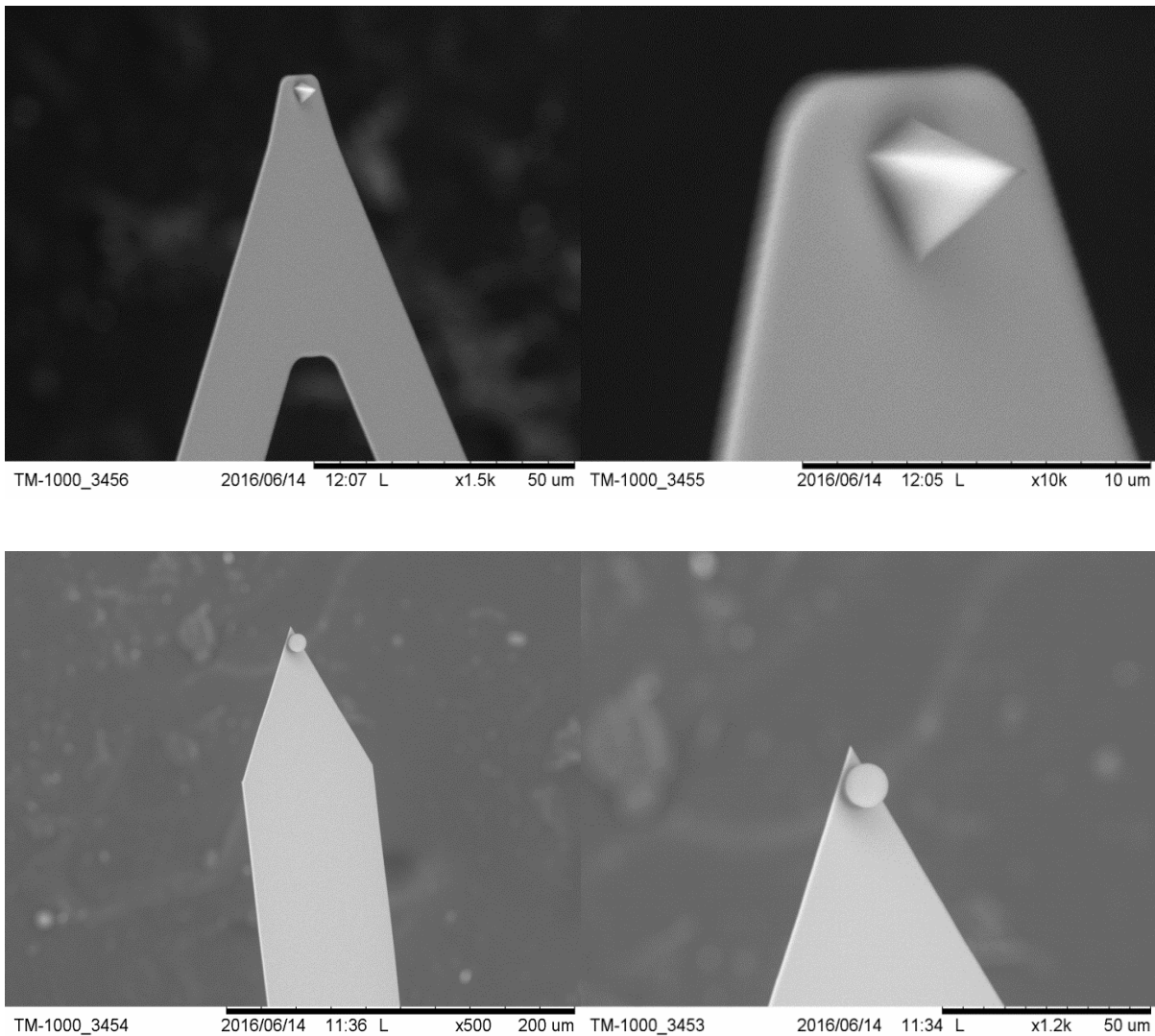
Figure 2.2 – Scanning Electron Microscopy images of the two types of indenters used for the AFM procedure. Images of pyramidal -A) 1.5kX B)10kX and spherical - C)500X D)1.2kX with FE-SEM Hitachi SU-6600.

To achieve this, characterisation of the tip is required, specifically an approximation of the tip geometry, which is essential to relate to force measurements. There are many possible ways of characterising the size and shape of the tip. In this study, the procedure used was SEM with an insulating material coated with a metal layer. The resolution is approximately 10nm but is dependent on the thickness of the coated layer on the surface (insulator/metal layer). The application of this technique is necessary to analyse for tip wear. It should be noted that SEM does not provide a calibrated image. Hence, the shape of the tip can only be semi-quantitative.

As seen in the SEM images (Figure 2.2), the tips have no obvious defects and there is correct placement of the microsphere on the tip. When comparing these two different geometries, it is important to realise that in experiments the pressure applied to the cell will be different for each, which will deform the cell differently. The area in contact with the cell when the spherical indenter is used is larger in comparison to the pyramidal indenter. The spherical indenter in Figure 2.2 was found to be 8µm in diameter which was confirmed with the use of AFM.

To obtain a more quantitative method for determining shape, transmission electron microscope (TEM) can be used as this gives defined images. This technology was not used in the current study. If assumptions were to be stated with regards to the tip or the surface not changing during an experiment they are likely to be wrong in the majority of cases. A study by Foster and co-workers produced a computer simulation to show the probability of the transfer of atoms as soon as contact is made, which emphasises the importance of avoiding cantilever contamination (Foster et al., 2001).

2.5.4. CALIBRATION OF AFM

The calibration of the cantilever is important to ensure the most accurate results are achieved. The procedure of calibration is well documented but there are different variations that are dependent on the type of AFM used (Cappella and Dietler, 1999, Butt et al., 2005, Hutter and Bechhoefer, 1993). Calibration should be conducted to reduce error and enable production of the best quality images. The two values that are required to calibrate the instrument are the deflection sensitivity and spring constant.

Firstly, the AFM laser spot needs to be positioned correctly on top of the cantilever, thus ensuring that the signal to noise ratio is minimised. Most AFM give a defined size of laser spot (normally ~50µm, which is the case for the Dimension Icon head). The setup for the Bruker FastScan gives three options: large spot, small spot and small diffracted spot. Also, if the laser spot is too large for the surface of the cantilever, the image will show artefacts similar to those shown below (Figure 2.3).
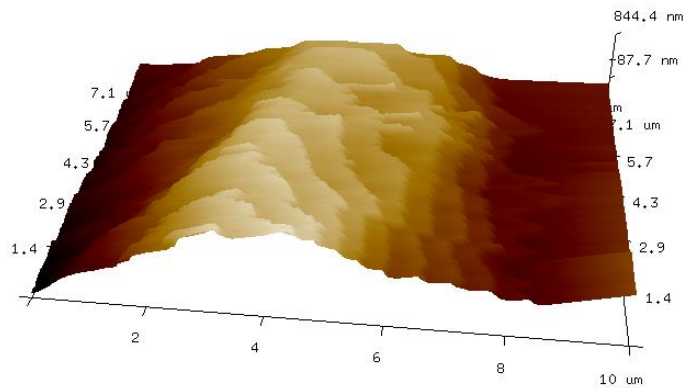
Figure 2.3 - Live cell imaging of a HepG2 cell. Artefact due to the AFM laser being incorrectly positioned and hence no surface detail can be clearly seen.

The deflection sensitivity is the relationship between the z-piezo movement and the laser spot position on the detector (units nm/V, for the case of AFM). The end value of deflection sensitivity can cause significant differences altering future results. Therefore, every type of cantilever (depending on resonance frequency/ spring constant) should have a range in which the deflection sensitivity should be. If a cantilever is to be reused this parameter should be relatively similar to that obtained before, and if this is not the case, the tip could be contaminated or defective. When attempting to obtain mechanical values by the use of AFM, the calibration has to be carefully undertaken. Calibration was undertaken on a glass sample, typically a ramp (force distance curve) would be conducted to achieve the value for deflection sensitivity. This value for deflection sensitivity has many variables and values should be kept constant. It should be emphasised that a very small quantity of force should be applied to the surface as greater forces can cause the tip to become blunt (Figure 2.4).
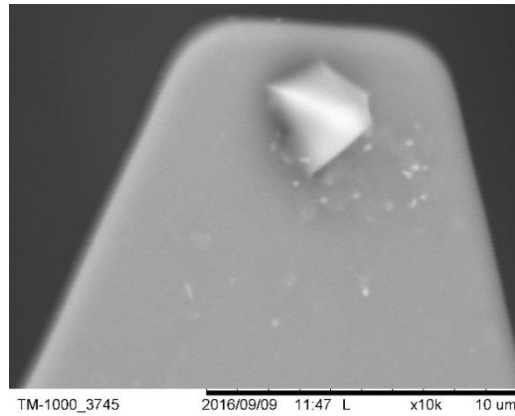
Figure 2.4 - Cantilever which had too much force applied to it. The surrounding area shows debris also from the tip.

The spring constant is an important value which is normally determined by the thermal noise method (Lübbe et al., 2013). Noise is produced due to the result of thermal fluctuations of the cantilever, while suspended away from any solid surface. The surrounding air bestows impulses to the cantilever which allows resonance to occur. Cantilevers are given an estimated spring constant by the manufacturer but each individual cantilever has a different value. This variation occurs because the manufacturing process is very delicate and can be difficult to carry out reproducibly. As explained, most studies regarding AFM use the thermal tune method to quantify the spring constant. To determine this value, the cantilever is excited to oscillation at well stabilised amplitude which produces a graph as seen in Figure 2.5. With this, the first mode can be highlighted and the software can calculate the spring constant. The range for the thermal tune method when using the Bruker software, ranges from 1- 100 kHz, which is not ideal for cantilevers that have low resonance frequency (especially if calibration measurements were conducted in water) and in some circumstances the peak obtained by thermal tuning cannot be clearly seen, see below (Figure 2.5). Hence, the spring constant value was obtained in air as the data were fitted with ease.
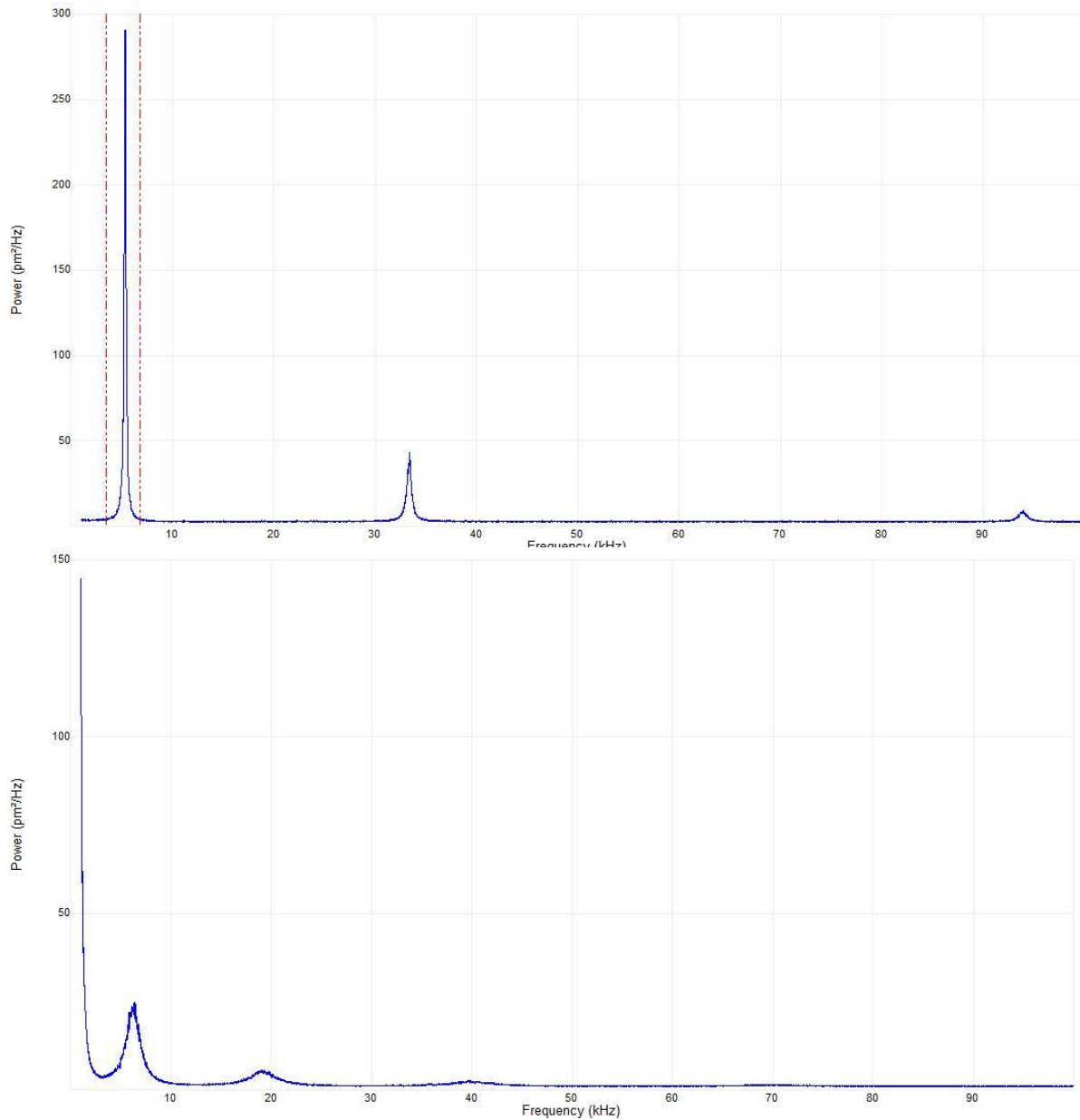
Figure 2.5 - Thermal tune method conducted on a cantilever with a low spring constant. a) Conducted in air the first peak appears at 6 kHz. b) Conducted in water, the peak is not fully plotted. This graph is required to obtain the value for the spring constant of the cantilever and is specifically needed for future mechanical measurements.

A correction factor (λ) takes into consideration the cantilever tilt which occurs with most AFM (schematic can be depicted in Figure 1.12). In most cases this can have an adverse effect on final mechanical measurements and increases the error value. There is an applet (Radmacher, 2014), where the thermal fit is applied to the thermal tune method obtained from the instrument which mathematically produces a more accurate value for the deflection sensitivity, taking into account the correction factor.

Overall to ensure the best results for mechanical measurements, a colloidal probe should ideally be used as the tip geometry is more easily defined. The spring constant should be calibrated by an interferometer and the deflection sensitivity measured should be in a region which can then be repeated (within 10%).

2.5.5. TIP QUALIFICATION

Tip qualification can assist in the estimation of the tip shape when calibrated on the correct surface (glass), and tip geometry estimation is the last parameter required for the calibration setup. The use of SEM can provide an estimation of tip geometry but to verify this value, an image of the tip can be captured using the AFM software.

An understanding of the software is required, when using the tip qualification/estimation icon in the NanoScope Analysis software (v1.5, Santa Barbara, USA). The software achieves this tip status (defining if the geometries comparable) by obtaining two cross sectional areas of the tip (Figure 2.6) after a small area of a relatively smooth surface is scanned by AFM. The cross sections create a ratio and this is compared to programmed threshold values (in the software) which will segregate the tip into good, bad and worn regions (example of this layout is shown on Figure 2.7). In most cases, the tips were found to be in a good condition but if found to in be bad condition they were discarded from any further experiments.
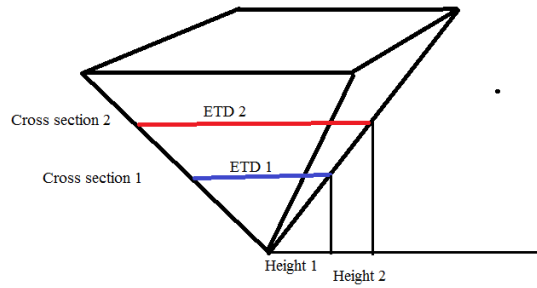
Figure 2.6 – Pyramidal tip estimation with the cross sections depicted. The tip estimation used by Bruker can assist with information about the tip status. The cross sections shown assist with obtaining apparent measurements of the tip at the two different heights. The effective tip diameter is defined as the area of a circle which has a similar area as that measured at the cross section which will give an aspect ratio.

In Figure 2.7, the layout of the tip qualification is displayed. Firstly, a height image is uploaded into the window which is obtained from scans (1µm) of the surface. Also, the tip could be sectioned to analyse the tip interface.
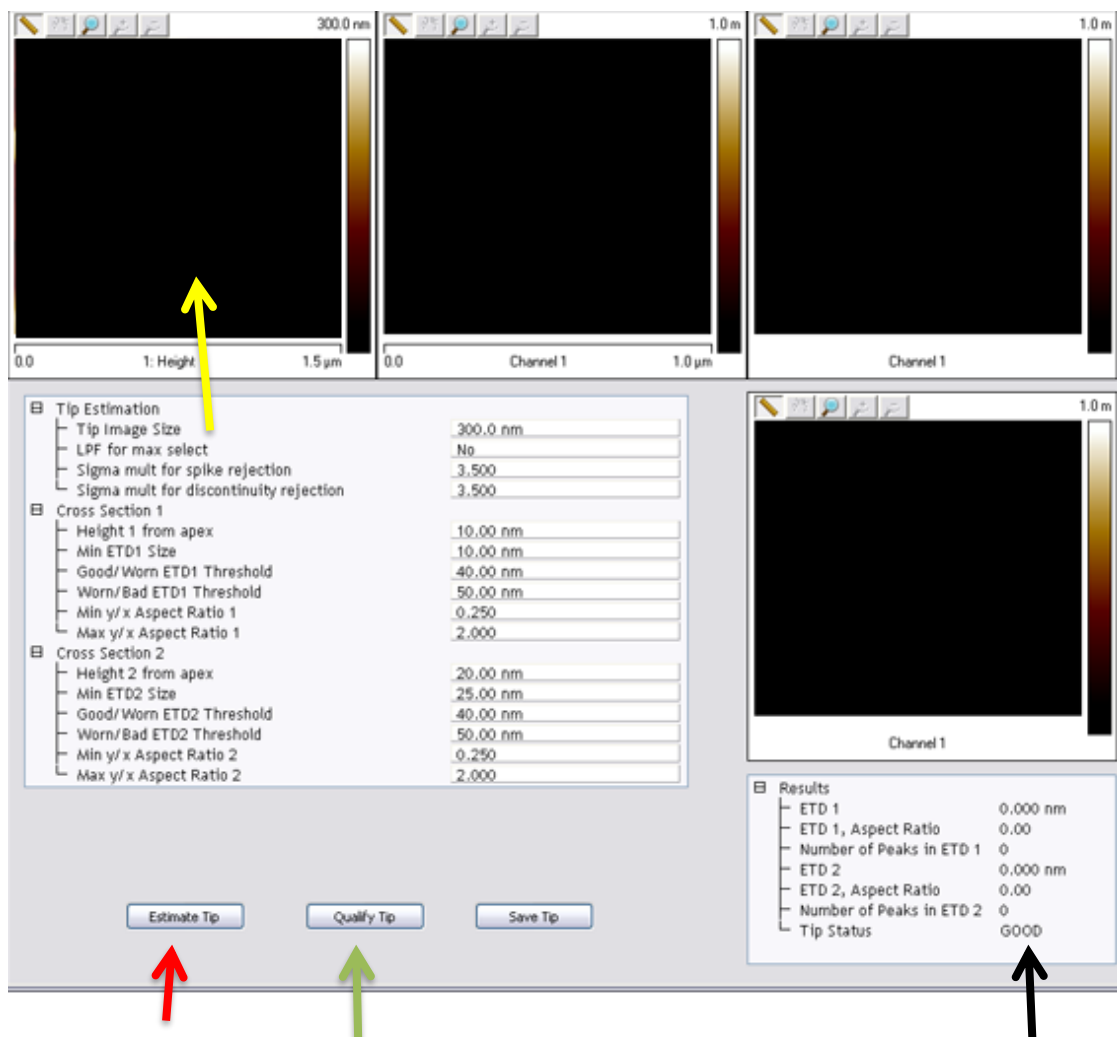
Figure 2.7 – Tip qualification window in the NanoScope software before calculation has been conducted.
Once the height image has been uploaded to this window, the tip geometry is estimated (red arrow) and then qualified (green arrow). The result gives information of the cross section and a suggested tip status (black arrow). The area in which the scan would be presented is shown by yellow arrow.

2.5.6. MICROSCOPE SETTING

Within the Nanoscope software assigned to the Bruker AFM, there are different modes to reduce the complexity of AFM. The Nanoscope software associated with the Dimension Icon has many variations of contact and tapping mode which gives the user options to manipulate to the software. The typical software layout obtained from the NanoScope can be seen in Figure 2.8, where different factors are highlighted and these can be altered to produce the desired image. When the desired aim is to investigate mechanical measurements, a lot of

considerations must be accounted for such as parameters which will be defined more clearly in section 2.5.6.4.
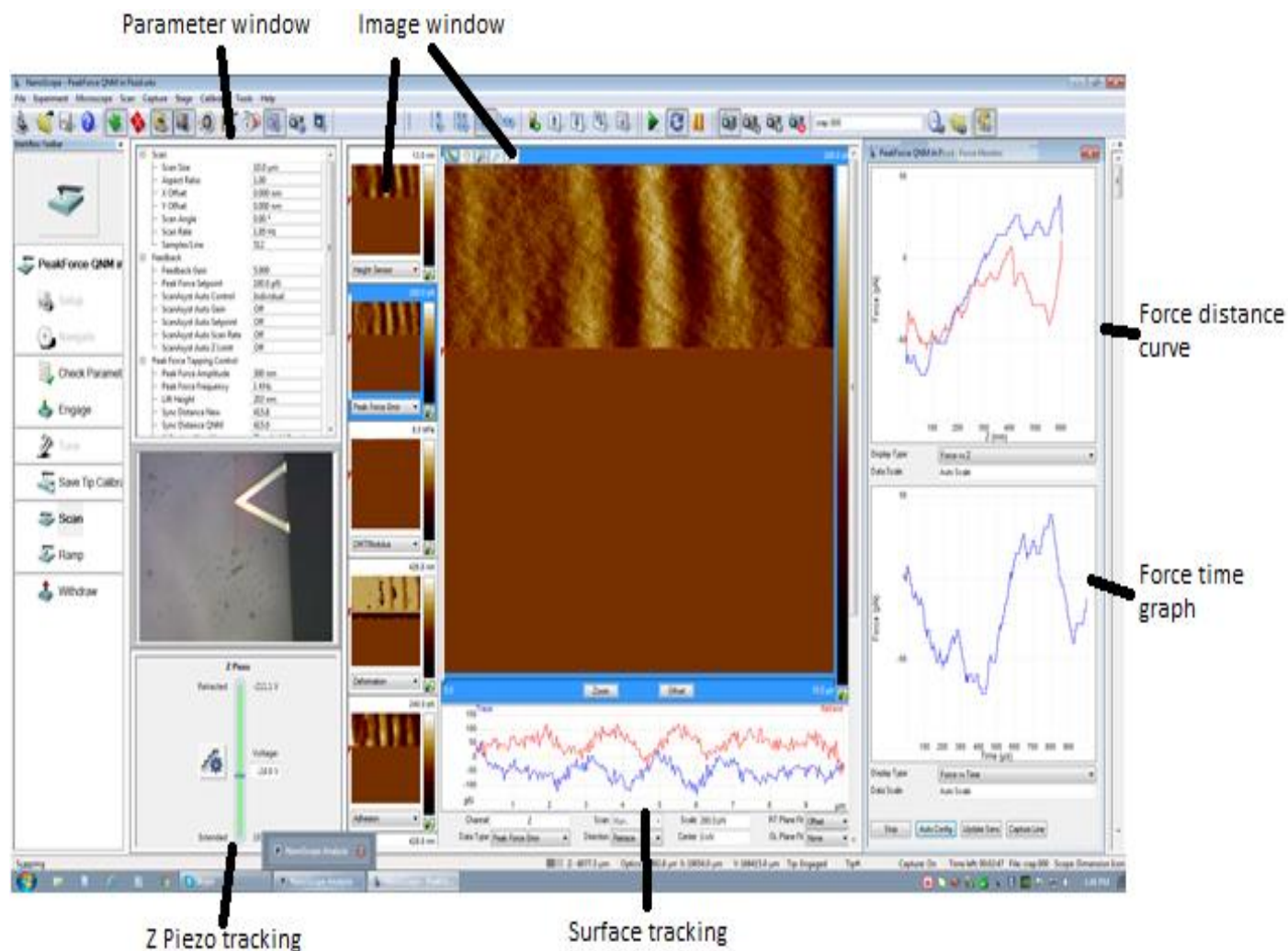
Figure 2.8 – Typical layout of the scanning window of the Bruker PeakForce QNM. The cantilever is scanning a glass surface in air. Important factors have been highlighted; the Z Piezo window should be in green, and if this was to change colour to red, the cantilever has either been retracted or extended away from the surface. Surface tracking is the approach to and retraction from the surface. These lines should follow each other, and parameters should be changed to allow that. The force monitor window should produce graphs similar to the ones that are shown on Figure 2.10.

In this study, most images were obtained during tapping mode or Peak Force QNM (differences are explained below). The force distance curves were obtained in the nanoindentation section of the Bruker software (section 2.5.6.4)

2.5.6.1.   TAPPING MODE

When imaging live cells, tapping mode reduces the problem obtained in contact mode with high lateral forces between the surface and the cantilever. Across the sample surface, the cantilever can change the oscillation amplitude and images that are obtained by tracking these changes. In comparison to the cantilever length, typical amplitudes of oscillation are relatively small, in the range of nanometres, and this emphasises the delicate nature of the procedure.

The quality factor (Q) in tapping mode needs to be considered. This value is a ratio of the stored energy divided by the energy lost per cycle. It is helpful to see this value if the system is lightly damped. The dynamics of tapping mode can be highly dependent on the sample properties and if there is a change in properties (for example, softness), the software can have difficulties.

In this mode, the cantilever needs to be tuned to the resonance frequency (Figure 2.9), and the peak should be well defined. There is an option for automatic tuning but the correct frequency must be applied.
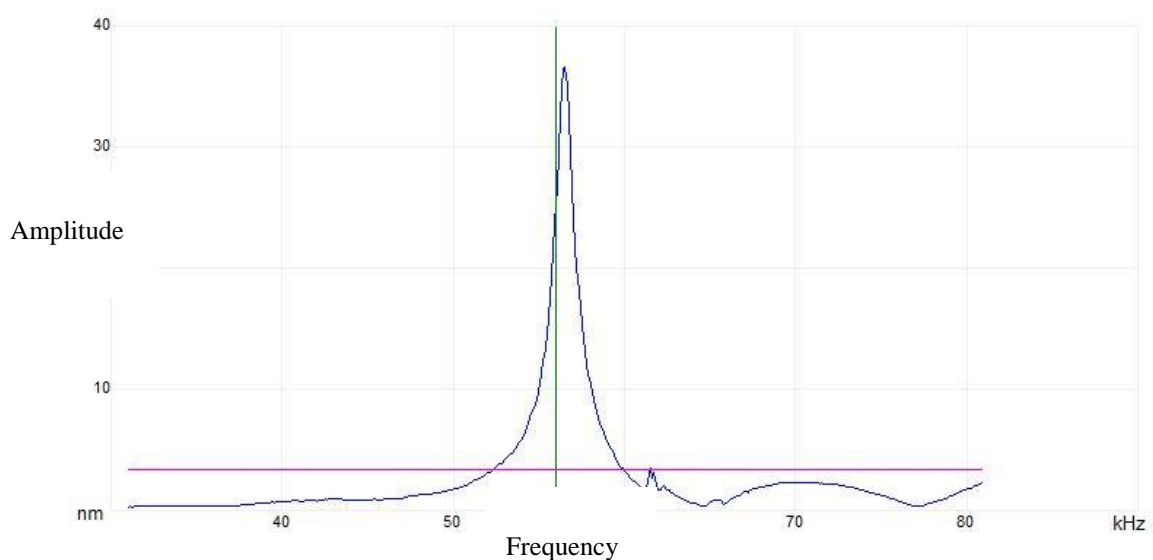
Figure 2.9 - Typical resonance frequency peak obtained in tapping mode. The cantilever used was SNL-C.

2.5.6.2. PEAK FORCE QUANTITATE NANOMECHANICAL MEASUREMENTS (QNM)

Peak Force QNM is constructed from the force volume approach but there is a significant increase in the approach and retraction velocities at which force curves are recorded, to produce images more quickly. This mode allows imaging of structure as well as physical properties at a relatively high speed and resolution. The tip of the cantilever contacts the surface very momentarily and therefore the shear force is minimised between the tip and sample. The cantilever used does not rely on resonance frequency (no need to tune) which has great advantages in liquid. The force curve is recorded at every pixel, which then enables production of a mechanical map (Figure 2.11). This mode separates information to give properties such as modulus, adhesion, deformation and dissipation. The layout of the software can be found in the appendix (Figure A4).
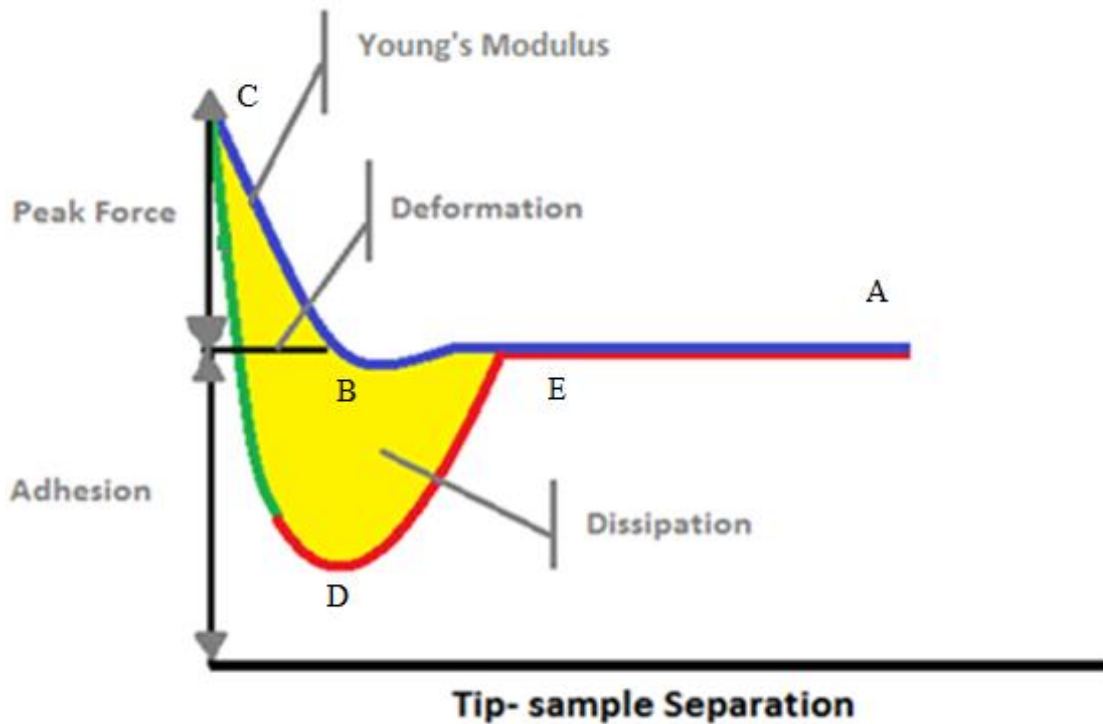
Figure 2.10 - Cantilever trace graph. Typical force curve produced from PeakForce QNM and possible mechanical information achieved from the curve. Young's modulus is obtained from the best fit of approach line. (Further details, 2.5.11). At point A, the tip is above the sample and then the Z-piezo pushes towards the sample. B- Tip makes contact with sample and Z-piezo pushes probe further until Peak Force measurement can be reached. C- The probe starts to withdraw from surface. D- Probe tip breaks free off sample at the maximum adhesion point. E- Probe back to starting point above sample surface. Graph B - Typical force curve produced from PeakForce QNM and possible mechanical information achieved from the curve. Young's modulus is obtained from the best fit of approach line (Further details, 2.5.11).

The frequency at which the cantilever is oscillated is important and should be kept constant throughout experiments to ensure the measurements are similar throughout. There are several different named parameters which can be altered in this mode, to achieve an understandable force curve. Such parameters include sync distance, peak force amplitude, lift height and drive frequency. The sync distance (value to achieve the best possible force curve) and feedback is vital for obtaining the peak force tapping curve which makes for accurate control and gentler tapping. Within the mode, there is an option, to capture each individual force curve taken across the cell; this can be very helpful but in most cases the approach velocity will be above 10µm/s (See 2.5.9.3). As explained, this mode does give many measurements

in the same scan and these are only in this part of the Bruker software (Figure 2.11). In Figure 2.11, there are four images shown and these are obtained with regards to the height image. The software produced three other images through mathematic manipulation, resulting in the four images being collected at the same time.
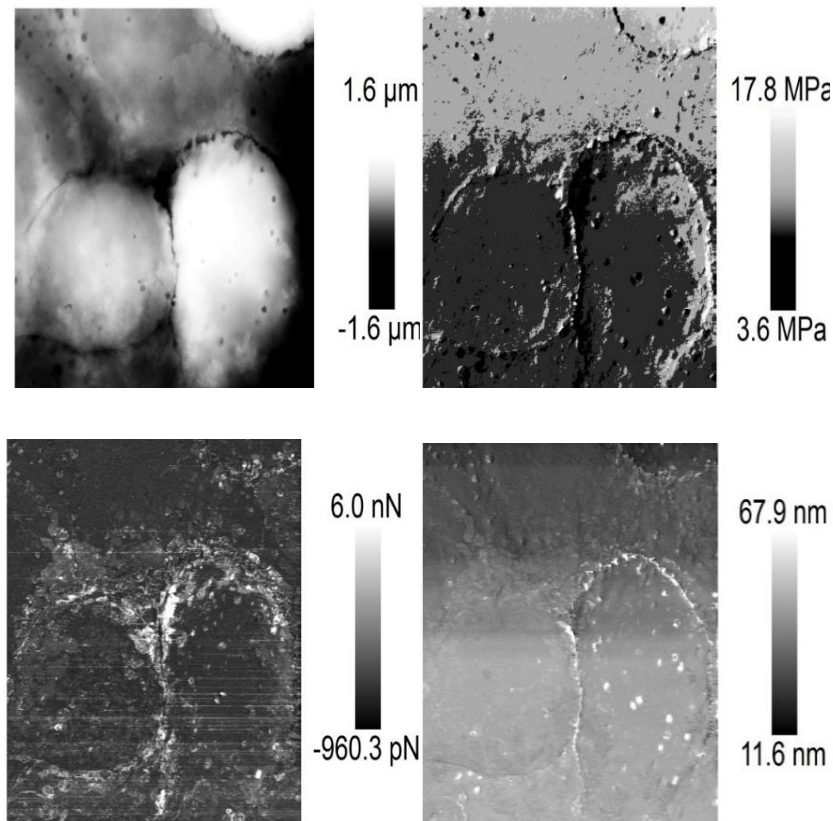
Figure 2.11 – Peak Force QNM images of dried HepG2 cells. This is an example of what PFQNM can produce in one scan, providing pictures with regard to height (top left), modulus (top right), adhesion (bottom left) and deformation (bottom right) of the cell. The software obtains these images due to mathematical manipulation of the height image.

Additionally, the mechanical maps produced by AFM can deduce more information about the cell surface such as roughness. Roughness can be calculated in a few ways such as the root mean square (RMS) or the roughness average (Ra). Roughness calculated by RMS is analysed by averaging the differences between the peaks and valleys and Ra obtains a value by averaging the area as a whole. RMS values were calculated throughout this thesis.

2.5.6.3.   SCANASYT

ScanAsyt is part of the software which is suggested for basic imaging. It is the straightforward approach to AFM but only if the sample is being imaged has no distinct changes such as stiffness or roughness of the surface. This part of the software is an "autopilot" function and is designed to make the user feel at ease. It also does not have a need for tuning, although, when in a fluid environment, the software tends to overcompensate with the feedback and can cause the cantilever to push into the cell surface more than necessary. As seen in Figure 2.12, the software has control of the feedback so the feedback gain and peak force setpoint is changed to suit the cantilever and surface.
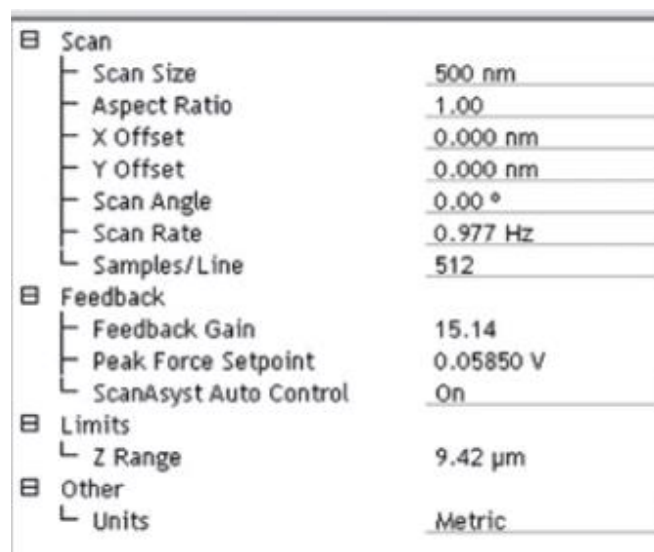
```
⊟ Scan
    ├ Scan Size              500 nm
    ├ Aspect Ratio           1.00
    ├ X Offset               0.000 nm
    ├ Y Offset               0.000 nm
    ├ Scan Angle             0.00 °
    ├ Scan Rate              0.977 Hz
    └ Samples/Line           512
⊟ Feedback
    ├ Feedback Gain          15.14
    ├ Peak Force Setpoint    0.05850 V
    └ ScanAsyst Auto Control On
⊟ Limits
    └ Z Range                9.42 μm
⊟ Other
    └ Units                  Metric
```

Figure 2.12 - ScanAsyt Parameters Table. Screen shot of the interface and all the feedback settings and scan rate which are automatically calculated by the AFM. This control can be removed whilst scanning if the gain or setpoint values are creating too much noise.

2.5.6.4.   NANOINDENTATION

The analysis of force-distance curves can assist in the understanding of the sample and the environment. Before the tip has contacted the surface, there should not be any significant deflection of the laser. When the cantilever encounters the surface, it begins to deflect and a repulsive force occurs. When the defined force set point has been attained, the indentation is stopped and the cantilever removed from the surface.

Figure 2.13- Indentation software layout incorporated into Bruker NanoScope. a) Screenshot of the indentation software, where there are many options which can be either additional or altered during the procedure. b) Some of the parameters are highlighted and can be seen on the screen. It should be emphasised that these are not the exact values used in the experiments. The ramp parameters need to be optimised for reproducible force curves to obtain end values such as Young's modulus. Other software windows can be found in more detail in the Appendix (Figure A.4).

Within the AFM software, there are many possible alterations which can optimise the experiment and help obtain reproducible force curves. The typical software layout for the indentation procedure can be seen below (Figure 2.13). This can give an indication of the range of parameters which can be altered. Specifically, the following parameters can be optimised; indentation speed, indentation force and indentation depth.

All the above parameters should be kept constant if an elasticity result is required. The optimal value for indentation force is dependent on the cell type and the AFM tip used. This is because different cell types vary in height and the pressure distribution will change with the different tip geometry. In the literature, the force applied to the cell has ranged from 100pN (Eaton and West, 2010) to 20nN (Wozniak et al., 2009). Initially, a range of 100pN to 15nN was used to analyse the immediate effect on the cells. After time, the loading force applied to the cells was 1nN which is a recommended value reported in the literature (Haase and Pelling, 2015).

The indentation depth is again dependent on cell type and tip geometry (seen in Figure 3.15b, ramp size). Many studies have stated that if this value is too great, it can show the cells to have a greater Young's modulus than anticipated. There is a plateau in modulus with regard to indentation depth and this is the ideal amount to indent the cell. Also, when a Hertz model is applied to the force curve, a minimum of 5% of cell height is required to be indented to fit the mathematical model. In the experiments reported in this thesis, the approach velocity had to be defined, and this was set to be 2µm/s as reported in the literature (Thomas et al., 2013).

After finalising the choice of indentation parameters, the cells were indented five times in the nuclear region with the spherical indenter and over 75 HepG2 cells were indented for each experiment. Each individual indentation produced a force curve which was examined by the Hertz model. Treatment of 5-FU (5µg/ml for 24 and 72h) and diclofenac (500µg/ml for 24h) was applied to HepG2 cells in separate experiments. In the experiment with 5-FU treated cells, a sharp tip was also used in addition to spherical tip for comparison purposes. Figure 2.14 shows a typical setup for the AFM experiment. Force curves obtained with indenting had a Hertz fit applied to it and values of Young's modulus were calculated (Section 2.5.12).

In this study, to ensure the value for tip size was correct the AFM microscope was used. Before the spherical probe was produced, the sphere could be clearly seen on the glass coverslip and its diameter confirmed. The pyramidal tip shape and size could be verified by use of the NanoScope, and this indicated whether the tip was good, or in worn or poor condition but also showed an outline of the tip. This was found to be only beneficial if the tip had even geometries (all sides have approximately the same dimensions) as this was required for application to the indentation experiments.
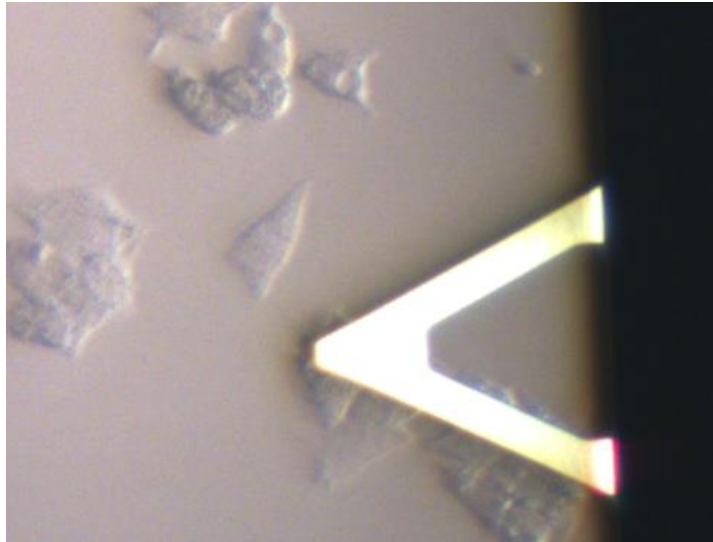
Figure 2.14 - Setup of indentation experiment. HepG2 cells on a petri dish, a small force is being applied to one cell by a cantilever.

2.5.7. LIMITATIONS WITH AFM

Calibration is a vital part of the AFM process if mechanical measurements are required. This is complex, but there are factors which can reduce error such as defined tip geometry and spring constant, as discussed.

There are limitations of force sensing and resolution which are affected by noise produced by the overall system. Thermal drift can be a hindrance and can give different force values from the start to end of the experiment. The vertical signal (z-piezo) is the value that can be noticeably changed. The slightest change in temperature can change the deflection signal and this is one reason why it is advisable to use uncoated cantilevers. The coated cantilevers will have different coefficients of expansion and therefore can cause a deflection in the cantilever.

Standardisation of data is crucial for reliable data, and is the easiest way to ensure that the data is reproducible. Also, it is important to ensure that every thermal tune and deflection sensitivity is recorded. More about controlling data reproducibility will be explained in later chapters.

2.5.8. SAMPLE SETUP FOR AFM

The main experimental set up used HepG2 cells as discussed in Chapter 1 (page 12). The cells were plated into petri dishes (60mm diameter). Even though HepG2 cells are an adherent cell line they were challenging cells to image because of their tendency to clump and when over confluent can form multilayers. In the literature, where the cells were imaged forces were applied to the cells in the range of 0.05-20nN (Shen et al., 2011). The fixation of the cells and then placing them in fluid simplifies the experiment, but in turn does not give the true surface. (more detail in section 2.5.11)

2.5.8.1. FIXED CELLS

To ensure the cells will not detach from the surface easily and to obtain a greater understanding of the force applied by cells there is an option to fix the cells. This was not often used in practice. Fixing was carried out by applying 4% paraformaldehyde for 15 minutes and then washing the surface with DPBS two times before viewing. The fixed samples were viewed and three images taken on one cell at different points. With the fixation of cell samples, it should be noted that the cell mechanics can be altered and more force could be applied compared to living unfixed cells.

2.5.8.2. LIVE CELLS

For live cell imaging, the cells were washed with warm DPBS to remove any debris and then 1ml of media added to the petri dishes. There are important factors which need to be considered such as temperature and carbon dioxide levels as these can alter the cell behaviour. Studies have shown that the temperature has a great effect over time on the elastic properties of cells (Espenel et al., 2008). Hence, it is important when trying to maintain an *in vivo*-like environment to maintain the experiment at 37ºC.

The AFM experiment in this situation is an open environment. An ideal situation to maintain the cells viability would to create an environment similar to the one achieved inside incubators at 37°C and in 5% CO_2 in air. The cells do not use the CO_2 themselves but the CO_2 ensures the bicarbonate buffer in media maintains physiological pH. Cells were only used for approximately 70 min and every 15min a pH strip was used to ensure the pH was in correct range.

In many studies, images of endothelial cells seem to be predominately used to investigate the capabilities and parameters of AFM. In comparison, hepatocytes (specifically HepG2 cells) are rarely utilised in the field of AFM. It was therefore found useful in initial studies, to use endothelial cells, to optimise parameters which would give most detail of the surface. The reasoning for this was because there were documented parameters in previous studies which were a starting point and the endothelial cells seemed more likely to stay adhered to the surface if the parameters changed. Also, it is thought that because endothelial cells, experience fluid flow more often than hepatocytes they adhere to the surfaces better (Barbee et al., 1994, Braet et al., 1998, Vargas-Pinto et al., 2013, Monkemoller et al., 2014, Thomas et al., 2013). The shape and height are different between hepatocytes and endothelial cell and as seen in image below, endothelial cells tend to be elongated (Figure 2.15). When imaging endothelial cells with AFM, it was observed a range of forces could be applied with ease and detailed images could be captured of the whole cell. However, imaging HepG2 cells was complex as several scans of the cells had to be aborted due to the cell movement. In the literature, there are few AFM studies with hepatocytes (HepG2 cells) in comparison to endothelial cells.
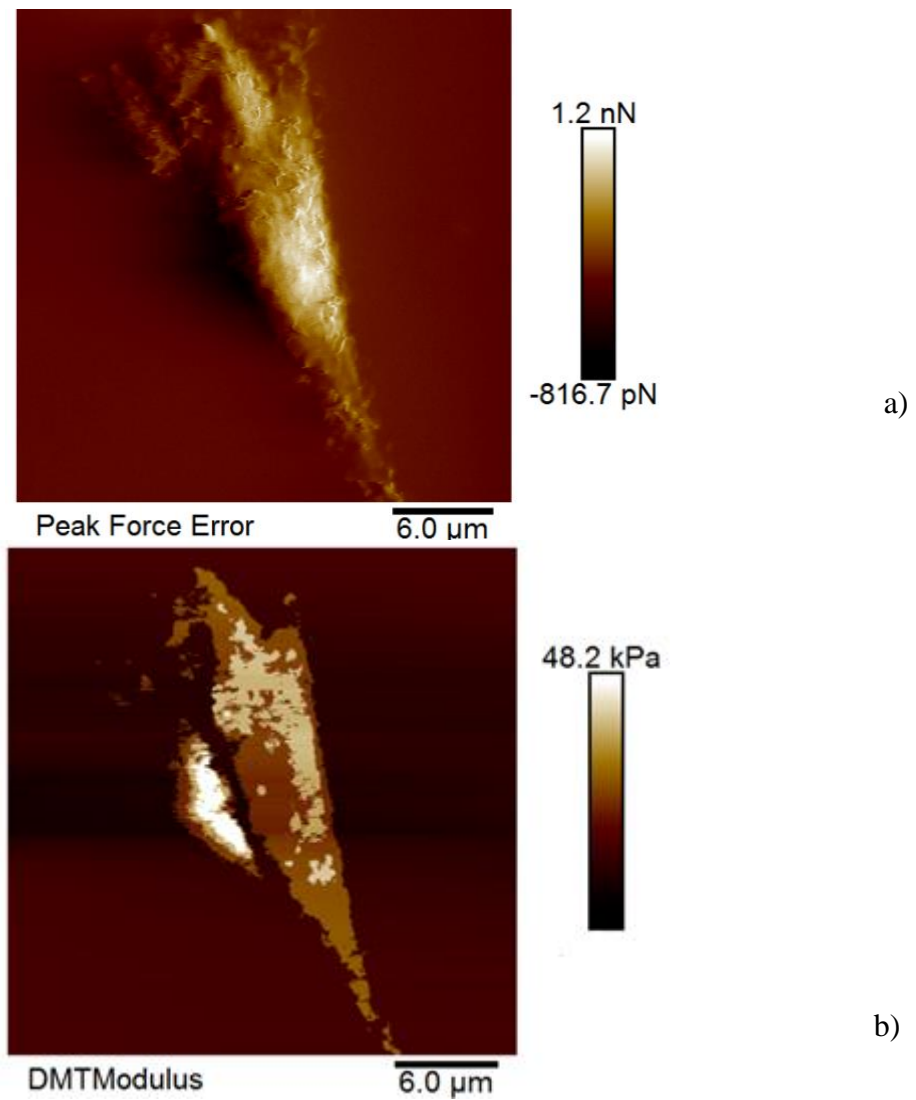
Figure 2.15 – AFM images of primary porcine endothelial cell which were harvested by excising a pulmonary artery. These cells were maintained in Primary Endothelial cell media comprised Gibco Medium 200 with 1.9% (v/v) Low Serum Growth Supplement and 0.9% penicillin-streptomycin (with 10,000units penicillin and 10mg streptomycin/ml). The pig hearts were donated by Robertson's Fine Foods (Ardrossan, Scotland) and cells isolated by Suky Kaloya and Ian Holland. The endothelial image was captured at scan rate 1Hz, amplitude setpoint, 250mV, drive amplitude 100mV and sample/line being 512.

The parameters within the AFM software can be altered to give different views of the cell surface. Every cell type is different in height, size and elasticity, so would require different parameters. Also, the correct parameters are needed to ensure there is no damage to the plasma membrane during AFM analyses. There are many possible parameter alterations which can be made, and a few of these are discussed below.

The optimisation of operational parameters for indentation measurements can be used to monitor the mechanical properties of the living cell. The indentation parameters for cells are dependent on cell type. Specifically, indentation parameters must be controlled or they can cause an inappropriate estimation of Young's modulus; these include parameters indentation depth, and the force and speed at which it is applied to the cantilever.

2.5.9.1. LOADING FORCE

The force which is applied to cells should be minimal, as particularly HepG2 cells were found to be easily removed from the surface. Various studies had suggested that forces of up to 20nN (Wozniak et al., 2009) should be used but if this was applied to HepG2 cells attached to a petri dish, they detached from the surface.

In the initial experiments, it was found that if high forces were applied to a cell, the approach curve showed unexpected peaks (Figure 2.16). These irregularities occurred after the cantilever had made contact with the surface. After these initial experiments, no loading forces above 10nN were used as these irregularities were noted and there was a high chance of the HepG2 cells being removed from the surface by the tip. In Figure 2.16, the indenter was shown to have double penetration which suggests a multi-membrane cell. As standard, the approach curve should be relatively smooth and to ensure it is not contaminated, the cantilever should be washed regularly to be sure it is still in working order. After initial experiments, the loading force applied to the HepG2 cells was 1nN and this value was kept constant.
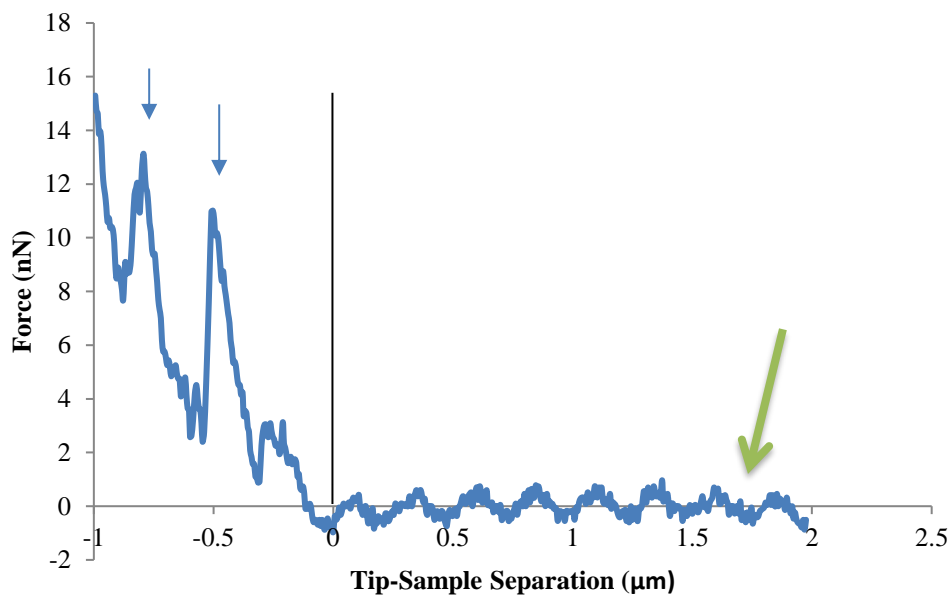
Figure 2.16- Approach curve when 15nN of loading force was applied to the cell surface with a pyramidal indenter. Unlike previous force curves where the approach curve had no clear irregularities (see Figure 2.10), this example does show irregularities (blue arrows). This suggests that the cell surface was not stable when the cantilever was applied. There is laser interference observed in the force curve (green arrow) and this can be prevented in future by repositioning the laser spot on the cantilever.

Force curves were obtained by indenting HepG2 cells to evaluate any changes in elasticity which were then related to other mechanisms which were occurring in the cell. To obtain the force distance curves, there is a conversion relating to the photodiode current and the piezoelectric translator height position. Two values need to be obtained - the zero distance and the sensitivity (Section 2.5.4). When analysing the force curve, the "contact point" can be assumed to be the zero distance and the slope of the curve is related to the sensitivity. There should be clarification regarding force curves, and assumptions should not be made that all force curves which are produced are "real" as noise can effect results (Hecht et al., 2015, Butt et al., 2005). An example of the noise affecting an image was given in Figure 2.3, where the laser produced additional artefacts.

It was found that if the HepG2 cells were subjected to a greater force than 10nN, the cells would detach from the surface and this could be associated with membrane rupture (Figure

2.16). This experiment was conducted with a pyramidal indenter and would be less likely to occur with a spherical indenter because the force is applied across a larger area. Hategan et al. (2003) reported that 10nN-30nN would penetrate the cell membrane of an erythrocyte. Additionally, other parameters such as approach velocity can affect the force curves produced and estimate mechanical parameters incorrectly. At high speeds, there will be a distortion of the elastic response due to viscous contributions (Butt et al., 2005).

2.5.9.2. INDENTATION DEPTH

Indentation depth is vital for mechanical measurements to assist with fit of the Hertz model to the force distance curve. If the indentation depth is too shallow, there will be an underestimation of Young's modulus. Values for elasticity are shown above (Figure 2.17) and to comprehend this graph, a schematic is shown (Figure 1.13), where the cantilever is observed to probe the cell. If the cantilever was to indent 100nm, it would apply the force to glycocalyx (for example). However, the more the cantilever indents the cell, more of a comparison can be calculated for the "whole" cell. Also, the increase in elasticity is most likely to be caused by the substrate or the tip altering the position of cellular components such as the nucleus which is stiffer than other cytoplasm components (Caille et al., 2002). In Figure 2.17, the relationship between indentation depth and Young's modulus is presented; the range applied was 100nm – 1200nm and it was observed that there would be an incorrect evaluation of the elasticity at this depth. The elasticity increased dramatically if the indentation depth was above 1000nm.
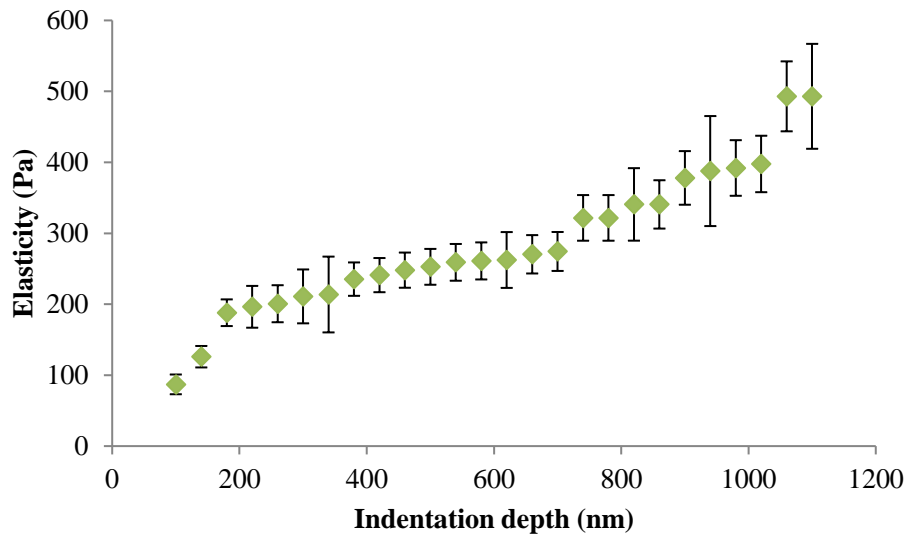
Figure 2.17 – Indentation depth against cell elasticity measured with a spherical indenter. These values were obtained at the point of contact between the sample and tip with small increasing increments (40nm) on HepG2 cells (n=4 ±SEM). At low indentation depth, an underestimation of elasticity was achieved but a plateau area at 400-600nm is shown.

The indentation depth was required to be defined and the range identified to agree with the Hertz model was found to be in the region of ~400 - 600 nm (Figure 2.17). Subsequently, these values were found to be in agreement with those in the literature defining the appropriate depth as approximately 5-10% of the total thickness of the sample. Without this range, there is a clear underestimation of values below 150nm and overestimation above 1000nm but this is dependent on cell height (Janmey and McCulloch, 2007). The overestimation can be related to the substrate upon which the cells adhere and therefore the Hertz model should not be applied to force curves greater than the 15% for a fit.

2.5.9.3. APPROACH VELOCITY

The velocity of the probe as it approaches the cell surface is an important factor when considering data acquisition from a soft sample as the stiffness of cells can appear larger at higher velocities (Janovjak et al., 2005). The apparent forces increase considerably at velocities greater than 12μm/s as there is a speed dependent hydrodynamic force acting on the cantilever. Similar values were found by Janovjak and co-workers (2005). Also, to minimise hysteresis the velocity of the probe should be minimal. This reduces the amount of

energy from the AFM tip dissipating into the cell. When indentation experiments were conducted, the approach velocity was set to 6µm/s.

2.5.10. INTERPRETATION OF YOUNG'S MODULUS

The measurement of Young's modulus in theory explains the elastic behaviour of a material as a constant value, but in true circumstances cells do harden upon multiple indentations. Information can be drawn from the contact area of the force curve to give an indication of the elastic behaviour of the material. Other considerations are taken into account such as the determination of the contact point of the curve, and when the model should be applied. Another value required to obtain Young's modulus is the Poisson ratio which is ratio of the strain from contraction to extension and in this case equal to 0.5. This defined value for Poisson ratio of cells is believed to deform elastically at small strains.

2.5.11. APPLICATION OF HERTZ MODEL

There are several mathematical models which can be applied to AFM data to assist in understanding of the mechanical measurements. All models are an approximation of forces relating to the acting force (from the cantilever) which is pressed against the cell surface. The parameters, which will differ depending on models, are the contact radius, applied force and/or the deformation. In most circumstances, the mathematical model applied is an adaptation of the Hertz model, with regard to choice of indenter used such as pyramidal, cylinder, cone or spherical.
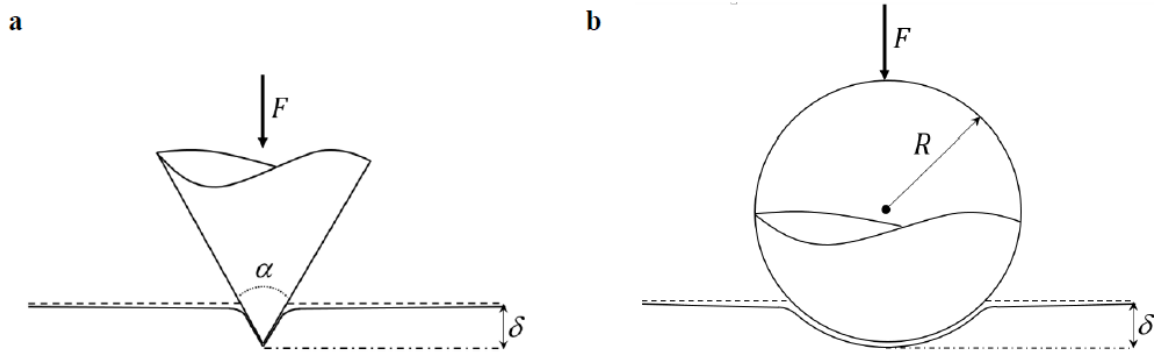
Figure 2.18 – Contact models which can be applied to the Hertz model. a) Conical indenter b) Spherical indenter; both indenters indent an elastic half-space. In both models, the force perpendicular to the surface is applied to the indenter. Therefore, knowing the values of loading force (F), indentation depth (δ), and tip geometry parameters (R or α) can assist in achieving a value for Young's modulus. The tip of the conical indenter is a point of infinite stress.

In Figure 2.18, two different types of indenter are used; these have great influence on the pressure applied to the surface. As shown, the area applied to the surface using the spherical indenter is larger than with conical or pyramidal indenters. For conical indenters, there is a constant ratio regarding the relationship between the radius of contact with the depth and surface of the cell, and it is independent of loading force. The sample conditions and experimental parameters must meet the requirements for the applied model. The Hertz model is not always true for biological samples, however alteration of indenter geometries can be accounted for (cone, pyramidal and cylinder) and applied to the model. All in all, after all parameters are met there is a degree of unavoidable error within the calculation as the living cell is complex, due to the heterogeneous structure.

2.5.12. FITTING THE HERTZ MODEL

To correctly fit the data by means of the Hertz model, the total sample depth should be indented by approximately 10% of the cell height. All parameters should be kept constant throughout; frequency, velocity, ramp size.

$$F = \frac{4}{3}\frac{E}{1-v^2}\partial^{3/2}\sqrt{R}$$

Equation 2.1 - Hertz model for spherical tip where F is the indentation force, E is the Young's modulus, v is the Poisson's ratio, and R is the radius of the sphere. Assumption of the cell being incompressible was made and the Poisson ratio value was 0.5.

In Equation 2.1, the Hertz model is shown for a spherical tip and the schematic for this is represented in Figure 2.18. Alterations to the equation need to be made when the geometry of the tip differs (cone, pyramidal, cylinder). In Table 2.1, the Hertz model is altered to suit the tip geometries as each tip will lead to different contact areas and pressure placed on the cells. In the literature, it has been stated that the pyramidal geometry can be approximated by equations for the conical geometry (Van Landingham, 2003). Assumptions made by Hertz model cannot be applied to most biological samples, hence a modification to account for different indenters can be used (Table 2.1).

Cone	Cylinder	Pyramidal
$= \frac{2}{\pi}\frac{E}{1-v^2}tan\alpha\,\partial^2$	$= 2a\frac{E}{1-v^2}\partial$	$= \frac{3}{4}\frac{E}{1-v^2}tan\alpha\,\partial^2$

Table 2-1 – Contact models of a tip indenting an elastic half space: force-indentation relationship.
Adapted from the Hertz model where all above equations are equated to the indentation force. E is the Young's modulus, v is the Poisson's ratio, R is the radius of the sphere, α is the opening angle (expressed in Figure 2.18), a is the radius of the cylinder. Assumption of the cell being uncompressible was made and the Poisson ratio value was 0.5

When fitting the Hertz model to a force curve using the Bruker Nanoscope software manual manipulation is required to interpret the correct depth for analysis. In Figure 2.19, an example of the Hertz model has been applied to a force curve and with this the area which could achieve a value of Young's modulus is the area in which the two lines make exact contact. The thickness of the material (cell thickness is >3000nm) is required as the thickness of the substrate below can alter the final Young's modulus values. Hence, specific areas of the cell (e.g. lamellipodia, <1000nm) cannot have the model applied to it.
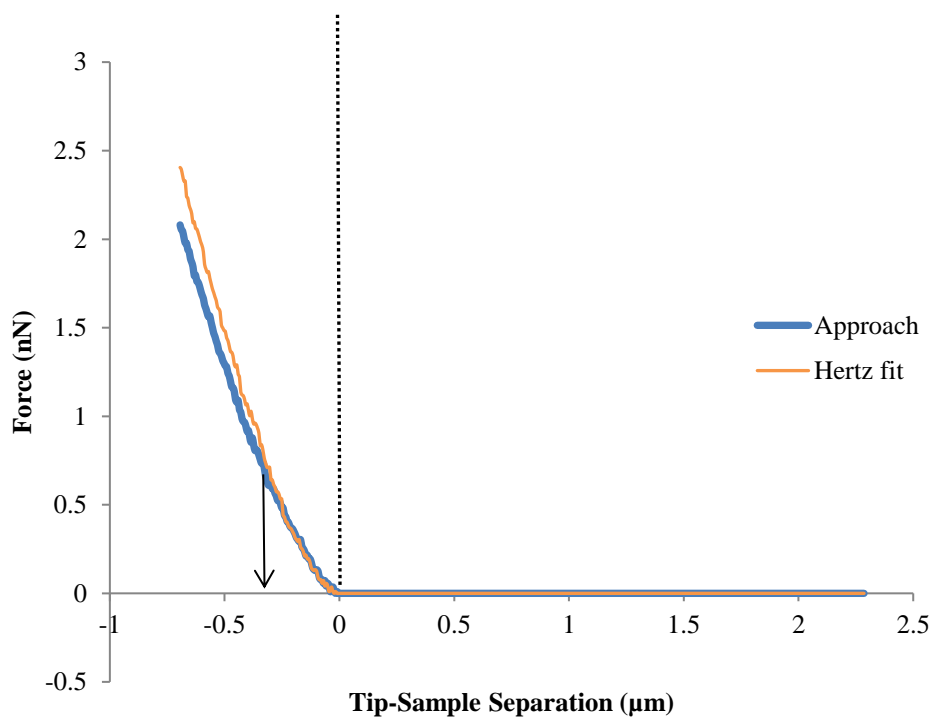
Figure 2.19 – Example of typical Hertz fit achieved from force distance curve. The blue line is the approach curve and the orange line denotes the Hertz's model which has been applied. The black dashed line is the area of first contact between these values and approximately where the arrow is, will be the zone to obtain the elasticity values.

The example in Figure 2.19, is approximately similar to force curves produced by a soft surface as at the contact point there is a negative tip-sample separation which confirms the material is deforming. The correct proportion of the force distance curve should be analysed to be able to achieve Young's modulus. In Figure 2.19, the area between the contact point and the arrow is the part of the fitted Young's moduli which is important.

There are occasions were the force distance curves produced cannot accurately fit the Hertz model (Figure 2.16) and the regression of the line should be minimal. In these cases, the model and data would not be in contact. If this was to occur, then the force curve would have to be discarded.

2.6.   STATISTICAL ANALYSIS

A one-way ANOVA test followed by Dunnett's multiple comparison tests was employed to the null hypothesis that two populations which were equal with significant difference. Data presented throughout this thesis are expressed as standard error of the mean.

Chapter 3 - Toxicity of 5-Fluorouracil in HepG2 cells

3.1. Introduction

Fluoropyrimidines are mainly used as chemotherapy drugs and included in this drug group is 5-fluorouracil (5-FU) which is commonly used for the treatment of HCC. 5-FU is an analog of uracil and uses the same metabolic routes and distribution pathways as this natural substrate. DNA synthesis is inhibited and apoptosis can be induced by 5-FU. In this chapter, the evaluation of the activity of this chemotherapeutic drug and the morphological change it induces will be related to biophysical changes occurring in the cell.

The experimental use of HepG2 has already been explained in detail in Chapter 1. This cell line has been used in the literature to evaluate the toxic effect of a wide range of drugs, including 5-FU. There are studies which suggest that apoptosis is occurring after 5-FU is applied, but nevertheless it is promising drug for cancer treatment (Yu et al., 2015, Tan et al., 2009).

Apoptosis is a distinctive and important mode of "programmed" cell death. It is an essential component of several processes ranging from ageing to embryogenesis, and can be a contributing factor in various health conditions, for example cancer. There are many conditions and stimuli which can induce apoptosis but in the case of chemotherapy DNA disruption is the main reason for apoptosis. On the cell surface, there is early recognition of phagocytic behaviour by adjacent cells towards apoptotic cells (Elmore, 2007). This phagocytic process ensures minimal effect to surrounding cells because the apoptotic cells are removed and do not leak inflammatory factors and signals into the environment. During apoptosis, the normally inward facing phosphatidylserine (PS), translocate the cell membrane and is expressed on the outer layer of the plasma membrane (Bratton et al., 1997). PS is a ligand which is used for recognition of apoptotic cell surface as normally PS is inaccessible on the inner membrane surface in living cells. Annexin V is a plasma protein and is a PS-binding protein. Experimentally, it is used to detect apoptotic events when labelled with a fluorescent stain, e.g. Fluorescein isothiocyanate (FITC)-Annexin V.

The intracellular arrangement of actin fibres can be a hallmark of apoptotic behaviour due to the reorganisation of these fibres (Desouza et al., 2012). The structural network of a cell is important for many biological functions. In apoptosis, actin fibres arrange themselves around the cell membrane, strengthening the membrane, and preventing the disintegration of the cell, and loss of its intracellular contents. Actin fibres are known to be degraded by caspases (Charras et al., 2006) which can be related to blebbing at the cell surface. Actin also plays an important role when it comes to regulating mitochondrial membrane permeability in mammalian cells (Calderwood et al., 2006). Several studies have suggested actin as an initiator of apoptosis pathways as the change in actin distribution results in subsequent morphological and biochemical actions throughout the cell (Desouza et al., 2012). The changes in the cytoskeleton could lead on to caspase activation which permanently fragments the actin filament. Caspase activation creates a contractile force generated by the actin structure and is believed to guide the formation of membrane blebs (Coleman et al., 2001).

Atomic Force Microscopy (AFM) is a versatile tool which has a wide range of possible applications. A well-documented application of AFM is force-distance measurements from which can be derived physical properties such as the estimation of elasticity of various sample types (Picas et al., 2012). In biological applications, this measurement of tissue and cell elasticity can be very advantageous, as it subsequently allows experiments with biological samples to occur in conditions where the mechanical properties mimic physiological conditions. However, there is complexity to AFM and the setup of experiments can be time-consuming, which was often found to limit progress.

As explained previously in section 1.8, force distance curves produced with the AFM can provide different information, for example, with the use of different frequencies elastic and viscosity measurements can be deduced. Before obtaining these force curves, three basic but important parameters are required: these are probe tip geometry, deformation of the sample and the degree of the cantilever deflection. Force measurements obtained by AFM are fundamental and the forces involved can range from electrostatic, magnetic, van der Waals, steric, hydration and hydrophobic forces (Müller and Dufrêne, 2011b).

The most important piece of hardware required for an AFM experiment is the cantilever. A cantilever can be produced in many shapes and sizes, and it is then mounted on a base which elongates to a tip (Chapter 1). Standard AFM probes (sharp tips) have a generic spring

constant and tip geometry provided by the manufacturer, but it is unusual to find two cantilevers with the same parameters, as described in Chapter 2. However, there are ways to minimise this issue. For accurate force distance measurements, these parameters relating to the cantilever should be well-defined. The analyses of soft materials, such as living cells are known to be heterogeneous and therefore will deform differently when a cantilever is applied. Additionally, adherent cell height is in the range of micrometres whilst the sharp tip of the cantilever is a thousandth of the size and it is complex to compare one cell to another.

Tip functionalisation is frequently used for soft samples; this was first proposed in 1991 (Ducker et al., 1991, Butt, 1991). Ducker and co-workers glued silica microspheres onto a tipless cantilever while instead Butt used glass microspheres in the same way. The microsphere setup allows measurements of force to be obtained at a minuscule range (picoN-nanoN), but over a larger area (2-15µm). As these microspheres have a generic geometry, the forces can be more quantitatively analysed and the measurements become more sensitive as the total force is higher.

Cellular mechanical properties can be altered for a range of reasons such as development of apoptosis, disease and many other pathophysiological processes (Cross et al., 2007). Many studies have attempted to correlate different diseases with the cells ability of cells to deform (Lekka, 2016, Lekka et al., 2012b, Lal and Arnsdorf, 2010), but the answer is more complex than first thought. Each cell type has different morphology and biophysical properties, therefore, the elasticity values vary. If there are biophysical or morphology changes within the cell, surface properties such as roughness or adhesion. The value of Young's modulus can assist in understanding these changes within the cell. However, in the literature there are a wide range of values for Young's modulus achieved by AFM. For example, a table in a review by Kuznetsova and co-workers demonstrated these large deviations and a range of values for Young's modulus of mammalian cells showed HUVEC cells to have a large range of values from 0.9kPa to 18kPa in untreated cells (Kuznetsova et al., 2007). These heterogeneities of results can be due to variation in the living biological samples but also in misunderstandings in the method of AFM being applied.

In this study, HepG2 cells were exposed to 5-FU to analyse the toxic effects in terms of cell viability, proliferation and morphology. Any significant changes within this cell line caused by specific concentrations of 5-FU were correlated with visualisation of apoptotic changes at

the cell surface, and changes in cell mechanics. As this drug inhibits and promotes different molecules within the cell it is believed to be beneficial to observe the changes which could occur at the cell surface. The observations emphasised the importance of the cell's elastic behaviour, and changes were related to the toxic events.

Aims

This chapter investigates a toxic effect induced by 5-FU and relates this to mechanical changes (Young's modulus). The toxic effects of 5-FU were assessed at different concentrations and time points by means of:

- NR and MTT assays to analyse the cell viability
- BrdU cell proliferation assay
- Flow cytometry to investigate apoptosis
- Fluorescent microscopy to analyse distribution of actin fibres and live/dead staining of the cells
- Atomic Force Microscope to investigate fine surface details, and mechanical properties of the cell
- Analysis of force distance curves produced after treatment with 5-FU
- Comparison of the pyramidal and colloidal probes to provide Young's modulus values after treatment with 5-FU

3.2. METHODS

The general methods used throughout this thesis can be found in Chapter 2. Specifically, the methods following are only used within this chapter.

3.2.1. TREATMENT OF CELLS WITH 5-FU

The cell viability experiment had a range of concentrations of 5-FU applied to HepG2 cells. This ranged from 0.01-1000µg/ml, over 24, 48 and 72h time points to analysis the toxic effects. In the case of BrdU, the one application of 5-FU was applied for 24 and 48h and lower concentrations (0.0001-1000µg/ml) were used

3.2.2. FLOW CYTOMETRY BY FLUORESCENCE-ACTIVATED CELL SORTING (FACS)

3.2.2.1. DETERMINATION OF APOPTOSIS

7-Amino-actinomycin (7-AAD), Annexin V-PE, CaliBRITE™ beads, FACS flow solution, the 12-well plates and the flow cytometry tube were obtained from BD Bioscience; Oxford. Annexin buffer contains 0.01M HEPES (4-(2-hydroxyethyl)-1-piperazineethanesulfonic acid), 0.14M NaCl and 2.5mM CaCl$_2$ which were all purchased from Sigma-Aldrich; Dorset, UK. The Parafilm® and TrypLE were obtained from Thermo Fischer.

The HepG2 cells were washed with versene and then TrypLE was used to dissociate the adherent cells from the culture flasks for 5min. The cells were transferred into a FACS tube and centrifuged at 200xg for 5 min. The supernatant was removed and the cells resuspended into 200µl of DPBS. As before, the cells were centrifuged and supernatant was aspirated. To ensure the cells were still viable, a sample amount of control cells was analysed by Trypan blue (see section 2.3.1). After the cells were again resuspended in 100µl of Annexin buffer, 5µl/sample of Annexin V- phycoerytrin (PE) and 0.25µg/5µl 7-Aminoactinomycin D (7-AAD) was added to each cell tube. The cells were vortexed for 15min at room temperature in the dark. Following the completion of the 15min incubation period, 200µl of both Annexin binding buffer and FACS Flow were added to tubes.

Firstly, it is required to set the fluorescence compensation and adjust the sensitivity and settings of the instrument. Three compensation measurements were required to define apoptosis (unstained, PE and PerCP staining compensation), this was achieved by take the

500µl FACS flow followed by drop of the compensation CaliBRITE™ beads. The data collection was undertaken on a BD FACS Canto™ Flow Cytometry and data was analysed using FlowJo software version 10. With each sample, the instrument had to record 20,000 events.

The output of the data could define if the cells were viable, necrotic, in early stages of apoptosis or in late stages of apoptosis. Each of these possible outcomes is typically represented within a quadrant, Figure 3.1. During early apoptosis, Annexin V can to bind to the negative to phosphatidylserine (PS) which is redistributed throughout the inner to outer layer of the cell membrane. To clarify, cells in early stages of apoptosis are not permeable to 7-AAD but are to Annexin V. In later stages of apoptosis, the cell membrane is compromised and both Annexin V and 7-AAD are allowed to bind. When cells have 7-AAD bound to DNA and not Annexin V, are expressed as necrotic due to mechanisms not being related to apoptosis.
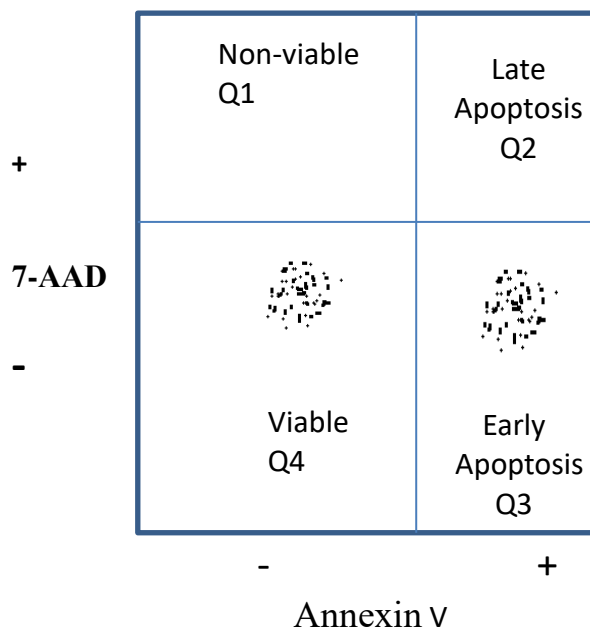
Figure 3.1 – Example of output given by Flow Cytometry Early apoptosis was defined using Annexin V conjugated to PI which allowed identification of the quadrant Q3. Each quadrant can be related to: Q1- Necrosis, Q2- Late apoptosis, Q3 – Early apoptosis, and Q4- Viable cells.

3.3. RESULTS

3.3.1. EFFECTS OF 5-FLUOROURACIL ON HEPG2 CELL VIABILITY AS ASSESSED BY NR AND MTT ASSAYS

A range of concentrations of 5-FU was applied to HepG2 cells over a period of 24, 48 and 72h. Over a 24h period, at concentrations above 100µg/ml, cell viability showed a linear trend for both assays used, NR and MTT (Figure 3.2). The toxicity as measured by different assays can be readily compared by calculating the concentration which decreases the cellular response of each assay by 50% (LD_{50} values), by linear regression over the linear portions of the dose response curves using the line of best fit to the data. The LD_{50} measurements of the cell metabolic activity by the MTT assay is a more sensitive assay and the LD_{50} value for 5-FU is significantly lower than that of the NR assay, after 48 and 72h exposure. After 24h exposure there is no significant difference between the LD_{50} values obtained from these two assays.
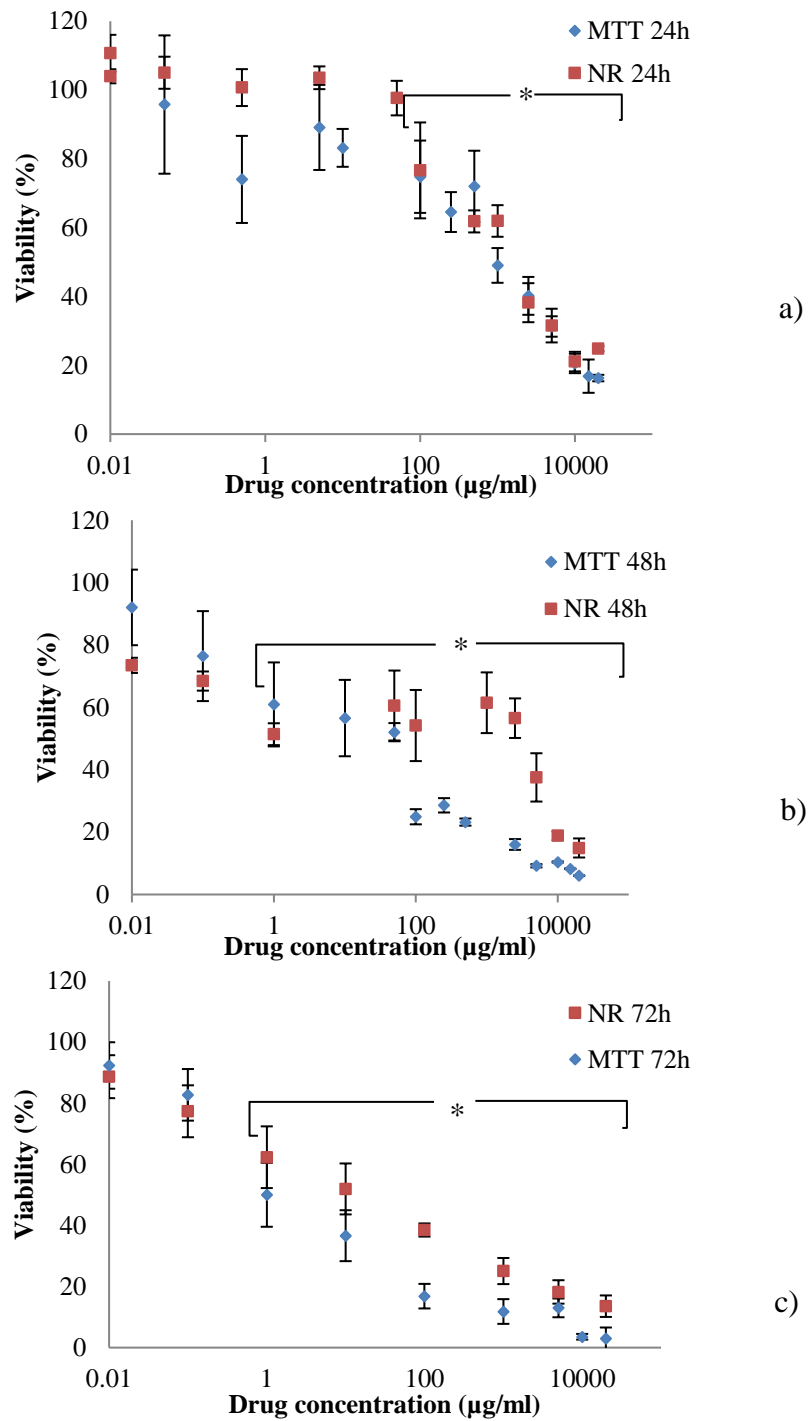
Figure 3.2 - Cell number (NR) and metabolic activity (MTT) of HepG2 cells treated with 5-FU. Control values were set to 100% viability. The viability values are percentage differences compared to controls (±SEM, n=6). After arbitrarily, a) 24h b) 48h and c) 72h exposure. By one-way ANOVA test followed by Dunnett's multiple comparison significant differences (*) were detected compared to the respective control values without drug (p<0.05).

LD$_{50}$	24 hours	48 hours	72 hours
MTT	1441± 113 µg/ml	9.40±0.41 µg/ml*	3.80±1.10 µg/ml*
NR	1434± 78.7 µg/ml	74.32± 31.96 µg/ml*ł	13.40 ±2.77 µg/ml*ł
BrdU	10.60±5.87 µg/ml ł	0.15 ±0.9µg/ml*ł	

Table 3-1- LD$_{50}$ of the HepG2 cells when treated with 5-FU for set time points. The LD$_{50}$ values are the concentrations of 5-FU which inhibited each response by 50%. By one-way ANOVA test followed by Dunnett's multiple comparison significant differences were detected over time (*) compared to 24h results and between assay type at the same time point (ł). ($p < 0.05$)

3.3.2. EFFECTS OF 5-FLUOROURACIL ON HEPG2 CELL PROLIFERATION BY THE BRDU ELISA METHOD

The BrdU cell proliferation assay was used at 24 and 48h time periods after treatment with 5-FU at different concentrations. There is a significant decrease in cell proliferation at concentrations higher than 0.01µg/ml after 24h of treatment (Figure 3.3). These concentrations were also used in parallel for cell number and metabolic studies in the NR and MTT assays, and the LD$_{50}$ values for all three effects are shown on Table 3.1. The LD$_{50}$ value for the BrdU response is markedly less than that for either NR or MTT, suggesting that the cells are most sensitive to the DNA synthesis inhibition of 5-FU.
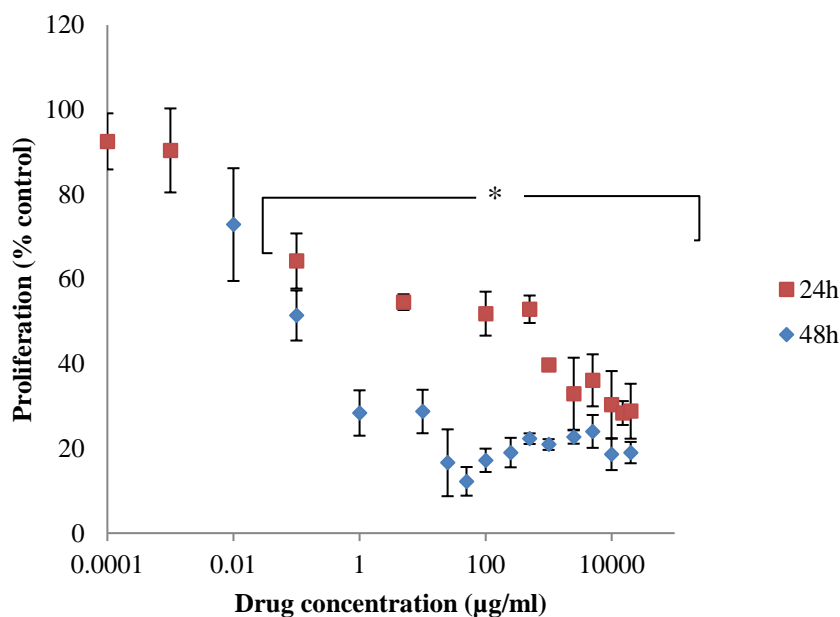
Figure 3.3 - Proliferation assay (BrdU) with HepG2 cells treated with 5-FU over a period of 24 and 48h. The proliferation is expressed as percentage compared to controls, which are expressed as 100% (±SEM, n=8). By one-way ANOVA test followed by Dunnett's multiple comparison significant differences (*) were detected compared to the control values (p<0.05)

3.3.3. EFFECTS OF 5-FLUOROURACIL ON HEPG2 CELL APOPTOSIS MEASURED BY FLOW CYTOMETRY

The procedure of flow cytometry can be used to distinguish between cells that are viable, in early or late stages of apoptosis or necrotic using Annexin V and 7-AAD stain (Figure 3.1). The Annexin V stain binds to the negatively charged phospholipid phosphatidylserine (PS) when it has relocated to the outer layer of the cell membrane during apoptosis. In early stages of apoptosis, the cell is not permeable to 7-AAD but in later stages it becomes permeable as the cell membrane becomes comprised. Necrotic cells have 7-AAD bound to DNA but are not Annexin V positive as they are not undergoing apoptosis.

The presence of apoptosis was determined by flow cytometry using Annexin V and 7-AAD after 24, 48 and 72h of treatment with 5-FU. The initial toxic effect was seen in the MTT experiments shown on Figure 3.2 at 100µg/ml at 24h so this concentration was used as a starting point for detecting early apoptosis. The quadrants which are produced by flow cytometry can define if the cell is viable, in early apoptosis, late apoptosis or necrosis (Figure

3.4). In Figure 3.4, there is a movement from viable cells to early apoptotic cells when analysing treated and untreated cell after 72 h. The cells in early apoptosis are located in quadrant three, and stained with Annexin-V only, and have not progressed to a late stage of apoptosis, where they would be stained with both Annexin V and 7-AAD.
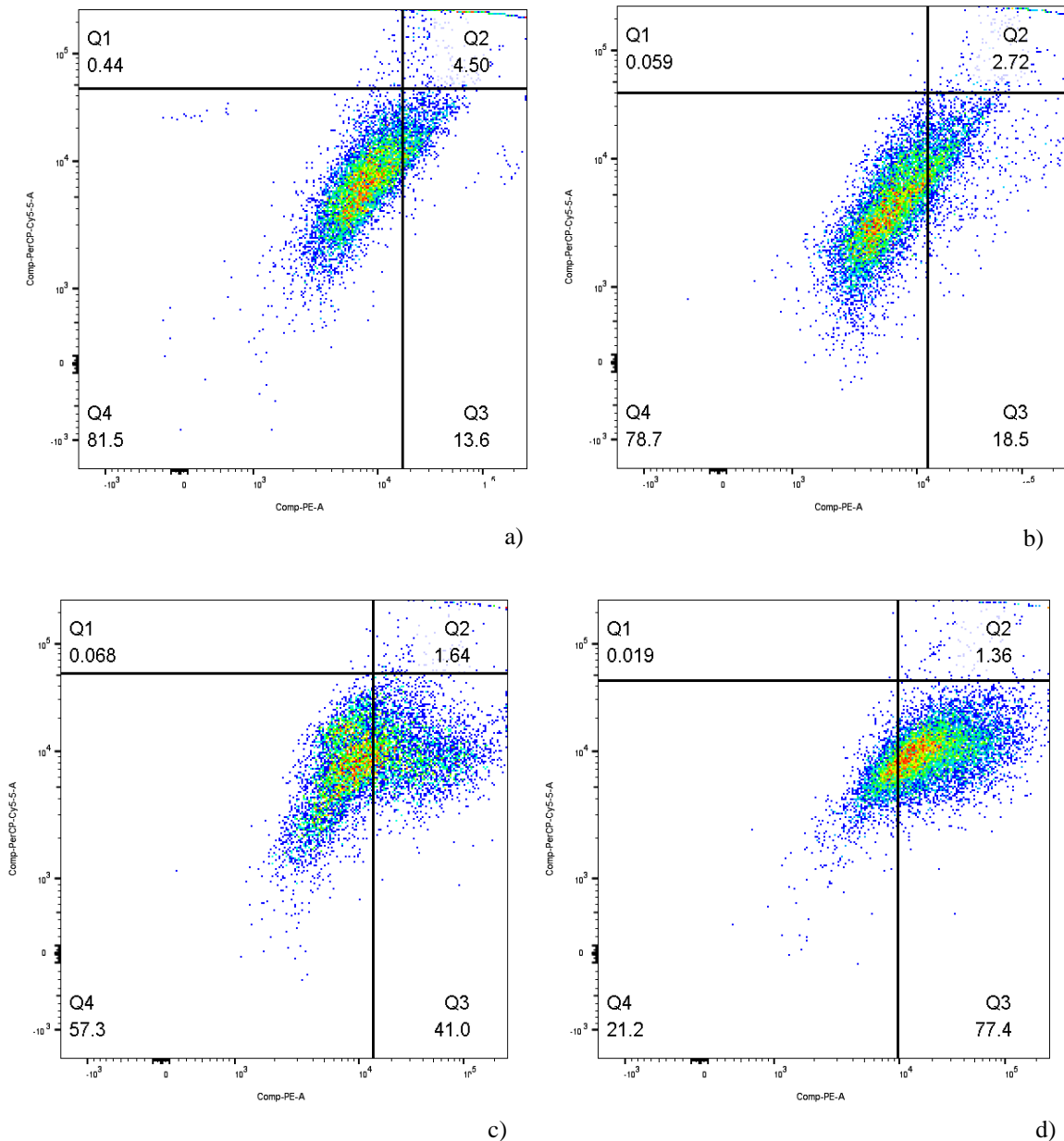
Figure 3.4 - Flow cytometry example of one experiment with HepG2 cells treatment with concentrations of 5-FU over a 72 h period. Early apoptosis was defined using Annexin V conjugated to PI which allowed identification of the quadrant Q3. Each quadrant can be related to: Q1- Necrosis Q2- Late apoptosis, Q3 – Early apoptosis and Q4- Viable cells. a) Control b) 0.05µg/ml c) 5µg/ml d) 500µg/ml

After repetition (n=5) of the flow cytometry experiment, a mean value can be achieved from the area of Q3 which is defined as the area of early apoptosis (Figure 3.5)
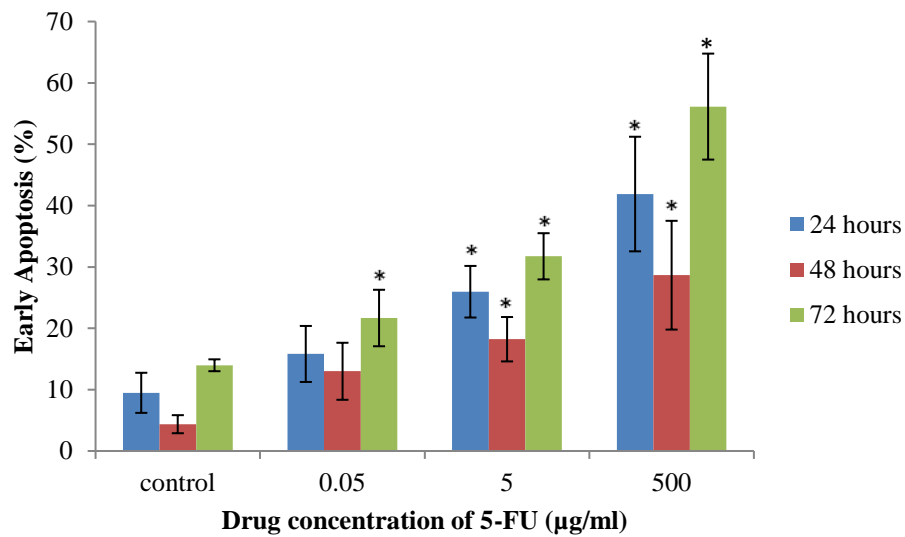
Figure 3.5 - Early apoptosis results after treatment with 5-FU are expressed as percentages of Q3 events measured by FACS. Results are mean values (±SEM, n=5). All experiments were performed independently at three time points. By one-way ANOVA test followed by Dunnett's multiple comparison significant differences (*) were detected compared to the control values (p<0.05)**.**

3.3.4. EFFECTS OF TREATMENT WITH 5-FLUOROURACIL ON MORPHOLOGY OF CELL INVESTIGATED BY LIGHT MICROSCOPY.

Cells were imaged using the light microscopy to determine if the cell morphology was affected by 5-FU (Figure 3.6). At lower concentrations of 5-FU, there is no visible difference between treated and untreated cells. However, there is a noticeable difference at the higher concentration where the cells have changed dramatically and shrinkage has occurred, with the cells having a rounded morphology (see Figure 3.6b).
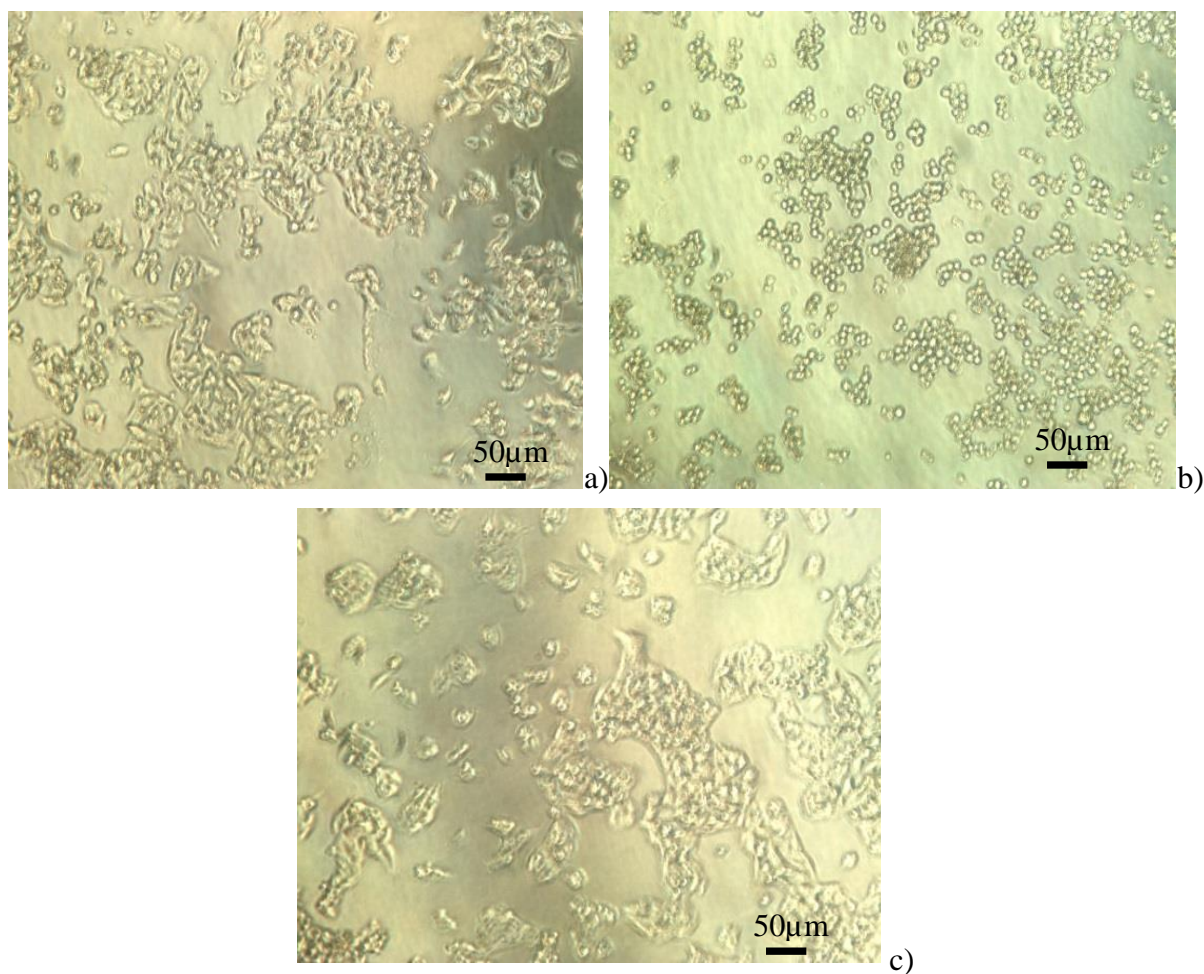
Figure 3.6 - Light microscopy (x20, Nikon Microscope) of HepG2 cells treated with 5-FU . Cells were seeded at $1x10^5$ cell/cm^2 for 24h and then 5-FU was applied for 48h with a concentration of 0.05µg/ml (a), 500µg/ml (b) and control (c). These images are representative of 4 different experiments. The scale can be applied throughout.

3.3.5. EFFECTS OF 5-FLUOROURACIL ON CELL MORPHOLOGY WITH USE OF FLUORESCENCE MICROSCOPY

The cell morphology was determined by fluorescence microscopy at three time points with three different concentrations of 5-FU. Propidium iodide (PI) and Acridine Orange (AO) stains were used on the HepG2 cells plated on 35mm^2 petri dishes and they were then analysed under a Carl Zeiss Axio Imager microscope using x20 (Numerical aperture, NA= 0.5) or x40 (NA=0.8) water lens. For the green fluorescence, the excitation wavelength was 450 - 490nm and emission wavelength was 515-565nm. With treatment, obvious changes can be seen in cell morphology when comparing the control and treated after exposure at certain time points.

94
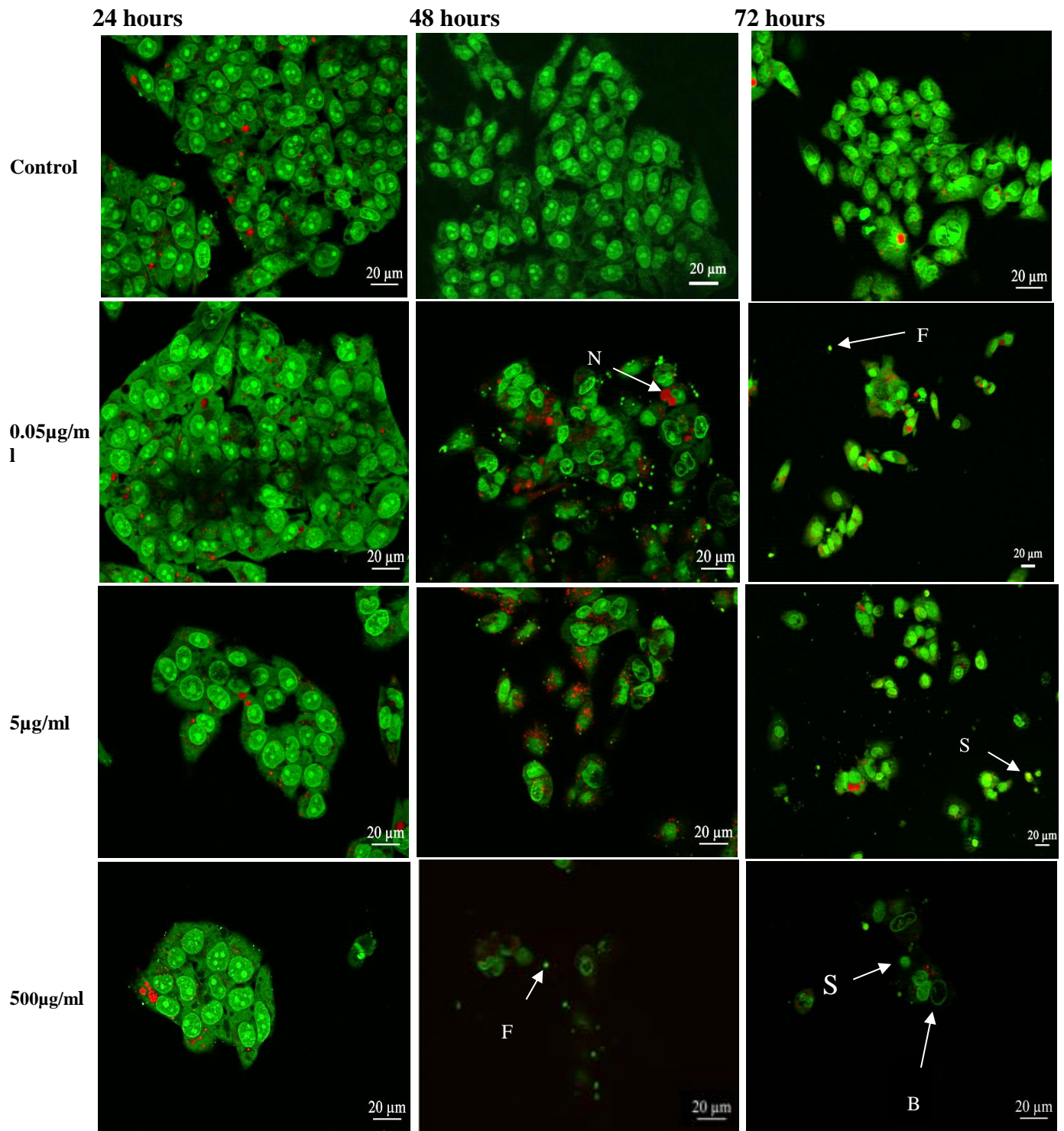
Figure 3.7 - Fluorescence microscopy images (20x) of HepG2 cells after staining with PI (Dead cells, red) and AO (Live cells, green) after exposure to different concentration of 5-FU . These images are representations of 5 different images at the set points (24, 48 and 72h). "B" indicates cell blebbing, "S" indicates cell shrinkage, "F" indicates fragmentation and "N" indicates necrotic and using the fluorescence microscopy at an excitation wavelength of 450 -490nm and emission wavelength of 515-565nm.

After exposure to 5-FU, cells were found to have evident changes in morphology in comparison to the control samples. After 72h, cells treated with 0.05µg/ml 5-FU did not seem to change morphologically, but over time there was a decrease in cell number when compared to control. In the presence of 5-FU at higher concentration, the cells appeared apoptotic showing indications of shrinkage and blebbing (Figure 3.7).
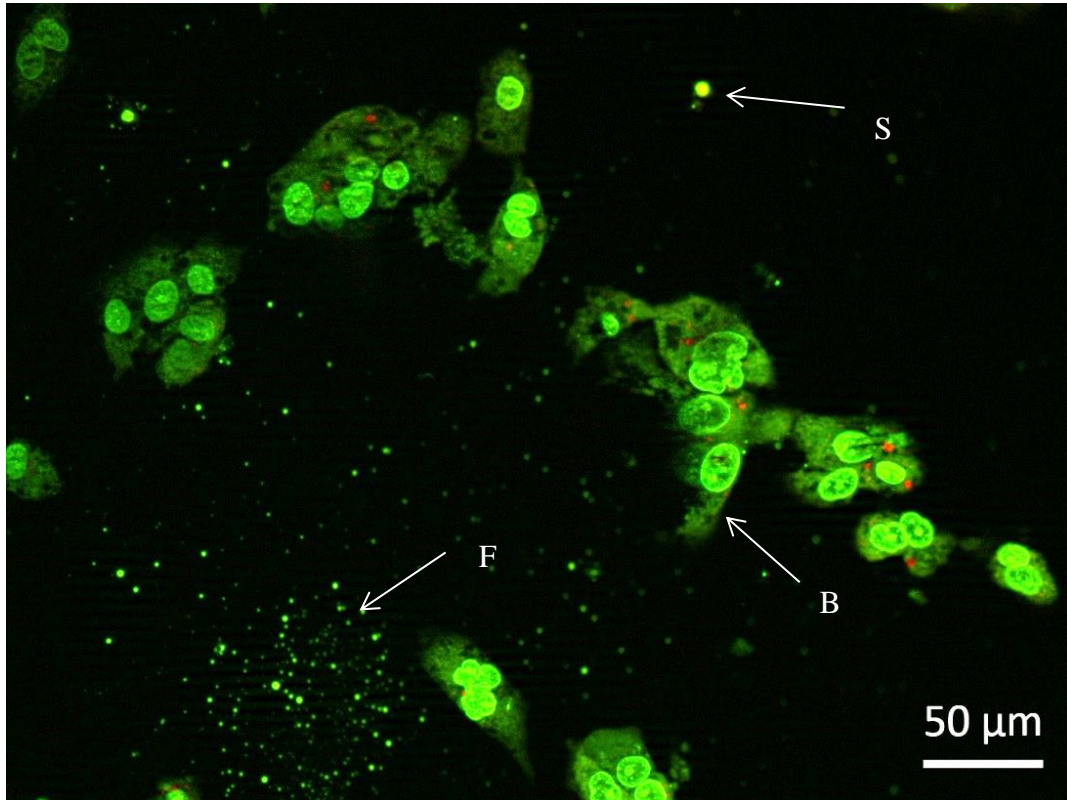
Figure 3.8 - Fluorescence microscopy image following PI (Dead cells, red)/AO (Live cells, green) staining of HepG2 cells treated with 5µg/ml of 5-FU for 48h. Magnified image (x40 water lens, NA=0.8) of HepG2 cells after treatment with 5-FU at 48h. "B" indicates cell blebbing, "S" indicates cell shrinkage and "F" indicates fragmentation and using the fluorescence microscopy at an excitation wavelength of 450 -490nm and emission wavelength of 515-565nm.

Figure 3.8 and Table 3.2 emphasise the effect of 5-FU on HepG2 cells. In magnified image (Figure 3.8), cells showed indications of blebbing and shrinkage. Over the range of concentrations, it was observed that cell number was affected and over longer periods of time the cells numbers began to diminish compared to the control cells. The cell numbers in Table 3.2 can be compared to Figure 3.1, where a rapid decline in cell number can be seen at 72h,

for example, using the NR assay. Cell numbers in the control sample, in contrast, have increased between 24 and 72h indicating cell proliferation.

	Mean number of viable cell (AO, live cells, green)			
	control	0.05µg/ml	5µg/ml	500µg/ml
24	47.50±1.49	41.38±2.79	21.125±1.74 *	9.75±0.71 *
48	51.78±1.92	26.13±1.17 *	14.53±0.69 *	4.5±0.54 *
72	58.13±2.45	19.55±0.64 *	11.33±1.89 *	2.89±0.34 *

Table 3-2 Mean number of viable HepG2 cells recorded by Confocal Laser Scanning Microscopy after staining with Acridine Orange and Propidium Iodide. Results are data across 25 independent images from each sample (mean ± SEM) Significant differences from the controls were determined by one-way ANOVA followed by Dunnett's multiple comparison test ($p < 0.005$).

Phalloidin-FITC, was used to examine at the actin fibres of the HepG2 cells after 5-FU treatment. At three time points (24, 48 and 72h), the cells analysed with the Carl Zeiss Axio Imager microscope, images were captured with the AxioVision 4.6 software. These images are shown in Figure 3.9, using the fluorescence microscopy at an excitation wavelength of 450 - 490nm and emission wavelength of 515-565nm. Additional images can be found in the appendix (Figure A5).
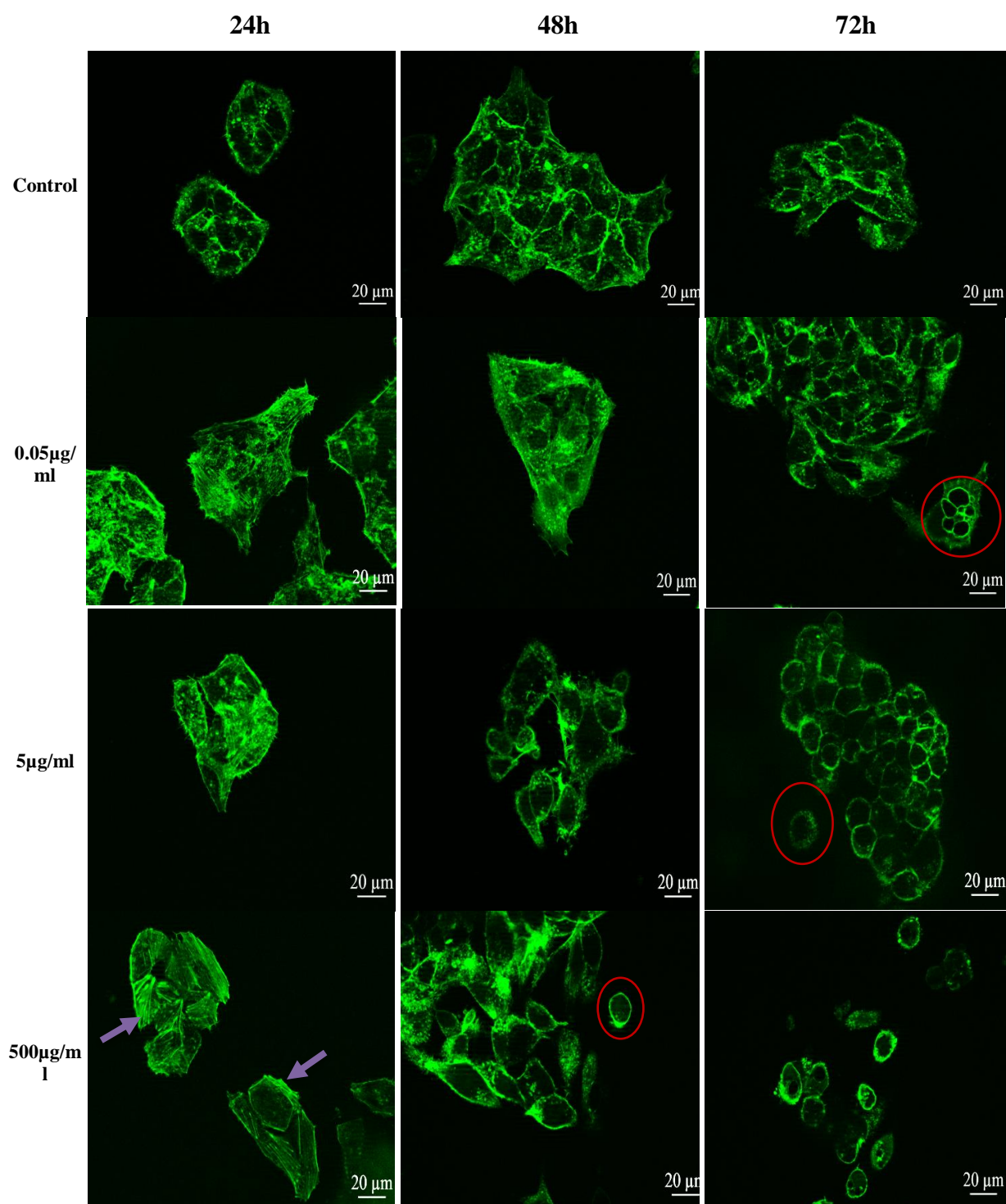
Figure 3.9 - Fluorescence microscopy images (40X water lens) following Phalloidin-FITC (actin) staining of HepG2 cells treated with 5-FU at three different concentrations of 5-FU (0.05, 5, 500µg/ml) after 24, 48 and 72h. The purple arrows indicate areas where the actin fibres are seen to be thick and prominent. Red coloured circles show some cells which have actin fibres around the circumference rather than an even distribution. Seven different images were taken for each control and treated sample at the end of each time point, and one from each is represented above.

The control cells were found to remain in clumps over the three time points, but this was less common in the treated cells. The treated cells, particularly those treated with 500µg/ml, have withdrawn from each other, and were mainly isolated cells rather than clumps. Over the first time point (24h), unconventional actin fibres can be seen at all concentrations compared to the control cells, where fibres are prominently thicker. At 500µg/ml, more emphasis of these fibres can be seen (highlighted by the arrows) where these parallel fibres are more prominent. After 48h, there is a change observed in distribution of actin fibres within the cells; the actin fibres reinforce the surface and at 72h clear indications can be seen that apoptosis is occurring.

3.3.6. EFFECTS OF 5-FLUOROURACIL ON CELL MORPHOLOGY WITH USE OF ATOMIC FORCE MICROSCOPY

AFM was used to show fine detail on the cell surface of one cell treated with 5µg/ml 5-FU for 72h. This image is a representation of 6 such images examined. In the image below (Figure 3.10), there are obvious signs of networking lines found throughout the surface. On the control cell (Figure 3.11), using the same amount of force (500pN), the same detail was not seen. The control cells were more complex to image than the treated HepG2 cell as shown in Figure 3.11. More observations can be made when altering the loading force to 100pN as the networking fibres are more apparent and appearances of circular protrusion can be seen (Figure 3.12). These were not observed in the control cells. After treatment with 5-FU, these protrusions were seen at 100pN in Figure 3.12. The amount of protrusions observed varied in each cell studied, and the size of the protrusions varied but appeared circular, as highlighted in the figure.

a)
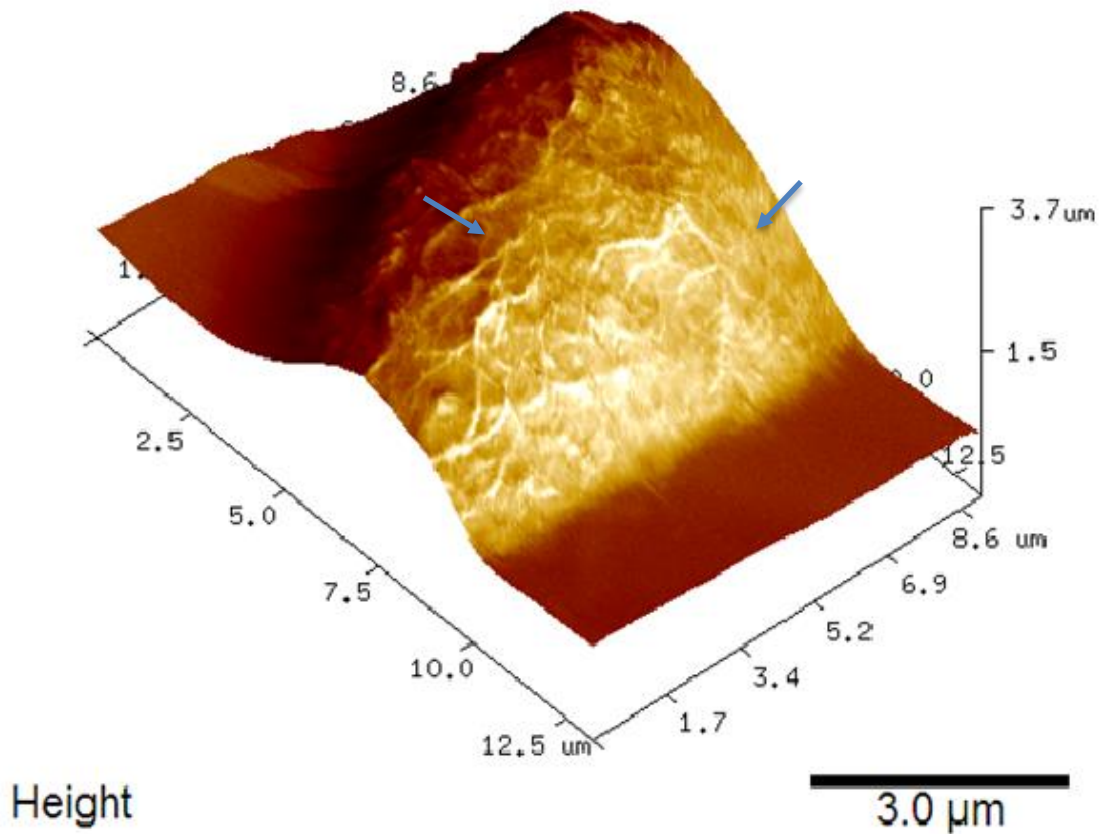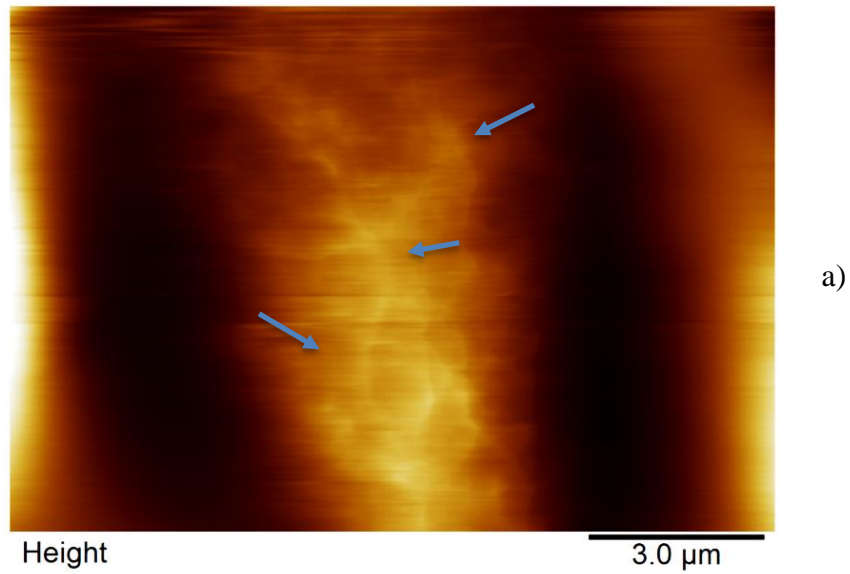
Figure 3.10 - HepG2 cell after treatment with 5µg/ml of 5-FU for 72h. The blue arrows indicate networking lines. a) 2D height image b) 3D height overlay of the HepG2 cell. This image was obtained in tapping mode and captured at a scan rate of 1Hz and loading force of 0.5nN.

Height   3.0 µm

a)

Height   3.0 µm
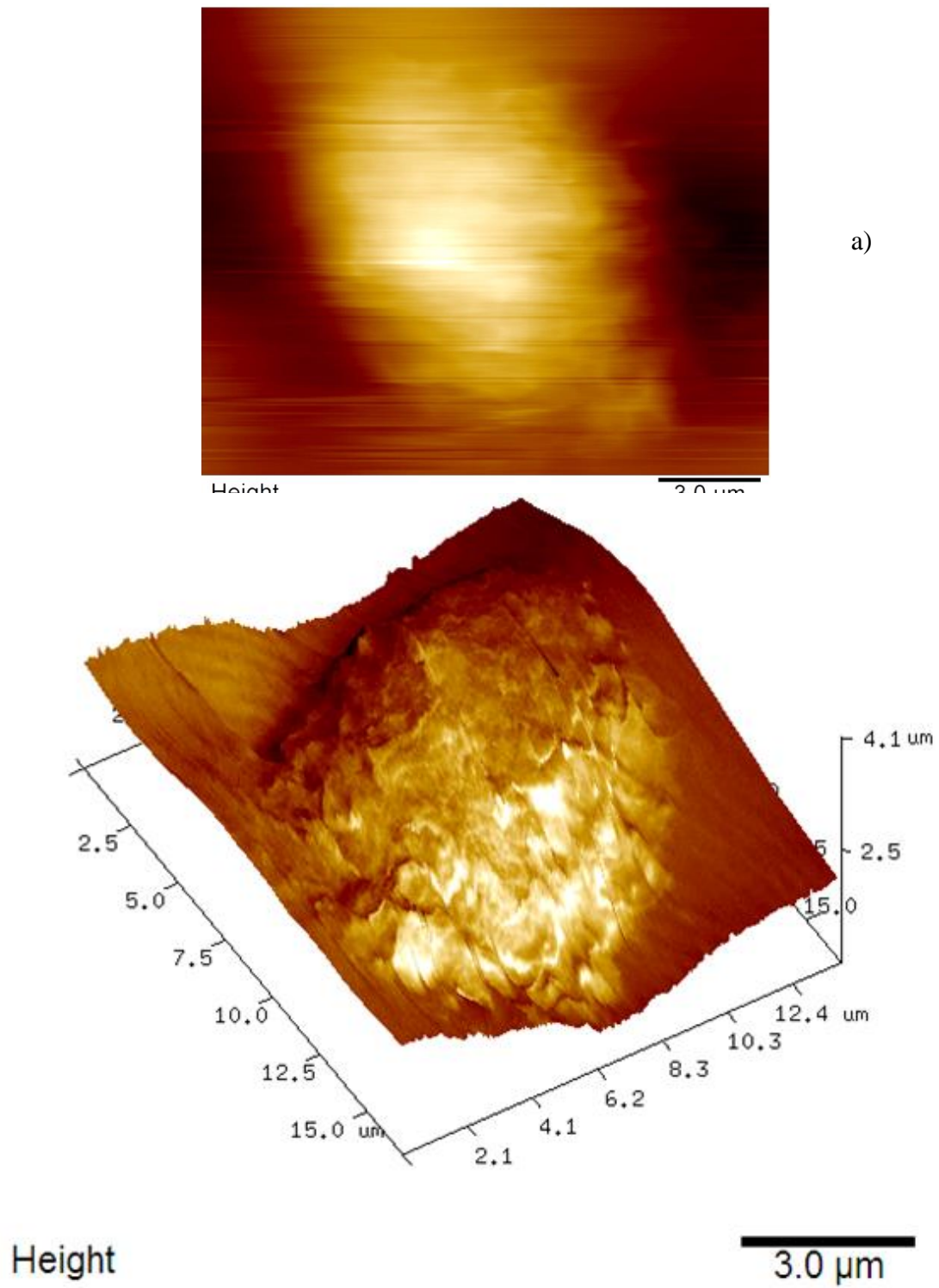
Figure 3.11 - HepG2 untreated control cell. There are no obvious protrusions seen on the cell surface in comparison to the treated cell. a) 2D height image b) 3D height overlay of the HepG2 cell. This image was obtained in tapping mode and captured at a scan rate of 1Hz and loading force of 0.5nN.
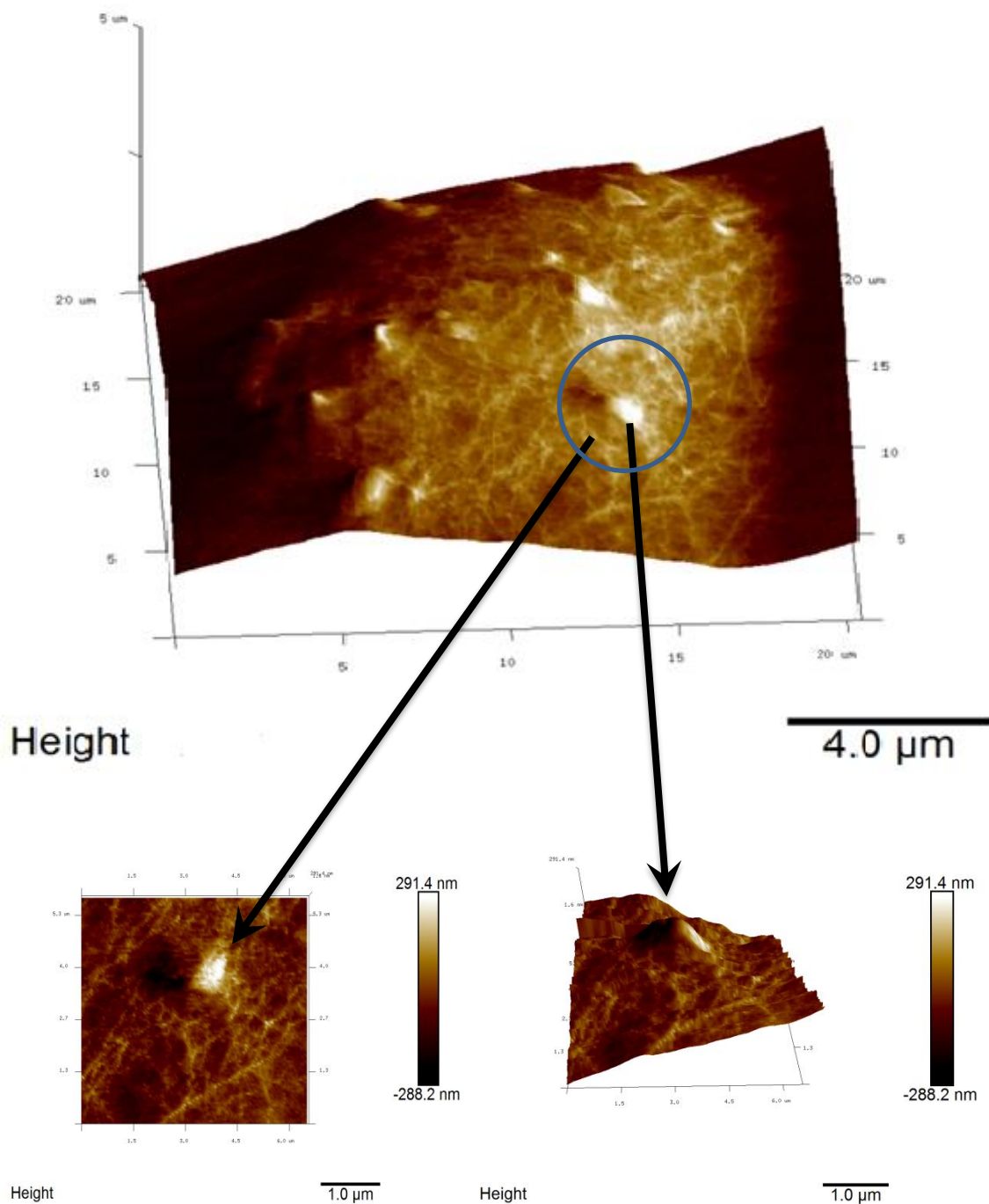
Figure 3.12 - 3D image of HepG2 cell after treatment with 5µg/ml of 5-FU for 72h. One point of the cell has been highlighted (blue circle) and in the zoomed in area, actin fibres can be seen and a protrusion is noticed. This image was taken in Bruker Peak Force QNM mode, with scan size of 20µm, scan rate of 0.5Hz and a loading force of 0.1nN. The cell can be seen to be uneven and protrusions are clearly seen on the cell surface.

The roughness of the cell surface was calculated in the Nanoscope software, over a scan size of 4µm². Over the six untreated cells, the roughness value was calculated to be 290.67 ± 14.72nm (n = 6, ±SEM). The roughness of the cell after application of 5-FU was increased to 372.0 ± 20.1nm (n = 6, ±SEM), even though the cell is presumably going through apoptosis and is shrinking. The increase in roughness after treatment with 5-FU could be related to the protrusion and networking fibres shown in Figures 3.10 and 3.12.

In this study, the aim was also to analyse Young's Modulus to see if alterations in cell stiffness occur after the treatment with 5-FU. Also, an investigation was carried out to analyse the effect on tip geometry on Young's modulus values. The elasticity results from the HepG2 cells were obtained by indentation with a sharp pyramidal tip (Bruker AFM probe) and a spherical microsphere mounted on a tipless cantilever (See section 2.5.3). As previously stated, every cell was indented five times over the nuclear region.

Individual force curves could be used to visually analyse any other interactions occurring between the cantilever and cell surface. The force curves which were obtained with the pyramidal indenter did not give any additional information apart from the Young's modulus values. This could be because the area in contact to the surface is smaller when the pyramidal indenter is used. However, the spherical probe shows that a large release of force occurs when the cantilever is removed from the surface of a cell after 72h exposure to 5-FU (Figure 3.13). There was no similar occurrence with the control and the 24h 5-FU treated cells.
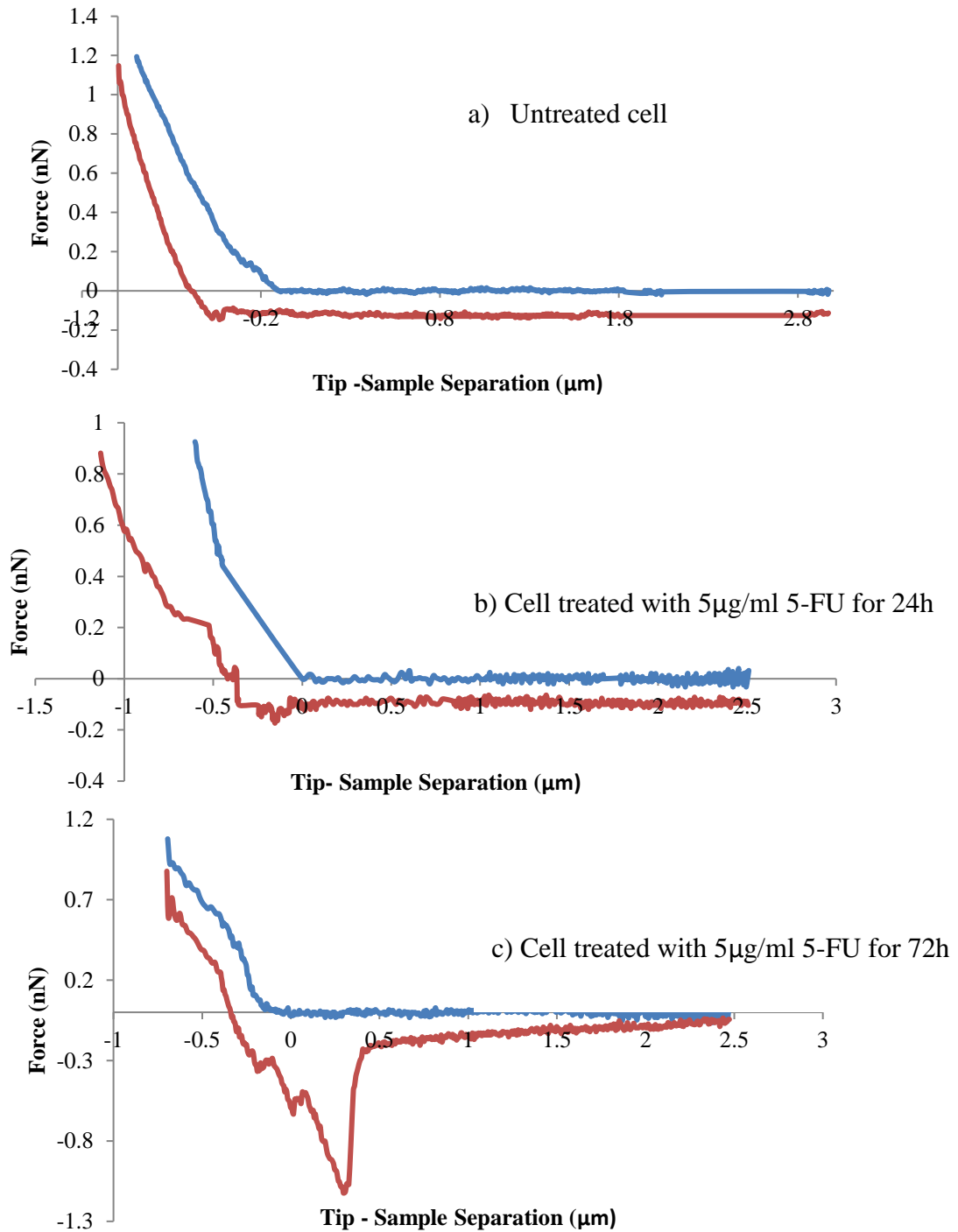
Figure 3.13 – Force distance curves on HepG2 cells treated with 5-FU. In these graphs, the line of approach is the blue curve and the retraction curve is orange. Cells had a loading force of 1nN and approach velocity of 2µm/s. a) Untreated HepG2 cell, b) HepG2 cell 24h after treatment with 5µg/ml 5-FU c) 72h after treatment with 5µg/ml 5-FU – in this figure, a negative force has occurred, this is due to the cantilever still being attached to the surface.

In total, 75 cells were indented for control cells, and cells treated with 5µg/ml 5-FU for 24h and 72h (Table 3.3). As seen in Table 3.3, the elasticity values obtained from the sharp pyramidal probe were at least four times higher those obtained when using the spherical indenter (in the case of the control). There is an increase in Young's modulus obtained between the two indenters after treatment with 5-FU, but no significant differences were detected between control and treated cells using pyramidal indenter. The cells indented with the spherical probe showed a decrease in Young's modulus after treatment with 5-FU over 24h and 72h. The significant differences of the Young's modulus calculated, with the pyramidal probe were shown to be large (Table 3.3). Standard error mean values suggest there were a few outliners, however, when analysing the data over 15% of the values were in the higher range. The outliers were not removed to express the variance of results produced.

Treatment with 5-FU (YM in kPa)		
Tip Geometry	Control	24 hours	72 hours
Spherical	0.49± 0.12	0.28± 0.08*	0.32 ±0.09*
Pyramidal	1.64 ± 2.52	2.02 ±2.72	3.47 ±2.98 ǂ

Table 3-3 – Young's modulus of HepG2 cells after treatment with 5µg/ml 5-FU for two time periods (24h and 72h) and using different indenters (spherical and pyramidal). In total force curves were obtained from 75 cells (±SEM) at 5 regions. By one-way ANOVA test followed by Dunnett's multiple comparison significant differences were detected compared to the respective control values without drug *, and differences between the two indenters used ǂ($p<0.05$).

Summary of main findings

In this section, the effect of treatment of 5-FU on HepG2 cells was analysed, in terms of cell viability, morphology, proliferation, apoptosis, surface appearance and mechanical properties.

- Concentrations of 5-FU above 5 µg/ml were observed to influence metabolic function after 48 hours
- High concentrations of 5-FU showed greater toxic effect and the BrdU assay was shown to be the more sensitive compared with MTT or NR assay
- Exposures to concentration of 0.05µg/ml for 24 h did not appear to affect cell proliferation but the effect became apparent after 72 h
- Apoptosis was observed to be more prominent after 72 h exposure, with the majority of treated cells (0.05-500µg/ml) showing clear signs.
- Actin fibres were observed to move towards the cell surface after treatment (> 5µg/ml, after 48h)
- 5-FU treated HepG2 cells have noticeable membrane protrusions and highlighted networking lines at the surface when imaged on the AFM
- Force curves obtained by AFM showed an unbinding force when the cantilever is being removed from the surfaces of cells treated with 5-FU
- Young's modulus of HepG2 cells did alter significant after treatment with 5-FU when the spherical indenter was applied
- The pyramidal indenter showed greater value of Young's modulus in comparison to the spherical indenter

3.4.   DISCUSSION

Several chemotherapy drugs exert their therapeutic effect by inducing or promoting apoptosis. One of the aims of research is to enhance the chemotherapeutic effect, but avoid increasing the toxicity of the existing drugs. 5-Fluorouracil is a chemotherapeutic drug that has an influence on many cellular processes within multiple cell lines. Specifically, 5-FU is used as first or second line chemotherapy treatment for metastatic HCC (Song et al., 2015). 5-FU works mainly by the incorporation of analogue nucleotides into nucleic acids which subsequently influences DNA synthesis and can also induce apoptosis.

In this study, 5-FU has been shown at high concentrations to be cytotoxic in HepG2 cells even at early time points after initiating exposure. The results shown by Neutral Red and MTT assays showed that with increasing periods of time, the LD_{50} concentration value became lower, showing a concentration and time dependent effect regarding cell viability. Over time, the concentration of 5-FU required to reduce the metabolic function in HepG2 cells decreases. The cytotoxic effect expressed with the MTT assay compared to the NR assay is greater because 5-FU affects the metabolic pathways that reduce MTT. MTT is only measuring intracellular reductases not general metabolism, 5-FU could directly inhibit these enzymes or decrease the supply of NADH and NADPH. At exposure of up to 72 h, there is a clear linear dose dependent trend in the decrease of cell responses for both NR and MTT assays as shown in Figure 3.2.

In this study, the BrdU assay was used to analyse the proliferation of HepG2 cells after treatment with 5-FU. In Figure 3.3, after 24h of treatment the cells follow a dose dependent inhibitory trend in proliferation, but after 48h at concentrations above 1µg/ml 5-FU caused a significant decrease in the proliferation of the cells to approximately 20%. A similar dose dependent trend was shown by Brenes and co-workers where MTT activity was measured in HepG2 and Hep3B cells over concentrations ranging from 100-5000µg/ml at 24h (Brenes et al., 2007). As the BrdU assay is a direct measurement of DNA synthesis using the incorporation of the nucleoside to obtain measurements of proliferation, the experiment is highly sensitive. 5-FU disturbs DNA synthesis by incorporating into the DNA molecule, and halting further synthesis. The LD_{50} for the BrdU assay at 48h is 0.15 ±0.9µg/ml, compared with 9.40±0.41 µg/ml for the MTT assay, thus the mechanisms of 5-FU toxicity are more dependent on inhibition of DNA replication rather than on the activity of reduction enzymes

or the glycolytic activity. A study conducted by Vu and co-workers, showed cell proliferation at lower concentrations of 5-FU which allowed the hepatic cancer cells to still function (Vu et al., 2013). The concentration of 3.45 ± 3.21 µg/ml in this study was shown to have a significant *in vitro* effect on the cells after a period of 24h.

Apoptosis is usually characterised by examining alterations in morphological and biochemical properties of cells, including metabolism and appearances of apoptotic bodies. Also, when cells are going through apoptosis the chromatin structure is affected, the total DNA content decreases as the DNA is broken down, and DNA fragmentation occurs. Thus, 5-FU exerts its chemotherapeutic effects by inhibiting DNA synthesis rather than disturbing cell metabolism.

In this study, HepG2 cells were treated with 5-FU resulting in formation of apoptotic bodies, alterations in metabolism and the cytoskeleton. When the cells were analysed using PI and AO, the number of live cells seen over the 72h exposure time dramatically decreased (Table 3.2). Firstly, the untreated HepG2 cells were observed to be clumped together and their sizes were above 16µm. Over the first 24 h, there were no significant changes in the 5-FU treated cells at the three concentrations tested in comparison to the control cells, shown in Table 3.2. After 48 hours, there were noticeable differences, and there was a high possibility that apoptosis was occurring as cells were observed to be surrounded by debris. This is emphasised in Figure 3.6b as at the higher concentration of treatment at 48 hours there are signs of shrinkage, rounding of the cell and fewer clumps Also, it was noticed that the cell number was dramatically reduced as proliferation is decreased and the cells are lost to apoptosis.

When differentiating between the early and later stages of apoptosis, flow cytometry can be used (Filgueiras et al., 2013, Abaci et al., 2014). This procedure is carried out in a suspension of cells. As HepG2 are an adherent cell line, it was thought that even with the control cells they would experience a higher than usual level of apoptosis because the enzymatic removal of attached cells into suspension by the action of TryEE (cell dissociation enzyme). To ensure this was not the case, Trypan Blue was used to ensure the control cell viability post detachment from the culture well plates was above 75%. After 72h treatment, the most significant change in viability was noticed (Figure 3.5), over three quarters (78.8%±5.8) of cells detected were found to be at the early apoptosis stage. Even at the lower concentrations,

there was a significant difference. Dihydropyrimidine dehydrogenase (DPD) is an enzyme which catabolises pyrimidines (uracil and thymine, as well as 5-FU). Furthermore, it has been stated DPD can cause resistance to 5-FU due to it being highly abundant in the liver (Longley et al., 2003), this resistance was not observed *in vitro* within this study.

The actin fibres within cell lines are effected by 5-FU, causing severe disruption in the cytoskeleton. The cytoskeleton framework is required to maintain the structure of the cell and if this is disturbed, the cells lose their integrity and this can lead to apoptosis (Chang et al., 2009). By use of the fluorescence microscope it was found that 5-FU induced disruption of actin fibres occurs in parallel to apoptosis detected by flow cytometry. In untreated HepG2 cells, long-form and regular actin fibres can be observed (Figure 3.9). There is disorganisation of actin cytoskeleton evident in Figure 3.9, where the exposure time and dose of 5-FU are dependent factors. At the first time point (24 h), there are noticeable differences with the actin fibres at all concentrations in comparison to the control cells. The cytoskeleton remodelling process has begun and an obvious disruption is occurring which can be related to the polymerisation of the actin fibres (Desouza et al., 2012). At later time points, it was found that high concentrations of 5-FU caused blebbing and shrinkage of the cell (Figure 3.8). In a study conducted by Gordon and co-workers, actin fibres were shown to be disorganised after treatment with 5-FU in rat endothelial cells (Gordon et al., 2005). After 72h of treatment, very few grouped cells could be found at the higher concentrations of 5-FU (500µg/ml) and a small number of necrotic cells were frequently observed. It could be that while there is apoptosis occurring, the cells also are going through a secondary necrosis mechanism. The cell proliferation is inhibited by 5-FU as cell cycle arrest in G1 phase has been induced; which promotes cellular morphology changes including a reduction in the number of actin fibres. The cells were shown to have a reinforced surface (Figure 3.9), as the actin fibres move toward the surface. This reinforced surface could in turn be related to the blebbing which is occurring as the debris was seen to be surrounded by actin fibres as in the formation of apoptotic bodies.

AFM has become a useful tool for biological surface analysis as it has the ability to image cells under physiological-like conditions at a high resolution alongside monitoring other possible applications such as mechanical alterations or molecular interactions. Cells are known to be viscoelastic materials and there is considerable complexity when attempting to map their behaviour with AFM. Many studies have attempted to validate cell viscoelastic

behaviour by novel procedures adapted from AFM to give quantitative results (Hecht et al., 2015). The idea of this research was to relate possible toxic effects caused by drugs and relate them to mechanical changes (Young's modulus).

Most tips of cantilevers are pyramidal shaped which is good for imaging if they are sharp (See section 2.5.3). During use, the tips contact area is changing with every indentation so force curves can never be linear. The loading force applied to the cell should be kept constant throughout experiments. When using the AFM, the same parameters were used throughout the experiment with the 5-FU treated and untreated HepG2 cells (Figure 3.10/3.11). The surface detail was only observed in cells which had been treated with 5-FU. After 72h of treatment, the cell surface shows long and dense lines; this is assumed to be actin fibres. It should be noted that we have no direct evidence for this, and future additional experiments with antibodies to actin adhered onto the AFM probe could be designed. A similar experiment was conducted by (Silberberg et al., 2013), where the actin cytoskeleton was monitored by a functionalised nanoneedle to measure the unbinding forces from the surface. At points throughout the cell surface, bundles of the fibres can be observed (Figure 3.10). This can be related to the fluorescent microscopy images (Figure 3.9) which showed the movement of the proposed actin fibres towards the surface after treatment. Studies have shown no obvious discrepancy in actin fibres after treatment with 5-FU in concentrations below 10µg/ml after a 24h period (Gordon et al., 2005, Filgueiras et al., 2013).

It was observed throughout the experiment, that the treated cells show signs of protrusions (Figure 3.12). Each of the protrusions observed had noticeable differences in surface area compared to the next protrusion. In Figure 3.12, a cell with multiple protrusions is shown and this particular cell has conspicuous protrusions compared to other treated cells. The analysis of each individual cell showed that no two cells had the same amount of protrusions. These protrusions were only clearly noted with the treated 5-FU cells. The cells at this time point (72h) and concentration (5µg/ml) are also show clear signs of blebbing and the protrusions could be related to this process. In the process of apoptosis, the generation of independent apoptotic bodies which travel away from the cell could lead to secondary necrotic membrane breakdown as a cascade of proteins are released. The difference between these phased transitions (early apoptosis to secondary necrosis) is the amount of intracellular proteins released during secondary necrosis.

One limitation of AFM is that the images achieved are not instantaneous, so scans can be time consuming (4-8 minutes). The scan rate could not be above 1Hz if the whole cell was imaged as the cantilevers approach velocity would result in the cell being removed from the surface. It was more complex to scan the surface of the untreated cell in comparison to the ones treated with 5-FU. When the cantilever is scanning the surface, just for imaging purposes, the amount of force required is lower (100-500pN) and hence there is no need to indent a great amount such as in nanoindentation, and the cell be made to deform in the micro-range (depending on the cell height). As the cell is very soft and is relatively stickier than most other sample types, the cantilever needs to have a large modulation (~600nm peak to peak).

In these experiments consistency is required to ensure that the Young's modulus achieved is comparable throughout. As explained previously, the Bruker software has multiple applications and alterations within the two main modes classically used (contact and tapping). In this study, to conduct these indentation experiments, the measurements were obtained using the nanoindentation part of the software. This ensured that the values were obtained by the user and not by the software and as such could be applied in the ScanAsyt module (See 2.5.6.3).

Analysis of multiple force curves can assist in visually detecting alterations in the control and treated cells. These force curves can become interesting if they differ from the standard forces curves. As explained previously, mechanical properties can be obtained from these curves but additionally specific interactions can also be noticed. When there are interactions between the tip and the surface, this can be described as a lock and key mechanism. The interpretation of force curves can give information about the sample such as roughness or adhesion properties. Often the approach and retraction parts of the force curve are not identical, and they can be used to deduce the properties of roughness and adhesion. To make this discussion comprehensive, the force curves produced will be broken down in relation to the pathway of the cantilever.

The cantilever will approach the surface and then jump to make contact, and it is within this contact area that suggestions can be made with regards to the cell surface. The contact area of the approach continues to move towards the surface. As mentioned briefly, the sharp tip cantilevers tend to affect the cell membrane, and if the loading force is high enough could

ultimately penetrate through it. Penetration of the cell membrane occurs with many cell types across a range of loading forces (10-20nN). In this study, the pyramidal indenter was observed to penetrate the cell membrane if the loading force was 15nN or greater; this is because the area to which the force is being applied is relatively small. In other studies, this incident happened due to the cantilever stiffness (for example, >5N/m) (Radmacher, 2002).

The trigger point of the force curve is set through the software where the cantilever begins to remove itself away from the surface. There will come a point where the cantilever will snap away from the surface. If the surface did not deform, or there were no surface interactions, the retract curve of the cantilever would be similar to the approach curve. This is not the case with cells as they deform when pressure is applied, which is in Figure 3.13, this is observed. Force curves produced in liquid show indications of hysteresis in the base line of the graphs, as in liquid, compared to air, thermal fluctuations are displayed more prominently. Hydrodynamic drag is induced on the cantilever as the end force does not return to the same start point, due to the viscosity of the liquid.

Figure 3.13 shows force curves after treatment with 5-FU. The control cells are shown to have relatively even approach and retraction curves, and these are similar to the 24h time point post 5-FU treatment. However, at 72h post treatment across a high number of curves (>75%), there is an irregular release of force after the tip and sample are no longer in "contact". Similar to the diclofenac treated cells (Figure 4.12), this could be related to surface alterations occurring in the HepG2 cells. In flow cytometry experiments, at the concentration of 5-FU (500μg/ml) applied at this time point, apoptosis was noticed. It may be that this interaction between the surface and the tip is due to movement of molecules towards the cell surface.

Young's modulus, in theory, is dependent on the organelles under the cell surface as well as on the strength of the cytoskeleton. Analysis of this information is difficult, but it is beneficial if measurements are completed only at one area on the cell surface, normally in the nuclear region. In this study, the Hertzian model was applied to these force curves to obtain a value for elasticity. Over one single cell, there should be a range of measurements compiled at different locations, and in this study 5 locations over the nuclear region were measured.

HepG2 and SK-Hep-1 cell are cancers cell lines, and although there are studies and reviews, relating the mechanical properties of cancer cells to the normal cell (Lekka et al., 2012a, Xinyi et al., 2014, Chen, 2014), these are limited when it specifically comes to the liver. In a study by Kim and co-workers (2013), it was found that the hepatocyte (THLE-2) had a higher Young's modulus in comparison to the hepatocellular carcinoma cell line, HepG2 cells (Kim et al., 2013). In this study, a conical and a spherical indenter were used, achieving a Young's modulus value of 3.48±0.56kPa and 0.26±0.26kPa respectively, for HepG2 cells. In this study, fewer numbers of cells (n=32 conical, n=11 spherical) were indented and the results can be seen to be comparable to the untreated HepG2 cells in Table 3.3. The results presented are comparable to values obtained in our investigation for control cells, and similar to our data the conical indenter gives a higher value for Young's modulus.

In relation to the two different indenters used, there was great variation in elasticity results, and this is related to the amount of pressure applied to a smaller cell area with the use of the sharp tip. The sharp tip indented a small surface area compared to the spherical indenter, therefore it can produce "stiffer" results (Table 3.3). The spherical tip did show significant differences in stiffness between control cells and cells treated with 5µg/ml of 5-FU for 24 or 72h (Table 3.3). However, there was not a significant change in stiffness when the sharp indenter is used to compare control cells and cells after the same treatment due to the large deviation over the sample size. The Young's modulus values are large which can be related to cytoskeleton or organelles moving toward the edge of the cell surface. Also, the area in which the cantilever was applied to was considerably smaller and hence these values from the sharp indenter analysed are localised. At first thought, it could be related to the F-actin fibres as they are relatively stiff in comparison to the whole cell, and actin fibres are known to move to the periphery of the cell as apoptosis develops. However, it must be stated that the error is greater with this tip so this needs to be considered.

It has been suggested in the previous study by Kim et al. (2013), that the AFM mechanical measurements and de-adhesion assay could be used for liver cancer diagnosis measuring the internal tension induced by actin with relation to normal and cancer cells (Kim et al., 2013). The de-adhesion assay uses microscopy to observe when the cells remove themselves from the surface and cells becoming more rounded recorded by the software. There are uncertainties about the practicalities of this experimental setup as there are other parameters

which would have to be considered, such as how to transfer this from *in vitro* to *in vivo* method with ease.

After drugs are applied to the cell, different mechanisms can occur which can trigger multiple interactions. 5-FU is a chemotherapeutic drug which influences the DNA synthesis of cells and can cause apoptosis. The cytoskeleton (actin fibres) has altered dramatically after treatment which is process presumed due to apoptosis. The fibrous structure has altered within the cell and moved towards the cell surface. The Young's modulus should relate to the processes which are occurring within the cell. As apoptosis develops, it is interesting to see if the Young's modulus would change as the cell begins to shrink and blebbing occurs. As the cell dynamics are changing, the Young's modulus has altered slightly to reflect the cell becoming softer. Apoptosis is a technique which the cell uses to protect their neighbouring cells and the cells die in solitude. In this study, all the above points can be brought together to give an indication on the health of the cell. The cells treated with 5µg/ml of 5-FU at 72h had distinguishable differences in presumed actin fibres which were captured by AFM. Additionally, the AFM produced images of cells with protrusions and force curves. However, we recognise that we have relatively few data, and have only investigated 5-FU in this section. An exciting future study would be to conduct experiments with other toxins which cause actin fibres to move to the cell surface during the process of apoptosis.

Overall, we observed that 5-FU altered HepG2 cell metabolism significantly over a period of 72hour. It was shown that the toxicity of 5-FU had a dose dependent trend, and that apoptosis occurred. The actin fibres were very prominent at the cell surface if the cell was going through apoptosis and this was also detected in the florescence microscope. The field of AFM is a vast and growing area of research with basic mathematics describing the theory of forces being applied to the tip. Once the correct procedure for calibration has been conducted, AFM provides the opportunity to obtain quantitative force measurements. Prominent fibres were also detected on AFM images of 5-FU treated cells, but at present these have not been identified for certain, but are suspected of being actin. It should be emphasised that the responses of the HepG2 cells to 5-FU in terms of detailed morphology are individual: no two cells showed the same response to the drug as would be expected. Knowledge of tip geometry is essential for repeatable and quantitative results and this is affected significantly by the type of probe used. AFM still has a lot to offer and nowadays a wide range of material properties can be quantitatively measured such as Young's modulus. To conclude, provided the

experimental parameters applied are consistent, AFM measurements could assist in understanding and improving liver cancer treatment and diagnosis, and particularly in determining mechanisms of action of chemotherapeutic drugs.

Chapter 4 - TOXICITY OF DICLOFENAC IN HEPG2 CELLS

4.1. INTRODUCTION

The mitochondrion has a central role in the energy production of the cell. For cell survival, the main source of energy comes in the form of ATP. A substantial amount of ATP is required to keep the cell functioning but specific requirements are tissue dependent. The liver requires a continuous synthesis of ATP, therefore hepatocytes contain of a high quantity of mitochondria. Additional, pathogenic diseases being related to alterations in the mitochondria (functional and structural), and these include diseases occurring in a wide variety of tissues from intestines to the skeletal muscles.

The hallmarks for defining cancer were established by Hanahan and Weinburg; which states differences between normal healthy cells and cancerous cells. Hallmarks of cancer cells are related to their self-sufficiency in growth signals, limitless replicative potential, antigrowth signals, sustained angiogenesis, tissue invasion and apoptosis (Hanahan and Weinberg, 2000). An amendment has since been suggested to include metabolic reprogramming (Tennant et al., 2009). The metabolism of cancer cells require a high rate of glucose uptake to aid in the maintain a replete oxygen environment. (Wise et al., 2008, DeBerardinis et al., 2007). It has been suggested that the mitochondria are working in cancer cells but just at very low capacity or in a completely different way to normal cells (Bellance et al., 2009). This is very dependent on the tumour type.

The HepG2 cell model can be employed for toxicity studies, in this case for detection of drug induced mitochondrial toxicants. HepG2 cells are known to be resistant to mitochondrial toxicants when placed in glucose containing media but are more susceptible to such toxicity when placed in galactose containing media (Marroquin et al., 2007). The reasoning for this is that the cells modify their metabolic pathway to be dependent on OXPHOS solely for energy production. Mitochondrial toxicity *in vivo,* can be complex to model hence a model of mitochondrial toxicity can be more easily defined *in vitro*.

The mitochondrial electron transfer chain has many possible inhibitors which can influence the function of the respiratory chain complexes. For example, NSAIDs can behave as oxidative phosphorylation uncouplers, but the mechanisms behind this are still unclear (Matsui et al., 2011). Diclofenac is a commonly used NSAID which has many different

clinical uses. Drug induced liver injury is common with diclofenac with contributory factors including mitochondrial damage and oxidative stress. There have been conflicting studies which gives uncertainty about whether or not the drug is a mitochondrial toxicant (Kamalian et al., 2015, Luo et al., 2012).
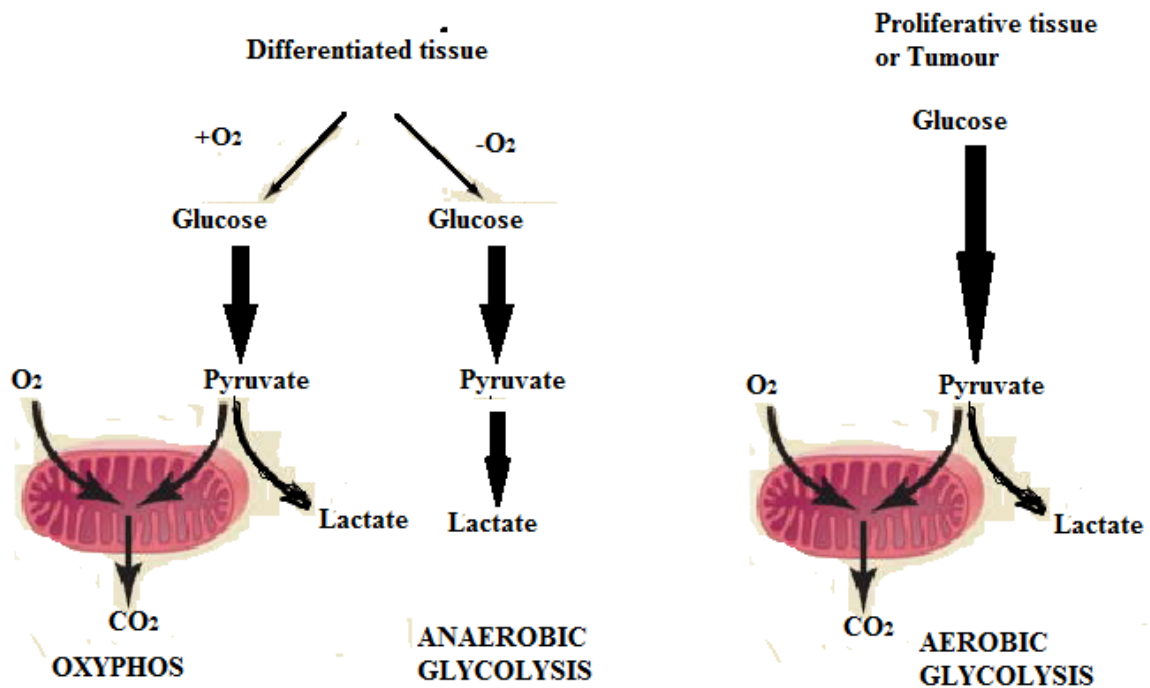
Figure 4.1 - Linking the difference between oxidative phosphorylation (OXPHOS) and glycolysis (both anaerobic and aerobic) Adapted from (Vander Heiden et al., 2009). Normal differentiated tissue can metabolise glucose to pyruvate if oxygen is present via glycolysis then proceeding to OXPHOS. Cells can redirect the pyruvate generated away from the mitochondria, when oxygen is limited. However, there is a minimal amount of ATP produced when anaerobic glycolysis is continual compared to OXPHOS. Aerobic glycolysis (Warburg effect) is observed when the glucose is transferred to lactate irrespective of whether or not there is oxygen present. Galactose is supplemented in medium in the absence of glucose, as it does not support the process of anaerobic glycolysis required within the cells. The galactose added to the cell lines is not readily oxidised into pyruvate without prior conversion to glucose.

In most mammalian cultured cell lines, glucose and glutamine two of the molecules which are catabolised in significant quantities (Vander Heiden et al., 2009, Dando et al., 2013). Hence, these molecules are required to ensure the cells can grow and divide. If the quantity of glucose was to be reduced or to be replaced, the cell dynamics would alter to ensure that the cells can still function. Every cell line reacts differently to this deprivation based on the number of mitochondria within the cells. To study this, galactose is supplemented in medium in the absence of glucose, as it does not support the process of anaerobic glycolysis required within the cells (Swiss and Will, 2011, Attene-Ramos et al., 2013). The galactose added to the cell lines is not readily oxidised into pyruvate without prior conversion to glucose, which consumes approximately two ATP molecules (Elkalaf et al., 2013). Detail image can be found in appendix showing the pathway of galactose if added to the cell (Figure A.3). Figure 4.1 shows the pathway involved in between OXPHOS, anaerobic and aerobic glycolysis and how they produce energy.

Overall, this process of understanding mitochondrial toxicants could be beneficial in the long-term treatment of HCC, as the cancer cells metabolic functions, as regards energy production, are different compared to normal hepatocytes. A clearer understanding of mechanistic relations between growth control and cellular metabolism would lead to better treatment for human cancer. The action of diclofenac as a mitochondrial toxicant is not clearly defined. If it proved to be a mechanism of toxicity, this could be used alongside chemotherapy drugs to benefit the treatment process for HCC.

Aims

To analyse the effects of diclofenac on HepG2 cells and determine if it acts as a mitochondrial toxicant, and whether this toxicity could be related to changes in cell surface properties and biomechanics, by means of:

- MTT, NR and CV assays to analyse the cell viability
- Fluorescent microscopy to examine the live/dead staining of the cells
- HPLC and Bioluminescence assays to investigate the ATP content of the cells
- Atomic Force microscopy to observe the surface of the cell and mechanical properties of the cells.

4.2. METHODS

The general methods can be found in Chapter 2. HepG2 cells were maintained in high-glucose (25mM) DMEM media and incubated at 37°C under air containing 5% CO_2. Specifically, with these experiments the HepG2 cells were collected after being trypsinised and washed with the required media; glucose or galactose containing media (DMEM containing 10mM galactose or 25mM glucose) and plated in 96 well plate (10^4cells/well) or 35mm^2 (10^5cell/well) petri dishes depending on what the cells were required for. Incubation with the specific media lasted for 4 h and then drug stock solution was diluted with the selected media and applied to the cells.

After 16, 24, 48 and 72 h of incubation with diclofenac; the MTT, NR and CV assays were conducted for measured carried out a viability. Cell morphology was analysed by means of fluorescence microscopy after 24 h of treatment with diclofenac at concentrations of 25 and 1000µg/ml.

4.2.1. BIOLUMINESCENCE ASSAY FOR MEASURING ATP CONTENT

The determination of ATP by use of bioluminescence is an established technique. This ATP bioluminescence assay (obtained from Roche, West Sussex UK. Kit version HS II), detects ATP by measuring luciferase catalysed oxidation of luciferin (McElroy et al., 1974).

Standards of ATP were diluted with distilled water by serial dilution in the range of 10^{-5} to 10^{-10}M. Cells were diluted to a concentration of 10^6cells/ml and added to a boiling suspension of 100mM Tris, 4mM EDTA at pH 7.75. The suspension was kept at 100 °C for 2 min and then centrifuged 1000xg for 60 sec. The supernatant was transferred and kept on ice until measured.

The standards and sample were individually placed in a 96 well plate and the luciferase reagent (50µl) added and measurement using Perkin Elmer Victor 2 plate reader. The blank (no cells) value was subtracted from the raw data and the ATP concentrations were calculated from a log-log plot of standard curve data.

4.2.2. HPLC METHOD FOR MEASURING ATP CONTENT

The HPLC method for measuring ATP was adapted from (Afolaranmi et al., 2011) where they measured ATP levels in suspensions of hepatocytes. Prior to analysis, standards of ATP containing 0.01, 0.1, 1, 10, 100μM were placed in HPLC vials.

The HepG2 cells were incubated at $5x10^6$cells/ml and left cultured as a monolayer for 24h. The cells were then incubated with the drug for 16 and 24 h. After this time, the cells were detached from the flask surface and suspended into a 1.5ml Eppendorf at a concentration of $5x10^6$cells/ml. To the suspension, 400μl of 8% perchloric acid was added and then the solution was centrifuged at 10,000g for 10 min. The supernatant (700μl) was removed and added to 40μl of 2M K_2CO_3 in 6M KOH which was then again centrifuged. Then the supernatant (100μl) was mixed with 50mM potassium phosphate buffer (pH 6) and placed into HPLC vials. To measure the ATP content, the solution (40μl) was injected onto a reversed phase C18 column (150mm x 4.6mm, particle size 5 μm) with a mobile phase of 50mM phosphate buffer (pH 6.0) (A) and methanol (B) flowing though the column at 1mL/min. The following gradient was applied for solvent A: 100% for the first 2 min, 87.5% at 10 min and then at 12 min, 100% at 17-19min. The samples were monitored by UV at 254 nm. The retention time for ATP was 3.5min and the concentrations were measured from 0.001μM. In Figure 4.2, a standard curve is shown where concentrations of ATP where applied to the HPLC.
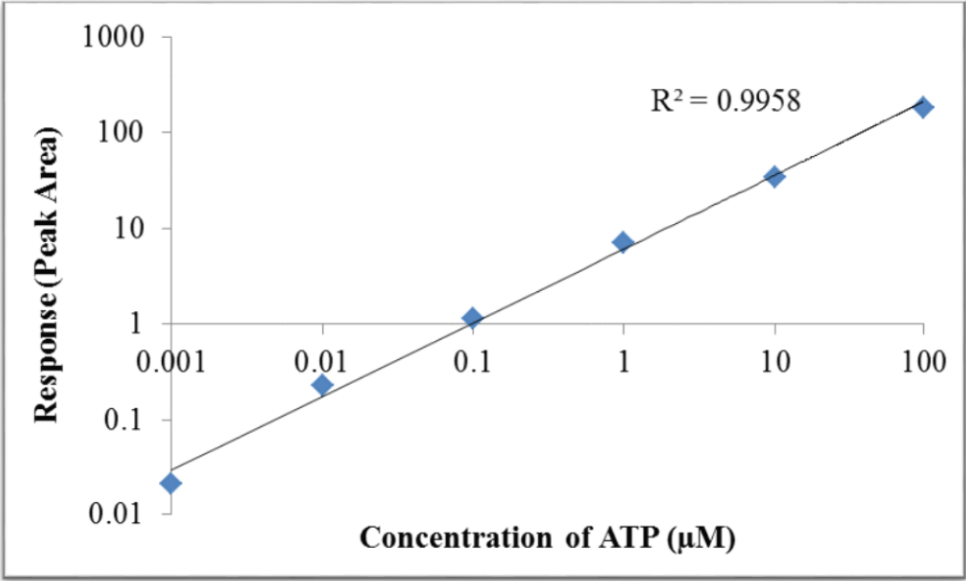
Figure 4.2 -Example of ATP standards achieved by HPLC to give a line of best fit.

4.3. RESULTS

Treatment of HepG2 cells resulting in a reduction in cell viability was detected by MTT, NR and CV assays. The cell morphology was analysed by fluorescence microscopy and AFM was used to determine alteration across the cell resulting in changes in the cell membrane and biomechanics.

4.3.1. EFFECTS OF DICLOFENAC ON HEPG2 CELL VIABILITY MEASURED BY MTT, CV AND NR ASSAYS

The cell viability was assessed in HepG2 cells with the two differently supplemented media (glucose, 25mM or galactose, 10mM) in combination with diclofenac. The following assays were conducted, MTT, CV and NR for analysis of toxic effects. In Figure 4.3, the MTT assay was conducted at four time points over a period of 72h and even after 16h any concentration above 200μg/ml was observed to have an effect on the cells viability.

In Figure 4.4, the CV assay was conducted at the same time points as the MTT assay, and decreased cell viability was measured at concentrations of diclofenac at concentrations above 50μg/ml at 16h.

In Figure 4.5, the NR assay was conducted in the same format as the previous assays (CV and MTT). With this assay, the toxic effects on cell viability were not observed to the same extent in comparison to the other assays even at the highest concentrations and extended time points (24 – 72h). Further investigation was required to understand the reason for this result
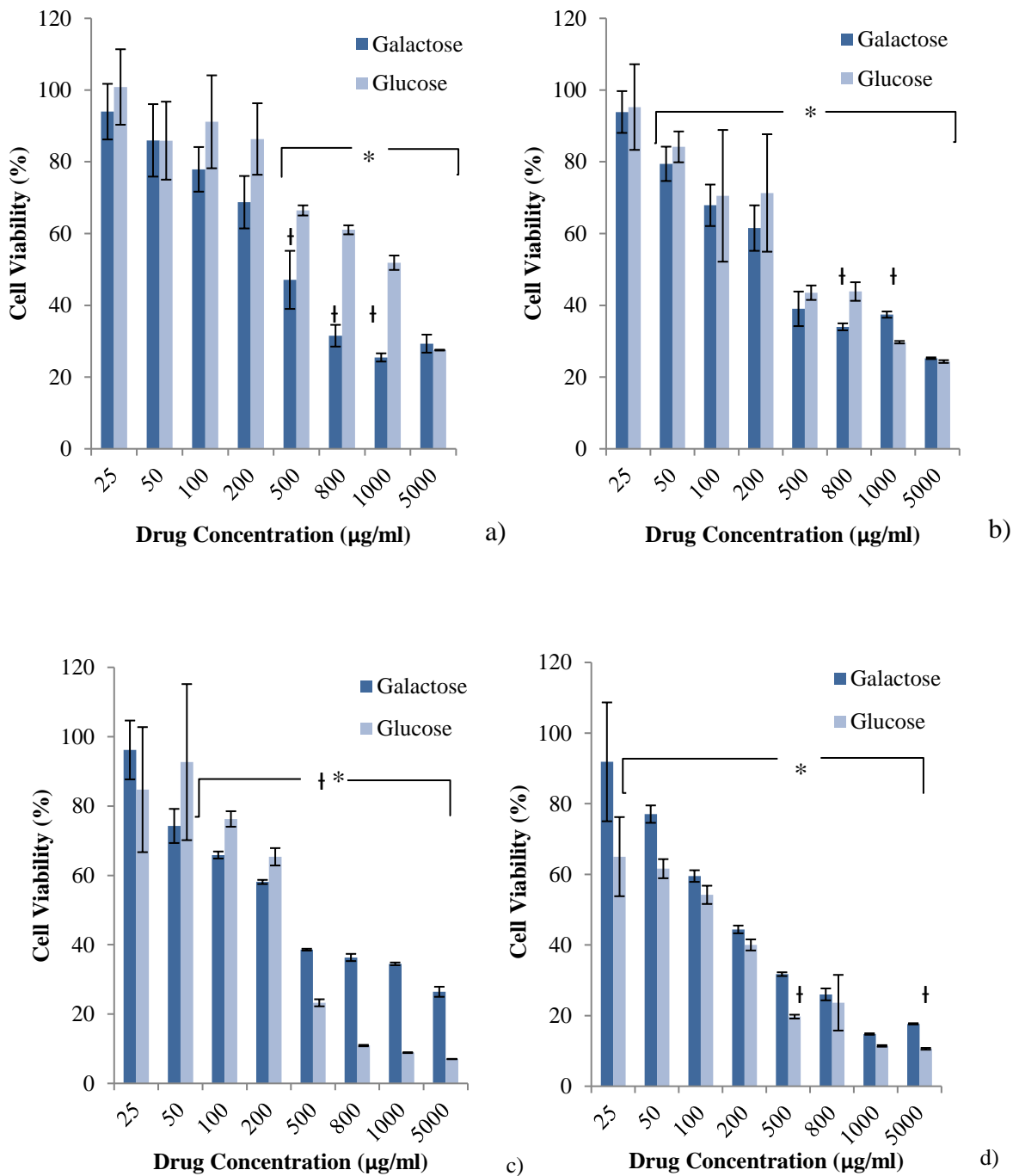
Figure 4.3 - MTT cell viability after treatment with Diclofenac. Cells were exposed to diclofenac for a period of 16h (a), 24h (b), 48h (c) and 72h (d). The viability values are percentage differences compared to controls (±SEM, n=8). By one-way ANOVA test followed by Dunnett's multiple comparison significant differences (*) were detected compared to the respective control values without drug (p<0.05). Significant differences were detected (ⱡ) between glucose and galactose supplemented media by 2 sample t-Test (p<0.05).
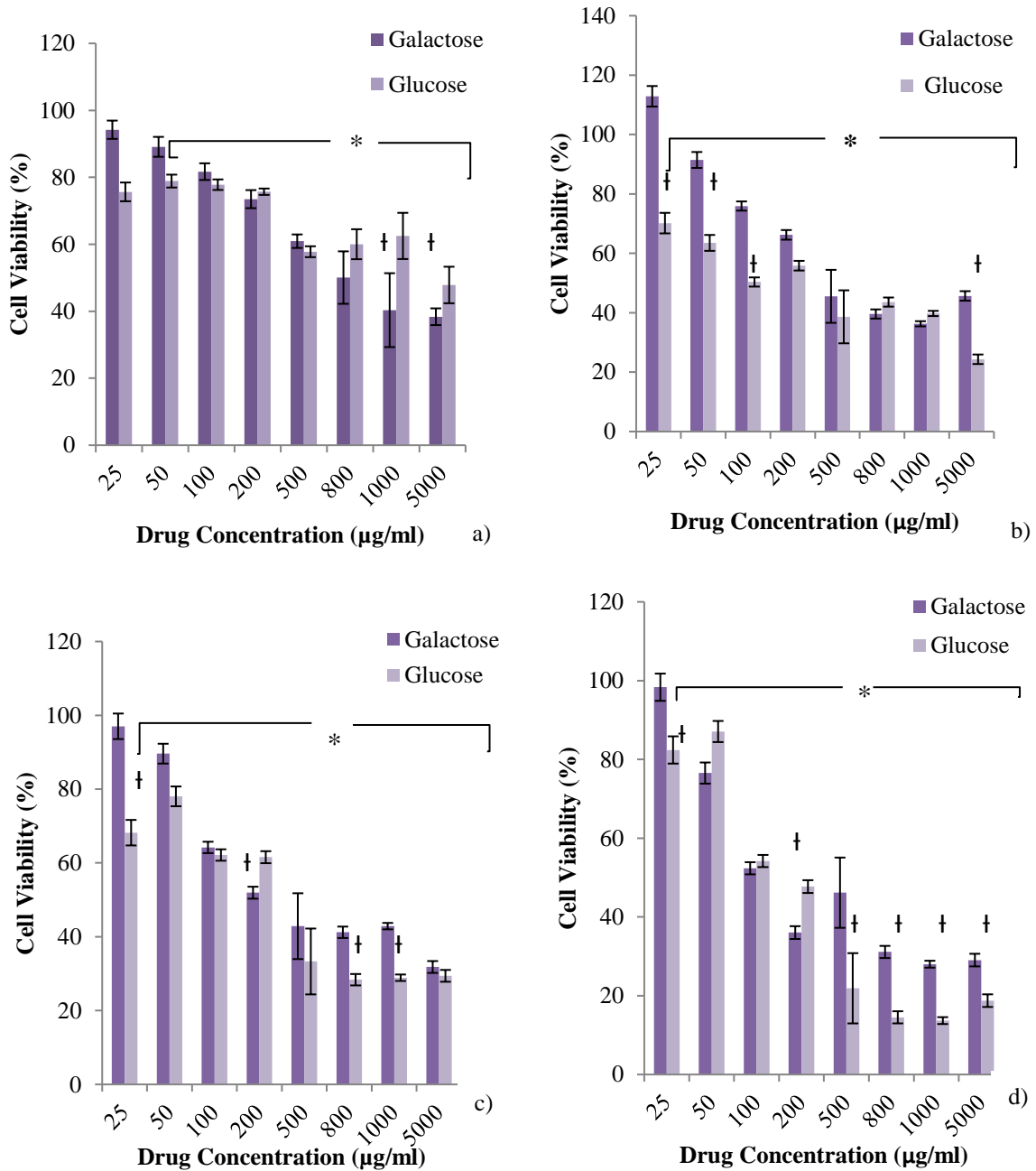
Figure 4.4 - CV cell viability graphs after treatment with diclofenac. Cells were exposed to diclofenac for a period of 16h (a), 24h (b), 48h (c) and 72h (d). The viability values are percentage differences compared to controls (±SEM, n=6). By one-way ANOVA test followed by Dunnett's multiple comparison significant differences (*) were detected compared to the respective control values without drug and differences between (p<0.05). Significant differences were detected (ɫ) between glucose and galactose supplemented media by 2 sample t-Test (p<0.05).

.
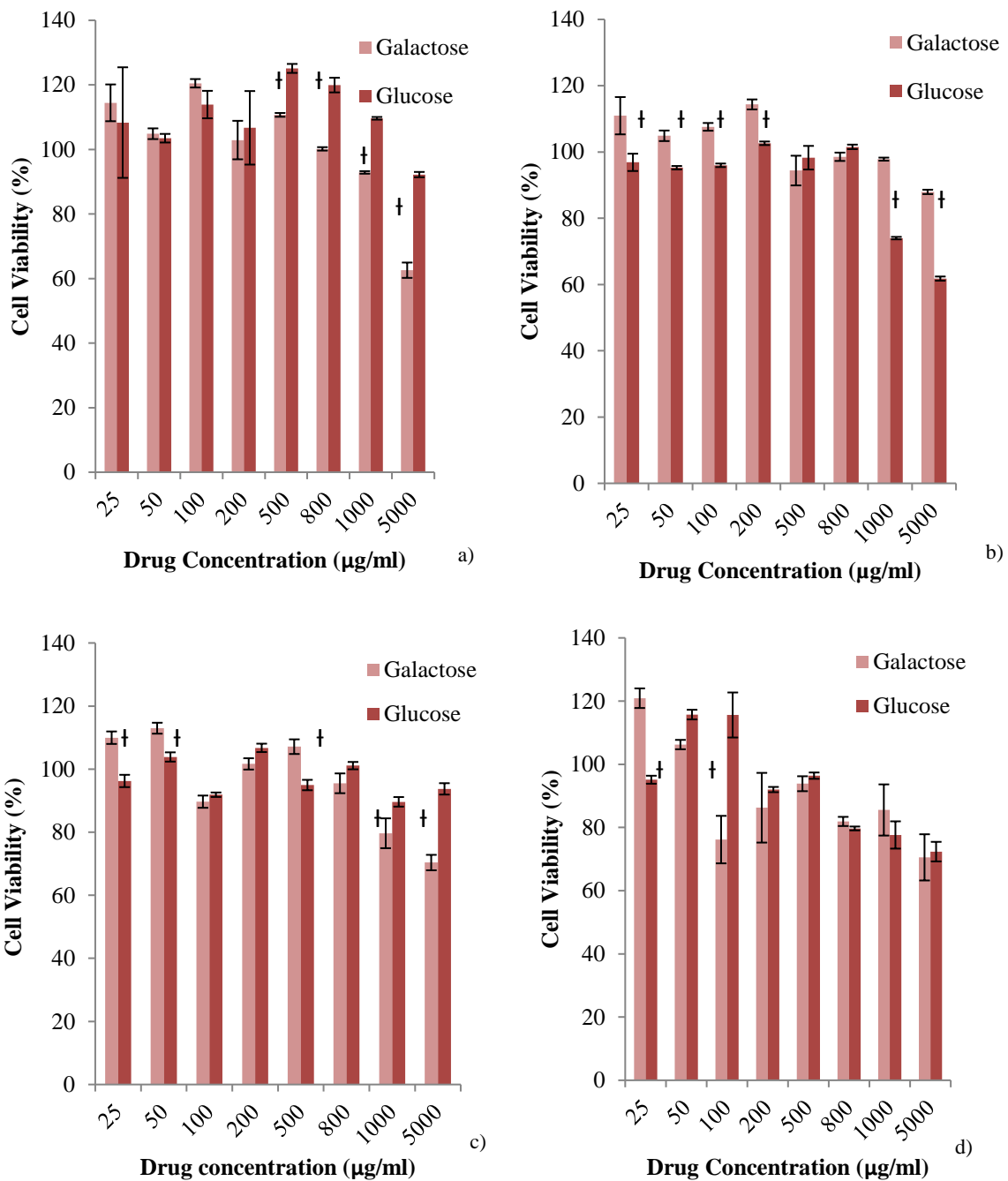
Figure 4.5 - NR cell viability graphs after treatment with diclofenac. Cells were exposed to diclofenac for a period of 16h (a), 24h (b), 48h (c) and 72h (d). The viability values are percentage differences compared to controls (±SEM, n=6). By one-way ANOVA test followed by Dunnett's multiple comparison significant differences (*) were detected compared to the respective control values without drug ($p < 0.05$). Significant differences (ⱦ) were detected between the medium types at the same time points ($p < 0.05$) by 2 sample t-Test ($p < 0.05$).

In Table 4.1, the MTT and CV assay results were analysed to calculate LD_{50} values for diclofenac incubated in both media types and over the four different time points. The calculations for the NR assay produced values for the LD_{50} of $> 2000\mu g/ml$, and these are not shown on Table 4.1.

	16h	24h	48h	72h
MTT	LD_{50} values ($\mu g/ml$)			
Glucose	1429.50± 57.18	498.78± 32.92*	160.95 ±12.39*	90.61± 5.25*
Galactose	534.01±17.61 ‡	411.49± 7.06* ‡	411.94 ±51.29 *‡	236.47± 37.58* ‡
CV	LD_{50} values ($\mu g/ml$)			
Glucose	2457.30 ± 89.97	234.60 ±15.34*	257.19±16.70*	179.93±29.06*
Galactose	807.24±25.07 ‡	786.51±35.82 ‡	564.52±41.92* ‡	283.57±9.94* ‡

Table 4-1- LD_{50} of HepG2 cells treated with diclofenac. The LD_{50} values for CV and MTT were calculated for both media used to analyse the differences in concentration required to decrease cell viability by 50%. By one-way ANOVA test followed by Dunnett's multiple comparison significant differences were detected over time compared to 16h exposure times (*) and between differently supplemented media (‡) ($p<0.05$) at the same time point.

4.3.2. EFFECTS OF DICLOFENAC ON CELL MORPHOLOGY DETECTED BY FLUORESCENCE MICROSCOPY

Cell morphology was examined by fluorescence microscopy at two time points after treatment of cells with diclofenac in the two differently supplemented media. These concentrations of galactose and glucose had been demonstrated to cause significant differences in terms of cell viability (Figure 4.3). Propidium iodide (PI) and Acridine Orange (AO) stains were used on the HepG2 cells which were plated on 35mm^2 petri dishes. Cells treated with diclofenac were showing indications of apoptosis, where shrinkage and blebbing of cells was observed. In Figure 4.6, the cells treated with the lowest concentration of diclofenac were comparable with the untreated control cells in terms of size and shape, but there was a noticeable build-up of red dye around the cells. The fluorescent red stain could be related to the AO concentrating in the lysosomes which will be explained in further detail in the discussion.
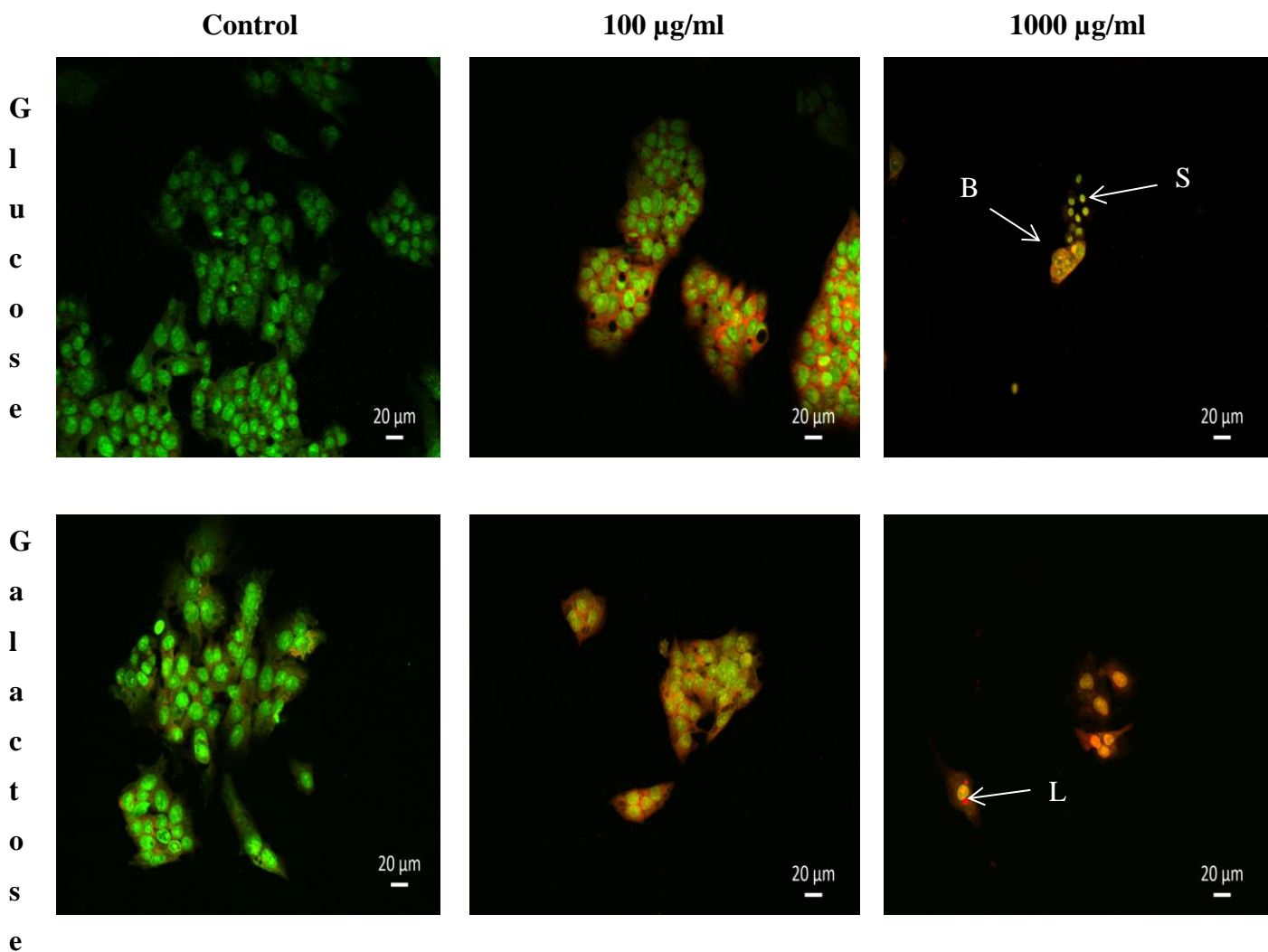
Figure 4.6 - Fluorescence microscopy images (20x water lens) of HepG2 cells after staining with PI (Dead cell, red) and AO (Live cells, green) at different concentrations of diclofenac with the different glucose and galactose containing media for 24h. These images are a representation of 10 different images. "B" indicates cell blebbing, "S" indicates cell shrinkage and "L" indicates lysosomes. There is a build-up of AO in areas of the cells which are known be acidic compartments of the cells and using the fluorescence microscope at an excitation wavelength of 450 -490nm and emission wavelength of 515-565nm.
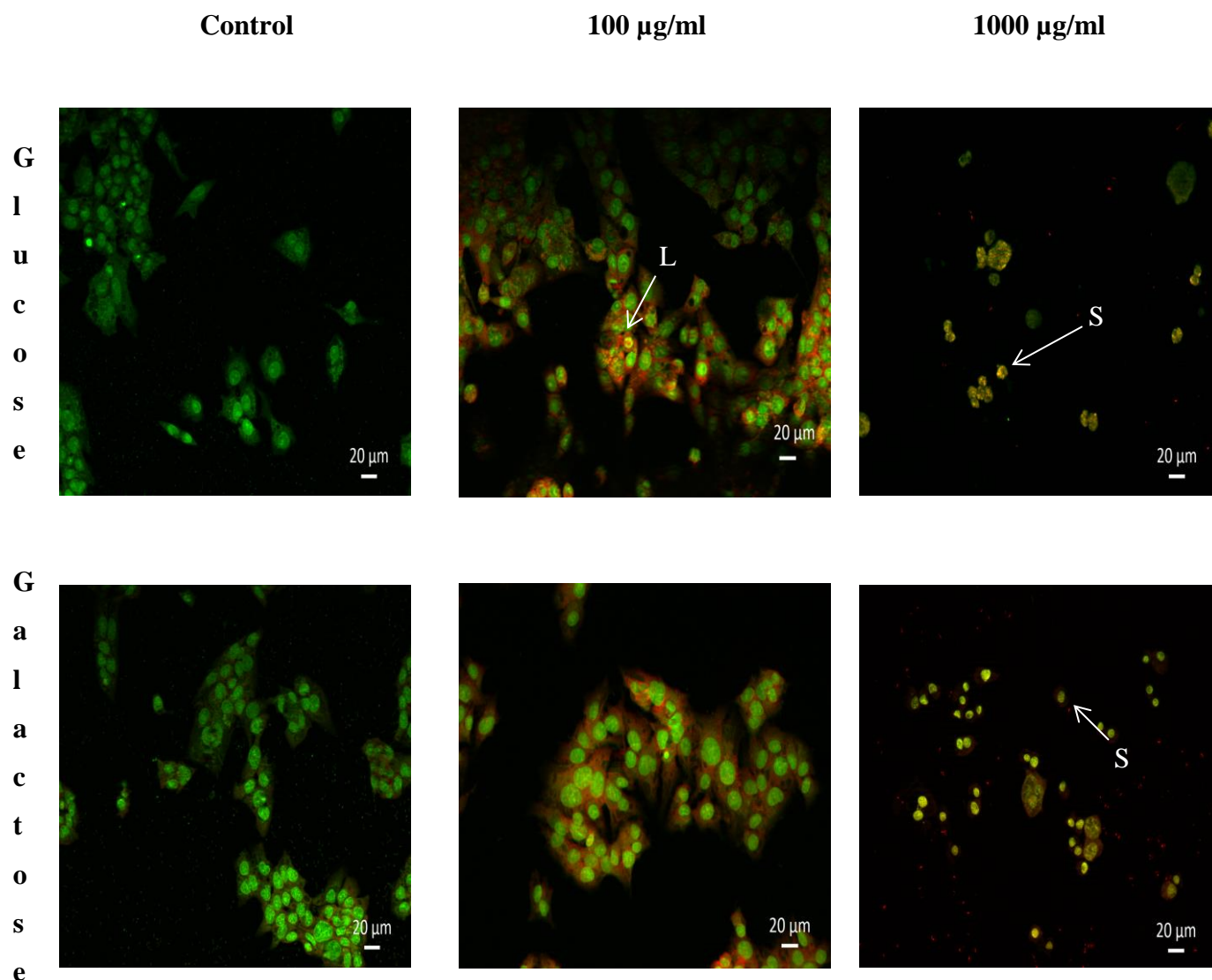
Figure 4.7 - Fluorescence microscopy images (20x water lens) of HepG2 cells after staining with PI (Dead cell/red) and AO (Live cells/ green) at different concentrations of diclofenac with the different glucose and galactose containing media after 72h. These images are a representation of 10 different images. "S" indicates cell shrinkage and "L" indicates lysosomes. There is a build-up of the AO in areas of the cells which are known to be acidic compartments of the cells and using the fluorescence microscopy at an excitation wavelength of 450 -490nm and emission wavelength of 515-565nm.

.

Over the range of concentrations of diclofenac, it was observed that cell number was affected and over longer periods of time the cell numbers began to diminish compared the number of the control cells (Table 4.2). The cell number can be compared to Figure 4.7, where a rapid decline in cell number can be seen when higher concentrations of diclofenac was applied to HepG2 cells.

	Mean number of viable cells (n=10, SEM)					
	24h			**72h**		
	Control	**100µg/ml**	**1000µg/ml**	**Control**	**100µg/ml**	**1000µg/ml**
Glucose	25.10±3.25	25.15±4.98	9.87±2.50*	40.32±4.80	33.51±6.56	5.00±1.25*
Galactose	22.45±4.56	18.15±4.87	11.45±1.65*	48±5.40	36.45±8.46*	5.35±4.25*

Table 4-2 - Mean number of viable HepG2 cells recorded by Confocal Laser Scanning Microscopy after staining with Acridine Orange and Propidium Iodide. Results are data across 10 independent images from each sample (mean ± SEM) Significant differences (*) from the controls were determined by one-way ANOVA followed by Dunnett's multiple comparison test ($p < 0.005$).

4.3.3. ANALYSIS OF ATP CONTENT IN HEPG2 CELL BY BIOLUMINESCENCE AND HPLC

As expressed in Chapter 1, the cell gets most of its energy from ATP generated in the mitochondria and it is important to monitor this to understand the role of mitochondria in the toxicity of diclofenac. In the control cells (glucose supplemented medium) there was an increase in ATP content between 16 and 24h which is thought to be due to the cell growth pattern. Both ATP content and cell numbers increase (~20%) over this period of 8h. The comparison of the controls at 16h and the 24h time point showed that there was a substantial difference in ATP levels if cells were deprived of glucose. As seen in Figure 4.8, the ATP content with the control cells in the galactose containing medium has been reduced (from 1.1±0.1µM to 0.84±0.09µM). It was observed in galactose supplemented media, that cell growth was only ~15% of that in glucose containing medium.
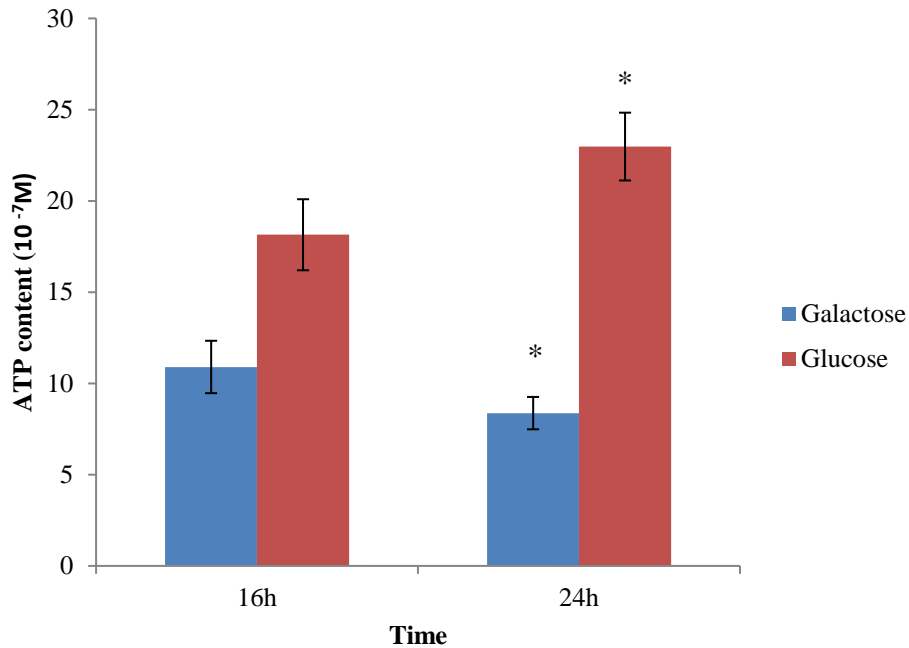
Figure 4.8 – ATP content in HepG2 control cells measured by the bioluminescence assay – Cells density for this experiment was 10^6 cells/cm^2. Over a 16h and 24h, cells were treated with glucose or galactose containing medium. By 2 sample T-test, significant differences (*) were detected between the medium types at the same time points (p<0.05).

In the graphs below (Figure 4.9), the bioluminescence assay for ATP content was conducted over 16h and 24h with the two different supplemented media after treating cells with diclofenac. At 16h, there was a substantial decrease in galactose supplemented cell with regards to ATP content. However, at 24h, the percentage difference of ATP content between glucose and galactose are comparable at 25μg/ml diclofenac at 24h. The glucose supplemented cells showed similar percentages 24h when treated with diclofenac.
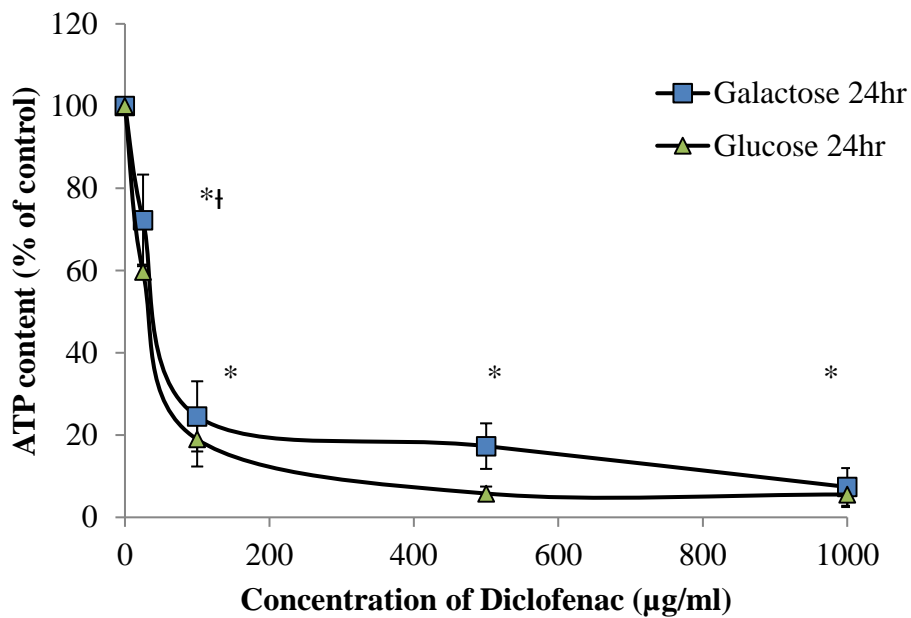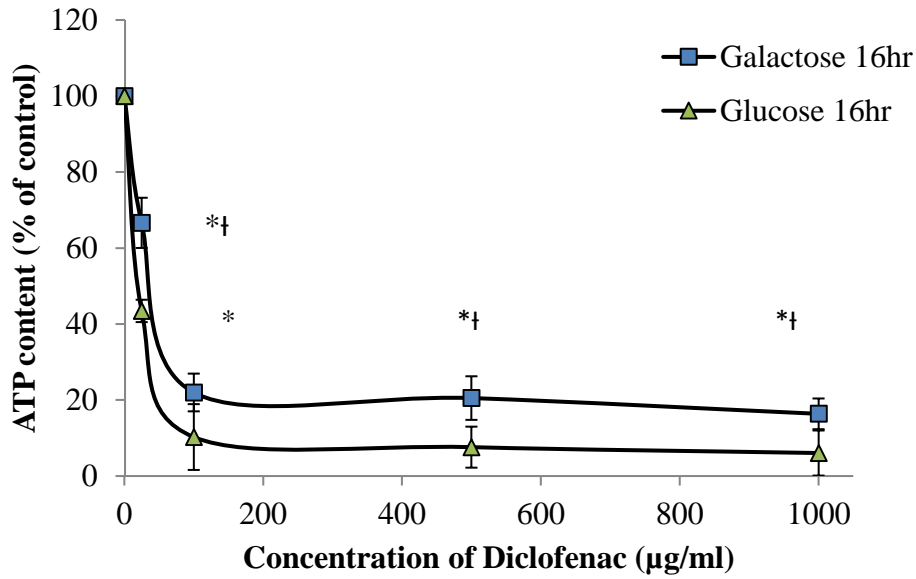
Figure 4.9 - ATP content of HepG2 cells measured by means of the bioluminescence assay. The viability values are percentage differences compared to controls (±SEM, n=8). By one-way ANOVA test followed by Dunnett's multiple comparison significant differences (*) were detected compared to the respective control values without drug ($p < 0.05$). Significant differences (ꝉ) were detected between the medium types at the same time points ($p < 0.05$) by 2 sample t-Test ($p < 0.05$).

The method of HPLC was also used to measure the ATP levels in cell treated with diclofenac in both media. Over these two-time points, a similar pattern could be seen in these graphs (Figure 4.10) as was measured with the bioluminescence assay.
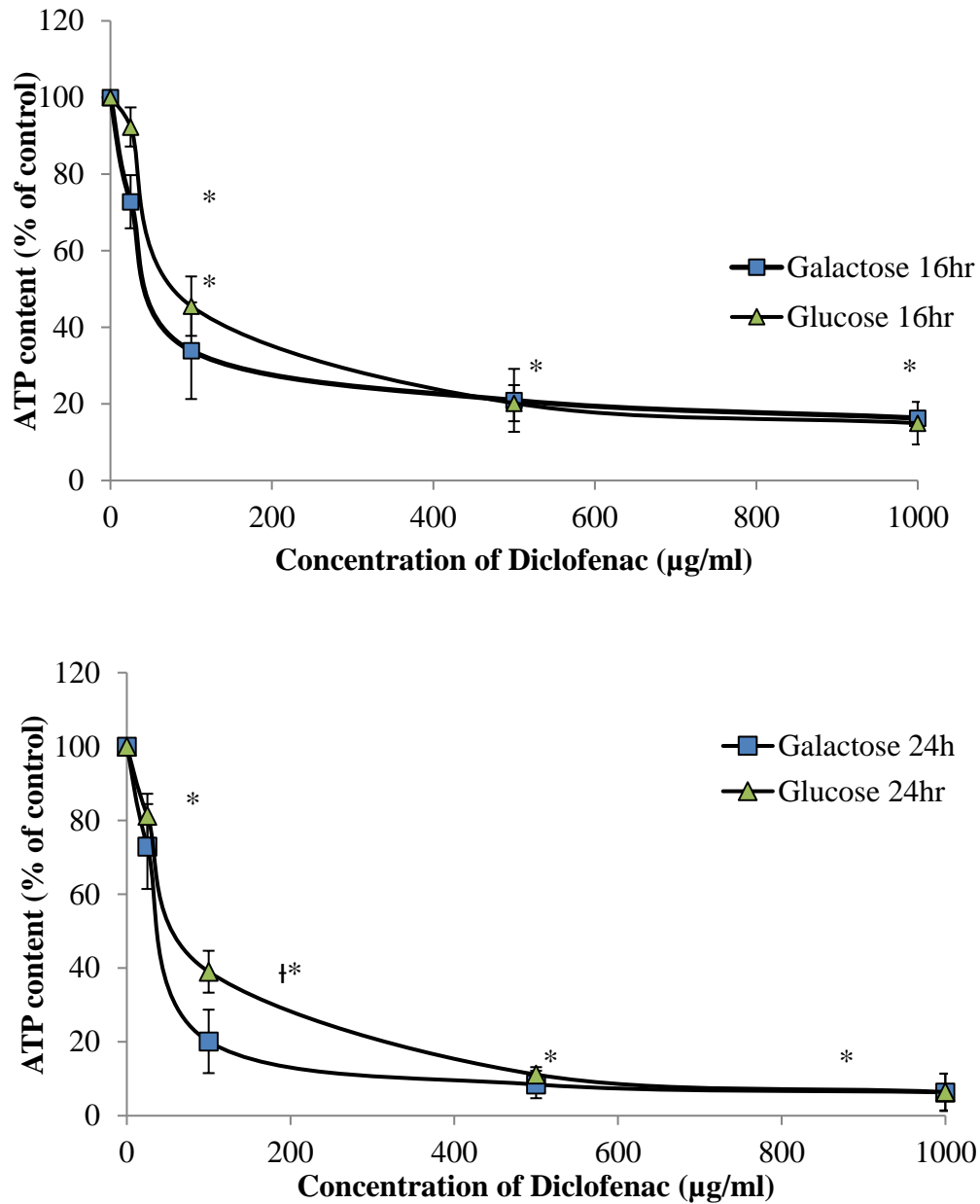
Figure 4.10 - ATP content of HepG2 cells measured by means of HPLC. The viability values are percentage differences compared to controls (±SEM, n=8). By one-way ANOVA test followed by Dunnett's multiple comparison significant differences (*) were detected compared to the respective control values without drug ($p < 0.05$). Significant differences (ɫ) were detected between the medium types at the same time points ($p < 0.05$) by 2 sample t-Test ($p < 0.05$).

Obtaining LD_{50} values for cytotoxicity and ATP content of the cells can give an indication whether a drug is a mitochondrial toxin (Swiss et al,. 2013, Kamalian et al,. 2015). In Table 4.3, the calculated LD_{50} value for MTT (cytotoxicity) is stated, indicating that it is less for cells grown in galactose media. A similar trend was also observed with the ATP content but the LD_{50} value is significantly reduced compared with that of the MTT tests. The ratios introduced in Table 4.3 are commonly used to define a drug or compound's behaviour in terms of mitochondrial toxicity. The two different ratios can allow two different aspects to be expressed (Swiss et al,. 2013, Kamalian et al,. 2015). Firstly, a LD_{50}-ATPglu/ LD_{50}-ATPgal ratio ≥ 2 would suggest mitochondrial liability after the application of galactose and the drug, - being related to the absence of glycolysis. This ratio for diclofenac is less than two at this time point and hence the cells are not affected by the absence of glycolysis. A LD_{50}-MTTgal/ LD_{50}-ATPgal ≥ 2 can confirm whether the mitochondrial impairment precedes cell death and this was case for the experiment conducted. Overall, diclofenac is not shown to be a mitochondrial toxin at this time point, however, cell death follows mitochondrial dysfunction. Future studies, should extend the range of time for which diclofenac is applied in order to confirm whether or not it involves mitochondrial toxicity.

	LD_{50} – MTT (µg/ml)		LD_{50} – ATP (µg/ml)		LD_{50}ATPglu/ LD_{50}ATPgal	LD_{50}MTTgal/ LD_{50}ATPgal
	Glucose	Galactose	Glucose	Galactose		
Diclofenac	498.78±32.92	411.49±7.06*	63.44±5.15	53.01±5.98*	1.19	7.67

Table 4-3 – The LD_{50} values for cytotoxicity and ATP content. The LD_{50} values for MTT and ATP content were calculated for both media used to analyse the differences in concentration required to decrease cell viability by 50%. The ratio (LD_{50}ATPglu/LD_{50}ATPgal) represents if the cells are effected by the absence of glycolysis. The ratio (LD_{50}MTTgal/LD_{50}ATPgal) signifies if the cells occur mitochondrial dysfunction due to toxin applied before cell death. By one-way ANOVA test followed by Dunnett's multiple comparison significant differences were detected between differently supplemented media (*) ($p<0.05$) at the same time point (24h).

4.3.4. Analysis of the changes in cellular morphology measured by use of AFM after treatment of HepG2 cells with diclofenac

AFM was used to analyse the HepG2 cell surface after treatment with diclofenac. The cells were treated for 24h with diclofenac (100µg/ml) with either the glucose or galactose containing media. All images captured had a scan size of 20µm and were cropped to the size of the cell. The completed scans were achieved in QNM mode and at the same scan rate (1Hz) and loading force (500pN). In Figure 4.11, the control HepG2 cell has a relatively uniform colour pattern throughout the scanned 2D area shown, whilst the treated cells (Figure 4.12a & 4.12b) have areas of constant disruption on the surface which suggest the scanned surface has areas of irregularity in height.
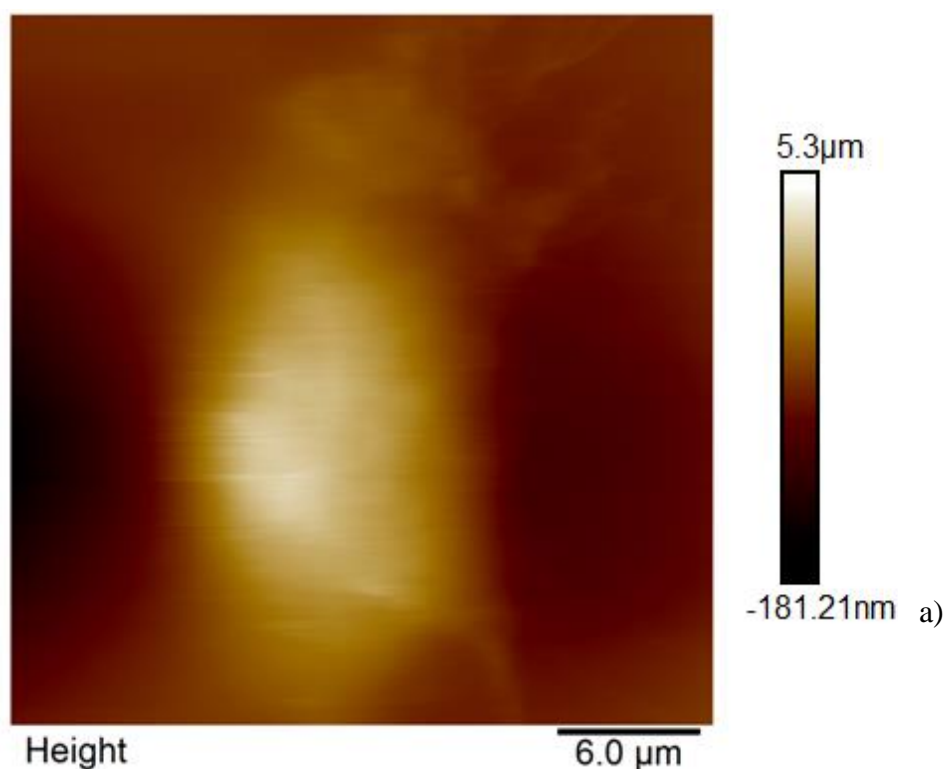
Figure 4.11 - AFM image of HepG2 control cell This image was captured using Tapping mode, with scan size of 20µm, scan rate of 1Hz and loading force of 0.1nN.

136
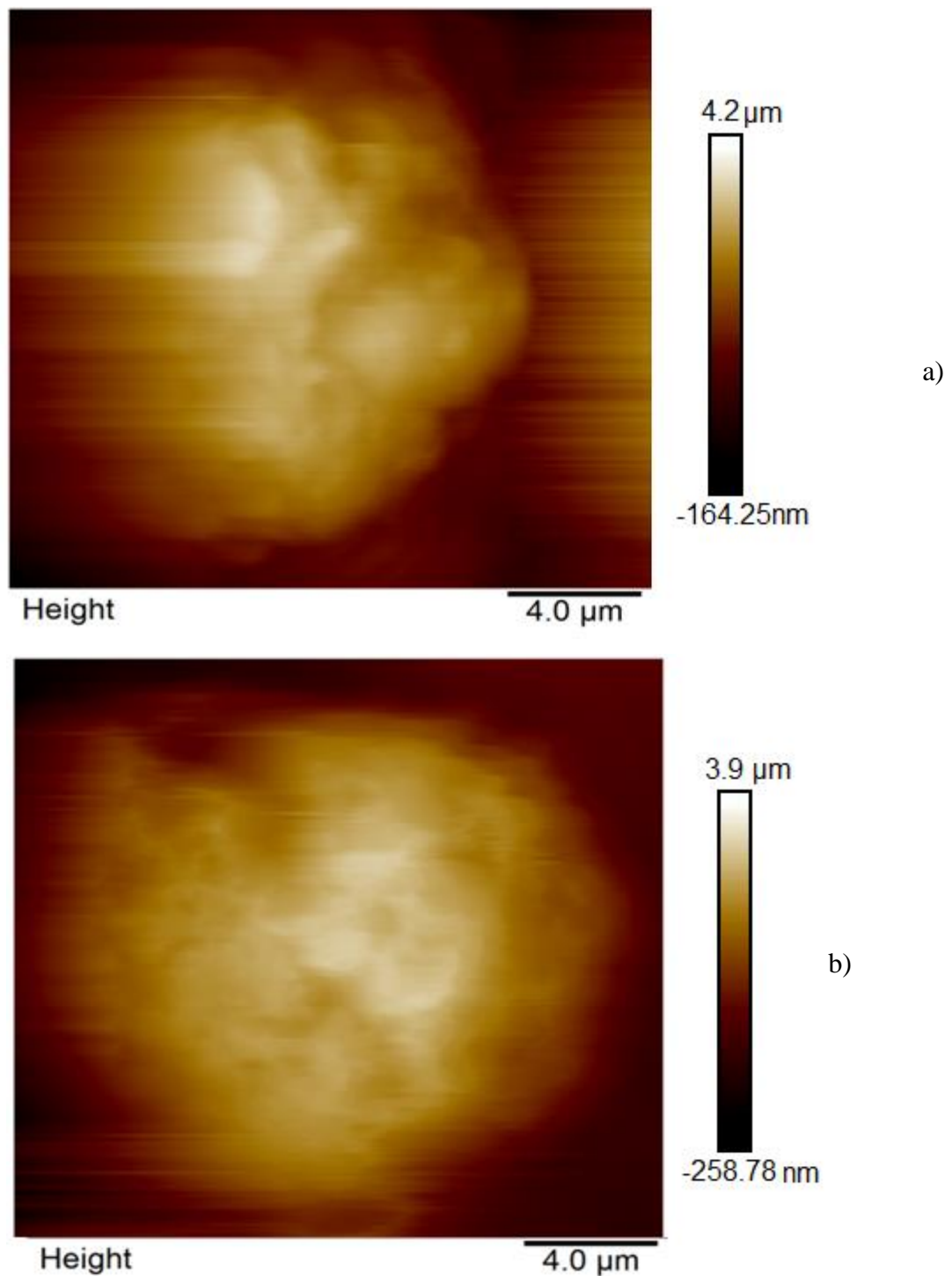
Figure 4.12 - AFM images of HepG2 cells, a) Diclofenac treated cell in glucose containing medium b) Diclofenac treated cell in galactose containing medium. These images were captured using Tapping mode, with scan size of 20µm, scan rate of 1Hz and loading force of 0.1nN. The treated cells are noticeably uneven in comparison to the control cell the surface of which is relatively even (Figure 4.11).
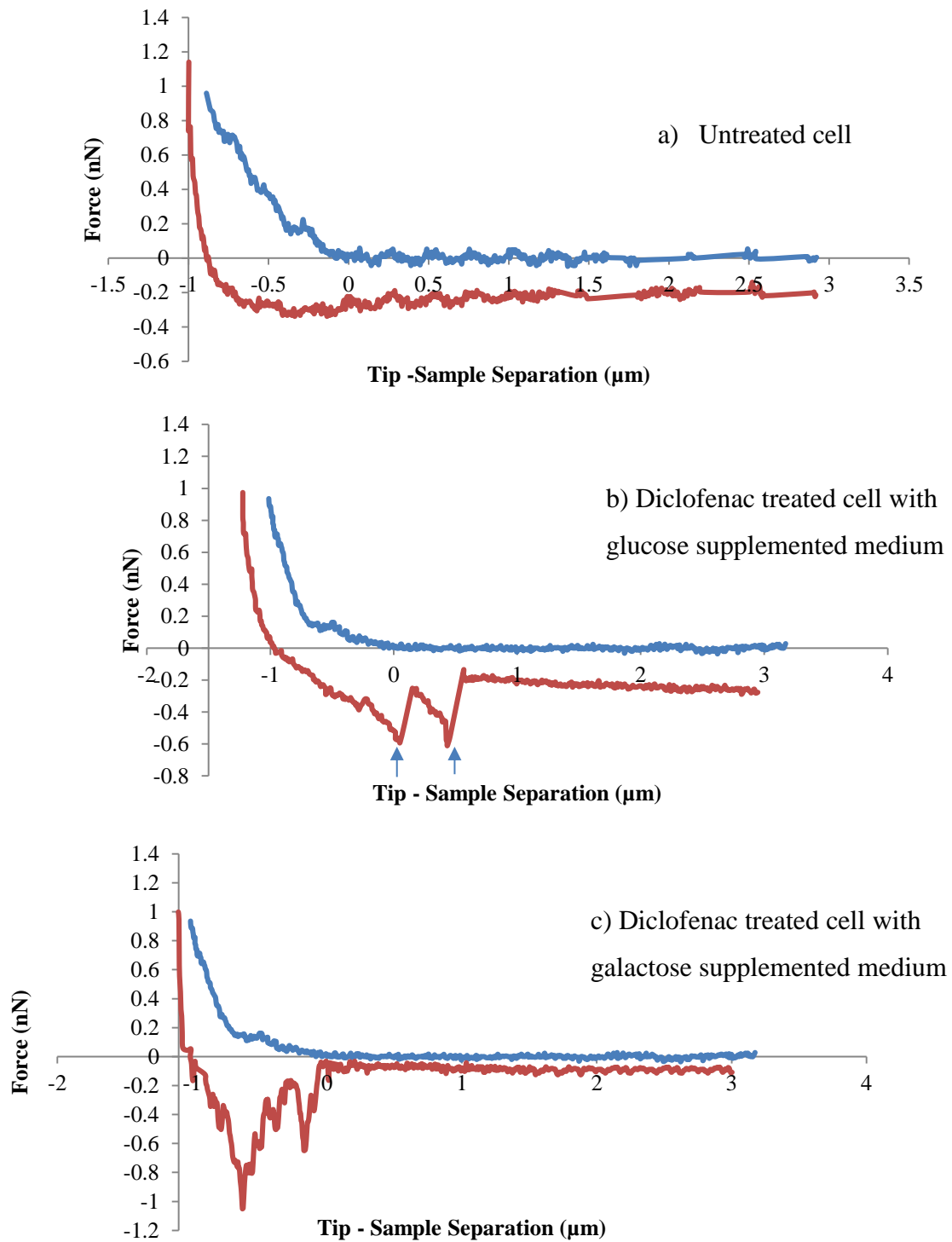
Figure 4.13 – Examples of Force curves obtained from HepG2 cells by AFM. In these graphs, the line of approach is the blue curve and the retraction curve is orange. Cells had a loading force of 1nN and approach velocity of 2µm/s. A) Untreated HepG2 cell with glucose supplemented medium, B) Diclofenac treated HepG2 cell with glucose supplemented medium. C) Diclofenac treated HepG2 cell with galactose supplemented medium. Arrows point to the areas of interest.

Force curves are produced throughout an AFM experiment, every time the cantilever touches the surface. In this study, HepG2 cells were indented to produce these force curves over 75 cells at 5 points across the nuclear region for each experiment. In Figure 4.13, HepG2 cells were treated with diclofenac at 500µg/ml in glucose containing medium for 24 h of treatment. Also, medium was supplemented with galactose containing medium instead of the normal glucose to see if there were any alterations in the response of the cells to diclofenac.

The noticeable differences between the three graphs are the area between the three curves and the rough retraction curve when the cells are treated with diclofenac. The multiple force curves produced did not show any additional or different effects when galactose was added to the medium instead of glucose.

As explained previously, the application of the Hertz model is required to achieve a value for Young's modulus from the indentation measurements. The variations in the final depth means the Hertz model cannot be applied to the whole curve using the Bruker NanoScope Analysis software and hence manual manipulation is required. This is explained in further detail in section 2.5.9.

YM in kPa	Glucose medium	Galactose medium
Control	0.44 ± 0.09	0.38 ± 0.06
Diclofenac	0.34 ± 0.07	0.30 ± 0.04

Table 4-4 – Young's modulus obtained over 75 cells (±SEM) at 5 different points across the cell, by applying Hertz model. This experiment was conducted over a period of 24h and the diclofenac concentration added to the cells was 500µg/ml. By one-way ANOVA test followed by Dunnett's multiple comparison no significant differences were detected compared to the respective control values without drug and, also compared between the two types of supplemented medium used ($p < 0.05$).

In Table 4.2, the Young's moduli values after treatment on HepG2 cells with diclofenac are presented after 24h exposure. Diclofenac treatment did not significantly alter the Young's modulus of the cells. The results presented also show that there is no significant effect on Young's modulus if galactose is supplemented in the medium instead of glucose.

Summary of the main findings

In this section, the effects of diclofenac in HepG2 cells were analysed, specifically cell viability, morphology and ATP content. The mechanical properties and surface characteristics of the cells after diclofenac treatment were investigated.

- Concentrations of diclofenac above 500 µg/ml were observed to influence metabolic function after 16 hours
- MTT and CV assays were more sensitive at detecting diclofenac induced toxicity than NR assay
- HepG2 cells grown in galactose supplemented medium in place of glucose were observed to slow down in terms of growth and metabolic activity
- LD_{50} values for CV and MTT assays were substantially reduced over time of exposure and at 72hr for both assays
- Images obtained by the fluorescence microscope showed indications of apoptosis at 1000µg/ml at 24 and 72h
- HepG2 cells were observed to fluoresce red after staining with propidium iodide and treatment of diclofenac indicating that cell death had occurred
- Bioluminescence and HPLC assays for measuring ATP content suggest that diclofenac causes depletion in ATP
- Diclofenac is revealed to cause mitochondrial dysfunction which precedes cell death
- Both the bioluminescence and HPLC assays showed a similar trend in cellular ATP content with diclofenac treatment to HepG2 cells
- AFM showed a change in appearance with regards to the cell surface after treatment with diclofenac, where roughness of the cell was altered
- Young's modulus of HepG2 cells was not altered significantly after treatment with diclofenac

4.4. DISCUSSION

Understanding the role of bioenergetics in cancer cells can be beneficial for novel approaches with regards to diagnosis and treatment. Liver cells contain roughly 1000-2000 mitochondria, which is approximately one fifth of the cell volume (Karp, 2008). The mitochondrial content of the cell (different cells vary in amount) affects the efficiency of mitochondrial OXPHOS which controls the bioenergetics of the cell (Jose et al., 2011). Diclofenac is thought to be a mitochondria toxicant, but many studies have debated that likely hood. It is believed to be dependent on the cell lines used in the experiments. The following studies have reported conflicting results for HepG2 cells exposed to diclofenac with the use of different assays (Bort et al., 1999, Kamalian et al., 2015, Eakins et al., 2016, Luo et al., 2012). Kamalian and co-workers used the glucose/galactose assay and stated diclofenac was a mitochondrial toxicant. The method used left HepG2 cells in two different environments (glucose or galactose supplemented media) and then a serial dilution of the drug was applied and after 2 hours the assays were conducted (LDH and Mitochondrial ToxGlow assay). However, Eakins and co-workers measured mitochondrial toxicity by an extracellular flux assay and suggested diclofenac was not toxic. This study assessed mitochondrial toxicity by defining the extracellular acidification rate, oxygen consumption rate and reserve capacity by utilising a flux analyser. Therefore, a standard *in vitro* assay should be used for defining mitochondrial toxicants.

In most *in vitro* cell culture experiments, the cells are supplied with high glucose conditions which *in vivo* would not be the case. The cell dynamics alter when galactose is supplied to the cells instead of glucose. The cell bioenergetic process changes from that in the glucose containing medium, which use glycolysis to help maintain ATP levels, whereas in galactose containing medium ATP production is forced through OXPHOS (Elkalaf et al., 2013). Hence, the metabolic pathway for energy production has changed to be wholly depending on OXYPHOS (Figure 4.1), and this now leads to a high chance of mitochondrial vulnerability.

In the present study, our results showed that diclofenac could induce toxicity in HepG2 cells and the toxicity expressed a dose dependent trend. Initially, the cell viability study for diclofenac was conducted by means of MTT and NR assay with a range of concentrations. After conducting both of these assays, it was noted that MTT results were not comparable to the NR assay. Over a period of 72h, the NR assay showed no significant change in cell

number over a large majority of the concentrations studied. Hence, the CV assay was also conducted alongside MTT and NR assays. It was then shown that CV and MTT were more comparable, suggesting that there was a cytotoxic response being induced over a range of different concentrations.

There are two considerations when analysing MTT assay (Figure 4.3), firstly the time elapsed and then the different media types used (glucose and galactose supplemented). Over the four time sets, there is a dose dependent trend which is more defined when examining the first and last time points. This significant difference between concentrations and the control cells appears to increase over time from 16h until 72h. When galactose is added to the cells instead of glucose, the cells need to adapt to this change and the response is not instantaneous. At high concentration of diclofenac (16h), the percentage difference of cell viability is less for the cells in the galactose supplemented medium in comparison to the cells in the glucose supplemented medium. The results suggest the cell mechanisms in relation to cell viability between the two media have altered. Similarly, the CV assay from the first time point (16h) to the last (72h) shows significant differences in cell viability. The first 16h showed a similar trend to MTT which is seen to be a dose dependent trend.

Overall, when comparing both assays there are no clear similarities when analysing the LD_{50} values but this can be related to the different pathways used for the two assays. The mechanisms between both assays differ as MTT relates to metabolic pathways and CV binds to DNA and proteins within the cell. Even though, the mechanisms are sought to be different, there needs to be emphases at 16h and 24h were a significant change has occurred. For both CV and MTT assays, at 16h LD_{50} values show the concentration of diclofenac required to influence the cell viability is substantially less in galactose supplemented media compared to glucose supplemented media (MTT- 63% less and CV – 68%). This suggests that at this time point, the cells are struggling to function normally if galactose medium is supplemented as the galactose is not being utilised for glycolysis, and cells are completely dependent on mitochondrial ATP production. Kamalian and co-workers suggested stating the change in ATP content may be due to a protective mechanism and the activation of cellular defence, this study by Kamalian et al, used a shorter time frame in comparison to the investigation in this thesis. Also, there is a dramatic drop in LD_{50} value for both assays with the glucose media at 24h which suggests that a toxic effect occurring within the cells with relation to diclofenac. The LD_{50} values achieved in this study are comparable with Otto et al, which

found the IC_{50} to be 151μg/ml over a 44h period compared to our 160.95±12.39μg/ml at 48h (Otto et al., 2008).

With the use of the fluorescent microscope, the HepG2 cells were analysed at 2 different time points after treatment with diclofenac. Once the cells have been treated with diclofenac for 24h there are no substantial visual differences at the lower concentration of treatment in comparison to the control cells (Figure 4.6 and Table 4.2). The number of cells at the lower concentration of diclofenac was comparable and no obvious signs of blebbing and shrinkage were noted. Although, at the higher concentration, the number of cells which have been altered visually was distinctly more if the medium contained with glucose. The glucose supplemented cells had reduced in size and numbers, and more cells were seen to be going through apoptosis. After 72h, it was shown that when the HepG2 cells were treated with diclofenac at 1000μg/ml, the cells had become fragmented and reduced in size. The mean size of the control cells was found to be 18.2±1.5μm and 13.1±2μm for cells treated with 1000μg/ml diclofenac for 72h. This cell shrinkage is a clear indication of apoptosis. However, it should be noted it is difficult to obtain accurate measurements of cell size by examining 2D microscopy images.

The lysosomal stability of HepG2 cells was altered when the cells were treated with diclofenac. The NR results correlate with AO fluorescent microscopy images as lysosomes preferentially accumulate the weak base (AO) (Yang et al., 2014, Repnik et al., 2014). There is a green fluorescence with AO when in the monomeric state which is visible when it binds to cytosolic and nuclear RNA and DNA. The accumulation of AO causes the formation of dimers, allowing the cells to fluoresce red. A high concentration of red fluorescence accumulates in cellular organelles, specifically lysosomes and mitochondria (Xie et al., 2011). A study conducted by Pourahmad and co-workers, applied diclofenac to hepatocytes with AO to analyse lysosomal membrane stability. The results showed that after incubation of diclofenac, the stain, AO, showed a significant release after 60-120 min which indicated severe damage to the lysosomal membrane (Pourahmad et al., 2011). In the fluorescent images, (Figure 4.6 and 4.7) at the higher concentration there was clear indication of apoptosis, there is a significant amount of debris and shrinkage of the cell. Some necrotic cells were found in microscope images which were observed to show red fluorescence throughout the cell.

The complexity of bioenergetics in tumours can be widely variant from glycolytic to oxidative phosphorylation (OXPHOS). When a cell has to be more biased towards OXPHOS for production of ATP, glucose and glutamine is required for mitochondrial respiration (Kaambre et al., 2014). As suggested (Gogvadze et al., 2010), the elimination of malignant cells might require a combination of modulating both mitochondrial and glycolytic pathways.

HepG2 cells have a high glycolytic capacity so are believed to be relatively resistant to mitochondrial toxicants (Rossignol et al., 2004). This is not the case if the main component of glycolysis (glucose) is removed, or reduced in concentration. Hence, susceptibility to mitochondrial toxicants will increase when cells are forced to oxidise galactose, as glucose is not readily available. The ATP content was measured in HepG2 cells by means of bioluminescence and HPLC, and both methods analysed the effect of diclofenac on ATP levels at 16h and 24h time points with glucose and galactose supplemented media.

When comparing the two different carbohydrate supplements added with the HepG2 cells, a substantial difference in ATP content was noticed using both assay methods (Figure 4.8, 4.9 and 4.10). At 16h, the ATP content in glucose supplemented cells was observed to be higher than in the galactose treated cells. This occurred because the galactose produced no net ATP increase unlike glucose which is normally converted into pyruvate, and giving a net gain of 30 ATP per molecule (Aguer et al., 2011). Over the 24h period, the ATP content in cells with glucose medium is increased, most likely due to the glucose still being readily available to the cells (Figure 4.8). Overall, these differences are thought to be due to metabolic reprogramming as the generation of ATP coming from the OXPHOS which reduces the ATP quantity (Figure 4.1). Similar studies used this galactose supplemented experiment to express this change from glycolysis to OXPHOS with cancer cells to show the usefulness of these mechanisms and assist a preclinical assay for detecting unknown drug induced mitochondrial toxicity. (Sirenko et al., 2014).

Over the experimental time (72h), HepG2 cells are attempting to adapt to the different environment when galactose is supplemented in place of glucose. As the bioenergetics of the cells changes at this point, drugs can be applied to see if there is additional effect. In Figure 4.9, the bioluminescence assay demonstrates how cells react to diclofenac with the different supplements present, and whether over time ATP content can insinuate the drug is a mitochondrial toxicant. In a study by Gómez-Lechón and co-workers, it was suggested that

when diclofenac was applied to hepatocytes, it caused an inability for mitochondria to produce ATP due to the toxicity of the drug (Gómez-Lechón et al., 2003). With regards to the bioluminescence assay, galactose supplemented control cells at the first time point (16h) showed a decrease in ATP in comparison to cells grown in glucose containing medium, which suggests there is a significant mitochondrial effect. However, at 24hr the ATP content at 25µg/ml is the only concentration where substantial difference is shown. Overall, this suggests diclofenac is having an additional toxic effect. This is emphasised as glucose supplemented cells are shown to have a comparable trend as the previous time point. Also, this is an indication that the bioenergetics of the glucose treated cells has not changed and there is no obvious reduction of the glycolytic pathway.

The AFM images show that structural change is taking place at the cell surface. The surface of untreated HepG2 cells was seen to be relatively smooth in comparison to the treated diclofenac cells. In relation to the surface alteration and mitochondria toxicity, there are not obvious differences as treated cells in both media showed similar alterations. The change in the cell surface is thought to be mainly due to the treatment of the diclofenac. However, there are no networking fibres observed after treatment with diclofenac, unlike with 5-FU. This observation could be related to the cytoskeleton not being significantly reinforcing at the cell surface at 24h, but further experiments need to be conducted to clarify this. In addition, the Young's modulus of the cell treated with diclofenac was not altered significantly unlike the treated 5-FU cells. It could be suggested that at a later time point, the cells treated with diclofenac would show similar trend. Additional experiments would need to be conducted to be able to compare both the toxins used.

In Figure 4.13, the force curves produced by the indentation of HepG2 cells with and without treatment with diclofenac show differences. The retraction curves are noticeably different. The treated cells are seen to produce an irregular release from the surface which suggests multiple binding sites between the cell and the tip. This release from the surface must be related to the diclofenac as it is the only obvious alteration made. This can be related to the surface roughness, or adhesion molecules, which may be present after treatment. Beyond the adhesion measurement, AFM opens opportunities for specific binding probes, which are a well-documented area (Rico et al., 2011). This study looked at the unfolding of proteins at submolecular resolution. This offers the potential to understand the cell surface once the cell had been treated with diclofenac.

Diclofenac is used normally as an NSAIDs but in this study, it was shown to have an additional effect on ATP content of HepG2 cell after a period of 24h. Allowing cell growth in galactose supplemented media can permit the investigation of mitochondrial bioenergetics. Overall, the effect of diclofenac in treated cells in this supplemented, galactose containing medium, highlights the importance of metabolic reprogramming and may assist in the future for targeted therapy of HCC.

Chapter 5 - Production and characterisation of liposomes for drug delivery to reduce the toxicity of 5-FU

5.1. Introduction

Liposomes are efficacious as delivery systems and have wide applications. In recent years, there has been growing interest in this area of drug delivery systems as liposomes have the possibility to improve targeting, bioavailability and circulation time (Bozzuto and Molinari, 2015). Also, the development of a new drug molecule is known to be very time consuming and expensive (Tiwari et al., 2012), whereas it is much cheaper to develop a new mode of drug delivery

There are many production methods for liposomes as explained in Chapter 1. The two methods which are conducted in this study are the thin film hydration method and a microfluidic based method, a relatively recently developed technique which is normally a single step process.

Thin film hydration is a well-established technique which uses a temperature above the phase transition to produce multilamellar vesicles (MLVs). This method is very time consuming and has been known to result in rapid leakage of active pharmaceutical ingredients from the vesicles (Payne et al. 1986). The structural framework to form liposomes is dependent on the lipid composition and temperature. Many lipid bilayers exhibit a predominant phase transition from the gel to liquid crystalline state. Specifically, 1, 2-dimyristoyl-*sn*-glycero-3-phosphocholine (DMPC) lipids phase transition occurs at below physiological temperature (~25°C). In general, temperature is an important parameter to be considered as physical instabilities can occur if liposomes are not correctly stored.

Microfluidics is the flow of a material in a controlled environment through a relatively small (~10-100µm) channel (Belliveau et al., 2012). Liposomes produced with this method follow the principles of laminar flow, the fluid streams can flow through a well-defined interface with no disruption between layers. Microfluidic production of liposomes is thought to result

in faster analysis, reduction in consumption of reagents and a higher level of throughput. Hence, microfluidics has been increasingly implemented in the production of liposomes and is likely to produce a technology that can be scaled up, but which is harder to translate due to costs (Bozzuto and Molinari, 2015, Li et al., 2015).

The pharmacokinetics of liposomes *in vivo* can assist in the understanding of their metabolism and distribution throughout different tissues. The primary sites of accumulation of drugs are reported to be the liver and spleen for carrier mediated agents compared to the non-carrier formulations. For most drugs, the liver is the site of greatest accumulation and the generous blood supply to the liver provides an explanation for this (Zamboni, 2008). Evidence has shown that liposomes are preferentially deposited in liver after systemic administration, resulting in prolonged retention within the organ and in some instances of significant hepatotoxicity (Gabizon et al., 2006).

The drug, 5-Fluorouracil, is administered either as an IV bolus injection daily for five days or by slow infusion cycles. This is used in order to improve the 5-FU treatment process, as the schedule aims to achieve optimal therapeutic benefits for patients as the half-life in plasma is relatively short (11.4 min). In most circumstances, this is administered in hospital and it is hoped in future to minimise the time patients need to stay in hospital. The development of the drug, 5-FU was anticipated to provide a drug with greater half-life that would extend patient exposure time and minimise toxicity as high concentrations of chemotherapeutic agents are used because tumours become resistant to the drugs (Kusunoki et al., 2000). There has been development of formulations for liposomal incorporation with 5-FU but no substantial changes to therapy has yet been made.

Aim

In this study, we prepared liposomes by using two methods (rotary evaporator and microfluidics) and investigated the morphology of the liposomes. The effect of the empty liposomes and the 5-FU free drug on the properties of HepG2 cells was investigated. These experiments were conducted by means of:

- Dynamic Light Scattering, NanoTracking analysis and AFM to measure the size of the liposomes
- NR and MTT assays to analyse the cell viability
- AFM to examine the surface detail of the liposomes and the cells
- Fluorescent microscopy to analyse the live/dead staining of cell

5.2. METHODS

5.2.1. THIN FILM HYDRATION WITH THE USE OF A ROTARY EVAPORATOR FOR LIPOSOME PRODUCTION

The rotary evaporator waterbath and solution for encapsulation (PBS) were pre-set to 40°C specific temperature for DMPC due to the temperature required to be above phase transition. To create the 2:1 (DMPC:cholesterol) ratio required for carrier formation, the following were weighed to produce a 1 ml suspension, 3.39 mg DMPC and 0.97 mg cholesterol (2: 1). In the fume cabinet, the lipid and cholesterol were dissolved in 1 ml chloroform in a pear-shaped flask (25cm^3). The flask was connected to the rotary evaporator with a luer lock and was set to rotate at 100 rpm. Once all the chloroform was evaporated, to produce empty liposomes 1 ml of PBS was added and the flask mixed well. The suspension was then sonicated in the waterbath at 40 °C for 30 min. and then was maintained at 40 °C for 1 h and centrifuged at 12,000 for 1 h. The supernatant was removed and then the liposomes were suspended in 100μl of PBS. The characterisation of liposomes was conducted as soon as formation had occurred and they were stored at 4°C if required.

5.2.2. MICROFLUIDICS METHOD FOR LIPOSOME FORMATION WITH USE OF THE NANOASSEMBLR

The NanoAssemblr (Figure 1.7) uses a microfluidics process (a rapid and controlled mixing procedure) using laminar flow to create the liposomes. The heating block was left for a period of time until it heated up to 40° C. A washing stage of the cartridge was conducted with two 1 ml syringes; one filled with ethanol and other with PBS. The stock solution contained 0.97mg of cholesterol and 3.39mg DMPC and these were dissolved in ethanol (1ml). There were two syringes in the system; one had the stock solution and the other a solution of 5-FU in PBS, or PBS alone. The appropriate parameters are inputted to the programme (e.g. flow rate, flow ratio and syringe size). The amount of waste and final volume values were also added to the software. The syringes are placed into the equipment as well as a 15ml centrifuge tube for waste and product. The lipids produced are unstable in ethanol and have to be diluted immediately into PBS. The washing stage was again repeated at the end of production process. The supernatant was removed and then the liposomes were suspended in 100μl of PBS. The characterisation of liposomes was conducted as soon as formation had occurred, and they were stored at 4°C as required.

5.2.3. LIPOSOME CHARACTERISATION

5.2.3.1. PARTICLE SIZE OF LIPOSOMES

The mean particle size was determined using Nanoparticle Tracking Analysis (NTA, NanoSight, United Kingdom) and dynamic light scattering (Malvern Zetasizer Nano ZS, Germany).

Nanoparticle Tracking Analysis has a Viton fluoroelastomer O-ring and a sample chamber with a 640nm laser. The particles had to be diluted with PBS when using the NTA to a concentration of approximately 10^4-10^8 particles/ml. The solution (~1000μl) was then injected with a sterile syringe into the NTA sample chamber where light was scattered and the particles captured by using a scientific digital camera. The software generates results relating to the solution, specifically size and concentration of particles. Over eight samples were measured three times and standard deviations could be calculated.

The particle size was also measured by dynamic light scattering equipped with a 633nm He-Ne laser which operated at 173°. After centrifuging the liposomes, the pellet was dispersed into PBS before analysis (500μl). The software was used to obtain and analyse the data (Dispersion Technology Software). Each sample (500μl) was measured in a polystyrene half-micro cuvette and for each sample, 15 runs were conducted lasting 10s each. The controlled temperature was at 25° and the size distribution and polydispersity index were obtained for the liposomes. The values are reported as the mean diameter ± standard deviation of eight measurements of the same sample.

5.2.3.2. MORPHOLOGY OF LIPOSOMES

The morphology of the liposomes was measured using the AFM in PeakForce QNM mode. The dispersed samples (100 µl) were diluted with 900 µl of distilled water to give a concentration in the range of 10^4 particle/ml. The metallic disc which the samples are viewed from, had a piece of mica tape to attract the liposomes towards the surface. 5 µl of the solution was left to dry on the disc for approximately 30 min and then was viewed on the AFM.

HepG2 cells were analysed by AFM after treatment with the liposomes, and the parameters used were scan specific and can be found on the designated figures. The liposome concentration applied to the cells was 10^3 particles/ml, and the cells were seeded (10^4 cell/cm^2) on a 35cm^2 petri dishes. Details of cell viability assays can be found in the general methods chapter.

5.3. RESULTS

5.3.1. LIPOSOME CHARACTERISATION

The liposomes were produced by two different methods, Thin Film Hydration (Rotary Evaporation) and Microfluidics (NanoAssemblr). They required to be sized to ensure they were in the correct size range for drug delivery. Three methods were used to size the liposomes as shown in Table 5.1.

Method	Size NTA /nm	Size DLS /nm	Size AFM /nm
Rotary Evaporation	244 ± 90	750 ± 500	360 ± 120
NanoAssemblr	126 ± 76	370 ± 170	256 ± 125

Table 5-1- Size characteristics of DMPC liposomes: The size was measured in three ways using the NanoTracking Analysis (NTA), Dynamic Light Scattering (DLS) and Atomic Force Microscope (AFM). (Average $\pm$ SD, n=8). Significant difference (*) in liposome size when using different sizing methods by one-way ANOVA test followed by Dunnett's multiple comparison (p<0.05)**.**
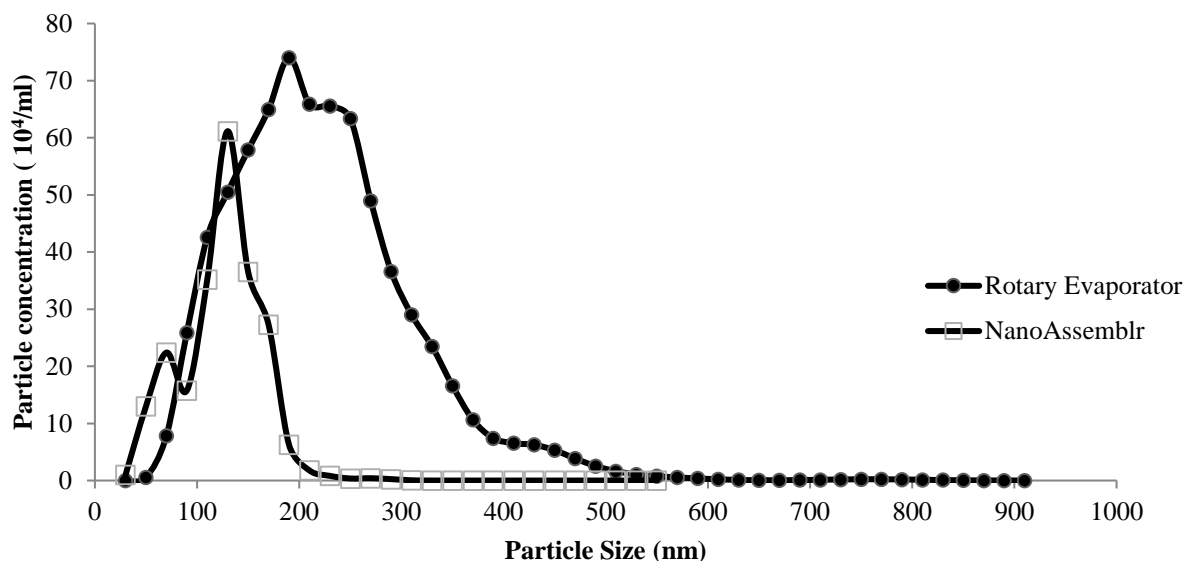
Figure 5.1 - Size distribution by use of NanoTracking Analysis (NTA). Example of one of the size distribution curve taken from NTA to emphasise the distribution from each production method, (1000μl from the final product). Particle size ranged from less than 100nm to above 400nm depending on the production method.

In Figure 5.1, the NTA sizing method was conducted on liposomes with both production methods used and it was shown that the Rotary Evaporator method had a broader size distribution in comparison to the NanoAssemblr produced liposomes. The morphology of the liposome is useful to understand the delivery pathway and drug uptake. In Figure 5.2, the morphology of the liposomes is presented. The NanoAssemblr liposomes were seen to be circular and homogeneous in shape, while the Rotary Evaporator produced liposomes are seen to vary in shape.

a)

b)
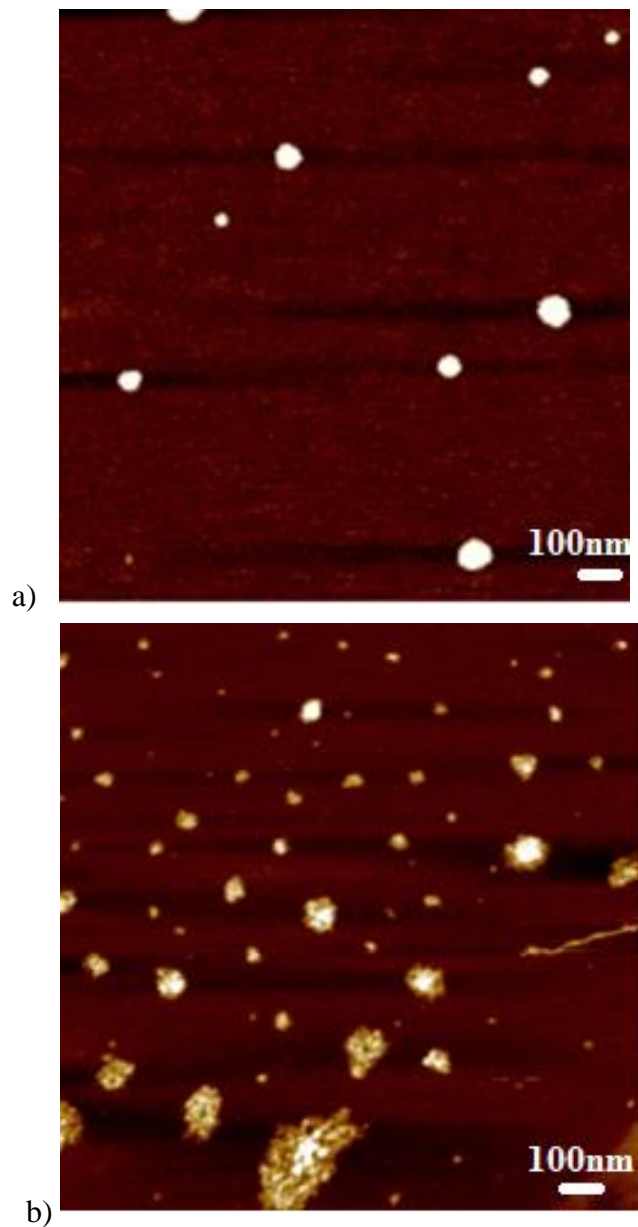
Figure 5.2 - AFM image of Liposomes produced by, a) NanoAssemblr b) Rotary Evaporator. Liposomes are more likely to have a homogenous shape if production was undertaken by the NanoAssemblr. The concentration of liposomes was found to show similarities to the nanotracking analysis. These images are one of 8 for each experimental set up.

Liposomes were added to HepG2 cell cultures to analyse possible reactions with the cell surface. Over the 14 samples analysed (Figure 5.3), there was found to be >70% showing indications that the liposomes were attached to the cell surface.
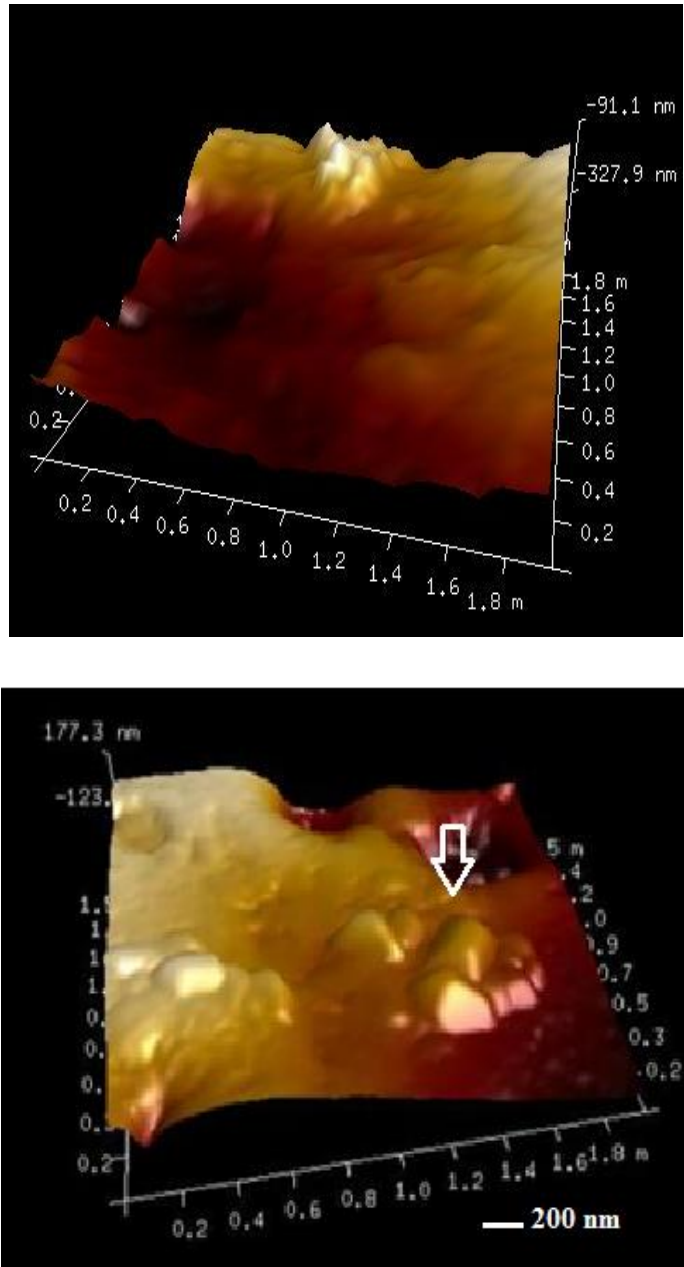
Figure 5.3 – HepG2 cell with liposomes fused to the surface. AFM conducted 24 hours after incubation of the cells with the DMPC liposomes. The arrow shown in the figure above, indicates a possible liposome on the cell surface. This was found to be the case in 10 cells over the examination of 14 cells.

The whole cell was analysed using AFM to observe any visual changes (Figure 5.4). The liposomes used were the NanoAssemblr liposomes as the size distribution was narrower. In Figure 5.4, the whole cell appeared to have a greater roughness after treatment with the liposomes
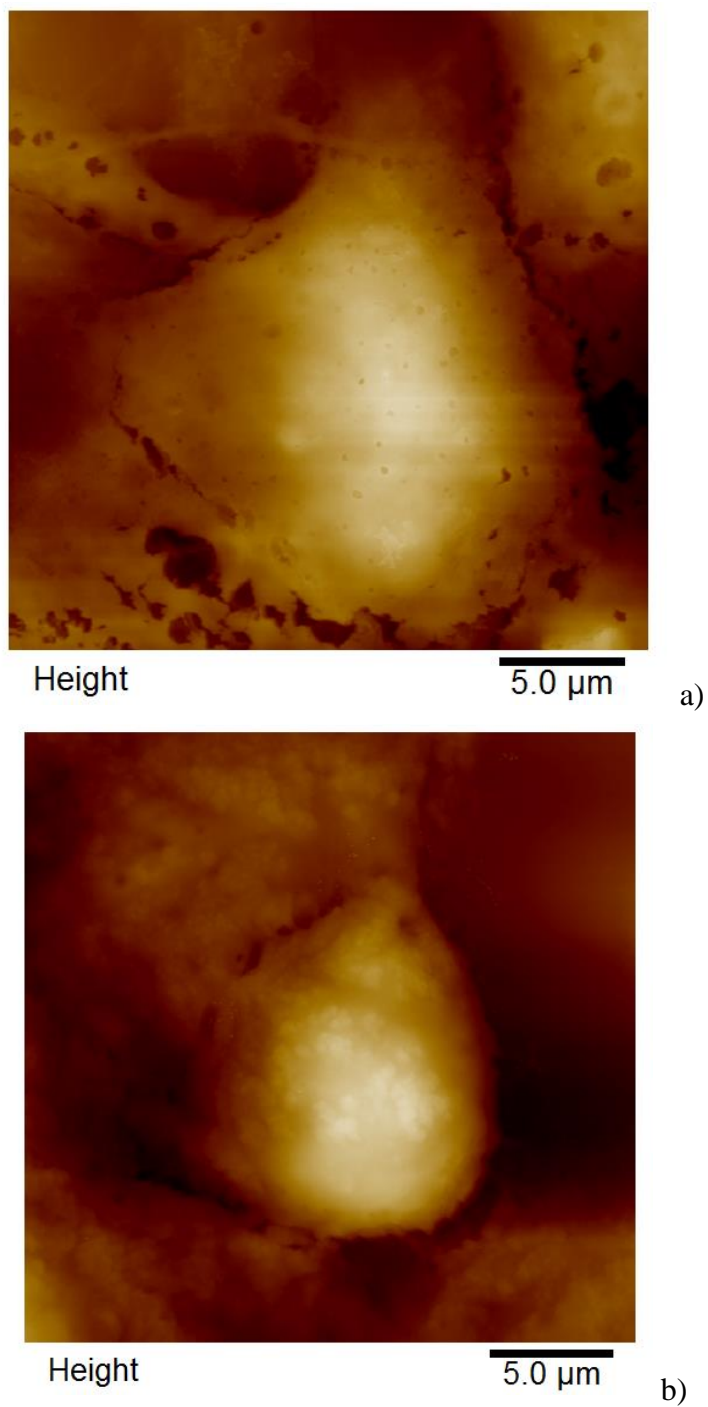
Figure 5.4 - Cell imaging, examining at the whole cell. These images were obtained using AFM and using force of 0.5nN at scan rate of 1Hz. a) Control HepG2 cell b) Cell treated with NanoAssemblr liposomes (10^3 particle/ml)

Two cell viability assays were conducted on HepG2 cells after a range of concentrations of liposomes were applied for a period of 72 h. In the graphs below (Figure 5.5), it was shown that even at the highest concentration of liposomes the cell viability was not significantly altered.
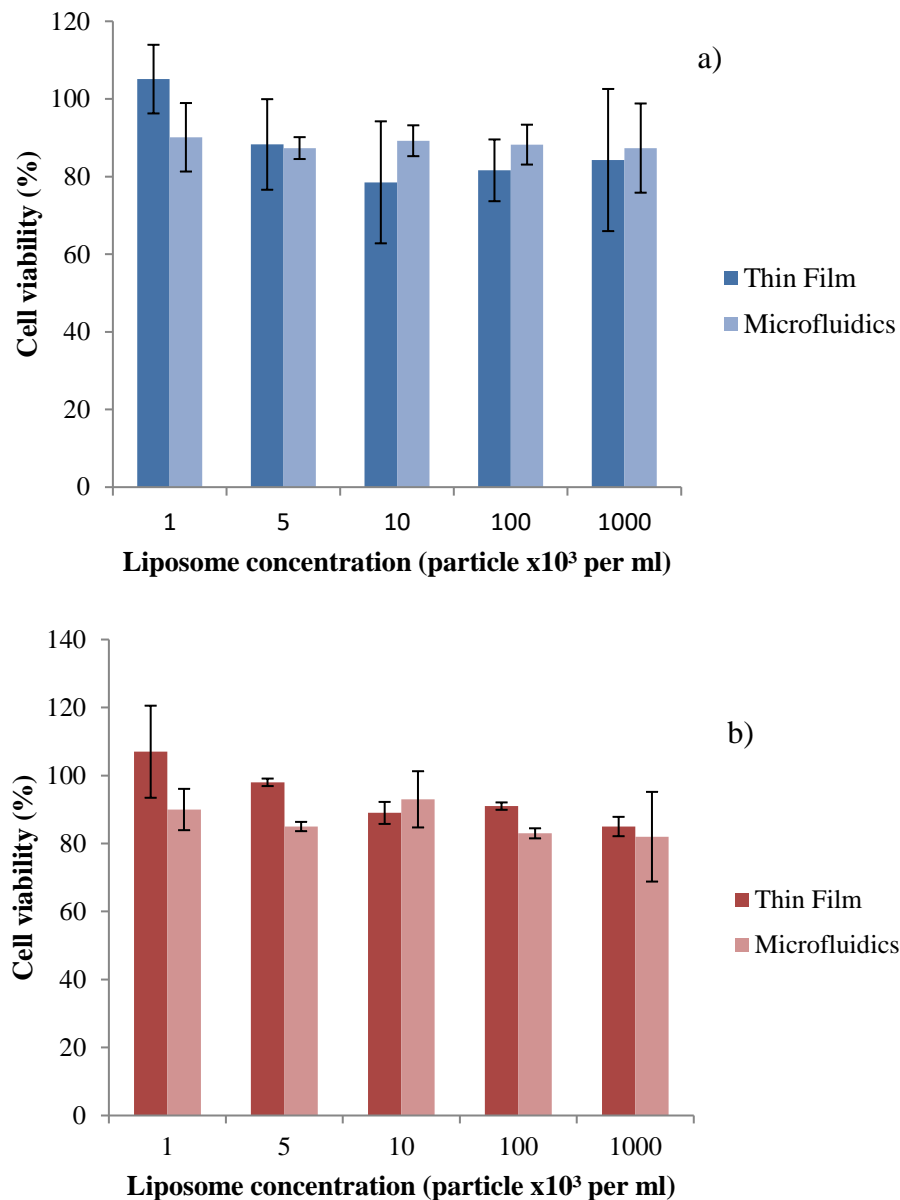
Figure 5.5 – Cytotoxicity assays conducted in the presence of DMPC empty liposomes (produced by the NanoAssemblr and Rotary Evaporator) for HepG2 cells over a period of 72hours. a) MTT assay b) Neutral Red assay. By one-way ANOVA test followed by Dunnett's multiple comparison no significant differences were detected compared to the control values ($p < 0.05$).

To verify that the liposomes had no effect on cell viability, fluorescent microscope was used. Two stains were applied (F-actin and DAPI) to observe any alterations occurring within the cell following treated with liposomes or 5-FU (Figure 5.6).
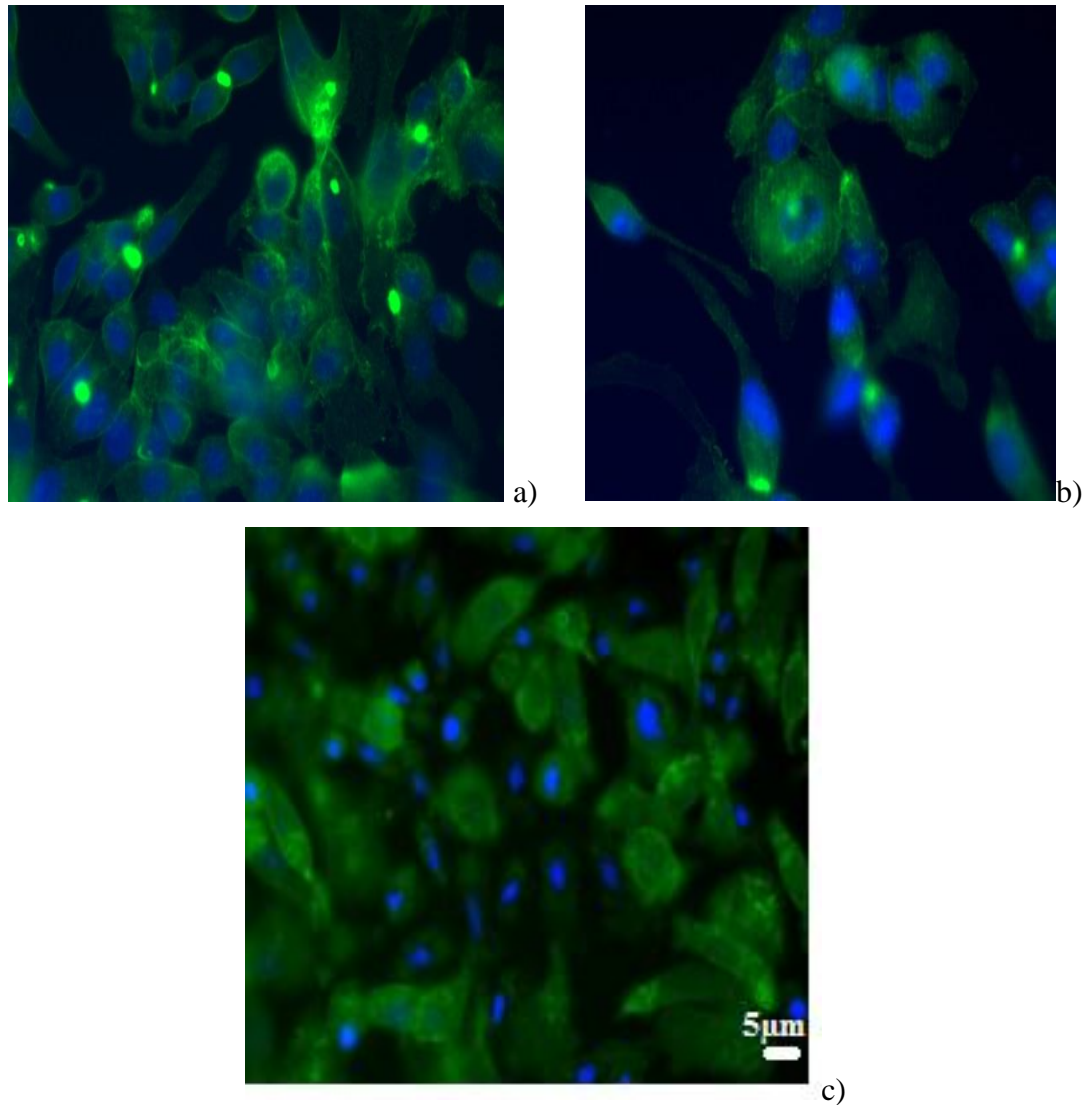
Figure 5.6 - Fluorescence images of HepG2 cells (x20 water lens) stained with FITC- Phalloidin and DAPI. a) Untreated HepG2 b) Empty Liposome Treated (concentration 10^3particles/ml) c) Drug only treated cells (concentration 0.5µg/ml). Images were taken 72 hours after treatment and the scale is the same throughout the images and using the fluorescence microscopy at an excitation wavelength of 450 -490nm and emission wavelength of 515-565nm.

The cells scanned by AFM can provide further information on physical characterisation as shown in Table 5.2. These parameters can assist with relating alterations which are occurring in the cell, to treatment. The surface area of the whole cell been calculated to decrease once 5-FU has been applied to the cells. However, the surface roughness was noted to increase which could be correlated with Figure 3.11, which showed protrusions from the cell surface. The liposome treated cells shown changes in surface area and roughness as both values increased. This could also be related to Figure 5.3, where liposomes were seen on the cell surface.

Cells	Height /μm	Surface Area / μm^2	Roughness / nm
Control	3.7 ± 0.3	254.6 ± 18.4	50 ± 17
Liposomes	3.5 ± 0.7	292.5 ± 14.3*	105 ± 14*
Drug Only	2.7 ± 0.4*	179.1 ± 20.2*	102 ± 20*

Table 5-2 - Properties of HepG2 cells measured by AFM for untreated or empty liposome treated cells (concentration - 10^{3}particle/ml) and drug treated cells (concentration - 0.5μg/ml) over a period of 72h. These values were achieved using the AFM in the QNM mode over 10 cells. The surface roughness was taken from 2μm^2 over 10 cells at three different points. Significant differences (*) in cell parameters comparing the untreated to the treated (liposomes and drug separately) by one-way ANOVA test followed by Dunnett's multiple comparison (p<0.05).

Summary of main findings

In this section, liposomes were produced by means of the thin film method and microfluidic method, described in Chapter 1.6 and Section 5.2. Liposomes were characterised for size and shape to ensure they would make a feasible drug delivery system. The ideal requirements for liposomes are to have homogenous size and shape, and be preferably under, 200nm in diameter.

- The microfluidic method of production produced liposomes with a narrow size distribution

- Liposomes engaged with the cell surface with respect to HepG2 cells

- Liposomes did not have effect on cell viability of HepG2 cells

There are many production methods to produce liposomes, some methods have been researched since the 1960s and others are more recent. In this study, an established method and recently developed method for the production of liposomes were compared. The established method is the thin hydration film method (using the rotary evaporator) and the more recently developed method, NanoAssembr (using microfluidics). For the liposomes to reach the target area as a drug, the delivery system should have the following homogeneous parameters; size and shape. It should be noted that penetrability of each tumour is highly variable. (Allen et al., 2013)

There are many studies stating the size of liposomes recommended for delivery of drugs to the hepatocytes. Ideally, the size should be below 200nm to facilitate passage through the pores in the blood vessels around the tumour site (Natarajan et al., 2014). Accumulation at the required target site is more likely to occur if the liposome size is below 200nm and this can reduce side effects relative to those of the free drug. There is an increase in the therapeutic index of drugs loaded in liposomes (Allen et al., 2013).

The size of the liposomes was characterised using three methods; NanoTracking Analysis (NTA), Dynamic Light Scattering (DLS) and AFM (Table 5.1). In Table 5.1, size measurements for all three methods are presented, and they show comparable results. The DLS results show larger sizes for liposomes compared to the other methods because the method possibly calculates the size of agglomerated particles as one. If the liposomes are agglomerated, there would be a high possibility that the drug would not reach its target site. This emphasises the importance of accurate measurement of the parameters of liposomes to be used for drug delivery. The filtration of the liposomes would be helpful to ensure removal of large agglomerates.

Figure 5.1 represents the distribution of the sizes of the liposomes by use of the NTA. When using the rotary evaporator to synthesise liposomes, their sizes give a broad distribution curve in comparison to the other synthesis method used. A previous study which also uses microfluidics platform to produce liposomes showed remarkable control of lipid nanoparticle size in the 20-100nm size range (Belliveau et al., 2012). For measuring the size of the liposomes, it was found that NTA was the better method as it provided useful results, in terms of distribution of size, and concentration of liposomes. Also, NTA software is advantageous

as a video can be recorded of liposomes which helped in visualising the flow of the liposomes.

Size is an important parameter but it is not the only one which is valuable when considering drug delivery. There is believed to be a relationship between particle size and the curvature of the liposome sphere which affects the opsonisation process (Moghimi et al., 2001). The AFM provides the ability to measure size and visual shape in fine detail. In Figure 5.2, the graph verifies the size distributions and helps visualisation of these liposomes. As shown (Figure 5.2a), the liposomes produced using microfluidics are circular particles with a relatively homogenous size range. However, the rotary evaporator (Figure 5.2b) produced liposomes which show a variety of irregular shapes ranging from circular to elongated wires. Shape is known to have an effect on delivery (Champion et al., 2007) but if the sample is not at all homologous then it will be hard to predict the delivery pathway. The only disadvantage to using AFM to measure the size of the liposome is that in solution they are floating, and or not bound to a surface. With the AFM, the mica tape (section 5.2, p143) will allow the liposomes to settle on the surface which in turn could let them spread out, so the environment is completely different to that experienced by the liposomes during drug delivery.

Stability of the liposomes is a vital parameter for a drug delivery system. In an ideal environment, the liposome would travel to the target site and release the drug slowly over time, but in practice this is rare. To minimise release before experiments, the organic solvent content would be removed from the solution. The rotary evaporator production method minimises the exposure to organic solvent compared to the microfluidic method, in which exposure to solvent would have to be minimised after the process had been completed.

The liposomes are required to bind to the surface of the cells but before this is achieved *in vivo*, there can be numerous barriers to overcome with regards to physiological and anatomical access to the target site. Liposomes can be designed to adhere to the cellular membrane to deliver a drug payload or simply transfer drugs following endocytosis (Bangham, 1995). In Figure 5.3, the liposomes are shown, likely fusing to the cell surface after a few hours of incubation. After a short time, the liposomes are attracted to the surface and then will be broken down which will result in the release the 5-FU.

One of the main concerns for the production of liposomes is advancing the methodology towards a scaled up version for commercial production. Recently, the company (Precision

Nanosystems) who developed the microfluidics equipment (NanoAssemblr) have advanced to processing up to 1 litre of end product which is beneficial for preclinical toxicology and other applications.

There are two main types of cell death which are recognised: apoptosis and necrosis (Zhang et al., 2011a), referred to in Chapter 1. Apoptosis can be triggered by different stimuli and mediated by alterations in enzymes and activated caspases. Apoptosis results in fragmentation of cells which are normally disposed of by support cells such as macrophages (Ojcius et al., 1998). The HepG2 cell line is a well-established cell line (Okajima et al., 2007, Li et al., 2011b) and the use of the liposomes to treat HCC would be beneficial. When conducting the cytotoxicity assays, it was found that the liposomes did not have a cytotoxic effect on the cells. Even though the concentration of liposomes was increased (10^6 particle/ml), there was no overt toxic effect when using either MTT or Neutral Red assay. This suggests that the liposomes would have no additional toxic effect in addition to that of the drug load they were carrying if used for drug encapsulation. It was first thought that as the NanoAssemblr method used a higher percentage of organic solvent, liposomes formed by this method may have an adverse effect on the cells, but this did not appear to be the case.

The functions of the actin cytoskeleton are essential for cell movement and structural support. Staining of F-actin and nuclear staining have shown that the liposomes do not have a noticeable effect on cytoskeletal or nuclear structure in HepG2 cells. The nuclei of the cells treated with drug only (Figure 5.6c) were shown to have decreased in size and fragmented. When this occurs it is known, to be related to apoptosis (Elmore, 2007). The optimisation of these interactions will enable more efficient chemotherapy for the treatment of cancer (Li et al., 2011a).

Table 5.2 shows the effects of treating the HepG2 cells with liposome or drug by height, surface area and roughness of the cells. The roughness of the untreated cell value is less than the cells treated with either the liposome or the free drug and this change in height could be due to the drug or liposome sitting on the cell surface. The liposome sizes range from 100 to 300nm and the increase in roughness may be due to possible liposome agglomeration on the surface. The higher the concentration of liposomes, the higher the agglomeration. Okajima et al, showed in their experiments the typical height for HepG2 cell to be 4µm (Okajima et al., 2007). The data from the table show that the cells were able to retain their structure after

treatment with empty liposomes or the drug. The surface area of the cell was seen to shrink with drug 5-FU, as can be also seen in the fluorescence microscopy images (Figure 5.6) of the cells and could indicate cells going through apoptosis. In a previous chapter, AFM revealed alterations in the cell surface after treatment with 5-FU (Figure 3.11). Protrusions were shown will influence the roughness result, and such effects are seen in the data on Table 5.2.

Liposomes as drug delivery systems have advanced to the commercial stage for clinical use. The aims of this chapter included investigation of the method of production. It was found that liposomes produced by the microfluidic preparation were more homogenous and circular in comparison to those produced by the method of thin film. The liposomes were found not to be cytotoxic and may therefore help reduce the toxicity issues of chemotherapeutic drugs towards non-cancerous tissue. It is anticipated that, liposomes would create slow release of 5-FU, which would reduce time for patients to spend in hospital, as this therapy could then be taken by the patients at home.

Chapter 6 - SUMMARY AND FUTURE WORK

6.1. SUMMARY OF THESIS RESULTS

In the UK, the number of new cases of HCC remains relatively stable nevertheless there is a suggestion by Health Board England that there is a fall in the number deaths (~11%)(Costella et al., 2016). These results are still preliminary, however, the outcome is believed to be due to a new treatment being implemented (directly acting antiviral, DAA). These DAA drugs are only reducing the premature mortality rates of HCC and are not related to prevention rates (Targett-Adams et al., 2011).

Drug research involves the development of novel drugs as well as analysis of the efficacy of established drugs to evaluate possible adaptations required for the improvement of treatment. The use of 5-FU as a chemotherapy drug has been around since the 1960s. Recently, instead of IV injections, patients are receiving treatment through an infusion pump, where they remain attached to this pump for up to five days at a time. Diclofenac is a NSAID which is mainly used as for inflammatory diseases but is known to have side effects relating to the liver. These two drugs, 5-FU and diclofenac have different metabolic pathways, but both can cause toxicity within the liver cells.

AFM is an invasive technique where a cantilever scans a surface to produce images. A force curve can be produced every time the cantilever contacts the surface. There are known limitations with the AFM (documented in previous Chapters) given the high chance of error or artefacts appearing on scans. Application of AFM to cells can produce detailed images of the surface as well as obtaining force curves. As explained previously, these force curves can assist in the understanding with cantilever-sample interactions and can produce values for quantities such as Young's modulus.

The current investigation has focused on the viability, morphology and toxicity of the drugs, 5-FU and diclofenac applied to HepG2 cells. The intention of this study was to explore the toxic effects of the two drugs which have different mechanisms of metabolism and relate it to mechanical measurements achieved by AFM. We examined the apoptotic effects caused by 5-FU and visualised the cell surface with the assistance of AFM. Results were also obtained

by application of diclofenac, to analyse energy production (ATP synthesis) in the cell, following the addition of either glucose or galactose to the medium. It was hoped that application of this drug would alter the energy processes within the cell and may aid chemotherapy, as it is known that the metabolism in cancer and normal cells are different. Liposomes are frequently being developed to assist in targeting bioavailability of drugs. There are several ways to produce liposomes but the end result requires liposomes to have homogenous characteristics.

In the following sections of this chapter, there is a summary of the main findings of this work and their implications for future drug research. Additionally, there are limitations of the study discussed which would improve procedures in future work.

6.1.1. TOXICITY OF 5-FU IN HEPG2 CELLS

HepG2 cells were exposed with 5-FU for 24, 48 and 72h at a range of concentrations. Cells incubated with the higher concentrations were observed to show indications of apoptosis at all time points. Apoptosis was more clearly defined at 72h using flow cytometry where ~78% of cells were in the process of cell death.

The actin fibres in the control cells were shown to be distributed throughout the cell, particularly around the nucleus. However, after treatment, the actin fibres moved towards the cell membrane. Also, the cells showed clear indications of fragmentation, shrinkage and blebbing, which are all signs of apoptosis. The AFM experiments scanned the cell surface of the control cells and then cells treated with 5-FU for 72h. The images revealed clear indications that the cell surface had been altered after treatment with 5-FU. Specifically, the cells were shown to have networking lines and protrusions, appearing at the surface.

After treatment with 5-FU, the Young's modulus did decrease when using the spherical indenter but not a significant amount. When the pyramidal indenter was used, it increased the values substantially due to the area indented being smaller (Figure 2.18) and therefore measured being dramatically smaller thus detecting properties of only certain components of the cell. Additionally, as the variance was high when the pyramidal indenter was used, no significant difference could be established. Force curves obtained typically showed an unbinding force when the cantilever was releasing from the surface of cells treated with 5-FU for 72h, but this was not seen in control cells, which suggests interactions occurring between

the surface of the treated cells and the cantilever. Although alterations in the membrane biomechanics in terms of Young's modulus were detected, the results were not conclusive.

6.1.2. TOXICITY OF DICLOFENAC IN HEPG2 CELLS

The energy production process inside HepG2 cells were altered when galactose was supplied to the cells instead of glucose. The cell viability was reduced when they were treated with diclofenac over a range of concentrations and time points (16, 24, 48 and 72h). The use of the NR assay produced what is thought to be a false result showing that the cell number was not significantly altered with application of diclofenac; even at the highest concentration applied. This result was then related to the fluorescence microscopy results, where high concentrations of (unexpected) red fluorescence was displayed. The explanation for this is believed to be related to acridine orange (AO) accumulation in acidic compartments possibly lysosomes. In these acidic components of the cell, there are dimers which take place causing the red fluorescence.

The ATP content was measured by both bioluminescence and HPLC assays. The results obtained showed depletion of ATP content after diclofenac had been applied. Analysis of the control cells showed the at ATP content of the glucose supplemented cells increased with time, whilst that of the galactose supplemented cells reduced.

Using AFM, there were alterations detected on the HepG2 cell surface after treatment with diclofenac where the cells appeared to become rougher. The spherical indenter was used in separate experiments for diclofenac. The force curves achieved showed interactions occurring after treatment with diclofenac, showing two points of release from the surface which was not seen in control samples. These results suggest at these time points, molecules appear underneath surface which could be related to the mechanisms of the drug. These alterations could be related to membrane changes due to the generation of apoptotic cells.

6.1.3. PRODUCTION AND CHARACTERISATION OF LIPOSOMES FOR DRUG DELIVERY TO IMPROVE TARGETING AND REDUCE THE TOXICITY OF 5-FU

Liposomes can be produced in numerous ways but the most advantageous technique would ensure the physical parameters of the liposomes are homogenous. In this section, two production methods (microfluidics and thin film method) were used to obtain liposomes. The liposomes produced by the microfluidics method (NanoAssemblr) had a more consistent homogenous size range and were observed to be spherical in shape. In comparison, the thin film method had a wide range in sizes and the shape did not always display consistency. The liposomes did not affect the HepG2 cell viability, and may accumulate on the cell surface after a short period of incubation.

6.2.   MAIN FINDINGS

The main findings of this thesis are:

- Concentrations of 5-FU above 5 µg/ml were observed to influence metabolic function after 48 h

- HepG2 cell proliferation was inhibited by 5-FU, with a significantly lower LD_{50} than that for MTT or NR assays

- MTT and CV assays were more sensitive at detecting diclofenac induced changes in cell viability than NR

- Apoptosis was prominent after 72 h exposure, with the majority of treated cells (0.05-500µg/ml) showing clear signs.

- Live cell imaging of HepG2 cell, before and after treatment with 5-FU

- 5-FU treated HepG2 cells have noticeable cell membrane protrusions and highlighted networking lines at the cell surface when imaged on the AFM

- HepG2 cells were grown in galactose supplemented medium in place of glucose which slowed down growth and metabolic activity at 16h as measured by MTT

- Diclofenac causes a depletion in ATP as measured by bioluminescence and ATP analyses

- AFM showed a change in appearance with regards to HepG2 surface after treatment with diclofenac and 5-FU

- Optimisation of software parameters, for the indentation of cells is vital to give reliable results

- Force distance curves demonstrated interactions with the cell surface after drug treatment

- Young's modulus of HepG2 cells did not alter significantly after drug treatment

- The microfluidic method of production produced liposomes with a narrower/more consistent size distribution

- Liposomes engaged with the cell surface with respect to HepG2 cells and did not have an effect on cell viability

6.3.   LIMITATIONS OF THESE STUDIES

Although this current thesis has shown work with HepG2 cells, observing the toxic effect of drugs and relating this to cell surface alterations. There are a few limitations within each of the studies. Firstly, the data achieved from *in vitro* may not reflect the situation of *in vivo* where different responses could result in different cell action, and the toxic effect in an *in vitro* environment is not a true reflection of the toxic response *in vivo*. The HepG2 cell line used has been experimented with since 1970s, and is known to express weakly at the gene expression level compared with primary hepatocytes. Newer cellular models (HepaRG) are being implemented in studies to improve upon the metabolic profiles observed in HepG2 cells and their responses may mimic that of primary hepatocyte more clearly. The drugs concentrations applied to the HepG2 cells were relatively high in comparison to quantities applied to *in vivo,* and circulating blood levels.

AFM has multiple capabilities and the application of these to experiments can be time consuming. The imaging process can however be relatively straight-forward and it should be ensured that noise is not affecting the final image. Artefacts produced can be related to the cantilever, and if there is contamination on the tip, this can lead to blurred scans. Also, the cantilever sharpness can improve image quality as there is a higher aspect ratio, defining area of detail. The complexity of this technique arises when analysing deformable materials in liquid such as cells, as hydrodynamic forces become more apparent due to the cantilever movement.

The calibration of the AFM for mechanical measurements needs to be carefully adhered to. If not this is when errors can occur and the end results may not make for sensible conclusions. Each cantilever type will have a region at which it is resonant and if this is not the case the cantilever should not be used for mechanical measurements.

The relationship between tip geometry and elastic measurements is important to observe as this can have a significant effect on results. There is a wide range of elasticity measurements in the literature as well as vast number of cell lines being studied. In this study, both spherical and pyramidal indenters were used. The spherical indenters were favoured as the tip gives an overall representation of elasticity behaviour of the cell rather than at a specific point of interest (~5nm) as with the pyramidal indenter.

The application of mathematical models to fit the force distance curve produced by AFM has limiting aspects to the procedure. It can be said, that there is no perfectly suited model for the indentation measurements. In an ideal circumstance, one aim of this study would have been to test a range of models and compared them in different situations. With the understanding of the Hertz model, an initial range of parameters was applied to ensure the model fitted successfully and produce reliable results. The number of cells indented was relatively high in comparison to other publications to ensure values were true to the experiment and to reduce the error.

Liposomes bring the opportunity to improve delivery parameters of established drugs. The production of liposomes used to be very time consuming but now the use of the microfluidics method such as the NanoAssemblr has reduced the production time dramatically. However, the main concern is with regards to the stability and targeting of the liposomes. In this study, liposomes were stored in a small quantity of organic solvent, which is not ideal for long term stability and so further procedures are required to enhance this.

6.4. FUTURE WORK

Certain aspects of this study displayed scope and promise for further investigation, these areas will be explained in detail below.

6.4.1. AFM AND ENHANCEMENT OF ITS CAPABILITIES

The technique of AFM allowed us to present detailed images of HepG2 cells after treatment with 5-FU showing networking lines and protrusions from the cell. In most studies, AFM is used to analyse the whole cell but it can be difficult to obtain finer details. The microfabrication process has improved the output of cantilevers, therefore the details on the surface can be seen more prominently and will eventually lead to atomic resolution. Also, the amount of force applied to the cell is related to the resolution of images produced by AFM. A study by Schillers and co-workers showed applied forces as small as 80pN could provide more detailed images of microvilli (Schillers et al., 2016).

Tip functionalisation has been conducted on many cell types in different studies (Grady et al., 2016). Using this technique, cellular actions at a single molecule level can be more clearly understood. This could demonstrate the molecule responsible for an effect on the surface by expression of various types of receptors. In this study, there were interactions shown between the spherical probe and the cell surface after drug treatment. There is potential to develop an AFM adhesion assay to investigate this in to cells after drug treatment (Figure 6.1). The interactions between the primary cell receptor CD44 and hyaluronic acid are well documented (Aruffo et al., 1990). Throughout the cell, this receptor participates in tumour growth (Klingbeil et al., 2009) and cell migration (Kajita et al., 2001). The spherical probe could be functionalised with the hyaluronic acid and if these receptors were found this could mimic different physiological conditions. Similar studies have analysed the interactions on the cell surface with other possible receptors, such as angiotensin II (Lamontagne et al., 2008).
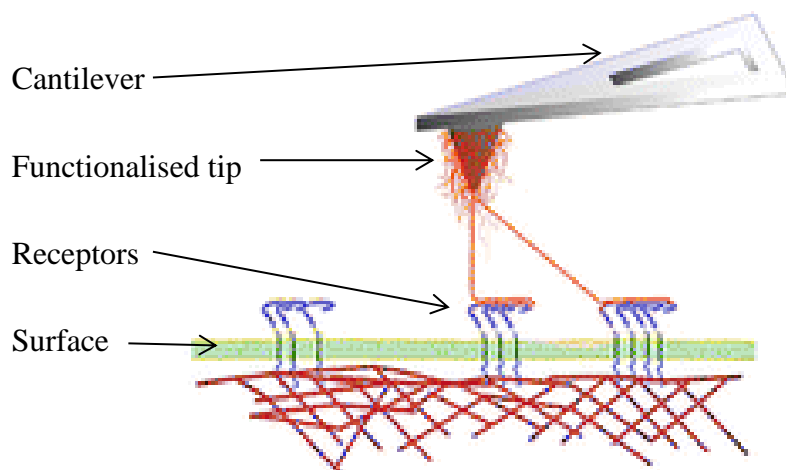
Figure 6.1 - Experimental setup for AFM functionalisation to stimulate the receptor on cell surface.

6.4.2. MITOCHONDRIAL TOXICITY

Mitochondria are vital for cell survival as they are involved in the production of ATP. As mentioned previously, the metabolism between normal and cancer cells functions differently. In this study, the ATP content was analysed but additional experiments are required to prove that diclofenac is a mitochondrial toxicant, ToxGlo assay which is mitochondria specific assay. The assay investigates biomarkers associated with alterations in cellular ATP levels relative to vehicle treated control cells and cell membrane integrity during exposure periods.

Recent developments of flicker-assisted localisation microscopy (FaLM) can resolve mitochondrial structure within the cell (Chalmers et al., 2016). In this study, Chalmers and co-workers investigated age-associated mitochondrial dysfunction and related the outcome to vascular diseases. The principle behind this is to record cationic fluorophore intensity to analyse the position and shape of the mitochondria from an electrical signal. The technique can provide information about the dynamics of the mitochondria and provide a link with mechanisms occurring in the cell due to mitochondrial toxicants.

Additionally, it would be beneficial to combine cellular and mitochondrial assays to aid in the prediction of drug-induced mitochondrial toxicity in the liver. It would also be advantageous

to use different and more organotypic cell lines (HepRG) to compare the drug metabolites with mitochondrial toxicity in the long term.

6.4.3. IMPROVISATION OF THE 5-FU PUMP WITH THE INCORPORATION OF LIPOSOMES

The use of 5-FU is becoming more common in the NHS environment with patients with different types of cancers being attached to a pump for 5 days on several occasions across a few months. Once successfully obtained, liposomes it could be advantageous to analyse the effects in a similar time frame as the traditional 5-FU pump. If the result proved to be positive, the finial result could be the patient can be removed from the pump sooner.

Initially, the release rate for 5-FU would need to be calculated and would hopefully is comparable to other studies. The liposomes would be produced from the NanoAssemblr and *in vitro* studies could be conducted to see the effectiveness.

6.4.4. RELATING TOXICITY OF DRUGS WITH SURFACE MORPHOLOGY

Results from this work have shown that the toxicity of two drugs with divergent mechanisms of action was accompanied by changes in the cell surface of the HepG2 cells. This study aimed to correlate changes in the cell surface with development of apoptosis, and while the results support this hypothesis, there are insufficient data to prove it. In Figure 6.2, an overview of the results with regards to the two drugs (5-FU and diclofenac) is presented. The drug, 5-FU is a known to halt DNA synthesis and in this thesis, apoptosis was observed. Additionally, the HepG2 cells were observed to have networking fibres which increased the roughness of the cell. Alterations in Young's modulus of HepG2 cells occurred at 72h after 5µg/ml of 5-FU was applied. When diclofenac was applied to HepG2 cells, a cytotoxic response and alterations to the cell surface was observed. However, there was no significant difference in Young's modulus over time. It is thought over a longer time period, Young's modulus would alter similarly to 5-FU but additional experiments need to be conducted. The results presented in this thesis give a comprehensive perspective for analyses of cytotoxic processes in HepG2 cells. The benefits of traditional methods for understanding cytotoxicity within the cell were exhibited but additionally the nanomechanical properties of the cells by

use of AFM can show us aspects of cell surface morphology which will add to our understanding of the events of apoptosis.
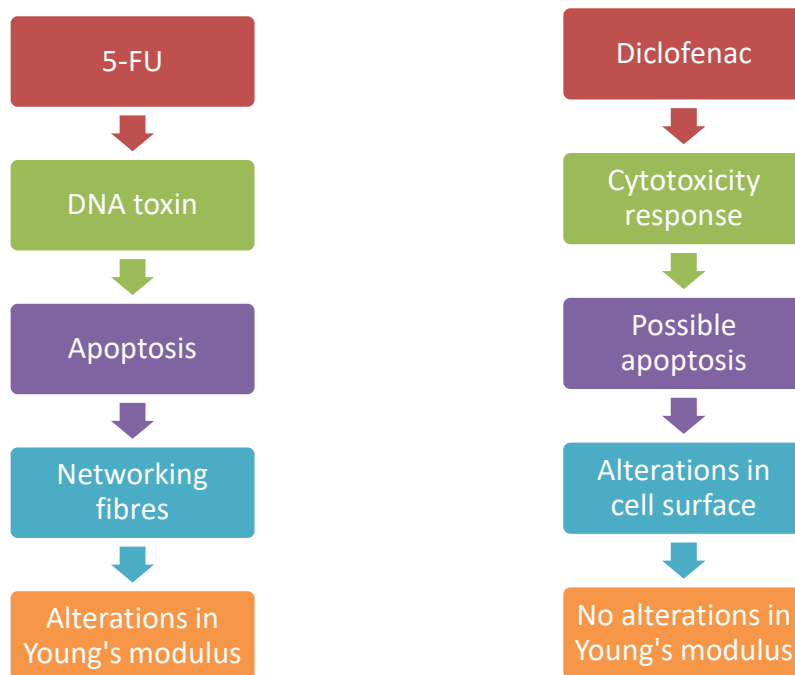
Figure 6.2- Flow chart of outcomes regarding the two drugs in this thesis. The processes above allow the comparison of the two toxins and express potential for future experiments.

The main limiting factor to progress was the time taken to establish, develop and apply AFM to measurements of morphology and biomechanical properties of live cells. I foresee that this technology will develop rapidly in this direction in the future. In conclusion, the AFM nanoindentation method could assist with quantitative values for Young's modulus and thereby could be a beneficial method for toxicity profiling in HepG2 cells at subcellular level.

List of Publications

Conference Proceedings

Kemp, O, Grant, M & Lamprou, D 2015, 'Microfluidics liposome formulation and investigation of liposome-cell interactions by atomic force microscopy' The 42nd Annual Meeting & Exposition of the Controlled Release Society, Edinburgh, United Kingdom, 26/07/15 - 29/07/15.

Kemp, O, Grant, H & Lamprou, D 2014, 'Atomic force microscopy (AFM) analysis of nanocarrier–cell interaction' *Toxicology Letters*, vol 229, no. Supplement, P-1.86, pp. S67. DOI: 10.1016/j.toxlet.2014.06.26667 1 p., P-1.86

REFERENCES

ABACI, H. E., SHEN, Y.-I., TAN, S. & GERECHT, S. 2014. Recapitulating physiological and pathological shear stress and oxygen to model vasculature in health and disease. *Scientific Reports,* 4**,** 4951.

ADEN, D., FOGEL, A., PLOTKIN, S., DAMJANOV, I. & KNOWLES, B. 1979. Controlled synthesis of HBsAg in a differentiated human liver carcinoma-derived cell line. *Nature,* 282**,** 615-616.

AFOLARANMI, G. A., HENDERSON, C. & GRANT, M. H. 2011. Effect of chromium and cobalt ions on phase I and phase II enzymatic activities in vitro in freshly isolated rat hepatocytes. *Toxicology in Vitro,* 25**,** 125-130.

AGUER, C., GAMBAROTTA, D., MAILLOUX, R. J., MOFFAT, C., DENT, R., MCPHERSON, R. & HARPER, M.-E. 2011. Galactose Enhances Oxidative Metabolism and Reveals Mitochondrial Dysfunction in Human Primary Muscle Cells. *PLoS ONE,* 6**,** e28536.

AHN, S., SEO, E., KIM, K. & LEE, S. J. 2013. Controlled cellular uptake and drug efficacy of nanotherapeutics. *Scientific Reports,* 3**,** 1997.

AKBARZADEH, A., REZAEI-SADABADY, R., DAVARAN, S., JOO, S. W., ZARGHAMI, N., HANIFEHPOUR, Y., SAMIEI, M., KOUHI, M. & NEJATI-KOSHKI, K. 2013. Liposome: classification, preparation, and applications. *Nanoscale Research Letters,* 8**,** 102-102.

ALLEN, T. M. & CULLIS, P. R. 2004. Drug Delivery Systems: Entering the Mainstream. *Science,* 303**,** 1818-1822.

ALLEN, T. M., CULLIS, P. R. & GSD 2013. Liposomal drug delivery systems: From concept to clinical applications. *Advanced Drug Delivery Reviews,* 65**,** 36-48.

ALSTEENS, D., DUPRES, V., YUNUS, S., LATGÉ, J.-P., HEINISCH, J. J. & DUFRÊNE, Y. F. 2012. High-Resolution Imaging of Chemical and Biological Sites on Living Cells Using Peak Force Tapping Atomic Force Microscopy. *Langmuir,* 28**,** 16738-16744.

ALTMANN, B., GISELBRECHT, S., WEIBEZAHN, K. F., WELLE, A. & GOTTWALD, E. 2008. The three-dimensional cultivation of the carcinoma cell line HepG2 in a perfused chip system leads to a more differentiated phenotype of the cells compared to monolayer culture. *Biomedical Materials,* 3**,** 034120.

ANKARCRONA, M., DYPBUKT, J. M., BONFOCO, E., ZHIVOTOVSKY, B., ORRENIUS, S., LIPTON, S. A. & NICOTERA, P. 1995. Glutamate-induced neuronal death: A succession of necrosis or apoptosis depending on mitochondrial function. *Neuron,* 15**,** 961-973.

ARUFFO, A., STAMENKOVIC, I., MELNICK, M., UNDERHILL, C. B. & SEED, B. 1990. CD44 is the principal cell surface receptor for hyaluronate. *cell,* 61**,** 1303-1313.

ATTENE-RAMOS, M. S., HUANG, R., SAKAMURU, S., WITT, K. L., BEESON, G. C., SHOU, L., SCHNELLMANN, R. G., BEESON, C. C., TICE, R. R. & AUSTIN, C. P. 2013. Systematic study of mitochondrial toxicity of environmental chemicals using quantitative high throughput screening. *Chemical research in toxicology,* 26**,** 1323-1332.

BAE, Y. H. & PARK, K. 2011. Targeted drug delivery to tumors: Myths, reality and possibility. *Journal of Controlled Release,* 153**,** 198-205.

BANDELE, O. J., SANTILLO, M. F., FERGUSON, M. & WIESENFELD, P. L. 2012. In vitro toxicity screening of chemical mixtures using HepG2/C3A cells. *Food and Chemical Toxicology,* 1653-1699.

BANGHAM, A. D. 1995. Surrogate cells or trojan horses. The discovery of liposomes. *BioEssays,* 17**,** 1081-1088.

BANGHAM, A. D., STANDISH, M. M. & WATKINS, J. C. 1965. Diffusion of univalent ions across the lamellae of swollen phospholipids. *J Mol Biol,* 13**,** 238-52.

BARAK, V., GOIKE, H., PANARETAKIS, K. W. & EINARSSON, R. 2004. Clinical utility of cytokeratins as tumor markers. *Clinical Biochemistry,* 37**,** 529-540.

BARBEE, K. A., DAVIES, P. F. & LAL, R. 1994. Shear stress-induced reorganization of the surface topography of living endothelial cells imaged by atomic force microscopy. *Circulation Research,* 74**,** 163-171.

BARBOSA, P. & PETERS, T. M. 1971. The effects of vital dyes on living organisms with special reference to methylene blue and neutral red. *The Histochemical Journal,* 3**,** 71-93.

BELLANCE, N., BENARD, G., FURT, F., BEGUERET, H., SMOLKOVA, K., PASSERIEUX, E., DELAGE, J., BASTE, J., MOREAU, P. & ROSSIGNOL, R. 2009. Bioenergetics of lung tumors: alteration of mitochondrial biogenesis and respiratory capacity. *The international journal of biochemistry & cell biology,* 41**,** 2566-2577.

BELLIVEAU, N. M., HUFT, J., LIN, P. J. C., CHEN, S., LEUNG, A. K. K., LEAVER, T. J., WILD, A. W., LEE, J. B., TAYLOR, R. J., TAM, Y. K., HANSEN, C. L. & CULLIS, P. R. 2012. Microfluidic Synthesis of Highly Potent Limit-size Lipid Nanoparticles for In Vivo Delivery of siRNA. *Mol Ther Nucleic Acids,* 1**,** e37.

BOLTJES, A., MOVITA, D., BOONSTRA, A. & WOLTMAN, A. M. 2014. The role of Kupffer cells in hepatitis B and hepatitis C virus infections. *Journal of Hepatology,* 61**,** 660-671.

BORNER, M. M., KNEER, J., CREVOISIER, C., BRUNNER, K. W. & CERNY, T. 1993. Bioavailability and feasibility of subcutaneous 5-fluorouracil. *British Journal of Cancer,* 68**,** 537-539.

BORT, R., PONSODA, X., JOVER, R., GÓMEZ-LECHÓN, M. J. & CASTELL, J. V. 1999. Diclofenac toxicity to hepatocytes: a role for drug metabolism in cell toxicity. *Journal of Pharmacology and Experimental Therapeutics,* 288**,** 65-72.

BOYER, T. D., WRIGHT, T. L. & MANNS, M. P. 2011. *Zakim and Boyer's Hepatology: A Textbook of Liver Disease*, Elsevier Health Sciences.

BOZZUTO, G. & MOLINARI, A. 2015. Liposomes as nanomedical devices. *International journal of nanomedicine,* 10**,** 975-999.

BRAET, F. & RADMACHER, M. 2012. Foreword to the special issue on AFM in biology & bionanomedicine. *Micron,* 43**,** 1211.

BRAET, F., ROTSCH, C., WISSE, E. & RADMACHER, M. 1998. Comparison of fixed and living liver endothelial cells by atomic force microscopy. *Applied Physics A: Materials Science & Processing,* 66**,** S575-S578.

BRAGUER, D., CARRÉ, M. & ESTEVE, M.-A. 2007. Microtubules in apoptosis induction: are they necessary? *Current cancer drug targets,* 7**,** 713-729.

BRANNON-PEPPAS, L. & BLANCHETTE, J. O. 2012. Nanoparticle and targeted systems for cancer therapy. *Advanced Drug Delivery Reviews***,** 206-212.

BRATTON, D. L., FADOK, V. A., RICHTER, D. A., KAILEY, J. M., GUTHRIE, L. A. & HENSON, P. M. 1997. Appearance of phosphatidylserine on apoptotic cells requires calcium-mediated nonspecific flip-flop and is enhanced by loss of the aminophospholipid translocase. *Journal of Biological Chemistry,* 272**,** 26159-26165.

BRENES, O., ARCE, F., GÄTJENS-BONICHE, O. & DÍAZ, C. 2007. Characterization of cell death events induced by anti-neoplastic drugs cisplatin, paclitaxel and 5-fluorouracil on human hepatoma cell lines: Possible mechanisms of cell resistance. *Biomedicine & Pharmacotherapy,* 61**,** 347-355.

BRUIX, J. & SHERMAN, M. 2011. Management of hepatocellular carcinoma: An update. *Hepatology,* 53**,** 1020-1022.

BURROUGHS, A. K. 2011. The hepatic artery, portal venous system and portal hypertension: the hepatic veins and liver in circulatory failure.

BUTT, H.-J. 1991. Measuring electrostatic, van der Waals, and hydration forces in electrolyte solutions with an atomic force microscope. *Biophysical Journal,* 60**,** 1438.

BUTT, H. J., CAPPELLA, B. & KAPPL, M. 2005. Force measurements with the atomic force microscope: Technique, interpretation and applications. *Surface Science Reports,* 59**,** 1-152.

CAILLE, N., THOUMINE, O., TARDY, Y. & MEISTER, J.-J. 2002. Contribution of the nucleus to the mechanical properties of endothelial cells. *Journal of Biomechanics,* 35**,** 177-187.

CALDERWOOD, S. K., KHALEQUE, M. A., SAWYER, D. B. & CIOCCA, D. R. 2006. Heat shock proteins in cancer: chaperones of tumorigenesis. *Trends in biochemical sciences,* 31**,** 164-172.

CANTON, D. A. & LITCHFIELD, D. W. 2006. The shape of things to come: An emerging role for protein kinase CK2 in the regulation of cell morphology and the cytoskeleton. *Cellular Signalling,* 18**,** 267-275.

CAO, H., PHAN, H. & YANG, L.-X. 2012. Improved Chemotherapy for Hepatocellular Carcinoma. *Anticancer Research,* 32**,** 1379-1386.

CAPPELLA, B. & DIETLER, G. 1999. Force-distance curves by atomic force microscopy. *Surface Science Reports,* 34**,** 1-104.

CHALMERS, S., SAUNTER, C. D., GIRKIN, J. M. & MCCARRON, J. G. 2016. Age decreases mitochondrial motility and increases mitochondrial size in vascular smooth muscle. *The Journal of physiology,* 594**,** 4283-4295.

CHAMPION, J. A., KATARE, Y. K. & MITRAGOTRI, S. 2007. Particle shape: A new design parameter for micro- and nanoscale drug delivery carriers. *Journal of Controlled Release,* 121**,** 3-9.

CHANG, H.-C., CHEN, T.-L. & CHEN, R.-M. 2009. Cytoskeleton Interruption in Human Hepatoma HepG2 Cells Induced by Ketamine Occurs Possibly through Suppression of Calcium Mobilization and Mitochondrial Function. *Drug Metabolism and Disposition,* 37**,** 24-31.

CHARRAS, G. T., HU, C.-K., COUGHLIN, M. & MITCHISON, T. J. 2006. Reassembly of contractile actin cortex in cell blebs. *The Journal of cell biology,* 175**,** 477-490.

CHEN, H.-W., SU, S.-F., CHIEN, C.-T., LIN, W.-H., YU, S.-L., CHOU, C.-C., CHEN, J. J. W. & YANG, P.-C. 2006. Titanium dioxide nanoparticles induce emphysema-like lung injury in mice. *The FASEB Journal,* 20**,** 2393-2395.

CHEN, J. 2014. *Nanobiomechanics of living cells: a review*.

CHO, K., WANG, X., NIE, S., CHEN, Z. & SHIN, D. M. 2008. Therapeutic Nanoparticles for Drug Delivery in Cancer. *Clinical Cancer Research,* 14**,** 1310-1316.

COLAÇO, R. & CARVALHO, P. 2013. Atomic force microscopy in bioengineering applications. *Scanning Probe Microscopy in Nanoscience and Nanotechnology 3.* Springer.

COLEMAN, M. L., SAHAI, E. A., YEO, M., BOSCH, M., DEWAR, A. & OLSON, M. F. 2001. Membrane blebbing during apoptosis results from caspase-mediated activation of ROCK I. *Nature cell biology,* 3**,** 339-345.

COSTELLA, A., GOLDBERG, D., HARRIS, H., HUTCHINSON, S., JESSOP, L., LYONS, M., MANDAL, S., RAMSAY, M. & SALMON, J. 2016. *Hepatitis C in the UK, 2016 report* [Online]. London: Crown. Available: https://www.gov.uk/government/uploads/system/uploads/attachment_data/file/565459/Hepatitis_C_in_the_UK_2016_report.pdf [Accessed 29/12/2016 2016].

CROSS, S. E., JIN, Y.-S., RAO, J. & GIMZEWSKI, J. K. 2007. Nanomechanical analysis of cells from cancer patients. *Nat Nano,* 2**,** 780-783.

CUBILLAS, P., ANDERSON, M. W. & ATTFIELD, M. P. 2013. Materials Discovery and Crystal Growth of Zeolite A Type Zeolitic–Imidazolate Frameworks Revealed by Atomic Force Microscopy. *Chemistry–A European Journal,* 19**,** 8236-8243.

DANDO, I., DONADELLI, M., COSTANZO, C., DALLA POZZA, E., D'ALESSANDRO, A., ZOLLA, L. & PALMIERI, M. 2013. Cannabinoids inhibit energetic metabolism and induce AMPK-dependent autophagy in pancreatic cancer cells. *Cell Death & Disease,* 4**,** e664.

DASH, T. K. & KONKIMALLA, V. B. 2013. Nanoformulations for delivery of biomolecules: focus on liposomal variants for siRNA delivery. *Critical Reviews™ in Therapeutic Drug Carrier Systems,* 30.

DE OLIVERIA ANDRADE, L. J., D'OLIVEIRA, A., MELO, R. C., DE SOUZA, E. C., COSTA SILVA, C. A. & PARANÁ, R. 2009. Association Between Hepatitis C and Hepatocellular Carcinoma. *Journal of Global Infectious Diseases,* 1**,** 33-37.

DEBERARDINIS, R. J., MANCUSO, A., DAIKHIN, E., NISSIM, I., YUDKOFF, M., WEHRLI, S. & THOMPSON, C. B. 2007. Beyond aerobic glycolysis: transformed cells can engage in glutamine metabolism that exceeds the requirement for protein and nucleotide synthesis. *Proceedings of the National Academy of Sciences,* 104**,** 19345-19350.

DEGLI ESPOSTI, D., HAMELIN, J., BOSSELUT, N., SAFFROY, R., #XEB, SEBAGH, M., #XE8, NE, POMMIER, A., MARTEL, C., #XE9, CILE & LEMOINE, A. 2012. Mitochondrial Roles and Cytoprotection in Chronic Liver Injury. *Biochemistry Research International,* 2012**,** 16.

DENG, L., REN, Z., JIA, Q., WU, W., SHEN, H. & WANG, Y. 2012. Schedule-dependent antitumor effects of 5-fluorouracil combined with sorafenib in hepatocellular carcinoma. *BMC cancer,* 13**,** 363-363.

DESOUZA, M., GUNNING, P. W. & STEHN, J. R. 2012. The actin cytoskeleton as a sensor and mediator of apoptosis. *Bioarchitecture,* 2**,** 75-87.

DORASAMY, S., NARAINPERSAD, N., SINGH, M. & ARIATTI, M. 2012. Novel targeted liposomes deliver siRNA to hepatocellular carcinoma cells in vitro. *Chemical biology & drug design,* 80**,** 647-656.

DÖRIG, P., OSSOLA, D., TRUONG, ANH M., GRAF, M., STAUFFER, F., VÖRÖS, J. & ZAMBELLI, T. 2013. Exchangeable Colloidal AFM Probes for the Quantification of Irreversible and Long-Term Interactions. *Biophysical Journal,* 105**,** 463-472.

DUCKER, W. A., SENDEN, T. J. & PASHLEY, R. M. 1991. Direct measurement of colloidal forces using an atomic force microscope.

DYKENS, J. A. Drug-induced mitochondrial dysfunction: an emerging model of idiosyncratic drug toxicity.

EAKINS, J., BAUCH, C., WOODHOUSE, H., PARK, B., BEVAN, S., DILWORTH, C. & WALKER, P. 2016. A combined in vitro approach to improve the prediction of mitochondrial toxicants. *Toxicology in Vitro,* 34**,** 161-170.

EATON, P. & WEST, P. 2010. *Atomic force microscopy*, Oxford University Press.

ELKALAF, M., ANDĚL, M. & TRNKA, J. 2013. Low Glucose but Not Galactose Enhances Oxidative Mitochondrial Metabolism in C2C12 Myoblasts and Myotubes. *PLoS ONE,* 8**,** e70772.

ELMORE, S. 2007. Apoptosis: a review of programmed cell death. *Toxicologic pathology,* 35**,** 495-516.

ESPENEL, C., GIOCONDI, M.-C., SEANTIER, B., DOSSET, P., MILHIET, P.-E. & LE GRIMELLEC, C. 2008. Temperature-dependent imaging of living cells by AFM. *Ultramicroscopy,* 108**,** 1174-1180.

ESREFOGLU, M. 2013. Role of stem cells in repair of liver injury: Experimental and clinical benefit of transferred stem cells on liver failure. *World Journal of Gastroenterology : WJG,* 19**,** 6757-6773.

FILGUEIRAS, M. D. C., MORROT, A., SOARES, P. M. G., COSTA, M. L. & MERMELSTEIN, C. 2013. Effects of 5-Fluorouracil in Nuclear and Cellular Morphology, Proliferation, Cell Cycle, Apoptosis, Cytoskeletal and Caveolar Distribution in Primary Cultures of Smooth Muscle Cells. *PLoS ONE,* 8**,** e63177.

FLEMING, G., SCHILSKY, R., SCHUMM, L., MEYERSON, A., HONG, A., VOGELZANG, N. & RATAIN, M. 2003. Phase I and pharmacokinetic study of 24-hour infusion 5-fluorouracil and leucovorin in patients with organ dysfunction. *Annals of Oncology,* 14**,** 1142-1147.

FOSTER, A., HOFER, W. & SHLUGER, A. 2001. Quantitative modelling in scanning probe microscopy. *Current Opinion in Solid State and Materials Science,* 5**,** 427-434.

FRESTA, M., VILLARI, A., PUGLISI, G. & CAVALLARO, G. 1993. 5-Fluorouracil: various kinds of loaded liposomes: encapsulation, efficiency, storage stability and fusogenic properties. *International Journal of Pharmaceutics,,* 99.

FRIEDRICHS, J., LEGATE, K. R., SCHUBERT, R., BHARADWAJ, M., WERNER, C., MÜLLER, D. J. & BENOIT, M. 2013. A practical guide to quantify cell adhesion using single-cell force spectroscopy. *Methods,* 169-178.

FUDGE, D. S., GARDNER, K. H., FORSYTH, V. T., RIEKEL, C. & GOSLINE, J. M. 2003. The mechanical properties of hydrated intermediate filaments: insights from hagfish slime threads. *Biophys J,* 85**,** 2015-27.

FULDA, S. & DEBATIN, K. M. 2006. Extrinsic versus intrinsic apoptosis pathways in anticancer chemotherapy. *Oncogene,* 25**,** 4798-4811.

FULDA, S., GALLUZZI, L. & KROEMER, G. 2010. Targeting mitochondria for cancer therapy. *Nat Rev Drug Discov,* 9**,** 447-464.

GABIZON, A. A., SHMEEDA, H. & ZALIPSKY, S. 2006. Pros and Cons of the Liposome Platform in Cancer Drug Targeting. *Journal of Liposome Research,* 16**,** 175-183.

GALLUZZI, L., JOZA, N., TASDEMIR, E., MAIURI, M. C., HENGARTNER, M., ABRAMS, J. M., TAVERNARAKIS, N., PENNINGER, J., MADEO, F. & KROEMER, G. 2008. No death without life: vital functions of apoptotic effectors. *Cell death and differentiation,* 15**,** 1113-1123.

GAN, T. J. 2010. Diclofenac: an update on its mechanism of action and safety profile. *Current Medical Research and Opinion,* 26**,** 1715-1731.

GARG, M. B., SEVESTER, J. C., SAKOFF, J. A. & ACKLAND, S. P. 2002. Simple liquid chromatographic method for the determination of uracil and dihydrouracil plasma levels: a potential pretreatment predictor of 5-fluorouracil toxicity. *Journal of Chromatography B,* 774**,** 223-230.

GOGVADZE, V., ZHIVOTOVSKY, B. & ORRENIUS, S. 2010. The Warburg effect and mitochondrial stability in cancer cells. *Molecular aspects of medicine,* 31**,** 60-74.

GOH, C. F. & LANE, M. E. 2014. Formulation of diclofenac for dermal delivery. *International Journal of Pharmaceutics,* 473**,** 607-616.

GÓMEZ-LECHÓN, M. J., PONSODA, X., O'CONNOR, E., DONATO, T., JOVER, R. & CASTELL, J. V. 2003. Diclofenac induces apoptosis in hepatocytes. *Toxicology in Vitro,* 17**,** 675-680.

GORDON, S. R., CLIMIE, M. & HITT, A. L. 2005. 5-fluorouracil interferes with actin organization, stress fiber formation and cell migration in corneal endothelial cells during wound repair along the natural basement membrane. *Cell Motility and the Cytoskeleton,* 62**,** 244-258.

GRADY, M. E., COMPOSTO, R. J. & ECKMANN, D. M. 2016. Cell elasticity with altered cytoskeletal architectures across multiple cell types. *Journal of the Mechanical Behavior of Biomedical Materials,* 61**,** 197-207.

HAASE, K. & PELLING, A. E. 2015. Investigating cell mechanics with atomic force microscopy. *Journal of the Royal Society Interface,* 12**,** 20140970.

HANAHAN, D. & WEINBERG, R. A. 2000. The hallmarks of cancer. *cell,* 100**,** 57-70.

HE, Y. F., WEI, W., ZHANG, X., LI, Y. H., LI, S., WANG, F. H., LIN, X. B., LI, Z. M., ZHANG, D. S., HUANG, H. Q., HU, B. & JIANG, W. Q. 2008. Analysis of the DPYD gene implicated in 5-fluorouracil catabolism in Chinese cancer patients. *Journal of Clinical Pharmacy and Therapeutics,* 33**,** 307-314.

HECHT, F. M., RHEINLAENDER, J., SCHIERBAUM, N., GOLDMANN, W. H., FABRY, B. & SCHAFFER, T. E. 2015. Imaging viscoelastic properties of live cells by AFM: power-law rheology on the nanoscale. *Soft Matter,* 11**,** 4584-4591.

HONG, C., LIBUTTI, S. & WOOD, B. 2013. Liposomal doxorubicin plus radiofrequency ablation for complete necrosis of a hepatocellular carcinoma. *Current Oncology,* 20**,** e274.

HOSOMI, Y., YOKOSE, T., HIROSE, Y., NAKAJIMA, R., NAGAI, K., NISHIWAKI, Y. & OCHIAI, A. 2000. Increased cyclooxygenase 2 (COX-2) expression occurs frequently in precursor lesions of human adenocarcinoma of the lung. *Lung Cancer,* 30**,** 73-81.

HSIAO, I. L. & HUANG, Y.-J. 2011. Effects of various physicochemical characteristics on the toxicities of ZnO and TiO2 nanoparticles toward human lung epithelial cells. *Science of The Total Environment,* 409**,** 1219-1228.

HUANG, Z., LI, X., ZHANG, T., SONG, Y., SHE, Z., LI, J. & DENG, Y. 2014. Progress involving new techniques for liposome preparation. *Asian Journal of Pharmaceutical Sciences,* 9**,** 176-182.

HUTTER, J. L. & BECHHOEFER, J. 1993. Calibration of atomic-force microscope tips. *Review of Scientific Instruments,* 64**,** 1868-1873.

JANA, N. 2008. NSAIDs and apoptosis. *Cellular and Molecular Life Sciences,* 65**,** 1295-1301.

JANMEY, P. A. & MCCULLOCH, C. A. 2007. Cell mechanics: integrating cell responses to mechanical stimuli. *Annu. Rev. Biomed. Eng.,* 9**,** 1-34.

JANOVJAK, H., STRUCKMEIER, J. & MÜLLER, D. J. 2005. Hydrodynamic effects in fast AFM single-molecule force measurements. *European Biophysics Journal,* 34**,** 91-96.

JEMAL, A., BRAY, F., CENTER, M. M., FERLAY, J., WARD, E. & FORMAN, D. 2011. Global cancer statistics. *CA: A Cancer Journal for Clinicians,* 61**,** 69-90.

JIANG, W., KIM, B. Y., RUTKA, J. T. & CHAN, W. C. 2008. Nanoparticle-mediated cellular response is size-dependent. *Nature nanotechnology,* 3**,** 145-150.

JOSE, C., BELLANCE, N. & ROSSIGNOL, R. 2011. Choosing between glycolysis and oxidative phosphorylation: a tumor's dilemma? *Biochimica et Biophysica Acta (BBA)-Bioenergetics,* 1807**,** 552-561.

KAAMBRE, T., CHEKULAYEV, V., SHEVCHUK, I., TEPP, K., TIMOHHINA, N., VARIKMAA, M., BAGUR, R., KLEPININ, A., ANMANN, T. & KOIT, A. 2014. Metabolic control analysis of respiration in human cancer tissue. *Mitochondria: the cell powerhouse and nexus of stress*, 72.

KAJITA, M., ITOH, Y., CHIBA, T., MORI, H., OKADA, A., KINOH, H. & SEIKI, M. 2001. Membrane-type 1 matrix metalloproteinase cleaves CD44 and promotes cell migration. *The Journal of cell biology,* 153, 893-904.

KAKIMOTO, P. A. & KOWALTOWSKI, A. J. 2016. Effects of high fat diets on rodent liver bioenergetics and oxidative imbalance. *Redox Biology,* 8, 216-225.

KAMALIAN, L., CHADWICK, A. E., BAYLISS, M., FRENCH, N. S., MONSHOUWER, M., SNOEYS, J. & PARK, B. K. 2015. The utility of HepG2 cells to identify direct mitochondrial dysfunction in the absence of cell death. *Toxicology in Vitro,* 29, 732-740.

KAMIMURA, K. & LIU, D. 2008. Physical Approaches for Nucleic Acid Delivery to Liver. *The AAPS journal,* 10, 589-595.

KARP, G. 2002. *Cell and Molecular Biology,* New York, John Wiley and Sons, Inc.

KARP, G. 2008. *Cell and Molecular Biology: Concepts and Experiments 5th Edition with Take Note Set*, John Wiley & Sons, Limited.

KASTNER, E., VERMA, V., LOWRY, D. & PERRIE, Y. 2015. Microfluidic-controlled manufacture of liposomes for the solubilisation of a poorly water soluble drug. *International Journal of Pharmaceutics,* 485, 122-130.

KERR, J. F., WYLLIE, A. H. & CURRIE, A. R. 1972. Apoptosis: a basic biological phenomenon with wide-ranging implications in tissue kinetics. *British Journal of Cancer,* 26, 239.

KIM, Y., HONG, J. W., KIM, J. & SHIN, J. H. 2013. Comparative study on the differential mechanical properties of human liver cancer and normal cells. *Animal Cells and Systems,* 17, 170-178.

KING, L. Y., KHALILI, H., HUANG, E. S., CHUNG, R. T. & CHAN, A. T. Diabetes mellitus is associated with an increased risk of HCC in a large prospective cohort with long term follow-up. Hepatology, 2014. WILEY-BLACKWELL 111 RIVER ST, HOBOKEN 07030-5774, NJ USA, 281A-281A.

KLINGBEIL, P., MARHABA, R., JUNG, T., KIRMSE, R., LUDWIG, T. & ZÖLLER, M. 2009. CD44 variant isoforms promote metastasis formation by a tumor cell-matrix cross-talk that supports adhesion and apoptosis resistance. *Molecular Cancer Research,* 7, 168-179.

KRÄMER, S. D. 2007. Liposome/Water Partitioning: Theory, Techniques, and Applications. *Pharmacokinetic Optimization in Drug Research.* Verlag Helvetica Chimica Acta.

KROEMER, G., GALLUZZI, L. & BRENNER, C. 2007. Mitochondrial membrane permeabilization in cell death. *Physiological reviews,* 87**,** 99-163.

KUMAR, N. & KUMAR, R. 2014. Chapter 2 - Nano-based Drug Delivery and Diagnostic Systems. *In:* KUMAR, N. & KUMAR, R. (eds.) *Nanotechnology and Nanomaterials in the Treatment of Life-Threatening Diseases.* Oxford: William Andrew Publishing.

KUMAR, S. & WEAVER, V. M. 2009. Mechanics, malignancy, and metastasis: The force journey of a tumor cell. *Cancer metastasis reviews,* 28**,** 113-127.

KUSUNOKI, M., YANAGI, H., NODA, M., YOSHIKAWA, R. & YAMAMURA, T. 2000. Results of pharmacokinetic modulating chemotherapy in combination with hepatic arterial 5-fluorouracil infusion and oral UFT after resection of hepatic colorectal metastases. *Cancer,* 89**,** 1228-1235.

KUZNETSOVA, T. G., STARODUBTSEVA, M. N., YEGORENKOV, N. I., CHIZHIK, S. A. & ZHDANOV, R. I. 2007. Atomic force microscopy probing of cell elasticity. *Micron,* 38**,** 824-833.

LAL, R. & ARNSDORF, M. F. 2010. Multidimensional atomic force microscopy for drug discovery: a versatile tool for defining targets, designing therapeutics and monitoring their efficacy. *Life Sciences,* 86**,** 545-62.

LAMONTAGNE, C.-A., CUERRIER, C. M. & GRANDBOIS, M. 2008. AFM as a tool to probe and manipulate cellular processes. *Pflügers Archiv - European Journal of Physiology,* 456**,** 61-70.

LEAL-EGAÑA, A., FRITSCH, A., HEIDEBRECHT, F., DÍAZ-CUENCA, A., NOWICKI, M., BADER, A. & KÄS, J. 2012. Tuning liver stiffness against tumours: An in vitro study using entrapped cells in tumour-like microcapsules. *Journal of the Mechanical Behavior of Biomedical Materials,* 9**,** 113-121.

LEKKA, M. 2016. Discrimination Between Normal and Cancerous Cells Using AFM. *Bionanoscience,* 6**,** 65-80.

LEKKA, M., GIL, D., POGODA, K., DULIŃSKA-LITEWKA, J., JACH, R., GOSTEK, J., KLYMENKO, O., PRAUZNER-BECHCICKI, S., STACHURA, Z., WILTOWSKA-ZUBER, J., OKOŃ, K. & LAIDLER, P. 2012a. Cancer cell detection in tissue sections using AFM. *Archives of Biochemistry and Biophysics,* 518**,** 151-156.

LEKKA, M., GIL, D., POGODA, K., SKA-LITEWKA, J. D., JACH, R., GOSTEK, J., KLYMENKO, O., PRAUZNER-BECHCICKI, S., ZBIGNIEW STACHURA, WILTOWSKA-ZUBER, J., OKON, K. & LAIDLER, P. 2012b. Cancer cell detection in tissue sections using AFM. *Archives of Biochemistry and Biophysics,* 518.

LI, J., CHEN, C., WANG, X., GU, Z. & CHEN, B. 2011a. Novel Strategy to Fabricate PLA/Au Nanocomposites as an Efficient Drug Carrier for Human Leukemia Cells in Vitro. *Nanoscale Research Letters,* 6**,** 29-29.

LI, J., WANG, X., ZHANG, T., WANG, C., HUANG, Z., LUO, X. & DENG, Y. 2015. A review on phospholipids and their main applications in drug delivery systems. *Asian Journal of Pharmaceutical Sciences,* 10**,** 81-98.

LI, Y., SUN, L., JIN, M., DUA, Z., LIU, X., GUO, C., LI, Y., HUANG, P. & SUN, Z. 2011b. Size-dependent cytotoxicity of amorphous silica nanoparticles in human hepatoma HepG2 cells. *Toxicology in Vitro,* 25.

LIN, J. H. & LU, A. Y. H. 1997. Role of Pharmacokinetics and Metabolism in Drug Discovery and Development. *PHARMACOLOGICAL REVIEWS,* 49**,** 403-449.

LIU, X., HUANG, N., LI, H., JIN, Q. & JI*, J. 2013. Surface and Size Effects on Cell Interaction of Gold Nanoparticles with Both Phagocytic and Nonphagocytic Cells. *Langmuir,* 29.

LLOVET, J. M., RUFF, P., TASSOPOULOS, N., CASTELLS, L., BRUIX, J., EL-HARIRY, I. & PEACHEY, M. 2001. A phase II trial of oral eniluracil/5-fluorouracil in patients with inoperable hepatocellular carcinoma. *European Journal of Cancer,* 37**,** 1352-1358.

LONDOÑO, M.-C., ABRALDES, J. G., ALTAMIRANO, J., DECAENS, T. & FORNS, X. 2015. Clinical trial watch: Reports from the AASLD Liver Meeting®, Boston, November 2014. *Journal of Hepatology,* 62**,** 1196-1203.

LONGLEY, D. B., HARKIN, D. P. & JOHNSTON, P. G. 2003. 5-Fluorouracil: mechanisms of action and clinical strategies. *Nat Rev Cancer,* 3**,** 330-338.

LÜBBE, J., TEMMEN, M., RAHE, P., KÜHNLE, A. & REICHLING, M. 2013. Determining cantilever stiffness from thermal noise. *Beilstein Journal of Nanotechnology,* 4**,** 227-233.

LUO, Y., RANA, P. & WILL, Y. 2012. Palmitate increases the susceptibility of cells to drug-induced toxicity: an in vitro method to identify drugs with potential contraindications in patients with metabolic disease. *Toxicological Sciences***,** kfs208.

LYUBCHENKO, Y. L. 2013. Nanoimaging methods for biomedicine. *Methods,* 60.

MAEDA, H. & MATSUMURA, Y. 1988. Tumoritropic and lymphotropic principles of macromolecular drugs. *Critical reviews in therapeutic drug carrier systems,* 6**,** 193-210.

MARROQUIN, L. D., HYNES, J., DYKENS, J. A., JAMIESON, J. D. & WILL, Y. 2007. Circumventing the Crabtree Effect: Replacing Media Glucose with Galactose Increases Susceptibility of HepG2 Cells to Mitochondrial Toxicants. *Toxicological Sciences,* 97**,** 539-547.

MASUZAKI, R., TATEISHI, R., YOSHIDA, H., SATO, T., OHKI, T., GOTO, T., YOSHIDA, H., SATO, S., SUGIOKA, Y., IKEDA, H., SHIINA, S., KAWABE, T. & OMATA, M. 2007. Assessing liver tumor stiffness by transient elastography. *Hepatology International,* 1**,** 394-397.

MATSUI, H., SHIMOKAWA, O., KANEKO, T., NAGANO, Y., RAI, K. & HYODO, I. 2011. The pathophysiology of non-steroidal anti-inflammatory drug (NSAID)-induced mucosal injuries in stomach and small intestine. *Journal of Clinical Biochemistry and Nutrition,* 48**,** 107-111.

MCELROY, W. D., SELIGER, H. H. & DELUCA, M. 1974. Chapter 8 - INSECT BIOLUMINESCENCE A2 - ROCKSTEIN, MORRIS. *The Physiology of Insecta (Second Edition).* Academic Press.

MI, L., LIANQING, L., NING, X., YUECHAG, W., ZAILI, D. & WEIJING, X. X. 2012. Atomic force microscopy imaging and mechanical properties measurement of red blood cells and aggressive cancer cells. *SCIENCE CHINA Life Sciences,* Vol.55 No.11: 968–973.

MI, L., LIANQING, L., NING, X., YUECHAO, W., ZAILI, D., XIUBIN, X. & WEIJING, Z. 2013. Mapping CD20 molecules on the lymphoma cell surface using atomic force microscopy. *Chinese Science Bulletin,* 58**,** 1516-1519.

MOEENDARBARY, E. & HARRIS, A. R. 2014. Cell mechanics: principles, practices, and prospects. *Wiley Interdisciplinary Reviews. Systems Biology and Medicine,* 6**,** 371-388.

MOGHIMI, S. M., HUNTER, A. C. & MURRAY, J. C. 2001. Long-Circulating and Target-Specific Nanoparticles: Theory to Practice. *PHARMACOLOGICAL REVIEWS,* 53**,** 283-318.

MONKEMOLLER, V., SCHUTTPELZ, M., MCCOURT, P., SORENSEN, K., SMEDSROD, B. & HUSER, T. 2014. Imaging fenestrations in liver sinusoidal endothelial cells by optical localization microscopy. *Physical Chemistry Chemical Physics,* 16**,** 12576-12581.

MULIER, S., NI, Y., JAMART, J., RUERS, T., MARCHAL, G. & MICHEL, L. 2005. Local recurrence after hepatic radiofrequency coagulation: multivariate meta-analysis and review of contributing factors. *Annals of surgery,* 242**,** 158-171.

MÜLLER, D. J. & DUFRÊNE, Y. F. 2011a. Atomic force microscopy: a nanoscopic window on the cell surface. *Trends in Cell Biology,* 21**,** 461-469.

MÜLLER, D. J. & DUFRÊNE, Y. F. 2011b. Force nanoscopy of living cells. *Current Biology,* 21**,** R212-R216.

MÜLLER, D. J., KRIEG, M., ALSTEENS, D. & DUFRÊNE, Y. F. 2009. New frontiers in atomic force microscopy: analyzing interactions from single-molecules to cells. *Current Opinion in Biotechnology,* 20**,** 4-13.

NAGARSENKER, M., JAIN, A. & SHAH, S. 2015. Functionalized Lipid Particulates in Targeted Drug Delivery. *In:* DEVARAJAN, P. V. & JAIN, S. (eds.) *Targeted Drug Delivery : Concepts and Design.* Springer International Publishing.

NANOSYSTEMS, P. 2015. NanoAssemblr™ v1.5 User Guide. *In:* NANOSYSTEMS, P. (ed.). Canada.

NATARAJAN, J. V., NUGRAHA, C., NG, X. W. & VENKATRAMAN, S. 2014. Sustained-release from nanocarriers: a review. *Journal of Controlled Release,* 193**,** 122-138.

NIKOLOFF, N., LARRAMENDY, M. L. & SOLONESKI, S. 2014. Assessment of DNA damage, cytotoxicity, and apoptosis in human hepatoma (HepG2) cells after flurochloridone herbicide exposure. *Food and Chemical Toxicology,* 233-241.

NOORDHUIS, P., HOLWERDA, U., VAN DER WILT, C. L., VAN GROENINGEN, C. J., SMID, K., MEIJER, S., PINEDO, H. M. & PETERS, G. J. 2004. 5-Fluorouracil incorporation into RNA and DNA in relation to thymidylate synthase inhibition of human colorectal cancers. *Annals of Oncology,* 15**,** 1025-1032.

OJCIUS, D. M., SOUQUE, P., PERFETTINI, J.-L. & DAUTRY-VARSAT, A. 1998. Apoptosis of Epithelial Cells and Macrophages Due to Infection with the Obligate Intracellular Pathogen Chlamydia psittaci. *The Journal of Immunology,* 161**,** 4220-4226.

OKAJIMA, T., TANAKA, M., TSUKIYAMA, S., KADOWAKI, T., YAMAMOTO, S., SHIMOMURA, M. & TOKUMOTO, H. 2007. Stress relaxation of HepG2 cells measured by atomic force microscopy. *Nanotechnology,* 18.

OTTO, M., HANSEN, S., DALGAARD, L., DUBOIS, J. & BADOLO, L. 2008. Development of an in vitro assay for the investigation of metabolism-induced drug hepatotoxicity. *Cell biology and toxicology,* 24**,** 87.

PANG, J. X. Q., ZIMMER, S., NIU, S., CROTTY, P., TRACEY, J., PRADHAN, F., SHAHEEN, A. A. M., COFFIN, C. S., HEITMAN, S. J., KAPLAN, G. G., SWAIN, M. G. & MYERS, R. P. 2014. Liver Stiffness by Transient Elastography Predicts Liver-Related Complications and Mortality in Patients with Chronic Liver Disease. *PLoS ONE,* 9**,** e95776.

PENTAK, D., SUŁKOWSKI, W. & SUŁKOWSKA, A. 2012. Influence of some physical properties of 5-fluorouracil on encapsulation efficiency in liposomes. *Journal of Thermal Analysis and Calorimetry,* 108**,** 67-71.

PERSAD, R., LIU, C., WU, T.-T., HOULIHAN, P. S., HAMILTON, S. R., DIEHL, A. M. & RASHID, A. 2004. Overexpression of caspase-3 in hepatocellular carcinomas. *Modern pathology,* 17**,** 861-867.

PETROS, R. A. & DESIMONE, J. M. 2010. Strategies in the design of nanoparticles for therapeutic applications. *Nat Rev Drug Discov,* 9**,** 615-627.

PETTERSEN, H. S., VISNES, T., VÅGBØ, C. B., SVAASAND, E. K., DOSETH, B., SLUPPHAUG, G., KAVLI, B. & KROKAN, H. E. 2011. UNG-initiated base excision repair is the major repair route for 5-fluorouracil in DNA, but 5-fluorouracil cytotoxicity depends mainly on RNA incorporation. *Nucleic Acids Research,* 39**,** 8430-8444.

PI, J., LI, B., TU, L., ZHU, H., JIN, H., YANG, F., BAI, H., CAI, H. & CAI, J. 2015. Investigation of quercetin-induced HepG2 cell apoptosis-associated cellular biophysical alterations by atomic force microscopy. *Scanning*.

PICAS, L., MILHIET, P.-E. & HERNÁNDEZ-BORRELL, J. 2012. Atomic force microscopy: A versatile tool to probe the physical and chemical properties of supported membranes at the nanoscale. *Chemistry and Physics of Lipids,* 165**,** 845-860.

PIROLLO, K. F. & CHANG, E. H. 2008. Does a targeting ligand influence nanoparticle tumor localization or uptake? *Trends in Biotechnology,* 26**,** 552-558.

POURAHMAD, J., MORTADA, Y., ESKANDARI, M. R. & SHAHRAKI, J. 2011. Involvement of Lysosomal Labilisation and Lysosomal/mitochondrial Cross-Talk in Diclofenac Induced Hepatotoxicity. *Iranian Journal of Pharmaceutical Research : IJPR,* 10**,** 877-887.

PULLARKAT, P. A., FERNÁNDEZ, P. A. & OTT, A. 2007. Rheological properties of the Eukaryotic cell cytoskeleton. *Physics Reports,* 449**,** 29-53.

RADMACHER, H. D., PHILIPP HAUPT. 2014. *HERTZ FIT APPLET* [Online]. Available: http://www.biophysik.uni-bremen.de/start/radmacher-group/data-analysis/hertzfit/#c5530.

RADMACHER, M. 2002. 4.-Measuring the Elastic Properties of Living Cells by the Atomic Force Microscope. *Methods in cell biology,* 68**,** 67-90.

RAI, N. K., TRIPATHI, K., SHARMA, D. & SHUKLA, V. K. 2005. Apoptosis: a basic physiologic process in wound healing. *The international journal of lower extremity wounds,* 4**,** 138-144.

RAO, C. V. & REDDY, B. S. 2004. NSAIDs and chemoprevention. *Current cancer drug targets,* 4**,** 29-42.

REPNIK, U., ČESEN, M. H. & TURK, B. 2014. Lysosomal membrane permeabilization in cell death: concepts and challenges. *Mitochondrion,* 19**,** 49-57.

RICO, F., SU, C. & SCHEURING, S. 2011. Mechanical mapping of single membrane proteins at submolecular resolution. *Nano letters,* 11**,** 3983-3986.

RIESS, W., STIERLIN, H., DEGEN, P., FAIGLE, J. W., GERARDIN, A., MOPPERT, J., SALLMANN, A., SCHMID, K., SCHWEIZER, A., SULC, M., THEOBALD, W. & WAGNER, J. 1978. Pharmacokinetics and Metabolism of the Anti-Inflammatory Agent Voltaren. *Scandinavian Journal of Rheumatology,* 7**,** 17-29.

RODRIGUEZ, M. L., MCGARRY, P. J. & SNIADECKI, N. J. 2013. Review on Cell Mechanics: Experimental and Modeling Approaches. *Applied Mechanics Reviews,* 65**,** 060801-060801.

ROSSIGNOL, R., GILKERSON, R., AGGELER, R., YAMAGATA, K., REMINGTON, S. J. & CAPALDI, R. A. 2004. Energy substrate modulates mitochondrial structure and oxidative capacity in cancer cells. *Cancer research,* 64**,** 985-993.

RYDER, S. D. 2003. Guidelines for the diagnosis and treatment of hepatocellular carcinoma (HCC) in adults. *Gut,* 52**,** iii1-iii8.

SARDO, M., RUANO, C., CASTRO, J. L., LOPEZ-TOCON, I., SOTO, J., RIBEIRO-CLARO, P. & OTERO, J. C. 2009. Surface-enhanced Raman scattering of 5-fluorouracil adsorbed on silver nanostructures. *Physical Chemistry Chemical Physics,* 11**,** 7437-7443.

SCHILLERS, H., MEDALSY, I., HU, S., SLADE, A. L. & SHAW, J. E. 2016. PeakForce Tapping resolves individual microvilli on living cells. *Journal of Molecular Recognition,* 29**,** 95-101.

SENOO, H. 2004. Structure and function of hepatic stellate cells. *Med Electron Microsc,* 37**,** 3-15.

SHAH, S. M., GOEL, P. N., JAIN, A. S., PATHAK, P. O., PADHYE, S. G., GOVINDARAJAN, S., GHOSH, S. S., CHAUDHARI, P. R., GUDE, R. P., GOPAL, V. & NAGARSENKER, M. S. 2014. Liposomes for targeting hepatocellular carcinoma: Use of conjugated arabinogalactan as targeting ligand. *International Journal of Pharmaceutics,* 477**,** 128-139.

SHAHBAZI, M.-A. & A SANTOS, H. 2013. Improving oral absorption via drug-loaded nanocarriers: absorption mechanisms, intestinal models and rational fabrication. *Current drug metabolism,* 14**,** 28-56.

SHARMA, S., CROSS, S. E., FRENCH, S., GONZALEZ, O., PETZOLD, O., BAKER, W., WALCZAK, W., YONGSUNTHON, R., BAKER, D. & GIMZEWSKI, J. K. 2009. Influence of Substrates on Hepatocytes: A Nanomechanical Study. *Journal of Scanning Probe Microscopy,* 4.

SHEN, Y., NAKAJIMA, M., KOJIMA, S., HOMMA, M., KOJIMA, M. & FUKUDA, T. 2011. Single cell adhesion force measurement for cell viability identification using an AFM cantilever-based micro putter. *MEASUREMENT SCIENCE AND TECHNOLOGY,* 22.

SHERMAN, M. 2014. Surveillance for hepatocellular carcinoma. *Best Practice & Research Clinical Gastroenterology,* 28**,** 783-793.

SILBERBERG, Y. R., MIEDA, S., AMEMIYA, Y., SATO, T., KIHARA, T., NAKAMURA, N., FUKAZAWA, K., ISHIHARA, K., MIYAKE, J. & NAKAMURA, C. 2013. Evaluation of the actin cytoskeleton state using an antibody-functionalized nanoneedle and an AFM. *Biosensors and Bioelectronics,* 40**,** 3-9.

SINGH, A. K. 2016. Chapter 2 - Structure, Synthesis, and Application of Nanoparticles. *Engineered Nanoparticles.* Boston: Academic Press.

SIRENKO, O., HESLEY, J., RUSYN, I. & CROMWELL, E. F. 2014. High-Content Assays for Hepatotoxicity Using Induced Pluripotent Stem Cell–Derived Cells. *Assay and Drug Development Technologies,* 12**,** 43-54.

SONG, M. J., BAE, S. H., CHUN, H. J., CHOI, J. Y., YOON, S. K., PARK, J. Y., HAN, K. H., KIM, Y. S., YIM, H. J. & UM, S. H. 2015. A randomized study of cisplatin and 5-FU hepatic arterial infusion chemotherapy with or without adriamycin for advanced hepatocellular carcinoma. *Cancer chemotherapy and pharmacology,* 75**,** 739-746.

SOUSA, M., POZNIAK, A. & BOFFITO, M. 2008. Pharmacokinetics and pharmacodynamics of drug interactions involving rifampicin, rifabutin and antimalarial drugs. *Journal of Antimicrobial Chemotherapy,* 62**,** 872-878.

SPENCE, T., DE SOUZA, R., DOU, Y., STAPLETON, S., REILLY, R. M. & ALLEN, C. 2015. Integration of imaging into clinical practice to assess the delivery and performance of macromolecular and nanotechnology-based oncology therapies. *Journal of Controlled Release,* 219**,** 295-312.

STAMENOVIĆ, D. 2008. Rheological behavior of mammalian cells. *Cellular and Molecular Life Sciences,* 65**,** 3592-3605.

STAMENOVIĆ, D., ROSENBLATT, N., MONTOYA-ZAVALA, M., MATTHEWS, B. D., HU, S., SUKI, B., WANG, N. & INGBER, D. E. 2007. Rheological Behavior of Living Cells Is Timescale-Dependent. *Biophysical Journal,* 93**,** L39-L41.

STEFAN B. KAEMMER, S. M., NATALIA ERINA, BEDE PITTENGER, ADAM MEDNICK, AND PETER DEWOLF 2013. Introduction to Bruker's ScanAsyst and PeakForce Tapping AFM Technology. *Application #133.* Santa Barbara.

SUN, S., SONG, Z., COTLER, S. J. & CHO, M. 2014. Biomechanics and functionality of hepatocytes in liver cirrhosis. *Journal of Biomechanics,* 47**,** 2205-2210.

SWISS, R. & WILL, Y. 2011. Assessment of Mitochondrial Toxicity in HepG2 Cells Cultured in High-Glucose-or Galactose-Containing Media. *Current Protocols in Toxicology***,** 2.20. 1-2.20. 14.

TAKEBE, N., ZHAO, S.-C., URAL, A. U., JOHNSON, M. R., BANERJEE, D., DIASIO, R. B. & BERTINO, J. R. 2001. Retroviral transduction of human dihydropyrimidine dehydrogenase cDNA confers resistance to 5-fluorouracil in murine hematopoietic progenitor cells and human CD34+ -enriched eripheral blood progenitor cells. *Nature,* 929.

TAN, X.-W., XIA, H., XU, J.-H. & CAO, J.-G. 2009. Induction of apoptosis in human liver carcinoma HepG2 cell line by 5-allyl-7-gen-difluoromethylenechrysin. *World Journal of Gastroenterology : WJG,* 15**,** 2234-2239.

TARGETT-ADAMS, P., GRAHAM, E. J., MIDDLETON, J., PALMER, A., SHAW, S. M., LAVENDER, H., BRAIN, P., TRAN, T. D., JONES, L. H. & WAKENHUT, F. 2011. Small molecules targeting hepatitis C virus-encoded NS5A cause subcellular redistribution of their target: insights into compound modes of action. *Journal of virology,* 85**,** 6353-6368.

THOMAS, G., BURNHAM, N. A., CAMESANO, T. A. & WEN, Q. 2013. Measuring the Mechanical Properties of Living Cells Using Atomic Force Microscopy. *Journal of Visualized Experiments : JoVE***,** 50497.

THOMPSON, C. B. 1995. Apoptosis in the pathogenesis and treatment of disease. *Science,* 267**,** 1456.

TIWARI, G., TIWARI, R., SRIWASTAWA, B., BHATI, L., PANDEY, S., PANDEY, P. & BANNERJEE, S. K. 2012. Drug delivery systems: An updated review. *International Journal of Pharmaceutical Investigation,* 2**,** 2-11.

TOH, M.-R. & CHIU, G. N. C. 2013. Liposomes as sterile preparations and limitations of sterilisation techniques in liposomal manufacturing. *Asian Journal of Pharmaceutical Sciences,* 8**,** 88-95.

TORCHILIN, V. 2008. *Multifunctional pharmaceutical nanocarriers*, Springer Science & Business Media.

UCHIBORI, K., KASAMATSU, A., SUNAGA, M., YOKOTA, S., SAKURADA, T., KOBAYASHI, E. ... SATO, N. 2012. Establishment and characterization of two 5-fluorouracil-resistant hepatocellular carcinoma cell lines. . *International Journal of Oncology***,** 1005-1010.

UMUT OZCAN, M., OCAL, S., BASDOGAN, C., DOGUSOY, G. & TOKAT, Y. 2011. Characterization of frequency-dependent material properties of human liver and its pathologies using an impact hammer. *Medical Image Analysis,* 15**,** 45-52.

VAN BALEN, G. P., MARTINET, C. A. M., CARON, G., BOUCHARD, G., REIST, M., CARRUPT, P.-A., FRUTTERO, R., GASCO, A. & TESTA, B. 2004. Liposome/water lipophilicity: Methods, information content, and pharmaceutical applications. *Medicinal Research Reviews,* 24**,** 299-324.

VANDER HEIDEN, M. G., CANTLEY, L. C. & THOMPSON, C. B. 2009. Understanding the Warburg Effect: The Metabolic Requirements of Cell Proliferation. *Science (New York, N.Y.),* 324**,** 1029-1033.

VANLANDINGHAM, M. R. 2003. Review of instrumented indentation. DTIC Document.

VARGAS-PINTO, R., GONG, H., VAHABIKASHI, A. & JOHNSON, M. 2013. The Effect of the Endothelial Cell Cortex on Atomic Force Microscopy Measurements. *Biophysical Journal,* 105**,** 300-309.

VARIOLA, F. 2015. Atomic force microscopy in biomaterials surface science. *Physical Chemistry Chemical Physics*.

VAUPEL, P. 2008. Hypoxia and Aggressive Tumor Phenotype: Implications for Therapy and Prognosis. *The Oncologist,* 13**,** 21-26.

VINOGRADOV, S. V., BATRAKOVA, E. V. & KABANOV, A. V. 2004. Nanogels for Oligonucleotide Delivery to the Brain. *Bioconjugate chemistry,* 15**,** 50-60.

VOLLMAR, B. & MENGER, M. D. 2009. *The Hepatic Microcirculation: Mechanistic Contributions and Therapeutic Targets in Liver Injury and Repair*.

VU, N. B., NGUYEN, T. T., TRAN, L. C.-D., DO, C. D., NGUYEN, B. H., PHAN, N. K. & PHAM, P. V. 2013. Doxorubicin and 5-fluorouracil resistant hepatic cancer cells demonstrate stem-like properties. *Cytotechnology,* 65**,** 491-503.

WAGNER, A. & VORAUER-UHL, K. 2011. Liposome Technology for Industrial Purposes. *Journal of Drug Delivery,* 2011.

WARBURG, O. 1956. On the Origin of Cancer Cells. *Science,* 123**,** 309-314.

WARNER, T. D., GIULIANO, F., VOJNOVIC, I., BUKASA, A., MITCHELL, J. A. & VANE, J. R. 1999. Nonsteroid drug selectivities for cyclo-oxygenase-1 rather than cyclo-oxygenase-2 are associated with human gastrointestinal toxicity: A full in vitro analysis. *Proceedings of the National Academy of Sciences,* 96**,** 7563-7568.

WISE, D. R., DEBERARDINIS, R. J., MANCUSO, A., SAYED, N., ZHANG, X.-Y., PFEIFFER, H. K., NISSIM, I., DAIKHIN, E., YUDKOFF, M. & MCMAHON, S. B. 2008. Myc regulates a transcriptional program that stimulates mitochondrial glutaminolysis and leads to glutamine addiction. *Proceedings of the National Academy of Sciences,* 105**,** 18782-18787.

WOZNIAK, M. J., KAWAZOE, N., TATEISHI, T. & CHEN, G. 2009. Monitoring of mechanical properties of serially passaged bovine articular chondrocytes by atomic force microscopy. *Micron,* 40**,** 870-875.

XIE, S.-Q., LI, Q., ZHANG, Y.-H., WANG, J.-H., MEI, Z.-H., ZHAO, J. & WANG, C.-J. 2011. NPC-16, a novel naphthalimide–polyamine conjugate, induced apoptosis and autophagy in human hepatoma HepG2 cells and Bel-7402 cells. *Apoptosis,* 16**,** 27-34.

XINYI, G., KEITH, B., KARIN, S. & MARTIN, G. 2014. The effect of neighboring cells on the stiffness of cancerous and non-cancerous human mammary epithelial cells. *New Journal of Physics,* 16**,** 105002.

YANG, M., ZHANG, M., TAHARA, Y., CHECHETKA, S., MIYAKO, E., IIJIMA, S. & YUDASAKA, M. 2014. Lysosomal membrane permeabilization: carbon nanohorn-induced reactive oxygen species generation and toxicity by this neglected mechanism. *Toxicology and applied pharmacology,* 280**,** 117-126.

YANG, W.-S., VA, P., BRAY, F., GAO, S., GAO, J., LI, H.-L. & XIANG, Y.-B. 2011. The Role of Pre-Existing Diabetes Mellitus on Hepatocellular Carcinoma Occurrence and Prognosis: A Meta-Analysis of Prospective Cohort Studies. *PLoS ONE,* 6**,** e27326.

YIN, P. H., LEE, H. C., CHAU, G. Y., WU, Y. T., LI, S. H., LUI, W. Y., WEI, Y. H., LIU, T. Y. & CHI, C. W. 2004. Alteration of the copy number and deletion of mitochondrial DNA in human hepatocellular carcinoma. *British Journal of Cancer,* 90**,** 2390-2396.

YOPP, A. C. & JARNAGIN, W. R. 2010. Randomized Clinical Trials in Hepatocellular Carcinoma. *Surgical Oncology Clinics of North America,* 19**,** 151-162.

YOUNG, D. B. 2010. Control of cardiac output. *Integrated Systems Physiology: From Molecule to Function,* 2**,** 1-97.

YU, G., CHEN, X., CHEN, S., YE, W., HOU, K. & LIANG, M. 2015. Arsenic trioxide reduces chemo-resistance to 5-fluorouracil and cisplatin in HBx-HepG2 cells via complex mechanisms. *Cancer Cell International,* 15**,** 1-12.

YU, S. J. 2016. A concise review of updated guidelines regarding the management of hepatocellular carcinoma around the world: 2010-2016. *Clinical and Molecular Hepatology,* 22**,** 7-17.

ZAMBONI, W. C. 2008. Concept and Clinical Evaluation of Carrier-Mediated Anticancer Agents. *The Oncologist,* 13**,** 248-260.

ZEISBERG, M., KRAMER, K., SINDHI, N., SARKAR, P., UPTON, M. & KALLURI, R. 2006. De-differentiation of primary human hepatocytes depends on the composition of specialized liver basement membrane. *Molecular and Cellular Biochemistry,* 283**,** 181-189.

ZHANG, G., SHI, L., SELKE, M. & WANG, X. 2011a. CdTe quantum dots with daunorubicin induce apoptosis of multidrug-resistant human hepatoma HepG2/ADM cells: in vitro and in vivo evaluation. *Nanoscale Research Letters,* 6**,** 418-418.

ZHANG N., Y. Y., XU S AND CHEN. W. 2008. 5-Fluorouracil: Mechanisms of Resistance and Reversal Strategies. *Molecules*.

ZHANG, Y., CAI, X., WANG, Y., ZHANG, C., LI, L., CHOI, S. W., WANG, L. V. & XIA, Y. 2011b. Noninvasive photoacoustic microscopy of living cells in two and three dimensions through enhancement by a metabolite dye. *Angewandte Chemie,* 123**,** 7497-7501.

ZHANG, Y., ZHANG, Y., CHEN, M., ZHOU, Y. & LANG, M. 2014. Galactosylated poly(ε-caprolactone) membrane promoted liver-specific functions of HepG2 cells in vitro. *Materials Science and Engineering: C,* 41**,** 52-58.

ZHAO, L. & BURT, A. 2007. The diffuse stellate cell system. *Journal of Molecular Histology,* 38**,** 53-64.

ZHAO Y., J. Q. A. L. G. 2013. Tumor markers for hepatocellular carcinoma (Review). *MOLECULAR AND CLINICAL ONCOLOGY*.

ZHOU, Z. L., NGAN, A. H. W., TANG, B. & WANG, A. X. 2012. Reliable measurement of elastic modulus of cells by nanoindentation in an atomic force microscope. *Journal of the Mechanical Behavior of Biomedical Materials,* 8**,** 134-142.

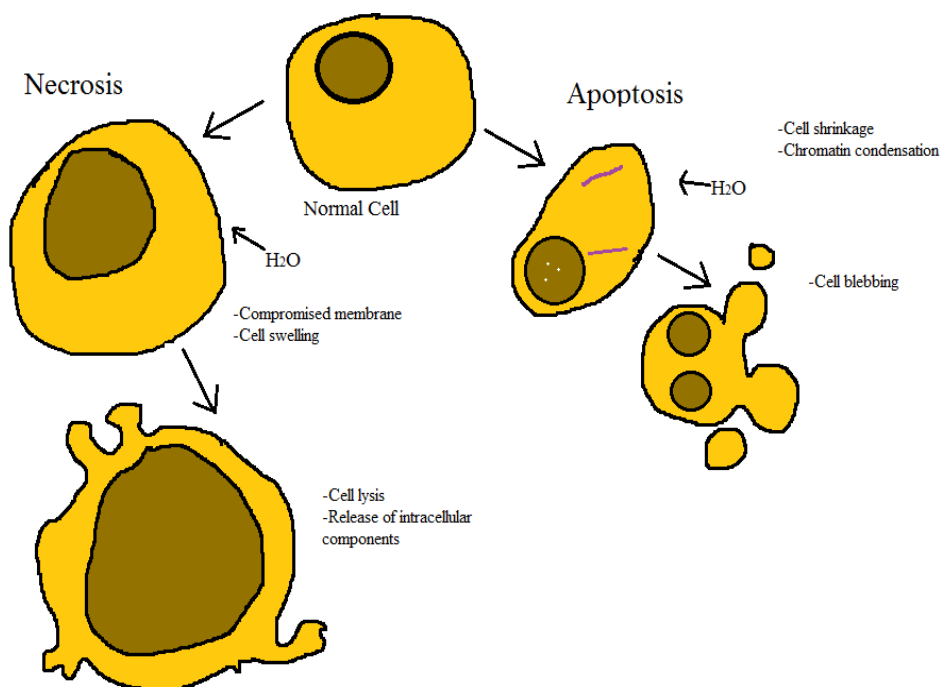ZIEGLER, U. & GROSCURTH, P. 2004. Morphological Features of Cell Death. *Physiology,* 19**,** 124-128.

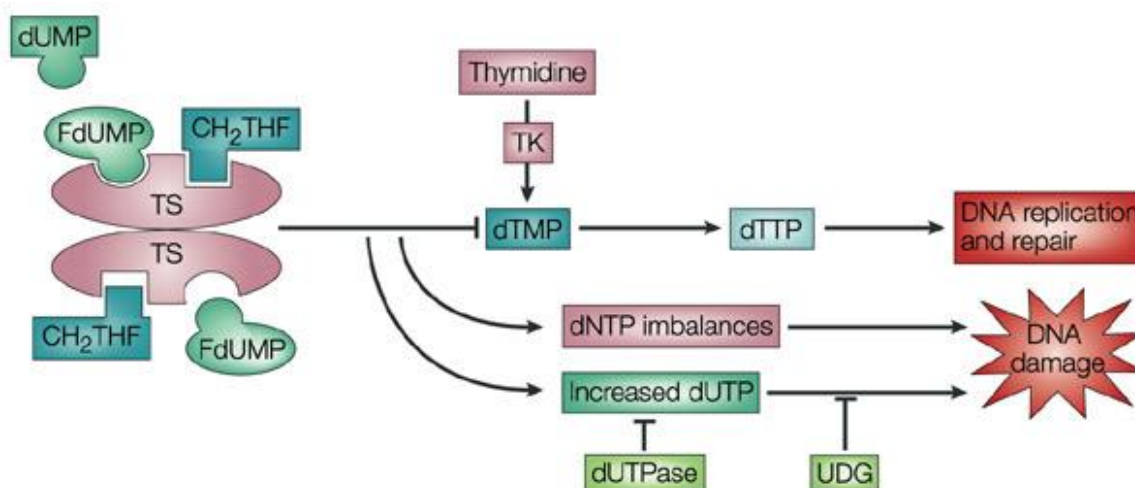Figure A-1 – Schematic showing the differences between apoptosis and necrosis modes of cell death

Figure A2 - The mechanisms of thymidylate synthase inhibition induced by 5-FU within the cell. The conversion of deoxythymidine monophosphate (dTMP) due to 5,10-methylene tetrahydrofolate (CH2THF). This image was obtained from Longley et al 2003.
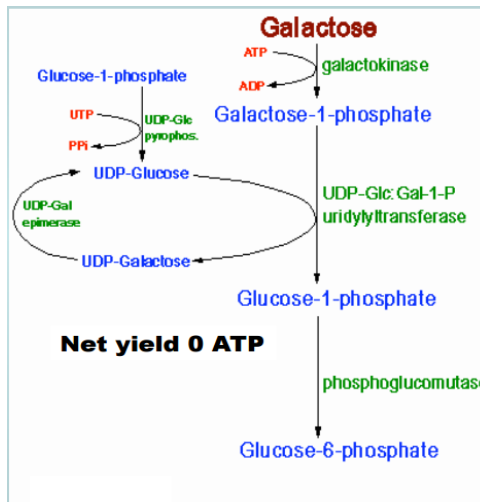
Figure A3 - Process of galactose metabolism intracellularly if glucose is not present for energy production (Dykens et al)
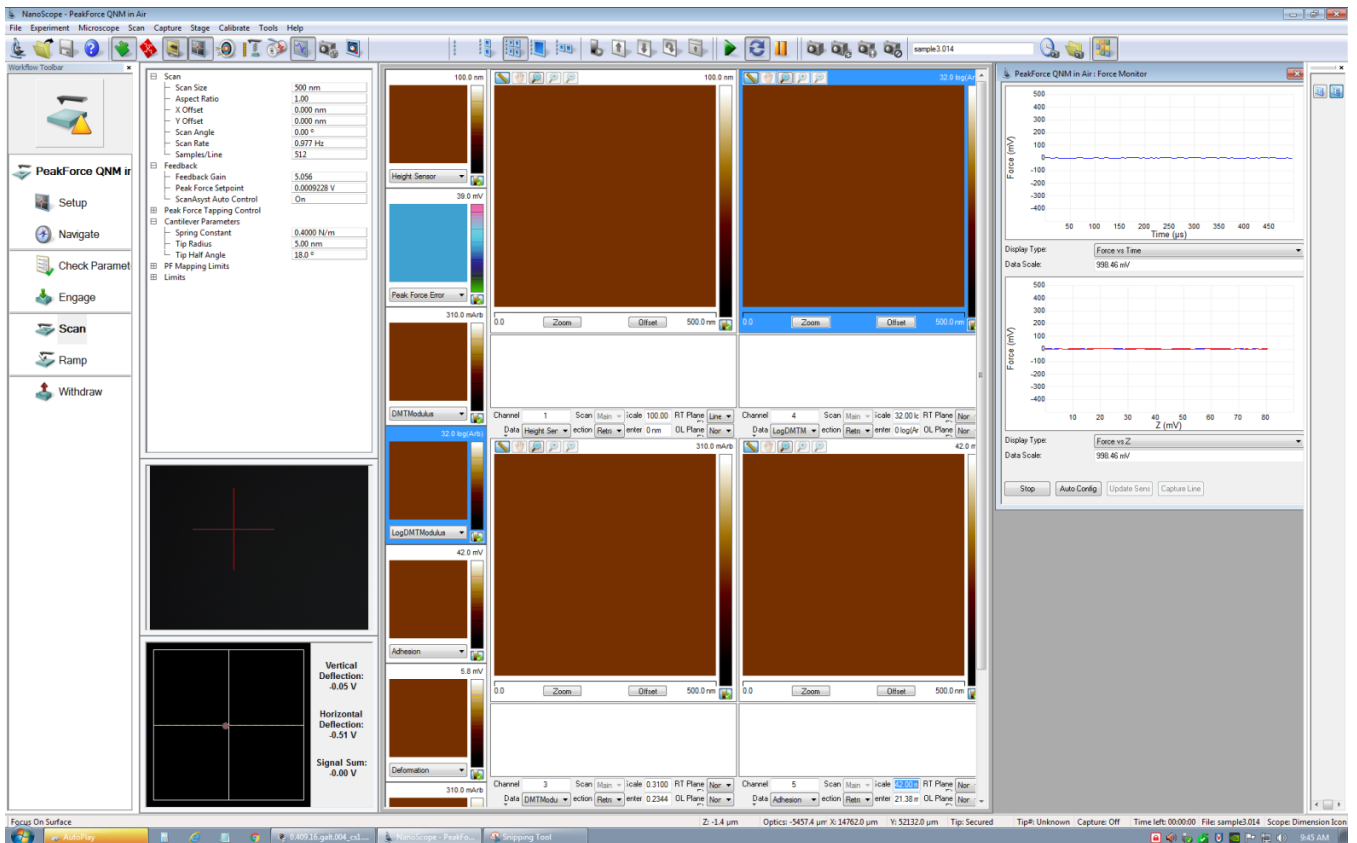

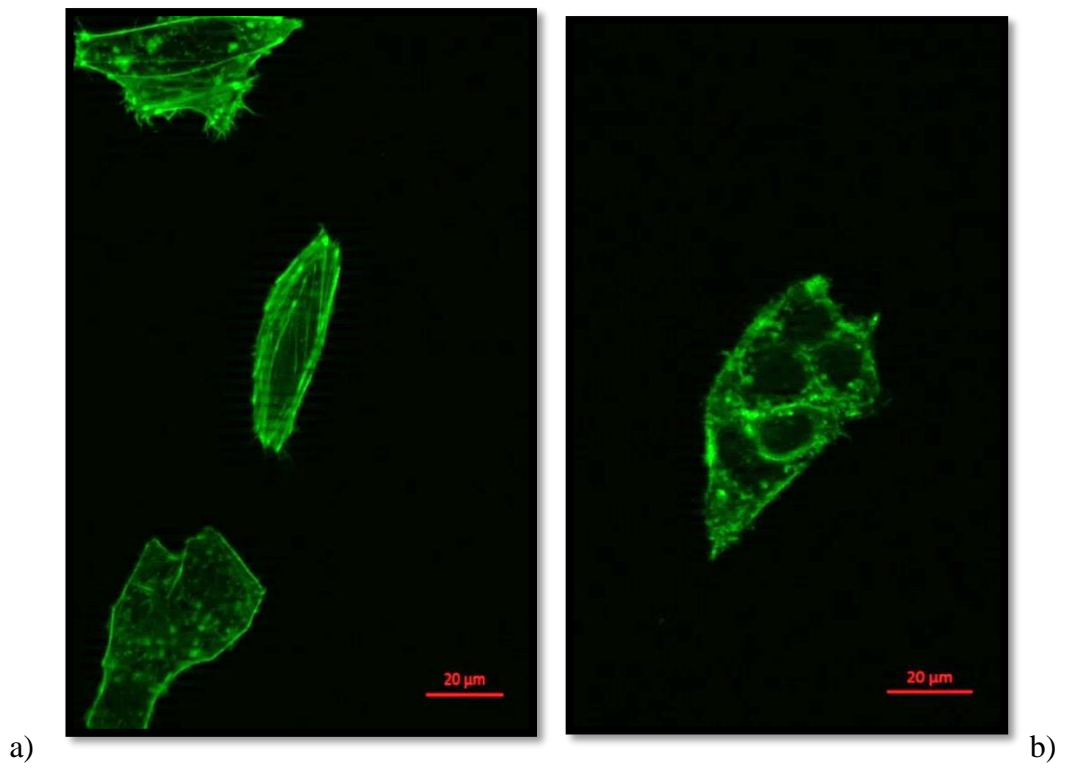Figure A4 - Layout for PeakForce QNM measurements.

a)

b)

Figure A5 - HepG2 cells actin fibres. a) After 24h of treatment with 5-FU b) control cells